**UNIVERSITY OF SOUTHAMPTON**
FACULTY OF NATURAL AND ENVIRONMENTAL SCIENCES
CHEMISTRY

# The Development and Application of Chromatography and Mass Spectrometry Techniques for the Analysis of Biodiesel and Fuel Related Compounds

by

Christianne Clare Wicking BSc (Hons) AMRSC

A thesis submitted in partial fulfilment of the requirements for the degree of Doctor of Philosophy

**June 2013**

**UNIVERISTY OF SOUTHAMPTON**

# ABSTRACT

FACULTY OF NATURAL AND ENVIRONMENTAL SCIENCES
Chemistry
Doctor of Philosophy

THE DEVELOPMENT AND APPLICATION OF CHROMATOGRAPHY AND MASS SPECTROMETRY TECHNIQUES FOR THE ANALYSIS OF BIODIESEL AND FUEL RELATED COMPOUNDS

by Christianne Clare Wicking

As world crude oil supplies deplete, research has heightened into alternative fuels. One such fuel is biodiesel which is used in varying percentages with petrodiesel *i.e.*B5, where 5 represents the percentage of biodiesel present. Biodiesel is composed of varying fatty acid methyl esters (FAME) % and these percentages are dependent on feedstock origin. FAMEs in biodiesel are composed of varying chain length and degrees of unsaturation. FAMEs have a propensity to auto-oxidise which increases fuel viscosity and introduces new species into the fuel cycle.

Chromatography and mass spectrometry have been applied to the analysis of rapeseed methyl ester (RME) and auto-oxidised RME. The benefits and disadvantages have been discussed, with each technique aiding the analysis. This research has demonstrated the complexity of RME auto-oxidation and the necessity of several techniques for analysis. Gas chromatography-mass spectrometry has provided information on small chain RME degradation products and FAMEs and supports auto-oxidation *via* homolytic β-scission and Russell mechanism auto-oxidation pathways. However, it also suggests the presence of an epoxide auto-oxidation route.

Positive ion ESI-MS techniques have demonstrated the presence of highly oxygenated species observed in auto-oxidised RME. Through the use of positive ion ESI-Fourier transform-ion cyclotron resonance MS suggested molecular formula have been detailed, with a $[C18:1/C18:2/C18:3 + nO + Na]^+$ series reported. MS/MS has been used

to identify the composition of a polymeric oxidation species and has been reported within.

Throughout analysis C18:1, C18:2 and C18:3, the major FAMEs in RME have been observed to deplete, this is coincident with observations of new species and increased viscosity. This research describes detection and identification of auto-oxidation markers: C8:0, nonanal and methyl *cis*-9,10-epoxystearate. These auto-oxidation markers have been discussed and compared to C18:0 FAMEs, with a correlation observed. C18:0:methyl *cis*-9,10-epoxystearate has been suggested to be a useful comparison to identify extent of auto-oxidation. However, further studies are required in RME of known auto-oxidation age, followed by application of RME of unknown auto-oxidation age and other feedstocks.

Also, investigated here is the use of electrochemistry coupled to a TOF-MS to investigate forced oxidation. Using electro chemistry positive ion ESI-MS, oxidation of RME has been shown to closely mimic auto-oxidation observed in natural auto-oxidation and forced oxidation studies. However, does not force oxidation through an epoxide route. Oxidation of RME using electrochemical techniques demonstrates a number of auto-oxidation products identified in natural and forced oxidation, further supporting the presence of auto-oxidation routes other than the epoxide route. Electrochemical oxidation was completed in minutes compared to forced oxidation (days) and natural auto-oxidation (years), potentially lending itself to be a quick screening technique for oxidation inhibitors.

Chromatography and mass spectrometry techniques have also been applied to the analysis of samples of a polyisobutylene (PiB) type dispersant synthesis. The resulting samples and starting reagents were not suitable to be analysed *via* other techniques due to the insolubility of these PiB type compounds in MeOH, MeCN and DCM. This analysis was completed to investigate the presence of a vinylimidazole graft on a PiB succinimide. The aim of the synthesis was to produce a multiply vinylimidazole grafted PiB succinimide. Analysis completed using positive ion ESI-supercritical fluid chromatography-ultraviolet MS has demonstrated this is not the case. UV and MS data suggest the presence of a singly vinylimidazole grafted PiB succinimide. It also highlights the presence of a PiB succinimide and residual starting reagents.

# Contents

# Figures

# Tables

# Declaration Of Authorship

I, Christianne Clare Wicking declare that this thesis and the work presented in it are my own and has been generated by me as the result of my own original research.

The Development and Application of Chromatography and Mass Spectrometry Techniques for the Analysis of Biodiesel and Fuel Related Compounds

I confirm that:

1. This work was done wholly or mainly while in candidature for a research degree at this University;

2. Where any part of this thesis has previously been submitted for a degree or any other qualification at this University or any other institution, this has been clearly stated;

3. Where I have consulted the published work of others, this is always clearly attributed;

4. Where I have quoted from the work of others, the source is always given. With the exception of such quotations, this thesis is entirely my own work;

5. I have acknowledged all main sources of help;

6. Where the thesis is based on work done by myself jointly with others, I have made clear exactly what was done by others and what I have contributed myself;

7. Either none of this work has been published before submission, or parts of this work have been published as: [please list references below]:

Signed:

Date:

*Per ardua ad astra*

# Acknowledgements

Someone once told me I was fuelled on happiness and optimism and many people have contributed to this in countless ways. I can only hope they appreciate the role they have played in getting me where I am today and wish them every happiness.

Most importantly I would like to thank my supervisor, John, for his support, patience, advice and faith throughout the last 4 years. For never doubting my skills even when I was armed with a screwdriver and a remaining piece from a recently reassembled MS.

Many thanks go to Julie for her guidance, ninja like skills and practical help, without which I would be lost. Tom and Sam, my industrial supervisors, for their support and advice. My group members past and present: Angie, Jo, Krina, Louisa, Stephen and Waraporn for facilitating my endless questions, sweet tooth and support throughout. My work colleagues for listening to my constant talk about my thesis, resemblance of my desk turning into a chaotic paper mountain, the unlimited chocolate supply and for understanding.

I owe many thanks, drinks, and hours to Row, Paolo, Stu, David, Sophie and Nathan, 'the lunch train', the Reid/Levason and the Raja group for the continuous supply of humour. Without their friendship, games, trips to the pub and dancing I'm sure I would be less sane. Writing my PhD has been a long process and without my housemates providing me with cake and doing my washing up it would have taken longer – thank you for bearing with me. Thanks goes to PRW for the continued support and escape, even when my PhD has taken me away from training.

My acknowledgements would not be complete without thanking my family. My parents, grandparents, Jo, Chris, Blaze, Billie-Anne, Angelique, Sam and Van, thank you for always being there and understanding the trials and tribulations of my PhD, especially the last few months. For listening even if you had no clue what I was talking about and for being your unique selves.

My last thanks go to my Granddad who throughout his life was the most encouraging, positive influence of my academic endeavours. Although he may not have supported my choice of hair colours through the years, he was the biggest champion of my education and without his belief and encouragement I wouldn't be where I am.

# Abbreviations

| | |
|---|---|
| API | atmospheric pressure ionisation |
| APCI | atmospheric pressure chemical ionisation |
| $CO_2$ | carbon dioxide |
| CRM | charge residue model |
| Da | Daltons |
| DAG | diacylglyceride |
| DEI/DCI | desorption probe |
| DIP | direct insertion probe |
| DTA | differential thermal analysis |
| EC | electrochemical |
| ECD | electron capture detector |
| EI | electron ionisation |
| EICC | extracted ion current chromatogram |
| ELSD | evaporative light scattering detector |
| ESI | electrospray ionisation |
| FAEE | fatty acid ethyl ester |
| FAME | fatty acid methyl ester |
| FID | flame ionisation detector |
| FT | Fourier transform |
| GC | gas chromatography |
| h | hours |
| HR | high resolution |
| *H* | height equivalent to one theoretical plate |
| HETP | height equivalent to one theoretical plate |
| HPLC | high performance liquid chromatography |

| | |
|---|---|
| ICR | ion cyclotron resonance |
| IEM | ion evaporation model |
| *k* | retention factor |
| L | length |
| LC | liquid chromatography |
| LOD | limit of detection |
| LR | low resolution |
| *m*/*z* | mass-to-charge |
| MALDI | matrix-assisted laser desorption/ionisation |
| MAG | monoacylglyceride |
| min. | minutes |
| MS | mass spectrometry |
| *N* | theoretical plate number |
| NMR | nuclear magnetic resonance spectroscopy |
| $NO_x$ | nitrogen oxide(s) |
| NP | normal phase |
| PiB | polyisobutylene |
| PiBSA | polyisobutylene succinic anhydride |
| QIT | quadrupole ion trap |
| *R* | resolution |
| RI | refractive index |
| RIC | reconstructed ion chromatogram |
| RP | reversed phase |
| RTFO | renewable transport fuel obligation |
| RME | rapeseed methyl ester |
| s | seconds |
| SFC | supercritical fluid chromatography |
| TAG | triacylglyceride |
| TCD | thermal conductivity detector |

| | |
|---|---|
| TGA | thermogravimetric analysis |
| TICC | total ion current chromatogram |
| TLC | thin layer chromatography |
| TOF | time of flight |
| $t_R$ | retention time |
| UV | ultra violet |
| VIMA | 1-vinylimidazole |
| $w$ | width |

# Chapter 1. Introduction

## 1.1. Transportation Fuels

Transportation fuels have traditionally been produced from crude oil *via* fractional distillation. Crude oil sources are depleting owing to ever growing demand. Whilst the search for novel crude oil sources is constant, viable alternative transportation fuels are needed. This need is driven by environmental, economical, political and ethical issues which are ever present, for example, sustainability, cost, greenhouse gas production, biodegradability, land use, food or fuel source, local development and government targets.

Research into alternative transportation fuels has rapidly developed within the last 20 years with practicable substitutes for petrol and petrodiesel identified. Petrol and petrodiesel surrogates can be produced from biomass and include ethanol, methanol, biodiesel, Fischer-Tropsch diesel, hydrogen and methane.[1] Other alternative fuels which are not produced from biomass directly include electric power and solar power and these can be used independently or together with petrol/petrodiesel in hybrid vehicles.

In Europe, bioderived fuels are used in blends with petrol and petrodiesel and through this partnership consumption of petrol and petrodiesel is being reduced. Presently, the Renewable Transport Fuel Obligation (RTFO) states that all petrol and petrodiesel that is supplied (in a significant quantity) and sold on UK forecourts must contain 5% (by volume) bioderived fuel, by the addition of bioethanol to petrol

and biodiesel to petrodiesel, with anticipation that the blend level will increase in line with pre-set targets.[2]

### 1.1.1. Petrodiesel

A popular fuel choice in Europe, petrodiesel is largely used in the compression-ignition engines of road and marine vehicles. Petrodiesel is largely composed of $C_8$-$C_{28}$ alkanes and is produced from crude oil by fractional distillation and is obtained from the 130-370 °C fraction. It boasts suitable properties for fuel use including a high energy content of 43 MJ/kg.[3-5]

However, petrodiesel is not without its problems; at low temperatures viscosity increases, the exhaust emissions are harmful, it compromises poor ignition qualities, doesn't easily biodegrade and contains unwanted species such as sulfur. Many of these issues can be overcome through purification/decontamination and the use of additives. To fully understand the issues presented in a compression-ignition engine it is important to understand the processes that occur.

#### 1.1.1.1. Compression-Ignition Engine

Compression-ignition engines are designed for use with petrodiesel and ignite fuel by compression, as discussed below. This is in contrast to a spark-ignition engine which uses petrol as the fuel source, with a spark needed to initiate the reaction.[6] Compression ignition engines can pose a problematic environment; engine temperatures range from low (-5 °C at start-up) to high (130 °C in

operation), combustion is not 100% efficient and is completed in normal atmosphere, lubricant containing additives circulate the engine and metal contaminants, free radicals and combustion by-products are present which can initiate unwanted chemical reactions within the engine.

Compression ignition engines typically work *via* four strokes and these will be discussed with the aid of Figure 1.1.

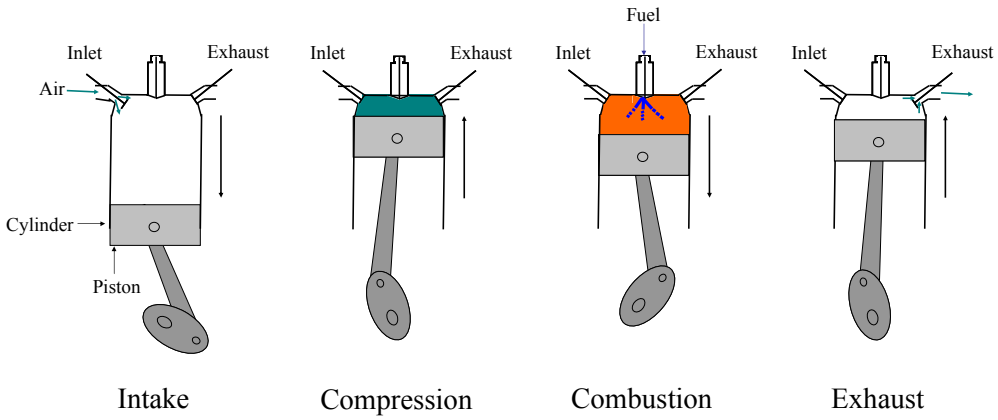


**Figure 1.1:** Schematic representation of petrodiesel combustion in a compression-ignition engine.

First, air is drawn into the cylinder *via* the inlet as the piston moves down the cylinder (intake, Figure 1.1). The piston then moves up the cylinder and the air is compressed, and thus heated (compression, Figure 1.1). Petrodiesel is injected and due to the high temperature, it combusts (combustion, Figure 1.1). Expansion of combustion gases forces the piston downwards and as the piston reaches the bottom of the cylinder the exhaust valve is opened forcing the exhaust gases out (exhaust, Figure 1.1). The piston then travels upwards where the inlet valve opens and the cycle is repeated.

This process is not 100% efficient and when petrodiesel undergoes combustion some fuel does not combust and some only

partially combusts.[6] The remaining uncombusted petrodiesel and partially combusted fuel exits the cylinder *via* the exhaust outlet, however minute amounts leak past the piston into the lubricant oil.[6] Over time these small traces of petrodiesel/partially combusted fuel can build up in the lubricant oil adversely affecting the lubricating oil chemically and physically.

Lubricant oil is needed to minimise friction and ensure smooth running of moving parts within the compression ignition engine. It is also employed to carry heat away from moving parts and through the use of additives combat chemical issues.[7] Specifically designed, lubricant oil must posses certain properties to target particular problems within the engine. Additives are needed and designed to counteract problems such as the formation of sulfuric acid, produced from sulfur and water in the fuel, and thus protect the combustion-ignition engine from chemical attack and deposits. Often one additive will be designed to target more than one issue.[7] Examples of additives include antiwear, antiscuff, antifoaming and antioxidants.[7] Lubricant oil must have suitable viscosity; if it is too thin temperatures increase and moving parts become worn, however if it is too viscous moving parts will stick.[7]

### 1.1.2. Biodiesel

An alternative to petrodiesel, biodiesel, is a fuel source that can be used neat or in blends with petrodiesel *e.g.* B100 (100% biodiesel) and B5 (5% biodiesel, 95% petrodiesel) with little or no modification needed to a compression-ignition engine. Of the biofuel supplied in the UK (as directed under the RTFO) in 2009/2010 71% was biodiesel,

with the remaining predominantly bioethanol (29%) and biogas (negligible).[8]

Biodiesel is defined as the alkyl esters of vegetable oil, animal fat, algae oil, or used/waste cooking oil feedstocks and is produced *via* a transesterification reaction (Figure 1.2).[9] Transesterification proceeds *via* the reaction of a short chain alcohol ($C_1$-$C_4$) with a triacylglyceride (TAG) from a feedstock oil source (Figure 1.2).[4, 9, 10]

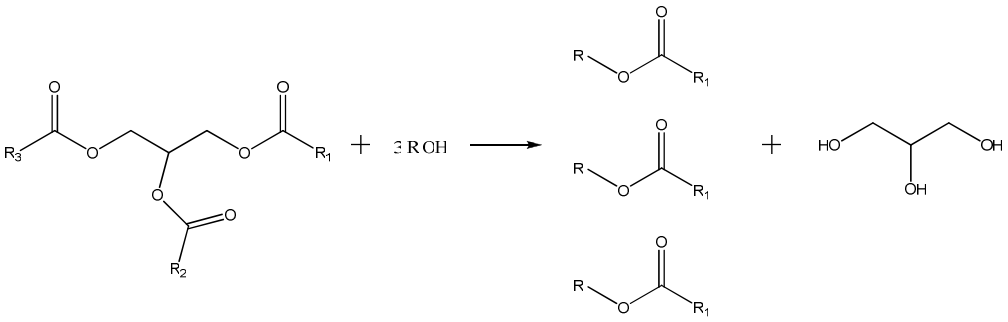


**Figure 1.2:** Transesterification reaction of TAG to produce alkyl esters used for biodiesel, where R = hydrocarbon of varying length and unsaturation and R' is a short chain hydrocarbon.

This reaction can be catalysed by an acid, base or enzyme, and is typically base catalysed, to produce three alkyl esters which are related to the starting TAG.[9, 10] Previous research has investigated the use of vegetable oils as a fuel source, however transesterification of the vegetable oil is needed; alkyl esters (compared to the starting TAG) are more volatile, boast viscosity more similar to petrodiesel and when used do not induce coking, carbon deposits, trumpet formation or ring sticking.[11] As with many reactions formation of by-products occurs, with glycerol being the principal by-product of transesterification. It is important that after transesterification, clean up steps are completed to ensure the biodiesel is of a high quality and is composed of alkyl esters

with no contaminants *i.e.* unreacted starting reagents, diacylglycerides (DAGs), monoacylglycerides (MAGs), catalyst, glycerol, trace impurities or water. Biodiesel contains trace amounts of impurities, with sterol glucosides the highest concentration and in higher concentration than the starting feedstock oil.[12] There is concern that these unreacted starting reagents and sterol glucosides will precipitate out during storage of biodiesel and when used as a fuel.[12-14] Precipitation of sterol glucosides in an engine could cause filters to plug or if allowed to build could cause engines to fail.[12-14]

Alkyl esters produced are dependent on the type of short chain alcohol that is used in transesterification, which is dependent on cost and availability of the alcohol with methanol and ethanol being the most popular.[4] In Brazil, ethanol is readily available and is cheaper than methanol, primarily owing to the sugar cane industry.[9] Therefore biodiesel in Brazil is composed of fatty acid ethyl esters (FAEEs).[9] This is contrary to Europe where methanol is the alcohol of choice resulting in the production of biodiesel composing of fatty acid methyl esters (FAMEs), with the terms biodiesel and FAME(s) often used synonymously. Research discussed from this point will be related to biodiesel composed of FAMEs.

Feedstock source also determines the composition of biodiesel. Choice of feedstock source is dependent on cost, availability, geographical location and properties it affords the fuel.[9] Many feedstock sources are available and are categorised into the following classes: vegetable oils, animal fats, algae oils and used/waste cooking oils. Vegetable oils provide the widest variety of feedstocks sources with 350 types of oil crops identified, of which several have been identified as appropriate biodiesel feedstocks including rapeseed, soybean, sunflower, palm, jatropha.[4, 15, 16] Rapeseed and soybean are

the most common feedstock sources used to produce biodiesel in the UK.[8] Each feedstock source has a unique composition of TAGs and this is translated to the refined biodiesel, where the finished fuel is composed of a unique composition of FAMEs. Additionally natural variance can influence FAME profiles observed in biodiesel, with the same feedstock source producing biodiesel with different FAME concentrations (Figure 1.3).[17] FAMEs vary in carbon chain length ($C_{14}$-$C_{24}$ for fuel purposes) and in degree of unsaturation (0-3 double bonds) and are commonly referenced relating to these chemical properties, *i.e.* CX:Y, where X denotes the length of the original fatty acid chain and Y denotes the number of double bonds (Figure 1.3, Figure 1.4).[4, 17] Typically, FAMEs containing an odd number of carbons in the fatty acid chain, *e.g.* C17:Y, are found only in feedstocks of animal origin.

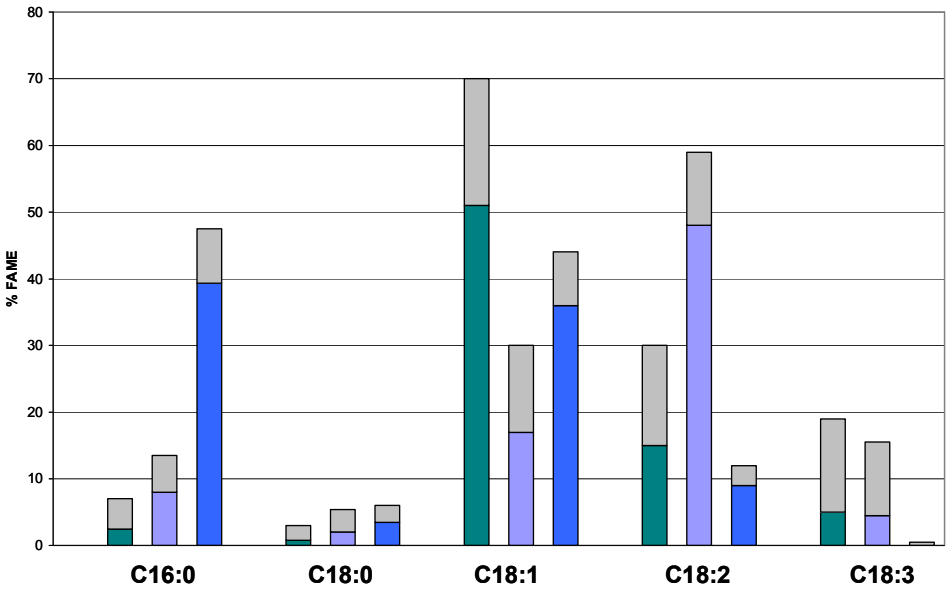


**Figure 1.3:** Fatty acid composition (%) of biodiesel feedstock oils, as measured by gas liquid chromatography, where green = rapeseed feedstock source, lilac = soya bean feedstock source, blue = palm oil feedstock source and grey = percentage range of fatty acid in the feedstock source.[17]

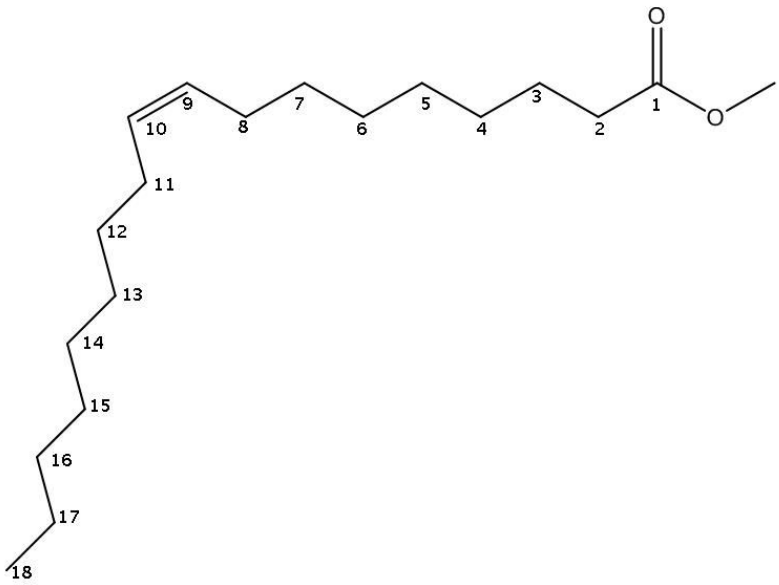


**Figure 1.4:** FAME nomenclature using methyl oleate, C18:1, as an example.

As a fuel biodiesel possesses many attractive features; it is non-toxic, biodegradable, contains no sulfur, has a similar viscosity to petrodiesel and has a higher flash point, therefore making it safe to handle and easy to transport.[4, 6, 18-20] When combusted biodiesel produces 39-41 MJ/kg with a slight reduction in power and torque observed, reduces most exhaust emissions, except nitrogen oxides ($NO_x$) which are slightly increased and improves anti-wear properties.[4, 6, 20] The use of biodiesel emits no new $CO_2$ into the atmosphere (Figure 1.5) and could potentially decrease the reliance on other countries for fuel, which in turn could; create more jobs, allow for easier monitoring of biodiesel quality and support sustainability and government targets whist decreasing the cost.[6, 19, 21]

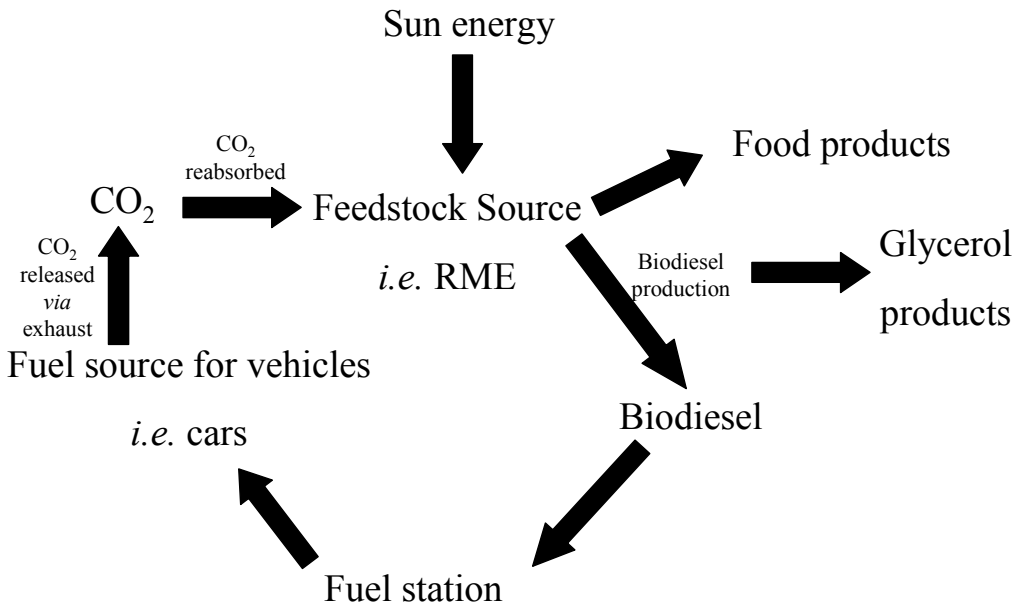


**Figure 1.5:** Life cycle of biodiesel produced from plant stocks, including the recycling of $CO_2$ that is produced as an exhaust gas.

Fuel stability is a major concern, with fuels often stored for many years before they are used. One of the major drawbacks of biodiesel as a fuel is its susceptibility to chemical oxidation and auto-oxidation, of which the latter is the focus for this project. Auto-oxidation describes the naturally occurring oxidation process of a substance with oxygen over time. Auto-oxidation is readily promoted by; air, raised temperature, light, oxidation promoters, free radicals, metal catalysts and humidity, all of which are common place in an engine. Through the auto-oxidation process FAMEs readily degrade and suggested auto-oxidation products include aldehydes, ketones, small chain hydrocarbons, epoxides, high MW polymers and free radicals. Auto-oxidation products are detrimental to fuel stability and can increase fuel viscosity, promote secondary reactions and compromise combustion efficiency. Furthermore, the addition of petrodiesel can further complicate auto-oxidation *e.g.* when used in a

blend or lubricant oil, as described previously. Auto-oxidation is suggested to be completed *via* a radical pathway and this will be discussed in more detail in Chapter 4.

Unsaturated FAMEs are particularly susceptible to auto-oxidation and their levels in the fuel can greatly influence the extent of auto-oxidation. Biodiesel containing FAMEs with increased number of multiple bonds are more vulnerable to auto-oxidation which can decrease fuel stability.[22] As the number of double bonds in a molecule increases, so does the number of pi bonds. Pi bonds have increased reactivity compared to sigma bonds and even more so when these bonds are conjugated, as observed in FAMEs C18:2 and C18:3. This characteristic of polyunsaturated (C18:2 and C18:3) compounds ensures that they react at a faster rate compared with monounsaturated (C18:1) or saturated (C18:0) molecules. This is the main reaction pathway for auto-oxidation of FAMEs, with the methyl ester functionality having little effect. This is evident in the reactivity of FAEEs (common biodiesel in Brazil) where the relative rates of auto-oxidation of C18:1, C18:2 and C18:3 have been shown to be 1:41:98, with a fuel containing high amounts of C18:2 or C18:3 less likely to be stable than a fuel containing predominantly C18:1.[23]

However, multiple double bonds can be an advantage, where biodiesel containing high concentrations of FAME possessing more than one double bond can improve, otherwise poor, cold flow properties of the fuel.[24] These properties highlight the need for a biodiesel fuel that contains a good balance of FAMEs.

Oxidation stability of a fuel, also referred to as the oil stability index, can be measured *via* an assortment of techniques including the Rancimat method, thermogravimetric analysis (TGA) and differential scanning calorimetry (DSC).[25, 26]The European standard EN14112

describes a standard method to analyse the oxidation stability of biodiesel using the Rancimat method.[26, 27] A Rancimat is an instrument used for determining the oxidation stability of biodiesel *via* determination of the induction period of oxidation of B100.[26] This method measures the production of volatile organic acids with an induction period of 6 or more hours acceptable.[26] Although this method can predict oxidation stability of biodiesel it can not identify the oxidation process. Auto-oxidation begins as soon as biodiesel comes in contact with air/$O_2$ and is hard to control. Measures which can be put in place to stop/slow auto-oxidation of biodiesel include storing the fuel under an inert atmosphere. However, the practicalities of storing large quantities of biodiesel under an inert atmosphere are infeasible. Alternatively, a more suitable option is to store biodiesel with as little air as possible, however containers that are not air tight will aid the auto-oxidation process. Without the aid of anti-oxidants biodiesel will begin auto-oxidation right away.

In Europe, rapeseed oil is a common biodiesel feedstock producing rapeseed methyl ester (RME), which predominantly contains C16:0, C18:1, C18:2 and C18:3, with minor constituents consisting of C12:0, C14:0, C16:1, C18:0, C20:0, C20:1, C22:0 C22:1, C22:2, C24:0 and C24:1 (Figure 1.3).[17] Auto-oxidised RME contains not only these FAMEs, but also numerous auto-oxidation products and can additionally contain petrodiesel and lubricant oil. The complex mixture of species present in auto-oxidised biodiesel, which have a range of different chemistries and polarities, requires separation and identification to fully understand this process. This project will focus on auto-oxidised RME and its analysis *via* chromatography and mass spectrometry.

## 1.2. Chromatographic Separation

Chromatography was first described in 1906 by Tswett, who first reported separation of plant pigments *via* a column of calcium carbonate or alumina using petroleum ether.[28-30] A versatile tool that is required by many researchers, chromatography is commonplace in modern day laboratories. The underlining principle involves the separation of components (analytes) within a mixture (sample) which is achieved through the use of two phases: the stationary phase and mobile phase.[31] The analytes partition between these phases depending on their relative affinities for each phase and it is this partitioning which determines the retention and thus the separation of the analytes.

Stationary phases may be solid, gel, liquid or a solid support coated in liquid and are immobile.[31] Many stationary phases are available and are produced from a wide range of compounds. Stationary phases vary in chemical composition and thus polarity, these properties dictate the ability of the stationary phase to separate analytes (Figure 1.6).

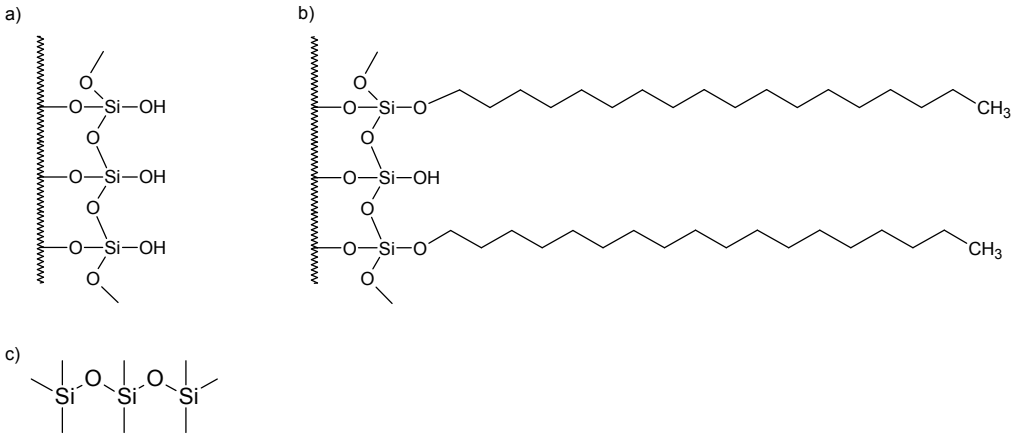


**Figure 1.6:** Structures of three common stationary phases and where they are used a) silica (SFC), b) $C_{18}$ (HPLC) and c) PDMS (GC).

The mobile phase is a fluid *i.e.* gas, liquid or supercritical fluid and is defined as a phase that moves in a definite direction.[31] Mobile phases can be single, binary or tertiary fluids. Modifiers and buffers can be added to the mobile phase, this changes the chemical composition and can aid analyses, for example by deactivation of silanols on a $C_8$ column.

Chromatography can be separated into two categories: planar and column chromatography.[31] Paper chromatography and thin layer chromatography (TLC) comprise planar chromatography, where the stationary phase is a plane support, with analytes migrating different distances across this support with the aid of a liquid mobile phase.[31] Column chromatography employs a column and two types of column are typically used; packed and capillary (Figure 1.7).[31] Capillary columns have a narrow internal diameter, range in length from 1-60 m and the inside walls are coated with the stationary phase. In contrast, packed columns have larger internal diameters, are much shorter (5-50 mm) and the stationary phase is bound to small deactivated particles *e.g.* diatomaceous earth, with a range of particle

sizes. Modern GC-MS is completed with capillary columns, with packed columns rarely used. Whilst SFC and HPLC are routinely accomplished using packed columns.

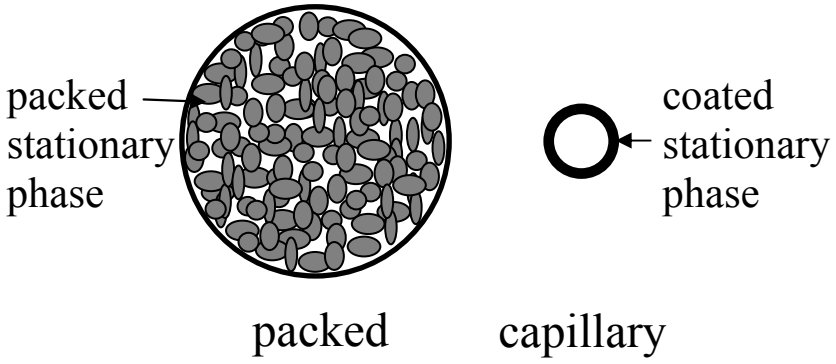


**Figure 1.7:** Pictorial representation of packed and capillary columns (not to scale).

Column chromatography includes gas chromatography (GC), high performance liquid chromatography (HPLC), supercritical fluid chromatography (SFC) and countercurrent chromatography (CCC) which utilise different stationary and mobile phases and afford other parameters that can be changed *e.g.* temperature and pressure.[31] HPLC, SFC and CCC can be described in terms of 'reversed phase' or 'normal phase'. Classification is dependent on the selection of the stationary and mobile phase. Reversed phase chromatography compromises a stationary phase that is of less polarity compared to the mobile phase. Normal phase is an opposite configuration, with the stationary phase more polar than the mobile phase.

Analysis of samples *via* one, two or all of these techniques can produce very different results dependent on the parameters of separation, namely the stationary and mobile phase and the chemistry of the analyte. These varying parameters do not allow direct

comparisons of chromatographic separations using different techniques. Therefore chromatographic separations are described *via* theoretical parameters described below.

### 1.2.1. Theoretical Measures of Chromatography

The retention factor (*k*) is a ratio of the length of time an analyte resides in the stationary phase relative to the time spent in the mobile phase compared to an unretained analyte eluted under identical conditions (Equation 1.1).[31] Long retention times ($t_R$) result in a large *k* value and *vice versa* for short retention times. Typical values of *k* are expected to be 1-10.

$$k = \frac{t_{an} - t_0}{t_0}$$

**Equation 1.1**[31]

Where $t_{an} = t_R$ of the analyte and $t_0 = t_R$ of an unretained compound

Resolution (*R*) is a gauge of how well two adjacent peaks are able to be separated. Samples often contain more than one analyte and under ideal chromatographic conditions all analytes would be baseline resolved, however some separations are completed with only the analyte of interest resolved from the rest of the sample components. Baseline resolution is achieved when $R > 1.5$.

Resolution is expressed as:

$$R = \frac{[t_{RB} - t_{RA}]}{0.5[w_A + w_B]}$$

**Equation 1.2**[31]

Where, $t_{RA} = t_R$ of analyte A, $t_{RB} = t_R$ of analyte B, $w_A$ = peak width of analyte A and $w_B$ = peak width of analyte B

Resolution is a measure of the efficiency of a chromatographic column and its ability to separate analytes within a sample. An alternate measure of efficiency is theoretical plates (Equation 1.3). The theoretical plate model divides the column into a number of theoretical plates (*N*) (Figure 1.8) and within each plate the stationary phase and mobile phase are at equilibrium.[31] A more efficient column will have faster equilibrium between the stationary and mobile phase and therefore a higher number of plates resulting in better resolution of peaks.

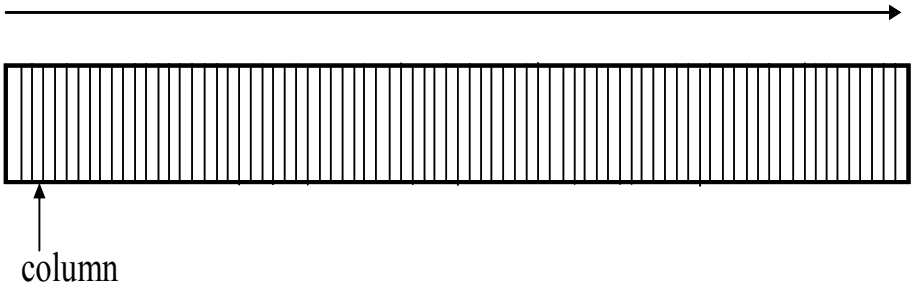


**Figure 1.8:** Schematic representation of theoretical plates in a chromatography column.

$$N = 16\left(\frac{t_R}{w}\right)^2 = 5.54\left(\frac{t_R}{w_{\frac{1}{2}}}\right)^2$$

**Equation 1.3**[31]

Where, w = peak width and $w_{1/2}$ = peak width at half-height

The height equivalent to one theoretical plate (HETP) (*H*) is another measure of efficiency and is related to *N*. HETP describes the length in which equilibrium between the stationary and mobile phase is established.[31] A column with high efficiency will have large *N* and small *H*.

$$HETP(H) = \frac{L}{N}$$

**Equation 1.4**[31]

Where, L = column length

Selectivity ($\alpha$) can assess a column's suitability to separate two analytes.[31] A ratio of the measured retention factors, selectivity values are always >1, with a selectivity of 1 indicating co-eluting peaks.

$$\alpha = \frac{k_B}{k_A}$$

**Equation 1.5**[31]

Changing the chromatographic parameters/instrument can result in vastly different data. Biodiesel and petrodiesel can contain

compounds of varying polarities, MW and composition and this is made more extensive by auto-oxidation. Through knowledge of how these techniques work, how changing specific parameters can affect analysis and understanding the chemistry of the analyte, analysts can tailor and predict how analytes will behave and thus optimise chromatographic separations.

### 1.2.2. Gas Chromatography

First developed in the 1950s GC is a separation technique in which the mobile phase, often described as the carrier gas, is a gas that is inert or unreactive *e.g.* helium.[31, 32] Not suitable for samples that are involatile or thermally labile and therefore typically molecules of less than 600 Da are analysed, GC can be used quantitatively as well as qualitatively.[33]

GC samples are injected (manually/autosampler) onto the column, entering the column as either a vapour or a gas. The GC column is seated in an oven which is capable of a wide range of temperatures (typically 0-400 °C) and can be programmed to be operated isothermally or with a temperature gradient. The analytes interact with the stationary phase and ideally are separated. As the analytes elute from the column they enter the detector (Figure 1.9).

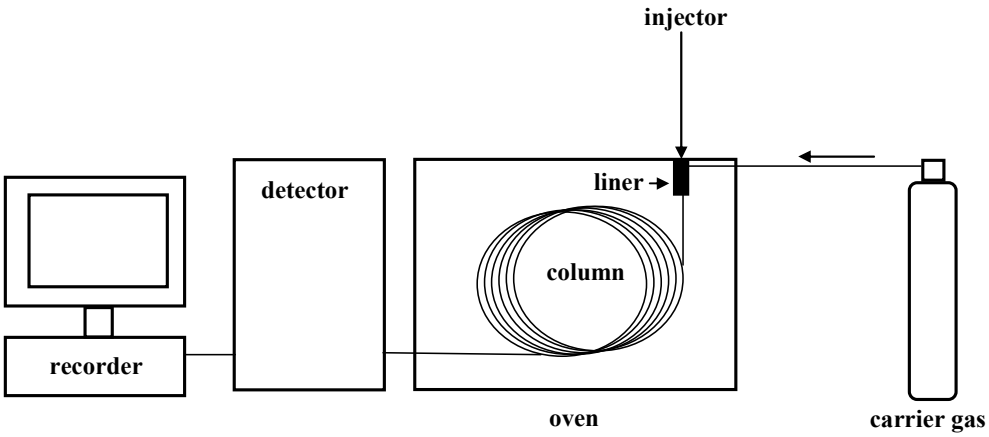


**Figure 1.9:** A basic GC configuration.

Common detectors used include a flame ionisation detector (FID) or a mass spectrometer, others routinely used include an electron capture detector (ECD) or a thermal conductivity detector (TCD).[33] GC affords a high number of theoretical plates, high resolution, can be used qualitatively and quantitatively, is reliable, relatively inexpensive and requires small amounts of sample (μg- ng). However it is only able to separate a small proportion of analytes due to limiting properties, such as volatility. As described in its name, this technique is completed in the gas phase. Analytes need to be sufficiently volatile to be vaporised to be 'swept' onto the column.

### 1.2.3. High Performance Liquid Chromatography

HPLC uses a liquid mobile phase and typically packed columns and unlike GC is not affected by volatility issues. Samples analysed *via* HPLC must be soluble in the mobile phase which is typically of varied composition. Separations in HPLC are largely dependent on the interaction of the analyte between the stationary and mobile phases. Through manipulation of the stationary and mobile phase,

selectivity can be drastically altered. Optimising these phases by changing not only the phase chemistry but other parameters, *e.g.* column dimensions, particle size, flow rates and column temperatures, can help obtain the optimal chromatographic separation.

HPLC is largely regarded as a reversed-phase technique where the mobile phase is polar *e.g.* methanol and water, and the stationary phase is non-polar *e.g.* $C_{18}$, used to separated compounds such as pesticides and proteins.[31] Normal phase HPLC which uses a non-polar mobile phase *e.g.* hexane and polar stationary phase *e.g.* silica, is sparsely used.[31] The sample is in liquid form, ideally dissolved in the mobile phase solvent and is injected into the mobile phase, which flows continuously through the system. This injection is carried onto the column, where the analyte is partitioned between the stationary and mobile phases. Samples that partition primarily in the stationary phase will take longer to elute off of the column and therefore have longer retention times, the opposite is true for analytes that partition in the mobile phase for longer. As analytes are eluted they are detected and detectors for HPLC include UV detector, refractive index detector (RI), fluorescence detector, evaporative light scattering detector (ELSD), charged aerosol detection (CAD), chemiluminescence nitrogen detector (CLND) and a mass spectrometry (MS) detector (Figure 1.10). Often a UV detector is used in conjunction with another detector.

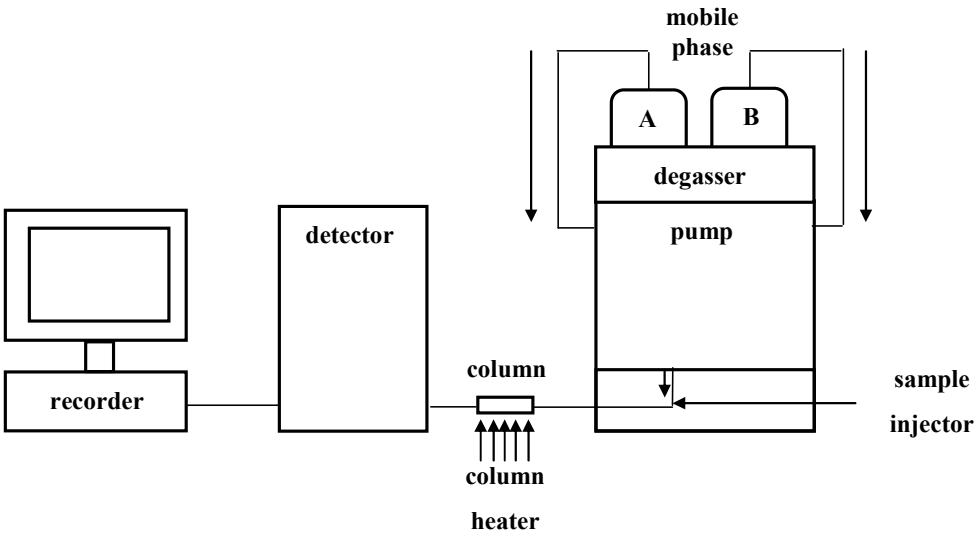


**Figure 1.10:** A common HPLC configuration.

Using HPLC, analytes of varying molecular weight, from small molecules to proteins, and of ranging polarities can be analysed. In comparison to GC, HPLC is less efficient affording lower plate numbers. Analytes take longer to equilibrate between the stationary and mobile phase and this is attributed to the packed nature of the column. However, retention times and therefore analysis times are generally quicker.

## 1.2.4. Supercritical Fluid Chromatography

A supercritical fluid is a substance that is above its critical temperature and pressure.[34] At critical temperature no matter how much the pressure is increased the substance can no longer exist as a liquid.[34] Similarly, critical pressure is reached when no matter how high the temperature is increased the substance cannot exist as a gas.[34] This is best described using a phase diagram, where the critical

temperature and pressure describe the critical point.[35] Figure 1.11 shows a phase diagram using $CO_2$ values as an example.[35]

Much debate remains over whether the mobile phase is in a supercritical form. Producing a supercritical fluid is a continuous process produced from i) heating a gas above its critical temperature or ii) compressing a liquid above its critical pressure.[35] Therefore it is hard to identify the phase $CO_2$ is in.

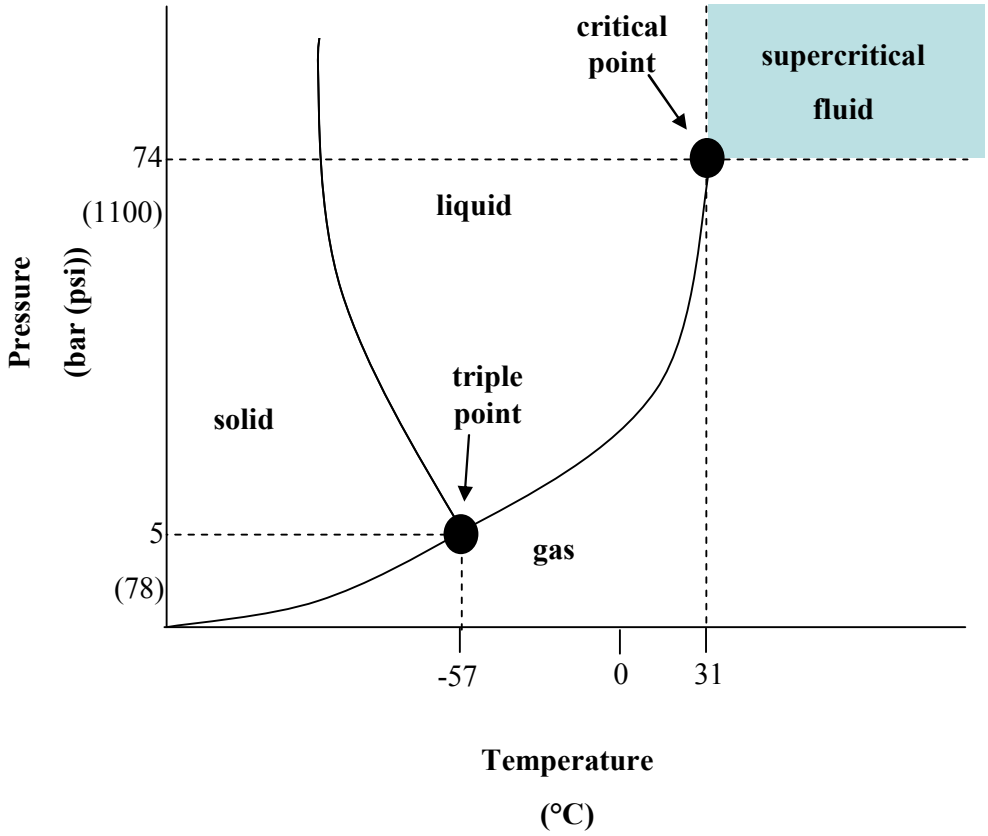


**Figure 1.11:** Phase diagram of $CO_2$.

Supercritical fluids possess qualities similar to both a liquid and a gas making them attractive mobile phases (Table 1.1).[34] Density, which influences solvating power, is similar to a liquid as is diffusivity (although it is an order of magnitude larger compared to the diffusivity of a liquid) whilst viscosity is closely correlated to a gas

(Table 1.1).[34, 35] Drawing on the optimum properties of a gas and liquid mobile phase, a supercritical mobile phase offers low viscosity enabling low pressures within the column and the system (compared to HPLC) therefore multiple columns can be added in series. Other benefits include an increase in the number of theoretical plates which influences resolution, selectivity and $t_R$.[34]

**Table 1.1:** Comparison of physical properties important to chromatography of a gas, liquid and supercritical fluid.[34]

| | **Density ($g\ cm^{-3}$)** | **Diffusion ($cm^2 s^{-1}$)** | **Viscosity ($g\ cm^{-1}\ s^{-1}$)** |
|---|---|---|---|
| **Gas** | $10^{-3}$ | $10^{-1}$ | $10^{-4}$ |
| **Supercritical fluid** | 0.8<br>Liquid-like | $10^{-4}$<br>Liquid-like | $5 \times 10^{-4}$<br>Gas-like |
| **Liquid** | 1 | $10^{-5}$ | $10^{-2}$ |

First suggested in the early 1960s, supercritical fluid chromatography is a technique that was superseded by HPLC.[36] However, in recent years SFC has seen resurgence. The ability to vary mobile phase composition, stationary phase chemistry, temperature and pressure to optimise chromatographic separations are attractive features.

SFC is considered a normal phase separation technique, with $CO_2$ typically used as the mobile phase. Other solvents can be used, however $CO_2$ affords a low critical pressure and a low critical temperature (Table 1.2). In addition $CO_2$ is non-toxic, non-flammable,

non-explosive and presents a low response, if any, in most detectors when used as the solvent.[34] However, $CO_2$ is non-polar and this can cause issues when trying to analyse polar compounds. Organic modifiers such as methanol, ethanol and acetonitrile, are often added to the $CO_2$ mobile phase to increase the polarity, with methanol being the most common modifier.[34] Addition of an organic modifier to the supercritical mobile phase changes the solvent strength which affects retention, efficiency, selectivity of the mobile phase and interactions with the stationary phase.[34] Furthermore, the mobile phase can contain additives, typically an acidic or basic additive added in a small amount and often analyte specific, which are used to increase chromatographic efficiency and obtain symmetrical, Gaussian peaks.[37, 38] As with HPLC, analysis can be undertaken isocratically, or using a mobile phase gradient. This in addition with stationary phase, mobile phase, modifier, additive, pressure, and number of columns allows many parameters to be manipulated to specifically tailor chromatographic analyses for individual analytes.

**Table 1.2:** Comparison of the critical temperatures and pressures of different solvents.

| **Solvent** | **Critical temperature (°C)** | **Critical pressure (bar)** |
|---|---|---|
| Carbon Dioxide ($CO_2$) | 30.95 | 73.76 |
| Water ($H_2O$) | 373.5 | 220.64 |
| Methane ($CH_4$) | -82.75 | 46.00 |
| Ethane ($C_2H_6$) | 32.15 | 48.74 |
| Propane ($C_3H_8$) | 96.65 | 42.46 |
| Ethylene ($C_2H_4$) | 9.25 | 50.36 |
| Propylene ($C_3H_6$) | 91.75 | 46.00 |
| Methanol ($CH_3OH$) | 239.45 | 80.86 |
| Ethanol ($C_2H_5OH$) | 240.75 | 61.40 |
| Acetone ($C_3H_6O$) | 234.95 | 47.01 |

Similarly to HPLC, samples must be dissolved in a solvent that is miscible with the mobile phase. The sample is injected (manually/autosampler) into the mobile phase ($CO_2$ and any modifiers/additives have already been pre-mixed), and loaded onto the column in a narrow band. As the analytes separate and elute they encounter a first detector, that is non-destructive, typically a UV detector. The analytes are then split, with analytes continuing to waste, fraction collection or a second detector, this can be completed pre/post or without a back pressure regulator.[39]

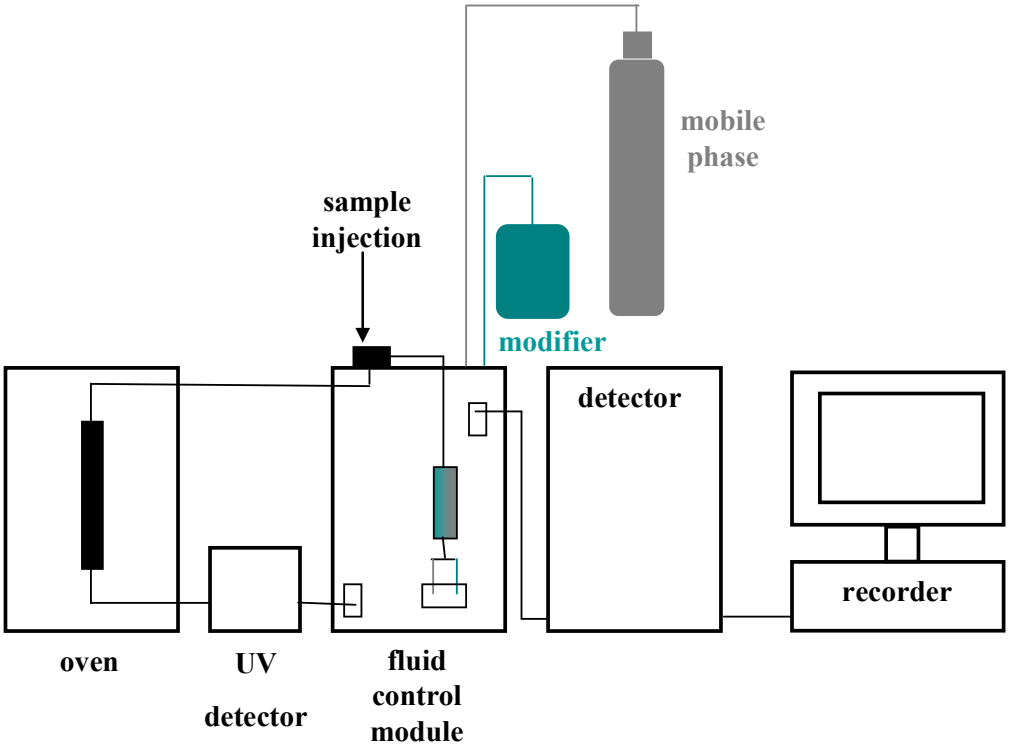


**Figure 1.12:** Schematic of a basic SFC configuration.

Although SFC is a normal phase technique, stationary phases used in reverse-phase HPLC can be selected *e.g.* $C_{18}$. An extensive range of stationary phases is available for analysis using this method and these can be divided into chiral and achiral stationary phases. Chirality of molecules is an important issue, especially in the design and development of pharmaceuticals and SFC can be applied to separate these on an analytical and preparative scale. Chiral stationary phases include CSP Chiralcel OD (cellulose tris[3,5-dimethyl-phenylcarbamate]), Chiralcel OJ (cellulose tris[4-methylbenzoate]) and Chiralpak AD (amylose tris[3,5-dimethylphenylcarbamate]). My work has focussed on the use of achiral SFC-MS, utilising silica based stationary phases.

Often regarded as a 'green' technique, SFC employs $CO_2$ that is captured from the environment or is a by-product of other

processes.[40] SFC also affords low organic solvent consumption, therefore liquid solvent waste is minimal.[40] SFC offers fast analysis, ease of fraction collection operation, at low pressure and can analyse a wide range of compounds typically ten times faster than HPLC with a high efficiency, fast column equilibration and easy hyphenation to detectors.[34] SFC allows a high number of detectors to be used, with GC and HPLC detectors both able to be coupled to SFC.

## 1.3. Detectors

Chromatographic techniques separate analytes from each other based on distinct properties of the analyte and once separated the analytes need to be detected. All detectors utilise some aspect of the analyte being detected *e.g.* UV absorbance, mass-to-charge ratio or fluorescence. Detectors are numerous and listing them here is not of importance, with GC alone having a choice of over 60 possible detectors of which 10-12 are typically used.[33]

Detectors can be categorised into selective or universal detectors and destructive or non-destructive, for example, UV is a common non-destructive detector in HPLC and SFC but is selective (must be set to a specific wavelength) contrary to a diode array detector (DAD) which scans a variety of wavelengths. From this the best wavelength can be chosen for analysis and peak purity identification is easier and more robust. Detectors can also be coupled together, naturally a non-destructive detector *e.g.* a UV detector can be placed before the terminal detector, affording more information and further identification of analytes.

Detectors coupled to chromatographic techniques must be compatible with the mobile phase composition, flow rates of the mobile phase, pressure of the system, the analyte(s) being analysed and temperature of analysis. Issues of compatibility with chromatographic techniques can limit the use of the detector. One detector that can be coupled to GC, HPLC and SFC that is universal but can be selective is a mass spectrometer. The three aforementioned chromatographic techniques have been coupled to mass spectrometers and have been used throughout this project.

### 1.3.1. Mass Spectrometry

Since mass spectrometry (MS) was first developed its popularity has soared rapidly placing it among the most important analytical techniques available today, with it being commonplace in many laboratories. Mass spectrometry is the measurement of the mass-to-charge ratio ($m/z$) of ionised analytes. It is a prevalent technique that is able to characterise many compounds including sugars, pharmaceuticals, metabolites, peptides, proteins, hydrocarbons, organic and inorganic compounds which highlights the broad range of applications of a mass spectrometer. Mass spectrometers afford low limits of detection, high sensitivity, accurate mass capabilities and can aid identification of chemical structures, elemental composition and molecular weight of compounds whilst only requiring small amounts (pg-ag) of analyte. Additionally mass spectrometers can be coupled to GC, HPLC and SFC instrumentation.

Mass spectrometers are composed of five sections: inlet, ionisation source, mass analyser, detector and a vacuum system. Each

section can be divided into several smaller components, allowing varying set-ups *e.g.* matrix-assisted laser desorption/ionisation-time of flight mass spectrometry (MALDI-TOF MS). Sample introduction *via* GC, HPLC and SFC has been used in this study as has direct infusion.

### 1.3.1.1. Ionisation Sources

It is the compound properties *e.g.* molecular mass and functional groups, which determine the optimal ionisation technique for analysis of particular analytes. For example, biodiesel is composed of molecules containing carbon, hydrogen and oxygen atoms and auto-oxidation products which will be of varying molecular mass, carbon, hydrogen and oxygen content, and volatility, whilst petrodiesel is predominantly composed of hydrocarbons.

A wide range of ionisation sources are available that encompass analysis of compounds ranging from non-polar hydrocarbons to large proteins. It is imperative that the correct ionisation technique is chosen to obtain information which can be used to investigate RME auto-oxidation with gas phase, solution phase and solid phase techniques all available.

#### 1.3.1.1.1. Atmospheric Pressure Ionisation

API sources operate at atmospheric pressure and this feature allows liquid to be easily transferred to the gas-phase *via* rapid heating of the solution followed by nebulisation by a nebulising gas. This is

essential for use with liquid samples and coupling to techniques which utilise a liquid mobile phase *i.e.* HPLC and SFC.[41]

## Electrospray Ionisation

Electrospray ionisation (ESI) is one of the most widely used ionisation techniques in mass spectrometry and is commonly termed a 'soft' ionisation technique.[41, 42] ESI is suitable for ionising samples that are polar, non-volatile and thermally labile and this allows for a wide range of compounds to be analysed, including pharmaceuticals, oligonucleotides, proteins, peptides, polymers, organometallics, macromolecules and salts.[41-45] Analysis can be completed using positive ion ESI or negative ion ESI and as a result the types of ions produced can differ. Positive ion ESI-MS can generate ions formed through adduction *i.e.* $[M + X]^+$ where examples of X include $H^+$, $NH_4^+$, $Na^+$ or $K^+$, these ions can also be multiply charged *i.e.* $[M + nX]^{n+}$, and contain multiple M *i.e.* $[yM + nX]^{n+}$ where y = an integer.[42, 43, 45] Negative ionisation can produce $[M - H]^-$ or $[M - nH]^{n-}$, or through adduction of M with anions such as $HCOO^-$, $Cl^-$, $Br^-$ or $I^-$. [43, 46]

Introduction of the sample into an ESI source is undertaken by dissolving/diluting the sample in solvent which is then introduced *via* FIA, HPLC/SFC column or directly infused. A range of buffers, acids and bases may be added at this stage to aid ionisation and/or adduct formation. As the solution passes through a small capillary a high potential difference (2-5 kV) is applied.[42, 43, 47] This results in accumulation of charge at the end of the capillary causing the solution to form a Taylor cone.[42, 48] Highly charged droplets break away from

the Taylor cone and through various suggested processes continue to form the ions observed in ESI-MS.[42, 46, 48, 49] This process is aided with the use of a nebulising gas, commonly nitrogen, or a heated capillary (Figure 1.13).[42]

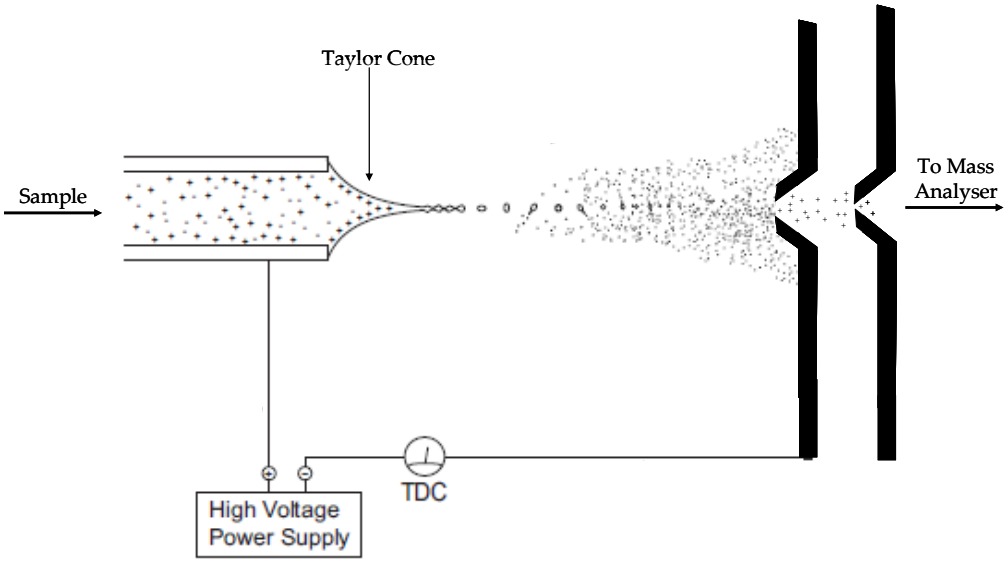


**Figure 1.13:** Schematic representation of an ESI source, adapted from [50].

Initially, solvent evaporates causing the charge density of the droplet to increase. When electrostatic repulsion exceeds the force of the surface tension fission of the droplet occurs. Smaller droplets are formed where production of ions occurs *via* two suggested models; the charge residue model (CRM) and the ion evaporation model (IEM) (Figure 1.14).[44, 49, 51, 52] The CRM and IEM are two theories proposed to model production of ions observed in ESI from charged droplets.[44, 49, 51, 52] Proposed by Dole, the CRM describes a series of fission events which result in extremely small droplets containing one analyte molecule. These undergo successive losses of solvent molecules and once all the solvent has evaporated the analyte remains in the gas phase with the charges that the droplet carried (Figure 1.14).[44, 52] The

IEM, as described by Iribarne and Thomson, suggests a mechanism based on desorption of ions directly out of the droplet.[49, 51] As the charged droplet undergoes evaporation the radius of the droplet reduces.[49, 51] The analyte is desorbed as an ion before the Rayleigh limit (radius <10nm) is reached.[49, 51, 53] These mechanisms are suggested to be non-competitive with larger biomolecules suggested to ionise *via* the CRM method and small molecules ionised *via* the IEM (Figure 1.1 and Figure 1.14).[53-59]

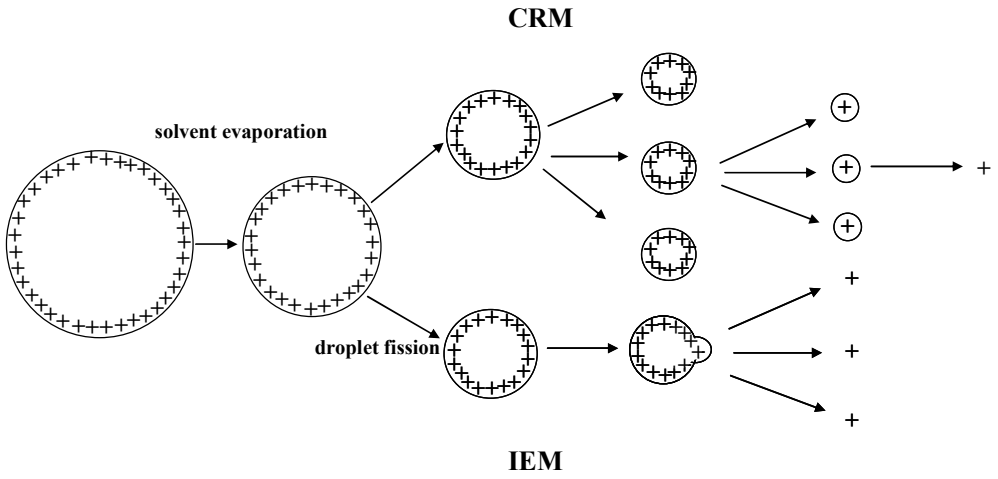


**Figure 1.14:** Diagram displaying the CRM and IEM ionisation models.

Once in the gas phase the ions travel towards the analyser through a series of skimmer cones which i) act as a counter electrode, ii) help the system reach lower vacuums needed for the mass analyser and iii) help reduce the number of neutral molecules that enter the mass analyser. Several set-ups of skimmer cones are available with different manufactures typically favouring particular set-ups, *e.g.* Waters use a Z-Spray source (Figure 1.15) which ensures neutral species are transported to the vacuum pumps therefore leaving a cleaner source when compared to traditional linear ESI sources (Figure 1.13).

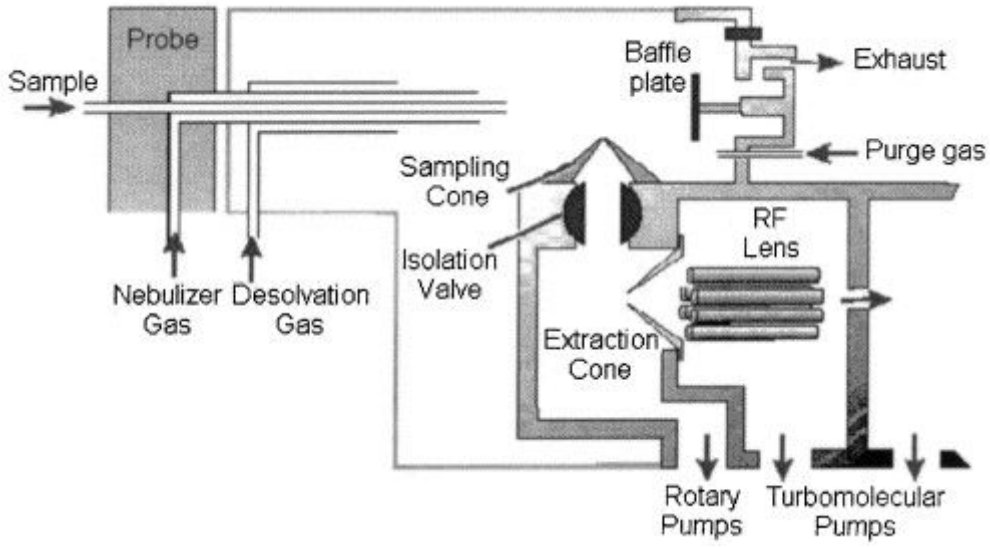


**Figure 1.15:** Diagram of a Waters Z-Spray ESI source (not to scale) reprinted with kind permission from Elsevier.[47]

ESI is a technique that poses significant benefits including high sensitivity, the ability to analyse a wide range of compounds containing heteroatoms and has many parameters that can be changed to ionise specific analytes. However, ESI processes are affected by salt and ion suppression effects are observed with hydrophobic compounds being ionised preferentially over hydrophilic compounds and solvent choice can also have detrimental effects.

## Atmospheric Pressure Chemical Ionisation

Similarly to ESI, atmospheric pressure chemical ionisation (APCI) can be undertaken using positive or negative ionisation and is completed at atmospheric pressure. Due to their similarities most ESI instruments are able to complete APCI with minor adjustments *e.g.* probe, addition of a corona discharge electrode. Often considered a

harsher ionisation technique compared with ESI, APCI is a gas-phase ionisation technique.[41] Compounds analysed using APCI can be of ranging polarities, with APCI able to analyse lower polarity compounds compared to ESI.[41] Analyses are completed with a top molecular weight of 1500 units and because of the ionisation process ions produced are typically singly charged *i.e.*$[M + H]^+$ or $[M - H]^+$.[41, 60]

Analogous to ESI, samples are introduced in liquid form into a small capillary from one of the methods as previously discussed. Towards the end of the capillary is a heater and this allows the sample and mobile phase to be vaporised. It is important that this is controlled, if the heater is too hot thermally labile compounds will degrade, if the heater is too cool analytes will be inefficiently vaporised.[41] Once in the gas-phase the molecules exit the capillary and encounter the corona discharge electrode where ionisation occurs. The corona discharge electrode produces electrons which ionise the gas molecules in the source, typically nitrogen and water vapour. These ions collide with the analyte and thus form the analyte ions. In negative ionisation a proton is abstracted or an adduct is formed. The ions then travel through the skimmer cones to the mass analyser (Figure 1.16). As with ESI different manufacturers have sources of different orientation and are generally of the same configuration as ESI sources (Figure 1.13) with the addition of a corona discharge electrode.

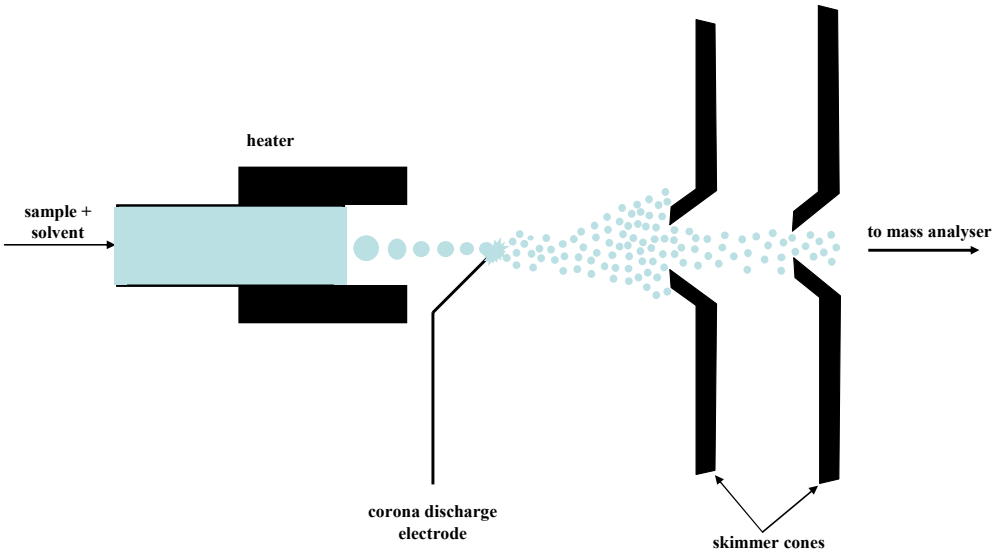


**Figure 1.16:** Basic schematic of an APCI source.

APCI is a popular ionisation source used widely in pharmaceutical analyses. The ability to ionise compounds of ranging polarity, handle large amounts of mobile phase and therefore be easily coupled to HPLC and the ease of switching between ESI and APCI set-ups afford this to be a valuable technique.[41, 60]

### 1.3.1.1.2. Vacuum Ionisation Sources

### Electron Ionisation

Electron ionisation (EI), formerly known as 'electron impact', is termed a hard ionisation technique.[61] When compounds are ionised *via* this method fragments are produced. Compounds fragment in often predictable ways, with good repeatability and spectra produced can be compared to EI libraries to identify analytes. The ability to predict fragmentation of compounds allows for the identity of unknown compounds to be largely deduced, if not identified. EI is a

technique suitable for volatile, thermally stable molecules and is typically used for small molecules (<600 molecular weight units) as opposed to ESI which can analyse very large molecules *e.g.* proteins.[33, 60]

EI is a gas-phase technique and once vaporised the molecules enter the EI source, from an appropriate inlet *e.g.* GC, where they are bombarded with electrons, produced from a filament (W or Re) which is held at 70 eV.[33, 60] The electrons cross the source in a helical path, achieved using two magnets on either side of the source, towards an electron trap. Bombardment with electrons causes an electron to be ejected from the analyte and a radical cation is produced ($M^{+\cdot}$) (Figure 1.17).[33] Fragmentation is commonplace in EI and is dependent on the stability of the molecular ion and fragment ions with some ions undergoing rearrangement.

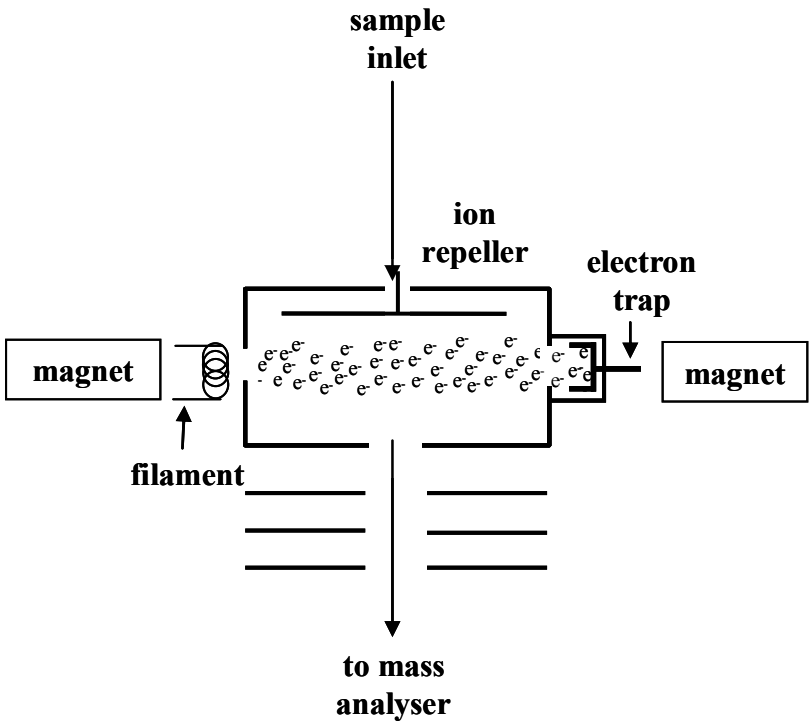


**Figure 1.17:** Diagram of an electron ionisation source.

### 1.3.1.2. Mass Analysers

Each ionisation technique produces a range of ions of varying mass-to-charge ratios that need to be detected and this is completed using a mass analyser. Mass analysers are kept under vacuum and choice of mass analyser is dependent on the requirements of analysis and ionisation source. Mass analysers include: quadrupole, quadrupole ion trap (QIT), time-of-flight (TOF) and Fourier transform ion cyclotron resonance (FT-ICR).[60]

#### 1.3.1.2.1. Quadrupole Mass Analyser

Quadrupole mass analysers are a type of scanning mass analyser typically used with HPLC, GC and stand alone instruments using API techniques. Quadrupoles consist of four cylindrical or hyperbolic rods that are placed equidistant from the centre and thus parallel, as outlined in Figure 1.18, these rods are placed after the source.[60, 62]

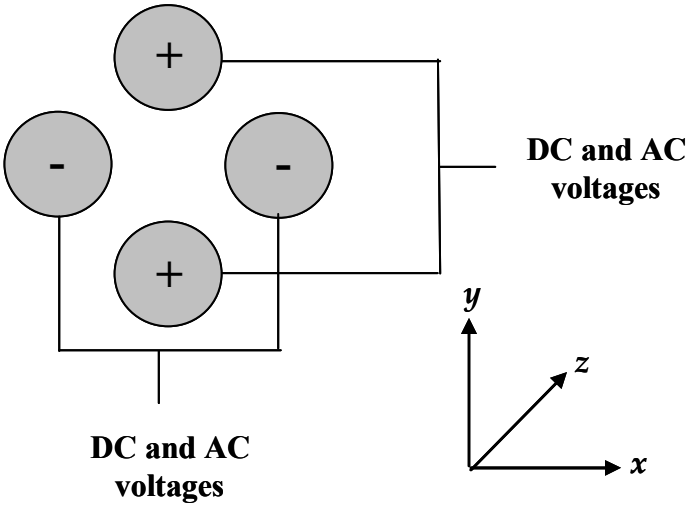


**Figure 1.18:** End-on diagram of a quadrupole and its suitable voltages.

First described by Paul and Steinwedel the principle of the quadrupole relies on how stable ion trajectories react in an oscillating electric field.[60, 62] DC and AC potentials are applied to the rods, with adjacent rods having opposite polarities (Figure 1.18, Equation 1.6 ).[60, 62]

$\Phi_0 = +(U - V \cos \omega t)$ and $-\Phi_0 = -(U - V \cos \omega t)$

**Equation 1.6**[60]

Where, $\Phi_0$ = potential applied to the rods, $\omega$ = the angular frequency, $U$ = direct potential and $V$ = 'zero-to-peak' amplitude of the RF voltage

The polarities of these rods are continuously switched and this creates an electric field. Ions entering the quadrupole enter this electric field and begin to oscillate. If the ion is positively charged it will be attracted to the negatively charged rods and repelled by the positively charged rods. The polarities of the rods are then switched and the ion is now repelled by the negatively charged rods which were

previously positively charged. This cycle is repeated and the polarities are rapidly switched, which causes the ions to travel through the quadrupoles in a spiral motion.[63]

The stability of the ions within the electric field can be described by their *a* and *q* values from the simplified Mathieu equation as described by Equation 1.7 and Equation 1.8. These equations express the relationship between the coordinates of an ion and time, whereby *x* and *y* describe the position of an ion from the centre of the rods. *x* and *y* must remain less than $r_0$ for the ion to pass through the quadrupoles successfully, otherwise the ion will crash into the rod and will not be detected. $r_0$ is a constant for a given quadrupole, with *U* and *V* the variables for mass filtering (Equation 1.7 and Equation 1.8).[60, 64]

$$a_u = a_x = -a_y = \frac{8zeU}{m\omega^2 r_0^2}$$

**Equation 1.7**[60, 64]

$$q_u = q_x = -q_y = \frac{4zeV}{m\omega^2 r_0^2}$$

**Equation 1.8**[60, 64]

*a* and *q* values obtained from Equation 1.7 and Equation 1.8 can be used to describe the co-ordinates of an ion and this informs of the stability of an ion. If these co-ordinates are within the stable region of the stability diagram the ions have a stable trajectory and are successfully transmitted through the quadrupole (Figure 1.19). However, if the co-ordinates lay outside the stable region of the stability diagram the ions will have an unstable trajectory and crash into the rod and will not be detected (Figure 1.19).[60, 64, 65]

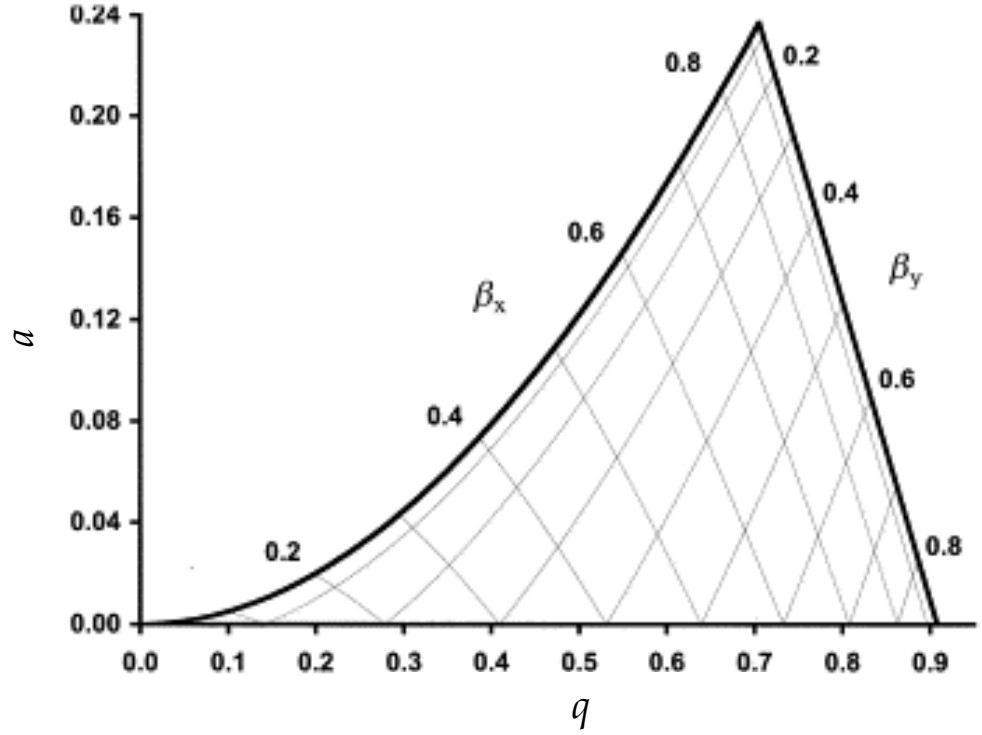


**Figure 1.19:** Stability diagram for a quadrupole mass analyser modified from [65].

Quadrupoles are low cost mass analysers that are relatively small in size and robust, however MS/MS cannot be completed on single quadrupoles, resolution is on a nominal scale and the mass range is limited to 4000 *m*/*z*.[60, 62] Additionally, quadrupoles can be used as ion guides (AC only quadrupole) or as a lens (DC only quadrupole).

### 1.3.1.2.2.Time-Of-Flight

A time-of-flight (TOF) mass analyser was first described by Stephens in 1946.[66] The TOF analyser consists of a flight tube, which is a field free region and kept under vacuum, acceleration plates and a

detector. Wiley and McLaren published the first design for a linear TOF and this is depicted in Figure 1.20.[67]

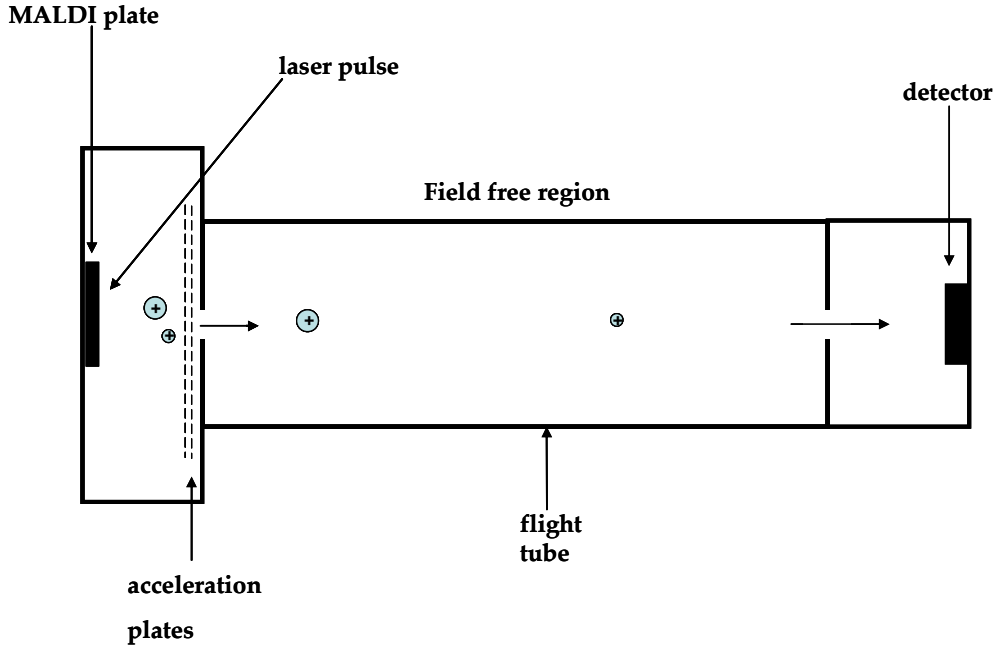


**Figure 1.20:** Schematic of a linear TOF analyser with a MALDI ion source.

Mass analysis is completed, as the name suggests, by measuring the time it takes for an ion of given *m*/*z* to travel a set distance and reach the detector. First ions are accelerated by an electric field which is of a known strength, with ions of the same *m*/*z* possessing the same energy and velocity. This acceleration subsequently causes the potential energy (Equation 1.9) to be converted into kinetic energy (Equation 1.10). As the ions leave the acceleration region the ions enter the field free region, where they are separated according to their velocities (and thus *m*/*z*) before reaching the detector (Figure 1.20). The velocity of an ion can be given by rearrangement of Equation 1.9 and Equation 1.10, where $E_p = E_k$, to obtain Equation 1.11.[60]

$$E_p = zeV_s$$

**Equation 1.9**[60]
Where $E_p$ = potential energy, $ze$ = total charge, and $V_s$ = accelerating potential

$$E_k = \frac{mv^2}{2}$$

**Equation 1.10**[60]
Where $E_k$ = kinetic energy, $m$ = mass of ion and $v$ = velocity

$$v = (\frac{2zeVs}{m})^{\frac{1}{2}}$$

**Equation 1.11**[60]

Ions have a constant velocity when they enter the field free region and this can be expressed in terms of the time ($t$) it takes to travel the distance of the flight tube ($L$) (Equation 1.12).[60]

$$t = \frac{L}{v}$$

**Equation 1.12**[60]

Equation 1.11 can be substituted into Equation 1.12 giving Equation 1.13. Which can be rearranged to obtain Equation 1.14, which shows the relationship between $m/z$ and flight time: ions of lower $m/z$ have a shorter flight time compared to ions of higher $m/z$.

$$t^2 = \frac{m}{z}\left(\frac{L^2}{2eVs}\right)$$

**Equation 1.13**[60]

$$(m/z)^{\frac{1}{2}} = \left( \frac{\sqrt{2eVs}}{L} \right) t$$

**Equation 1.14**[60]

Mass resolution is proportional to flight time and can be improved by lengthening the tube (Equation 1.14).[68] However, this has limited applicability, performance can be decreased through loss of ions by scattering if the flight tube becomes too large.[68] Manipulation of the acceleration voltage can also improve resolution however this affects sensitivity and higher concentrations are required.

Resolution is a key concern in TOF analysers and can be affected by factors which cause ions of the same *m*/*z* to be distributed, such as velocity of the ion as described previously. This can be improved through the use of delayed pulse extraction or using the TOF analyse in reflectron mode.

Delayed pulse extraction,[69] also referred to as time-lag focussing,[67] and pulsed-ion extraction,[70] reduces the distribution of ions of the same *m*/*z* by introducing a time delay between ion formation and extraction. This occurs by first allowing ions to expand into a field-free region of the source where ions are separated according to their kinetic energy.[60, 69] The ions are then extracted, with ions of the same *m*/*z* but lower kinetic energy receiving more energy and thus forming a tighter packet of ions as they enter the field-free region of the flight tube.[60, 69] These ions possess smaller energy dispersion, thereby resulting in narrower peaks and thus better resolution.[60, 69]

Alternatively a reflectron can be used to increase the length the ions travel and thus improve resolution. The reflectron is a series of electrostatic reflectors that are situated at the opposite end of the flight

tube to the ionisation source.[71, 72] As ions are accelerated and move through the flight tube they possess a velocity. Ions of the same *m*/*z* may have slightly different velocity and will be dispersed, therefore taking a different amount of time to travel the tube. This dispersion is utilised and ions with more velocity will enter the reflectron to a greater extent compared with the same ions with less velocity.[72] As these ions are reflected and travel back down the flight tube the ions reach the detector (situated next to or off-axis to the source) at the same time.[60, 71, 72] Whilst this improves resolution, it is at a loss of sensitivity and limits the mass range.[60, 71]

TOF mass analysers are typically coupled to MALDI and API ionisation sources due to the fast analysis speed, high transmission rates and the detection of high mass ions.[60, 71] Within this study positive ion ESI-TOF-MS has been used to investigate electrochemical auto-oxidation of RME.

#### 1.3.1.2.3. Fourier Transform-ICR Mass Analyser

In contrast to quadrupoles, FT-ICR mass analysers have a high resolving power with the ability to separate isobaric ions. They can analyse ions of higher *m*/*z* value, and are able to complete tandem mass spectrometry and are extremely sensitive (compared with quadrupoles).[73] However, require high vacuums, suffer with long duty cycles and possess a reduced dynamic range of $10^5$.[74] Biodiesel and auto-oxidised biodiesel have been investigated using this technique, allowing identification of nominal mass ions.

FT-ICR mass analysers consist of an ICR cell that is composed of three key components, excitation, detection and trapping plates (Figure 1.21). ICR cells are available in several different configurations, including cubic, cylindrical and infinity trap, with Marshall *et al.* listing these configurations.[73]

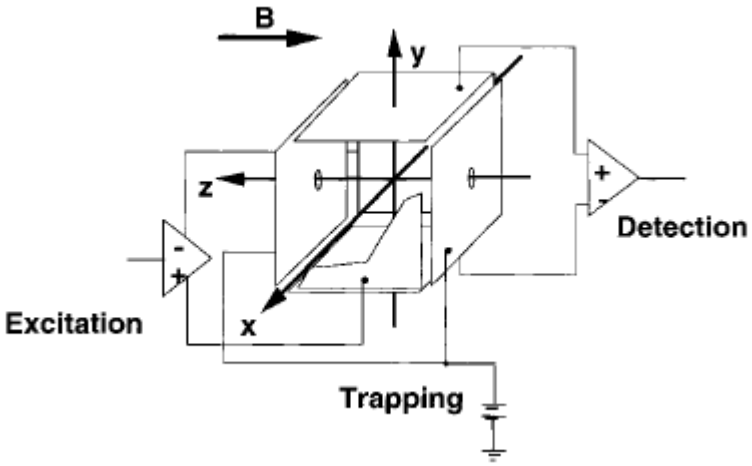


**Figure 1.21:** Schematic of a cubic FT-ICR cell, reprinted with kind permission from Wiley online.[73]

As ions enter the magnetic field they are subjected to a force, the Lorentz force, which is perpendicular to their motion (Equation 1.15).[73] This causes the ions trajectory to be bent into a circular movement.[73]

$$F = zvB$$

**Equation 1.15**[60]
Where, $F$ = force, $q$ = total charge, $B$ = magnetic field

The ICR frequency of an ion is dependent on its mass-to-charge, as observed from the cyclotron frequency equation (Equation 1.16).[73] This feature is not dependent on velocity, therefore focussing is not

required to obtain accurate *m*/*z* values where high resolution is required.[73]

$$F_c = \frac{zB}{m2\pi}$$

**Equation 1.16**
Where, *z* = number of charges and *m* = mass of the ion

The ions inside the ICR cell undergo two other motions in the ICR cell: trapping and magnetron.[73, 75] The trapping motion is a simple harmonic restoring force, whereby ions oscillate in the direction of the electric field created by the trapping plates.[73] Magnetron motion is caused by a combination of the electric and magnetic fields. Typically, magnetron motion and trapping motion are not detected, owing to their usually smaller frequencies, however if detected can suggest possible issues, such as, misalignment of the magnet axis.[73]

To measure the ICR frequency of several ions, they are simultaneously excited.[60] This is completed by scanning a large frequency range which ensures all ions present are excited, this excitation is completed in a short time period (1 μs) by the excitation plates (Figure 1.21).[60, 74, 75] Concurrently the radius of the cyclotron motion increases and the ions move in a spiralling motion as the ions absorbs energy.[73] It is necessary for the ions cyclotron motion radius to be increased in order to detect the ions.[60, 75] Scanning a large frequency range ensures a range of *m*/*z* values are excited, specific RF voltages, characteristic to specific *m*/*z*, are applied to the excitation plates to increase the ion cyclotron radius of particular *m*/*z* values.[73]

Detection of the ions is completed using the detector plates (Figure 1.21). The ions pass close to the detector plate, where an 'image current' is induced and the resulting ion frequency signals are

detected (Figure 1.21).[73] This detection produces a time-domain free induction decay (FID), sometimes referred to as a transient. The FID can be mathematically transformed using a Fourier transform (FT), this converts the time-dependent function into a frequency dependent function, the mass spectrum.[73, 76]

## 1.4. Aims

As biodiesel auto-oxidises it becomes more viscous. This increased viscosity is suggested to be linked to production of auto-oxidation species and thus, depletion of FAMEs. A series of auto-oxidised RME, forced oxidised RME and electrochemically oxidised RME at different stages of auto-oxidation will be investigated.

This study aims to develop a rational method(s) to investigate RME auto-oxidation using GC-MS, HPLC-MS, SFC-MS and direct infusion positive ion ESI-MS. Through the use of these chromatography-mass spectrometry techniques different characteristics of FAME auto-oxidation will be investigated.

Initially, depletion of FAMEs will be explored in varying RME samples and will aim to identify the key FAME contributors to auto-oxidation. Through the use of GC-MS it is postulated that quantification of FAMEs can be used to monitor FAME depletion. These depletions can then be compared to viscosity with any relationship detected.

Auto-oxidation products will be studied through the use of multiple chromatography-mass spectrometry techniques. Once auto-oxidation products have been detected and identified they can be used to describe auto-oxidation pathways and auto-oxidation species detected and pathways suggested will be compared to the literature. Key auto-oxidation products will be identified which can be suggested to be used as auto-oxidation markers.

Auto-oxidation markers suggested will be investigated through different RME oxidation techniques (natural auto-oxidation, forced oxidation and electrochemical oxidation). Quantification of these

markers will be explored, alongside direct comparisons of FAMEs depletion and viscosity of these samples to establish any relationships present.

Additionally, the chromatography-mass spectrometry techniques developed will be applied to other fuel related compounds to demonstrate the comprehensive use of these techniques.

# Chapter 2. Experimental

This chapter describes the instrumentation, conditions and chemicals used. Deviations from these conditions are explained in the relevant chapter.

## 2.1. Instrumentation

Positive ion ESI-FT-ICR MS spectra were acquired using a Bruker Daltonics solariX FT-ICR mass spectrometer equipped with a 4.7 Tesla actively shielded superconducting magnet (Billerica, MA, USA) with an external Apollo ESI ion source. The capillary voltage was set at 4000V. The nitrogen drying gas flow rate of 4.0 L/min. and gas pressure of 1.2 bar were applied to the nebuliser. The positive ions were accumulated for 0.001 s.

Samples were injected *via* direct infusion at a rate of 120 μL/hour. All samples were diluted into MeOH and analysed at a concentration of 1 μL/mL. The instrument was calibrated using sodium formate. Data acquisition and analysis was completed using DataAnalysis version 4.0 (Billerica, MA, USA).

GC-MS data were obtained using a ThermoQuest Trace GC-MS (ThermoFisher Scientific, UK), fitted with a Stabilwax column, 30 m x 0.25 mm i.d., 0.25 μm film thickness (Thames Restek Ltd, Saunderton, U.K.). Electron ionisation mass spectrometry was used with a detector voltage of 350 V. The sample was injected splitless at a volume of 1 μL. The injector port was held at 240 °C and a gradient temperature

programme was used. The initial temperature was 40 °C which was held for 5 minutes, the temperature then increased at 5 °C/min. until 240 °C was reached, where it was held for 16 minutes, equating an hour run time. All data was acquired in full scan mode, with a 10 minute solvent delay. RME samples were analysed at concentrations of 1 mg/mL, pure FAMEs were analysed at 0.01 mg/mL and B20 was analysed at 0.1 mg/mL. A series of ten different samples at concentrations in the range (0.05 – 100 μg/mL) were analysed to determine the LOD.

HPLC positive ion ESI-MS were completed using a Platform LC (Waters, Manchester, UK) with an XBridge $C_{18}$ column, 2.1 x 50 mm, 5 μm. The cone voltage was 20 V, source block temperature 120 °C and desolvation temperature 250°C. An Agilent (Santa Clara, USA) 1050 pump, UV detector and autosampler were used. Water with 0.1% formic acid (A) and acetonitrile with 0.1% formic acid (B) were used at 0.3 μL/min. on the gradient programme outlined in Table 2.1 . Data was analysed using MassLynx version 3.5. All samples were diluted in MeOH and were analysed at 0.1 mg/mL (RME and B20). The samples were injected at 10 μL.

**Table 2.1:** Gradient programme used in HPLC positive ion ESI-MS.

| Time | A% | B% |
|---|---|---|
| 0 | 80 | 20 |
| 2.0 | 80 | 20 |
| 12.0 | 0 | 100 |
| 16.0 | 0 | 100 |
| 20.0 | 80 | 20 |
| End | 80 | 20 |

Positive ion ESI-MS data were obtained *via* infusion at 300 μL/hour on a Platform LCZ quadrupole mass spectrometer (Waters, Manchester, UK) equipped with a Z-Spray source. The cone voltage was 30 V, source block temperature 120°C and desolvation temperature 250 °C. All samples were diluted in MeOH and were analysed at 0.1 mg/mL (RME and B20) and 0.01 mg/mL individual FAME. A series of ten different samples at concentrations in the range (0.05 – 100 μg/mL) were analysed to determine the LOD. Data was analysed using MassLynx version 3.5.

Positive ion APCI-MS data were obtained *via* infusion at 300 μL/hour on a Platform LCZ quadrupole mass spectrometer (Waters Manchester, UK) equipped with a Z-Spray source. The cone voltage was set at 30 V, source block temperature was 140 °C and the APCI probe temperature was 425 °C. RME was diluted in MeOH at 0.1 mg/mL. Data was analysed using MassLynx version 3.5.

Electrochemical oxidation was completed using an Antec ROXY potentiostat (Zoeterwoude, The Netherlands). Electrochemical oxidation was completed using the μicroprep cell with a glassycarbon electrode, oxidised at 0 V and 1.8 V. Samples were directly infused at

a rate of 50 μL/min.. RME and individual FAMEs were prepared in 75:25 $H_2O$:MeOH at 1 μg/mL. This was coupled to a maXis ESI-TOF-MS.

Positive ion ESI-MS in electrochemical studies were acquired using a Bruker (Billerica, MA, USA) maXis TOF-MS. The capillary voltage was set at 4000 V. The nitrogen drying gas flow rate of 4.0 L/min. and nebulising gas pressure of 2 bar were applied to the nebuliser. This was completed in reflectron mode.

Positive ion ESI-SFC-UV MS data was obtained using a Berger Minigram system (Waters, Manchester, UK) completed at a flow rate of 3 mL/min. and pressure of 150 bar. The mobile phase was SFC Grade $CO_2$, with a methanol modifier (amount indicated in relevant sections). A silica column (Princeton Chromatography, Cranbury, New jersey, U.S.A) was used for analysis (250 x 4.6 mm, 5 μm, 60 Å) and on occasion an additional silica column (250 x 4.6 mm, 5 μm, 60 Å) was used and this is indicated in the relevant chapters. This instrument was coupled to a Knauer K-2501 UV detector at wavelength 210 nm. Additionally, this instrument was coupled to the pre-described Platform LCZ quadrupole mass spectrometer (Waters) in positive ion. A make-up flow of 0.1 mL/min. MeOH/$NaNO_3$ was used post column and BPR to aid ionisation and sample introduction into the mass spectrometer. Sample injection volume was 10 μL and samples were analysed at a concentration of 0.1 mg/mL for RME/B20 and 0.01 mg/mL for individual FAMEs. SFC ProNTo version 1.5 and MassLynx version 3.5 were used for data analysis.

Data acquired that is used in Figure 3.14 and Figure 4.4 was obtained at Bruker, in Bremen by Dr Matthais Witt. This was completed using a Bruker solariX FT-ICR MS in positive ion with a 12 Tesla actively shielded magnet. This instrument was fitted with an

Apollo II Dual ESI/MALDI source. The capillary voltage was set at 4000 V. The nitrogen drying gas flow rate of 4.0 L/min. and nebulising gas pressure of 1.2 bar were applied to the nebuliser. The positive ions were accumulated for 0.001 s. Samples were analysed in MeOH at 5 μL/mL. Data was acquired and analysed using DataAnalysis 4.0 (Billerica, USA).

MS/MS was completed (Figure 4.15) on the above FT-ICR instrument with the same instrument set-up. The collision voltage for acquisition was 24 V.

## 2.2. Chemicals

RME, SME, PiBSA, VIMA, VIMA intermediate, final dispersant and diesel were supplied by BP (Pangbourne, UK). Methyl stearate (>99.5%), methyl oleate (>99.0%), methyl linoleate (>98.5%) and methyl linolenate (99.0%) were purchased from Sigma-Aldrich Company Ltd (Gillingham, Dorset, UK). Methyl Octadecanoate-d35 was purchased from CDN isotopes (Quebec, Canada). Methanol (LC-MS), acetonitrile (LC-MS) and water (LC-MS) were purchased from Fisher Scientific (Loughborough, UK). SFC grade $CO_2$ was purchased from BOC (Poole, UK).

## 2.3. Forced Oxidation Engine Simulation Studies

Forced oxidation tests were completed by the oxidation team at BP (Pangbourne, UK). 250 mL RME was heated and kept at a constant temperature of 165 °C throughout analysis. This was stirred (to introduce air into the sample) at 1300 rpm and aliquots were taken

periodically (0, 10, 17, 18, 19, 21, 23, 24, 25, 26, 42, 43, 44, 45, 46, 47, 50, 51, 52, 66, 67, 70 hours). Viscosity of these aliquots were measured at 40 °C as defined by EN ISO 3104:1994.[77] The test was stopped once the viscosity, as measured by the KV40, had doubled. Aliquots were then analysed using GC-MS and ESI-FT-ICR MS instrumentation.

# Chapter 3. Detection of Biodiesel Using Chromatography Coupled to Mass Spectrometry

As the world pushes towards 'greener' fuels and better practices, biodiesel is being increasingly used and in rising blend percentage. This heightens the importance of many concerns including storage of biodiesel, addition of biodiesel to matrices, adulterant compounds and techniques available to identify these issues.

Formation of auto-oxidation products in biodiesel increases the number of compounds present, therefore increasing the complexity of the sample and its analysis. As biodiesel ages an increased number of auto-oxidation products are present which affects the quality of the fuel resulting in an undesirable fuel mixture. Through investigation using chromatography and mass spectrometry techniques a number of auto-oxidation products have been identified these will be discussed in more depth in Chapter 4.

Several standards are in place, listed in BS EN 14214:2008+A1:2009 (Automotive fuels. Fatty acid methyl esters (FAME) for diesel engines. Requirements and test methods), which ensure that biodiesel is a high quality fuel and meets pre-set criteria before it is used either neat or in blends.[78] These standards ensure no residual starting reactants, partially reacted reagents (DAGs or MAGs), catalyst, alcohol or glycerol remain.[78] Different properties of the fuel, similar to petrodiesel standards, are measured, such as cold flow properties, and through these assessments poor fuel stocks can be identified and removed from the fuel cycle for disposal or repurified.[78]

The focus of this Chapter is the application of chromatography and mass spectrometry to the analysis of biodiesel, typically RME, of varying ages and thus varying extent of auto-oxidation. Ideally, analysis using chromatography and mass spectrometry would; separate all components in the sample; separate at baseline resolution; be qualitative and quantitative; aid structural elucidation; and identify trace components such as auto-oxidation products and adulterants.

Certain criteria are desired for biodiesel analysis; firstly, the technique must be suitable to detect FAMEs and auto-oxidation products. Secondly the technique should aid study of all these components with the ability to track/monitor their increases or depletions within various samples. Thirdly, where possible, components should be separated from matrices, such as petrodiesel or lubricant. This is ideally expected to be completed quickly with minimal sample preparation and ease of analysis as well as having minimal cost and being 'green'. Historically, analytical techniques are not considered 'green'. Large amounts of hazardous solvents, additives and use of high amounts of energy all have an environmental impact.

It is expected that through the development of chromatography and mass spectrometry techniques for the analysis of biodiesel and auto-oxidised biodiesel that markers associated with auto-oxidation can be established. These developments will assist the identification and tackling of degraded fuel stocks, adulteration and identification of original fuel source.

## Analytical Methods in Biodiesel Analysis

Petrodiesel has been largely characterised and researched over the last 50 years. Traditionally, and still a necessary technique, GC-FID is applied to petrodiesel analysis. More recently, petrodiesel has been investigated using FT-ICR MS and this branch of analysis is typically described as petroleomics. Whilst other analytical techniques have been used, a comprehensive review of modern (2008-2011) contributions to petroleum product analysis is discussed by Rodgers and McKenna.[79]

Two typical detectors used for the analysis of FAMEs are flame ionisation detectors (FID) and MS. One of the most favoured detectors is the FID, with B100 typically analysed using GC-FID.[80] This is most evident in standard EN 14103:2011.[80] FID is a non-selective detector that is ideally suited for the analysis of hydrocarbons, such as petrodiesel. However, when molecules contain heteroatoms the FID is less efficient and difficulties can arise in analysis relating to the molecules carbon deficiency. Ulberth, Gabernig and Schrammel investigated the GC-FID response of FAMEs, FAEEs, fatty acid propyl esters (FAPEs) and fatty acid butyl esters (FABEs) and compared the obtained results with calculated theoretical values.[81] This study proposes GC-FID is most suited for FABE analysis with smaller differences observed between experimental and theoretical carbon deficiencies.[81] When assigning FAMEs a larger disagreement (compared to FABE) was observed.[81] These differences could cause confusion especially if FAMEs are being analysed in a hydrocarbon matrix such as petrodiesel.

Other issues relating to FID include the identification of unknowns containing heteroatoms. Analysis of unknowns requires appropriate standards to be analysed from which retention times and detector response can be compared. If FID analysis is completed on a small data set, such as fresh biodiesel, results obtained can be used valuably. However, predicting every component of a more complex sample, such as auto-oxidised FAME, would require a large number of standards to correctly identify auto-oxidation products and would be a lengthy and costly task. Auto-oxidised FAME samples require a more universal detector which can (preferably) aid molecular/structural elucidation without the need for multiple standards.

Mass spectrometers can be coupled with relative ease to chromatography instrumentation, with particular partnerships commonly used, such as GC-EI-MS. Unlike the FID, mass spectrometers can be used non-selectively allowing for a larger subset of samples to be analysed. Benefits of mass spectrometers compared to FID include lower sensitivity, higher selectivity, a broader range of compounds that can be easily analysed and they afford more informative data. Tandem mass spectrometry has been used to elucidate the structure and position of double bonds.[82, 83]

An analytical technique that is often used to analyse biodiesel is Fourier transform-infra red (FT-IR), typically mid-IR or near-IR (NIR).[84, 85] This analysis is completed by measuring the intensity of the C=O stretch in the spectrum to identify FAME which possess a C=O, in diesel and is used in BS EN 14078.[84, 85] However, this technique cannot be used quantitatively on composite samples other than petrodiesel, the absorption strength of the C=O band is strongly affected by water and additives, such as ZDDP.[84] Nuclear magnetic resonance spectroscopy (NMR) is used to detect the changing

unsaturation within FAMEs as auto-oxidation products are produced.[86-90] Additionally electron paramagnetic resonance spectroscopy has been used to investigate oxidation stability of lipids.[91]

As with petrodiesel, biodiesel has been predominantly analysed by GC-FID or GC-MS. This is a common technique that is extensively used for FAME analysis, especially derivatised lipids, whereby fatty acids are derivatised into their more volatile FAME counterparts.

GC analysis of FAMEs is typically completed using capillary columns with a polar, or more recently ionic liquid, stationary phase. Many columns (not an exhaustive list) have been investigated for FAME analysis,[21, 92-100] with Eder reviewing GC analysis of FAMEs,[101] however wax columns are being used more frequently and have been used for this investigation and in standard BS EN 14103:2011.[19, 80, 81, 100, 102, 103]

More recently, GC×GC-FID and GCxGC-TOF-MS have been used to analyse FAMEs.[104-106] GC×GC techniques utilise a polar/non-polar column set-up and are used to target individual separation of FAMEs and separation of FAMEs from hydrocarbon matrices, such as petrodiesel. However, this is typically completed at extended run times with Adam *et al.* reporting an analysis time of 125 minutes.[104] Whilst able to separate FAMEs from the hydrocarbon matrices, this is not a realistic analysis time for a routine, high throughput analysis.

Other chromatography techniques have been employed in the analysis of biodiesel, namely HPLC. Similarly to GC, FID and MS have been utilised as the detection technique with additional detection using ELSD and UV, detectors that are not compatible with GC.[107] FAMEs have been analysed typically using (reversed phase (RP)-HPLC,[95, 96, 99, 108-111] however successful separation and identification of

FAMEs has also been achieved using normal phase (NP)-HPLC.[107, 112] Chromatography using silver columns is also a common theme in lipid analysis and has proved useful for the separation of isomers of FAMEs, however this can increase analysis times.[106]

Similar to NP-HPLC, studies have investigated the use of SFC, typically with a FID, although MS and ELSD have also been used.[113-119] These studies have investigated separation of FAMEs from; other compounds *e.g.* petrodiesel; and each other.[114-119] These analyses are typically completed in excess of 20 minutes, with some analysis taking over 60 minutes.[114, 115, 117-119] Research undertaken here will exhibit the successful analysis of FAMEs in petrodiesel in under 4 minutes.

HPLC and SFC when coupled to MS typically use an API technique, typically ESI, APCI and APPI have been used independently with positive identification of the FAMEs achieved.[120-126] Many papers report the use of chemometrics with API techniques in the analysis of biodiesel, which has not been applied in this study. Chemometrics is a method whereby the data is processed statistically and is multi-disciplinary, used in areas such as *e.g.* chemistry and biochemistry. In biodiesel, chemometrics is typically completed on data sets requiring either characterisation of FAMEs or separation of FAMEs from matrices.[120, 121, 125, 126] This technique can be time consuming requiring many data sets and results can be easily misinterpreted.

Additional oxygen atoms, varying chain lengths and unsaturation in auto-oxidised biodiesel further enhances the complexity of the aged biodiesel. As FAMEs degrade there is an increase in auto-oxidation products, this adversely affects the performance of the fuel which can cause issues when used in an engine, such as thickening of the fuel and lubricant. Other issues

relating to supply/shelf life are apparent when compared to petrodiesel, with FAMEs possessing a shorter supply/shelf life. It is expected that initial auto-oxidised biodiesel will either consist of molecules composed of shorter chains with a decreased number of oxygen atoms compared to the starting FAMEs or additional oxygen atoms compared to the starting FAMEs, with molecules such as epoxides, aldehydes and ketones expected.

Detection of auto-oxidised biodiesel is an area which is gaining much interest. It is important to understand the processes by which biodiesel auto-oxidises and to understand the chemistry, so measures can be taken to reduce or prevent auto-oxidation. To achieve this, analytical techniques are required that can detect auto-oxidation products, ideally with separation. Currently, the most favoured technique to identify biodiesel auto-oxidation is through the use of the Rancimat instrument. Whilst standards are in place to analyse multiple properties of biodiesel, presently few standards are available that addresses biodiesel oxidation.

Oxidation stability of biodiesel, as described in BS EN 14112:2003, is measured using a Rancimat instrument and is completed by utilising the induction period which is a measure of the time taken for the production of volatile acids to be produced.[127] Biodiesel that has an induction period in excess of 6 hours is deemed suitable for use as a fuel. BS EN 15751:2009 is another measure of oxidation which again uses the Rancimat instrument, however this targets the oxidation stability of biodiesel when in petrodiesel blends.[128] BS EN 16091:2011 also measures oxidation stability of biodiesel, however this is completed in a reaction vessel and is termed 'rapid small scale oxidation'.[129] This standard is sensitive to

experimental conditions, certain FAMEs and presence of ignition improvers, resulting in fuels exhibiting lower oxidation stability.

Some studies have been conducted into the detection and identification of auto-oxidised products together with biodiesel. However, more research is required to better understand biodiesel auto-oxidation including determining the identities of the auto-oxidation products generated, likely pathways of oxidation and how this affects other properties, such as viscosity. This information coupled with FAME analysis will allow a clearer picture of biodiesel as a fuel.

For RME and auto-oxidised RME samples a naming system is in place: $RME_x$ where x represents the length of time, in years, that the RME has been oxidised, where 0 denotes fresh RME.

## 3.1. Gas Chromatography-Mass Spectrometry

Traditionally, GC-MS is conducted using EI, a hard ionisation technique whereby FAMEs can be detected and successfully identified. Fragmentation is a particular feature of EI, with molecules fragmenting in often predictable ways. This is observed for FAMEs, for example, fragmentation occurs producing fragment ions at 74 *m*/*z* (*via* the McLafferty rearrangement) and 87 *m*/*z* through bond cleavage (Figure 3.1).[130] The relative abundance of fragment ions 74 *m*/*z* and 87 *m*/*z* become less prominent with increased carbon chain length and number of double bonds (Figure 3.2).[130]

Predictable fragmentation is particularly useful for identifying unknowns, with spectra either compared to a compound library or is deduced manually. GC-MS is a vital tool for the identification of

FAMEs and auto-oxidised FAMEs aiding the identification of low-molecular weight auto-oxidation products.

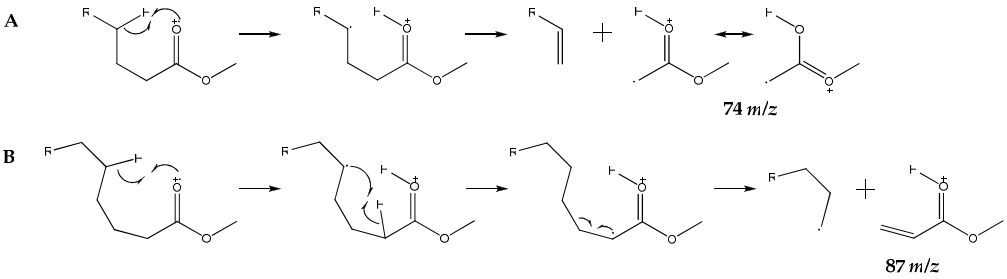


**Figure 3.1:** Fragment ions typically observed in EI when analysing FAMEs.

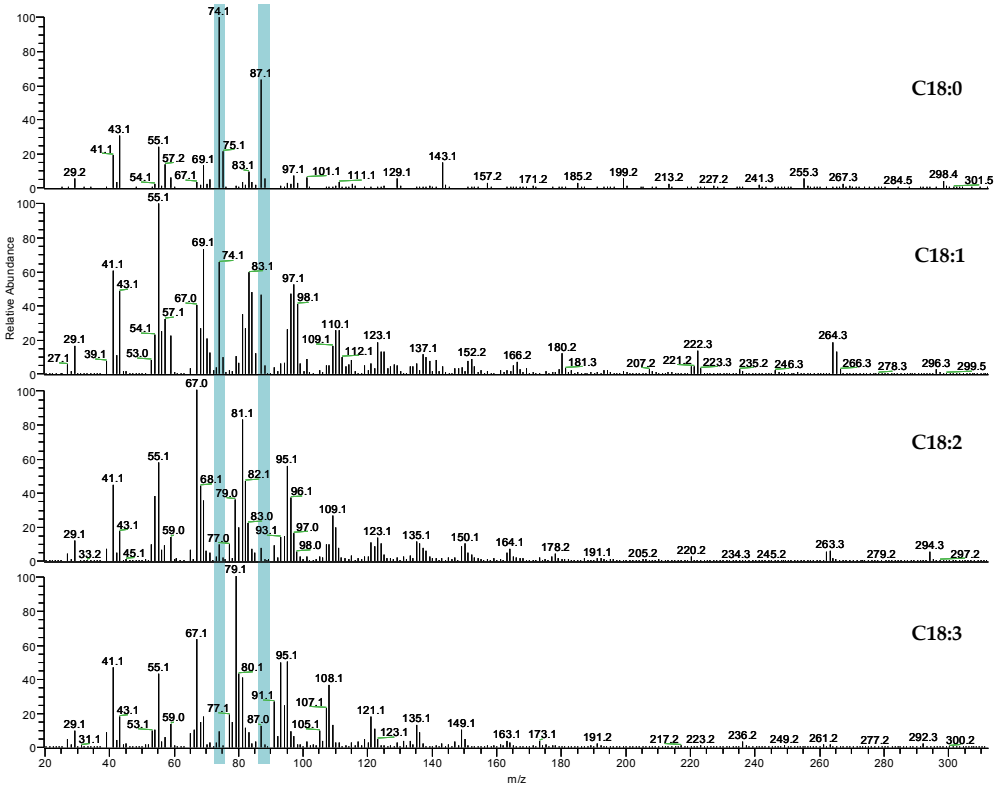


**Figure 3.2:** EI mass spectra of C18:0, C18:1, C18:2 and C18:3 obtained using GC-MS demonstrating the effect of unsaturation on production of fragment ions 74 and 87 *m/z* (highlighted) from C18:X FAMEs.

GC-MS was initially used to explore biodiesel auto-oxidation. Individual FAMEs were analysed *via* GC-MS and it was observed (Figure 3.3) that C18:1, C18:2 and C18:3 elute at different retention times and are baseline resolved when using the GC-MS method outlined in Chapter 2. Total ion current chromatogram (TICC) baseline resolution was also observed when analysing RME (Figure 3.4) and can be observed for all FAMEs in fresh RME ($RME_0$) (Figure 3.5).

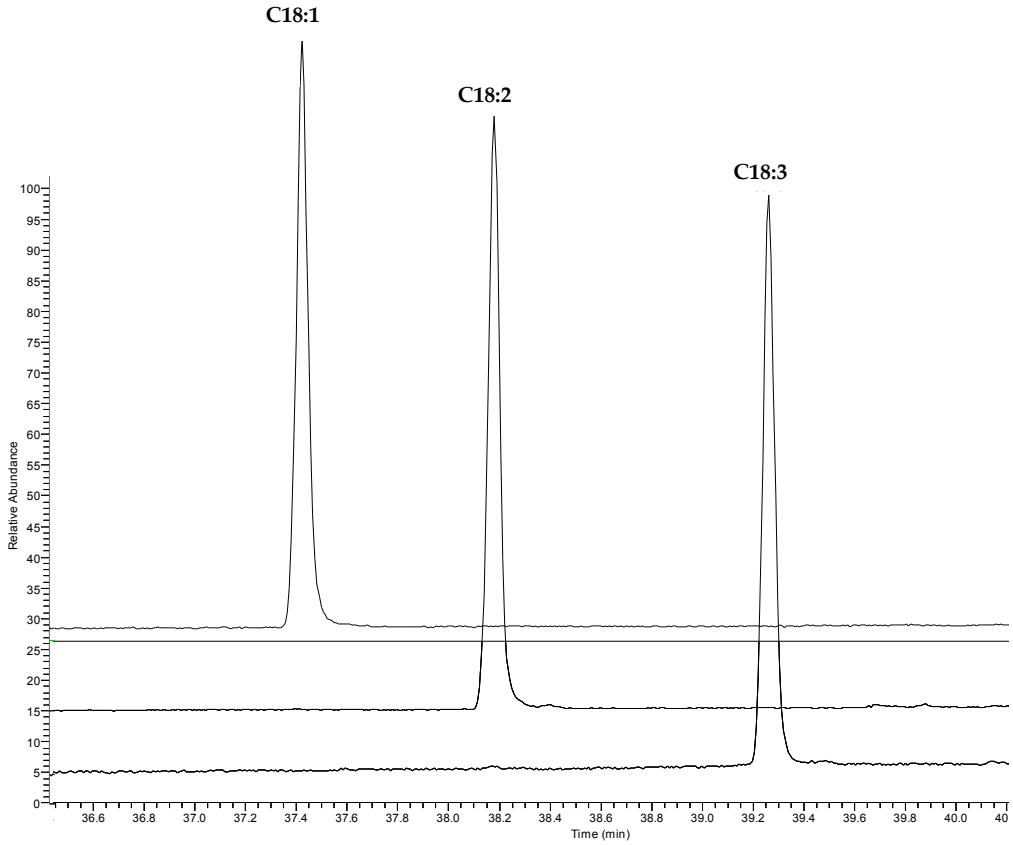


**Figure 3.3**: Overlay of GC-MS TICCs of C18:1, C18:2 and C18:3 clearly displaying baseline separation.

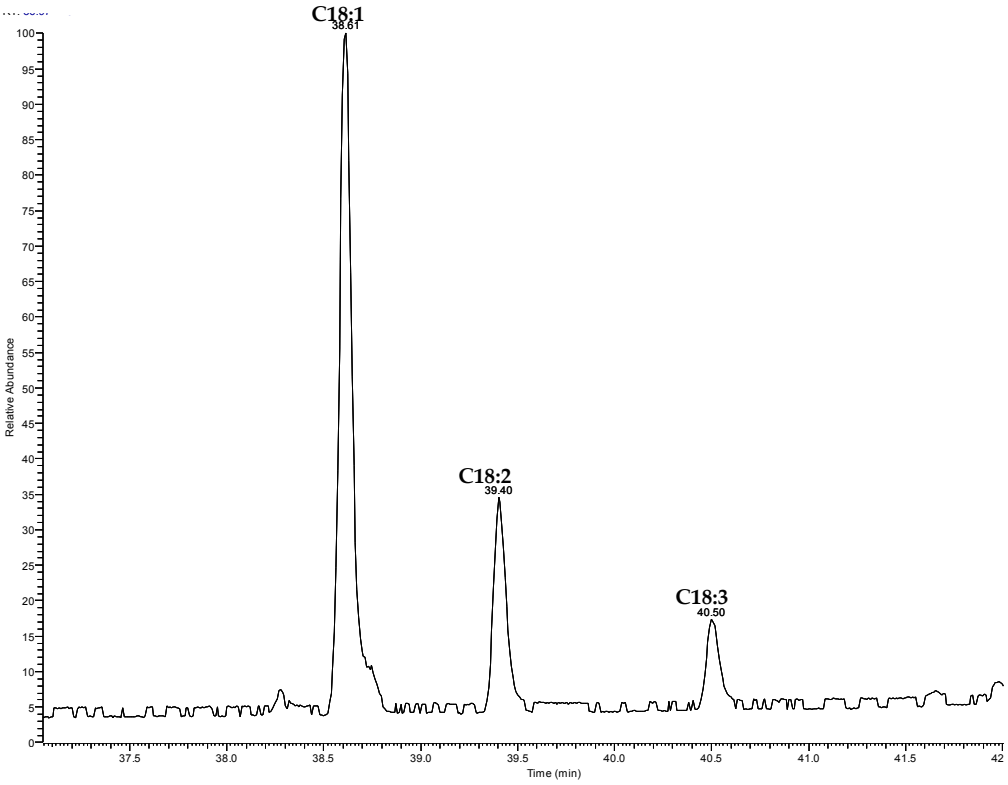


**Figure 3.4:** GC-MS TICC of $RME_0$ clearly displaying baseline separation of C18:1, C18:2 and C18:3.

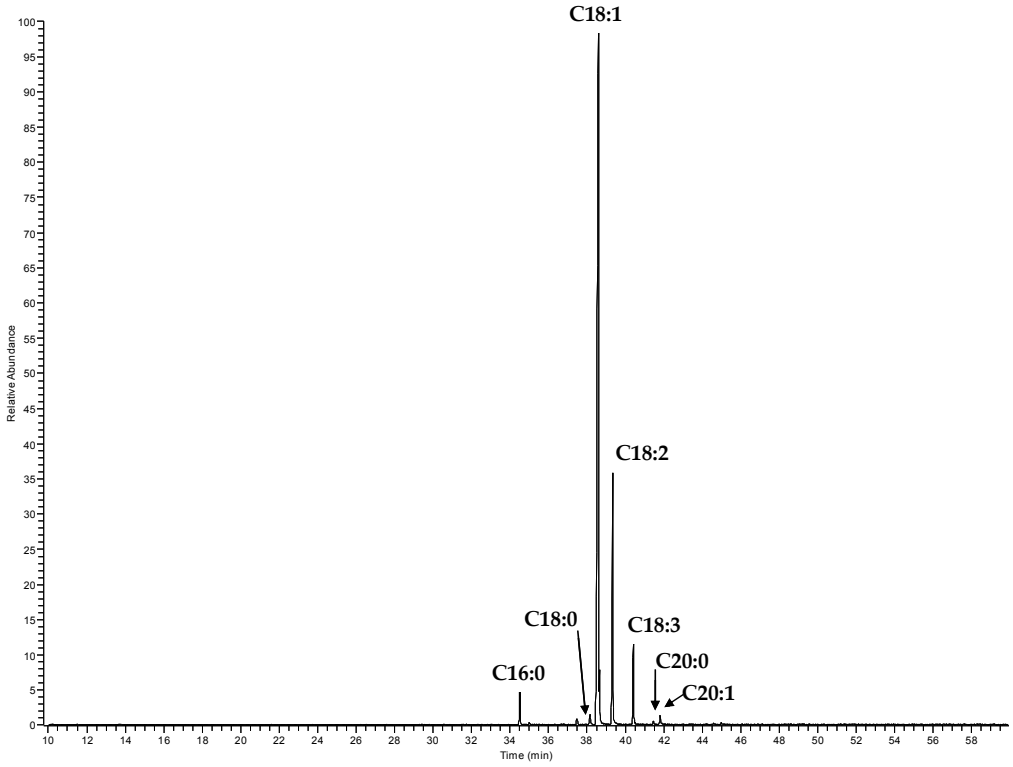


**Figure 3.5:** GC-MS TICC of $RME_0$ displaying separation of FAMEs in RME.

FAMEs are positively identified and structurally elucidated *via* fragmentation patterns which can be compared to the NIST library and positive matches obtained (Figure 3.6). Comparisons are completed and given an SI number which is a measure of how well the unknown spectrum and suggested compound match, these values are displayed in Table 3.1 for FAMEs C16:0, C18:0, C18:1, C18:2, C18:3, C20:0 and C20:1 in RME from Figure 3.5.

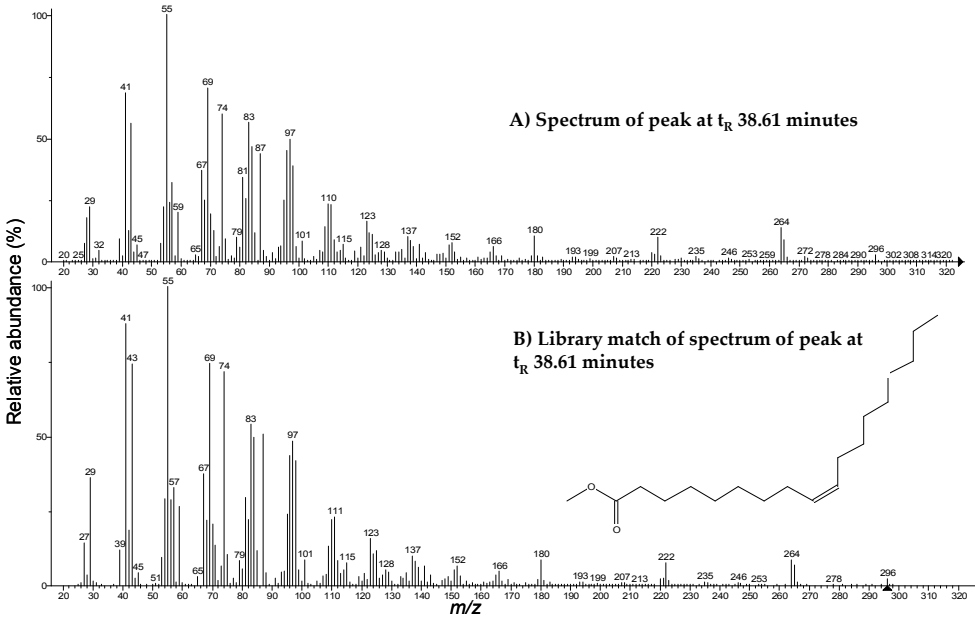


**Figure 3.6:** EI mass spectrum of A) peak at $t_R$ 38.61 minutes $RME_0$ Figure 3.5 and B) library match (SI = 941), obtained using GC-MS.

**Table 3.1:** SI values of FAME peaks compared to library matches.

| FAME | SI value (arbitrary units) |
|---|---|
| C16:0 | 932 |
| C18:0 | 891 |
| C18:1 | 941 |
| C18:2 | 925 |
| C18:3 | 884 |
| C20:0 | 911 |
| C20:1 | 917 |

Separation of FAMEs is an important aspect of analysis; it allows changes in abundance to be closely monitored, as well as detection of other species, which will ideally be separated from the FAMEs. Another advantage is that GC-MS can be used quantitatively, allowing FAMEs to be tracked over time.

Alongside identification of FAMEs and monitoring of various species over time, GC-MS can be used to identify original feedstock sources. Different feedstock sources produce biodiesel with different FAME compositions (Figure 1.3) and this can be distinguished by GC-MS, as demonstrated in Figure 3.7 which shows the different compositions of FAMEs in biodiesel derived from rapeseed and soybean.

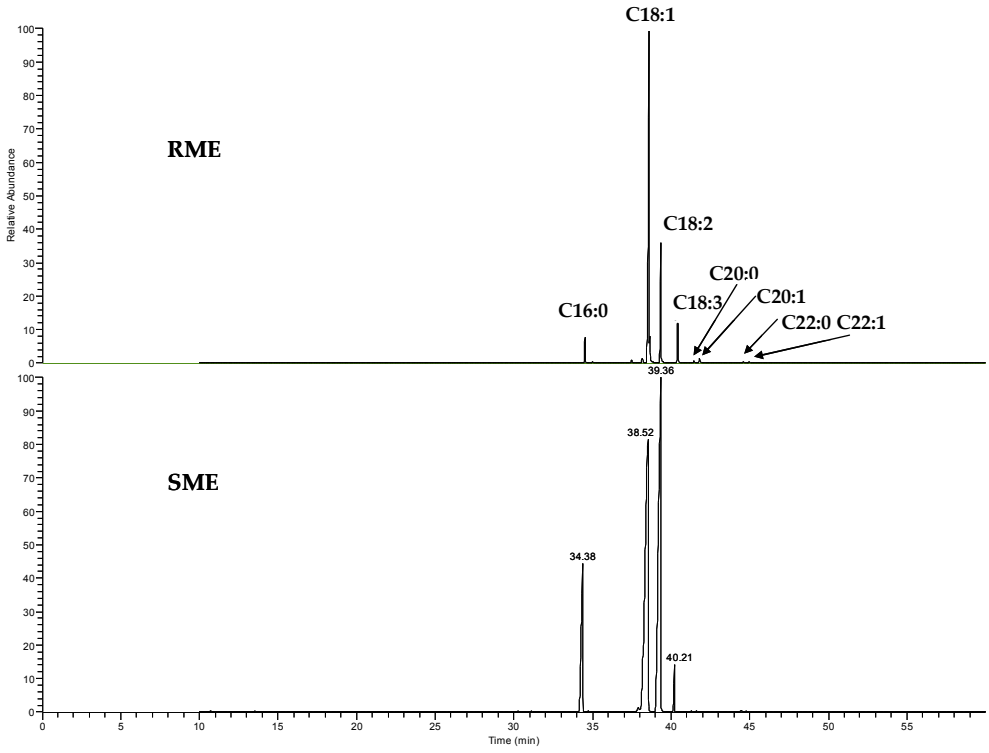


**Figure 3.7:** GC-MS TICCs of $RME_0$ and $SME_0$ clearly displaying the different FAME distribution (Figure 1.3).

Quantitative GC-MS is completed using an internal standard. An internal standard should be as closely related to the analyte of interest as possible. Ideally a deuterated or isotopically labelled version of the analyte of interest should be used, however these can be costly and difficult to obtain. If not available, a homologue should be used, *e.g.* C17:0. This research has used methyl octadecanoate-d35

(Figure 3.8); a deuterated C18:0 with all hydrogen atoms of the original fatty acid backbone replaced by deuterium atoms. This molecule was used to quantify FAMEs and some auto-oxidation products present in RME and auto-oxidised RME samples.

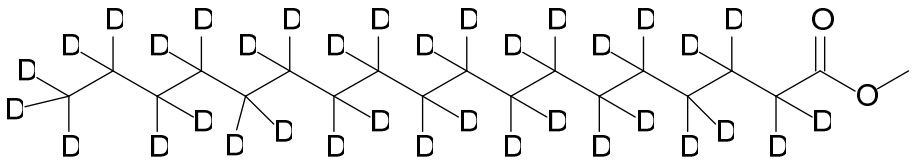

**Figure 3.8:** Methyl Octadecanoate-d35.

Homologue internal standards have been used in standard methods, *e.g.* methyl nonadecanoate (C19:0) for BS EN 14103:2011[80] However, the use of homologues can cause some issues. Previously, BS EN 14103:2003 used methyl heptadecanoate (C17:0) as the internal standard. This presents an issue when analysing biodiesel produced from animal feedstocks or waste oil. These biodiesel sources are composed of FAMEs of even and uneven chain fatty acid chain length, unlike vegetable oil which is composed solely of even FAMEs. Therefore, when analysing biodiesel from an unknown or animal/waste feedstock source *via* this method calculations using the internal standard area are compromised due to (potential) contributions from this FAME.[131]

Another important factor for any analysis is the limit of detection (LOD) of the measurement. The LOD describes the lowest possible concentration of a given substance that can be detected and is dependent on instrument and analysis conditions. Typically, the LOD is defined as the amount of a substance which can be detected to give a signal:noise ratio of 3:1. To obtain an LOD, for a specific compound or

group of compounds, a standard is analysed at a series of concentrations and completed in triplicate (at least). The lowest concentration detected producing a signal:noise ratio of 3:1 (Figure 3.9) is considered the LOD. The LODs of the FAMES methyl oleate, methyl linoleate and methyl linolenate attained using GC-MS were 0.10, 0.25 and 0.25 ng on column, respectively. Reconstructed ion chromatograms (RIC) were completed for LOD GC-MS analysis of RME samples with the following m/z values used; methyl oleate - m/z 55.1, 74.1, 84.1, 180.3, 222.4, 264.4, 296.5; methyl linoleate - m/z 55.1, 67.1, 81.2, 95.2, 220.4, 263.4, 294.5 and methyl linolenate - m/z 55.1, 67.1, 79.1, 95.1, 108.2, 149.2, 261.4, 292.4.

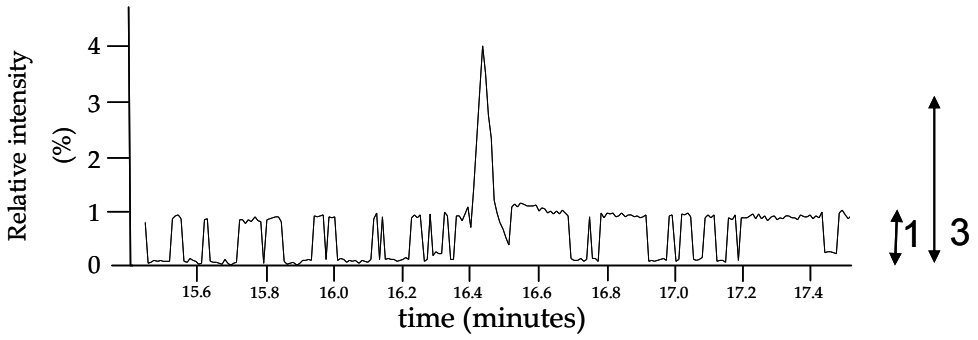


**Figure 3.9:** Example of signal to noise at 3:1 ratio.

GC-MS is well suited for the analysis of initial auto-oxidation products and FAMEs. Auto-oxidation products are expected to be composed of C, H and O, with various functionalities, e.g. aldehydes and ketones, and have a low molecular weight (<400 Da). Comparison of RME of different ages, therefore at different extents of auto-oxidation, clearly demonstrates an increase in species detected in further auto-oxidised samples. These species have predominantly been baseline separated from other new species and FAMEs (Figure 3.10). Analysis of mass spectral data suggests previously undetected

peaks present in advanced age samples are products relating to auto-oxidation, clearly highlighting the ability of this technique to analyse RME and auto-oxidised RME. These species and the obvious depletion of C18:X FAMEs (observed throughout all techniques) will be considered in Chapter 4.

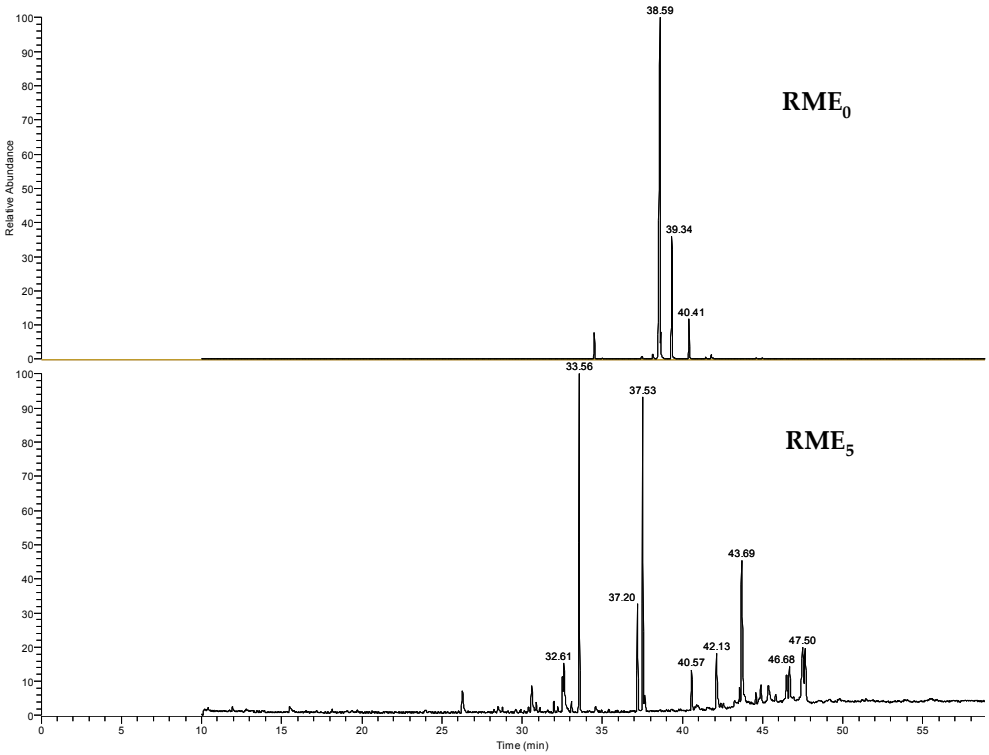


**Figure 3.10:** GC-MS TICCs of $RME_0$ and $RME_5$.

As biodiesel is further auto-oxidised it is expected that auto-oxidation species will increase in size and thus molecular weight. Described here as a polymeric species, these products are less volatile and contain additional oxygen atoms when compared with starting FAMEs and initial auto-oxidation products. These properties render these molecules unsuitable to be detected using GC-MS.

Biodiesel is often diluted into various matrices, these include petrodiesel, which is primarily hydrocarbons and therefore non-polar and lubricant oil which is composed of compounds of wide ranging functionality and polarity.

Whilst GC-MS is suitable for hydrocarbon analysis, co-elution can cause some issues. As observed in Figure 3.11, hydrocarbons relating to petrodiesel can be separated from each other and the C18:X FAMEs. However, some co-elution with shorter chain FAMEs such as C16:0 is observed. Hydrocarbons elute within the same retention time window as some of the auto-oxidised species (10-33 minutes (Figure 3.10)), if co-elution does occur then mass spectral data could be complex and difficult to interpret. Techniques are available whereby matrices are 'invisible' throughout analysis and this will be discussed at a later point.

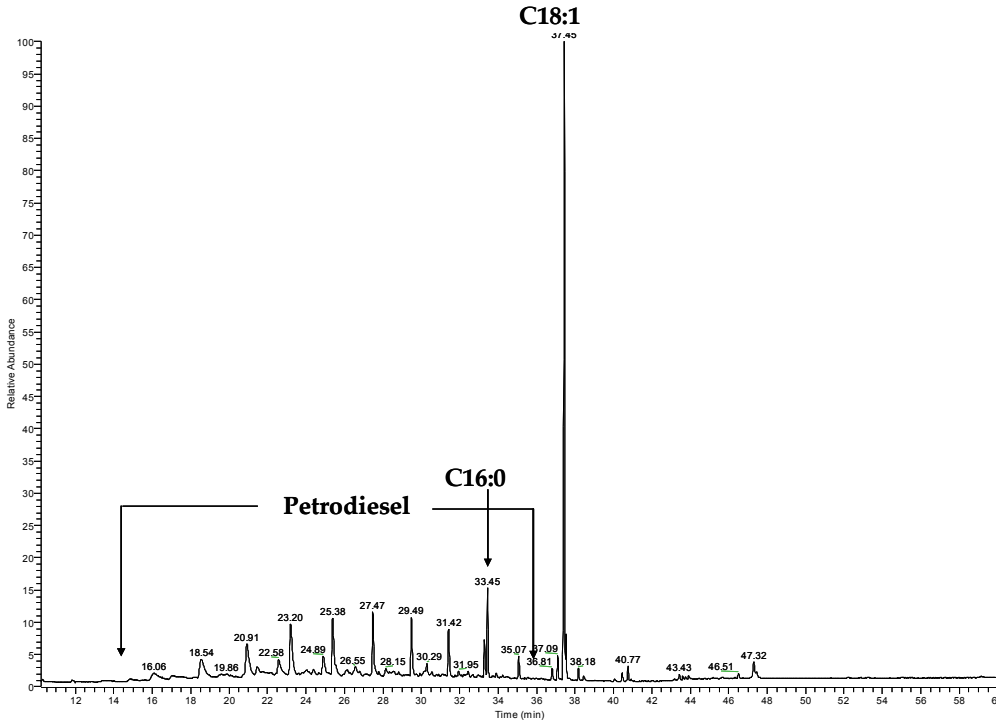


**Figure 3.11:** GC-MS TICC of B20 (RME).

The ability of GC-MS to detect biodiesel and matrices is an important tool. Analysis of jet fuel is an example where this is utilised. When fuel is transported throughout the United Kingdom joint fuel lines are used which transport petrodiesel, petroleum, marine

petrodiesel, biodiesel as well as the aviation fuel kerosene. Sharing of transport lines can cause cross-over of fuel and thus contamination. Biodiesel is considered an adulterant in aviation fuel, with a maximum level of 5 ppm of biodiesel accepted in aviation fuel.

Separation of individual FAMEs and auto-oxidation products comes at a time cost with GC-MS analysis times in this method (Chapter 2) being 60 minutes long. This time constraint permits a maximum of approximately 20 samples to be analysed per day per instrument, when accounting for additional time required for the instrument to re-equilibrate between analyses. Whilst methods can be altered and shorter run times obtained, this is typically at a loss of information or compromised separation. This, together with the need for a technique to analyse polymerised auto-oxidation species, warranted the use of another technique.

## 3.2. Electrospray Ionisation-Mass Spectrometry

ESI-MS is ideally suited for the analysis of both low and high molecular weight polar molecules (non-polar molecules are rarely ionised) and has been used within this project to analyse RME samples. Termed a 'soft' ionisation technique, ESI-MS typically does not induce fragmentation and ions observed are intact species that are protonated or cationised molecules in positive ion ESI-MS, or conversely deprotonated molecules in negative ion ESI-MS.

Initially, direct infusion low resolution positive ion ESI-MS was used to analyse FAMEs, *i.e.* no chromatography (Figure 3.12 and Figure 3.13). FAMEs primarily ionised *via* the formation of sodium

adducts; $[M + Na]^+$, and it is in this form the ions were observed (Figure 3.12 Figure 3.13 and Figure 3.14).

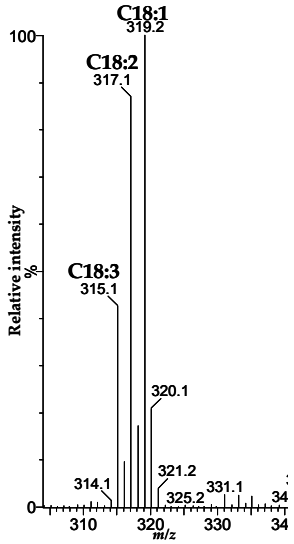


**Figure 3.12:** C18:1, C18:2 and C18:3 observed in $RME_0$ using positive ion ESI-MS, detected in the sodiated adduct form $[M + Na]^+$.

Positive ion ESI-MS is a technique whereby $[M + Na]^+$ ions are formed through chelation of a sodium ion to the molecule. ESI is a competitive process and ionisation can be dependent on molecular composition. Lone pairs on oxygen atoms primarily aid this process and molecules containing increased amounts of oxygen atoms will ionise preferentially, such as multiple oxygen atom containing auto-oxidation species. For example, molecules with basic or acidic sites are more likely to ionise in comparison with hydrocarbons which ionise poorly *via* ESI-MS and thus be detected using either positive ion ESI-MS or negative ion ESI-MS correspondingly. Compounds containing multiple $\pi$ bonds are preferentially ionised and this can be observed in the C18:X series, where C18:3 is preferentially ionised compared with C18:1 and C18:2.

Freshly produced RME ($RME_0$) is predominantly composed of C18 FAMEs (C18:1, C18:2 and C18:3 present at a minimum of 71%, Figure 1.3) as previously discussed. These species can be seen in Figure 3.12 and Figure 3.13 where $[C18:1 + Na]^+$, $[C18:2 + Na]^+$ and $[C18:3 + Na]^+$ (319, 317 and 315 *m*/*z* respectively) were identified. Ratios of C18:X FAMEs obtained using positive ion ESI-MS appear to be as expected (Figure 1.3), however due to preferential ionisation cannot be used quantitatively without the use of specific calibration protocols.

Using this knowledge of ionisation can be advantageous; auto-oxidation products are produced from the original FAMEs and possess similar characteristics, with many products having additional oxygen atoms. Increased oxygen content ensures preferential ionisation, forming stronger chelation with sodium. This potentially suppresses other ions with lower ionisation efficiencies and thus lower affinities for sodium chelation. This characteristic of ESI-MS would ensure that as auto-oxidation proceeds molecules that possess increased oxygen content ionise preferentially thus are more readily detected. Auto-oxidation products which are preferentially ionised could be used as markers to identify the extent FAMEs auto-oxidation.

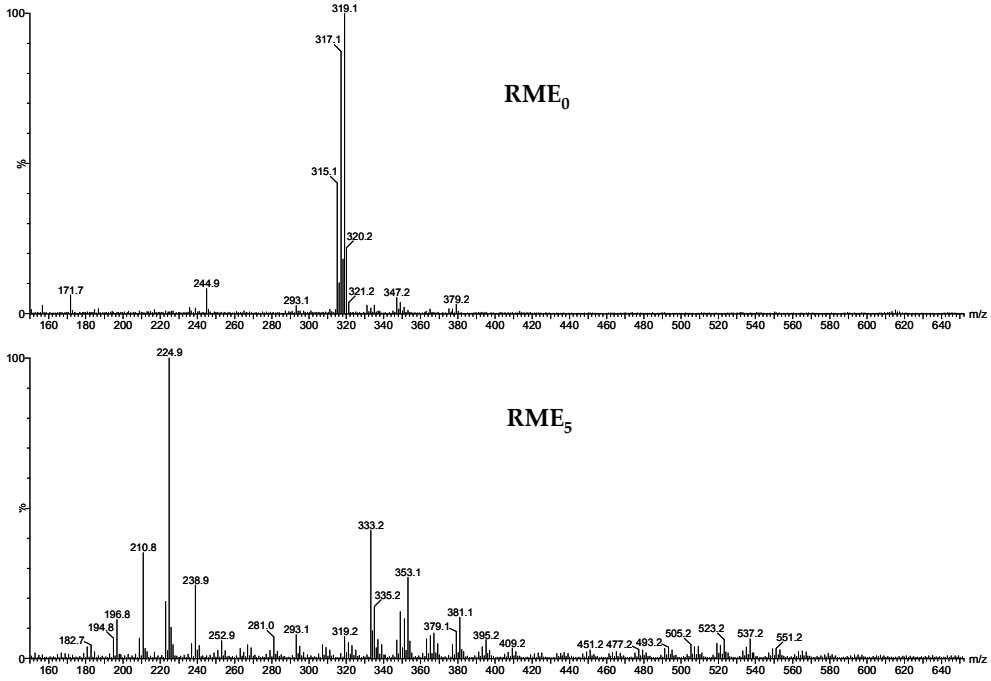


**Figure 3.13:** Low resolution positive ion ESI-MS of $RME_0$ and $RME_5$.

Analogous to GC-MS, distinct differences are observed when comparing RME of different ages (Figure 3.13 and Figure 3.14) using positive ion ESI-MS. C18:X FAMEs ($[C18:1 + Na]^+$, $[C18:2 + Na]^+$ and $[C18:3 + Na]^+$, *m*/*z* 319, 317 and 315 respectively) intensities are noticeably decreased in aged RME. Other ions are present which are not observed in fresh RME and these are attributed to auto-oxidation products.

Analysis of RME samples using direct infusion positive ion ESI-MS is completed within minutes compared to the GC-MS method (Figure 3.5) which requires a 60 minute analysis time. This rapidity could be exploited and positive ion ESI-MS could be used as a quick screening technique. RME samples could be screened for initial auto-oxidation with results that indicate samples have begun to auto-oxidise tested further.

However, as with all techniques limitations are present. Low resolution (LR)-positive ion ESI-MS (Figure 3.13) does not possess

sufficient mass resolution to separate nominally isobaric ions, *i.e.* whose differences are less than 1 *m*/*z* unit. LR-ESI-MS instruments are low cost and commonplace in many laboratories with many used in conjunction with LC techniques. High resolution (HR) instruments boast increased capability compared with low resolution instruments, comprising lower LOD and have an increased ability to separate nominally isobaric ions. HR instruments, such as, TOF-MS are becoming more widespread in laboratories, whilst magnetic sectors and FT-ICR mass spectrometers are not so common. However, sensitivity and resolution is enhanced when compared to TOF-MS which is required to fully investigate these samples. Increased resolution means these instruments are more expensive and complex. Positive ion ESI-FT-ICR MS has been used for analysis of auto-oxidised RME in this study.

RME of varying age has been investigated using LR-ESI-MS and HR-ESI-MS. LR positive ion ESI-MS of aged RME ($RME_5$)(Figure 3.13) appears complex with ~250 nominal mass ions (excluding $^{13}C$ isotopes) present compared to $RME_0$ with 10 ions relating to starting FAMEs. However, when positive ion ESI-FT-ICR MS was used over 5000 ions (excluding $^{13}C$ isotopes) were evident (Figure 3.14). Comparison of GC-MS, LR-ESI-MS and ESI-FT-ICR MS displays these differences (Figure 3.10, Figure 3.13 and Figure 3.14 ). Whilst positive ion ESI-FT-ICR MS separates nominally isobaric ions, with multiple ions found at most nominal *m*/*z* values (Figure 3.15), isomers are not separated, so potentially there are more species present for each *m*/*z*.

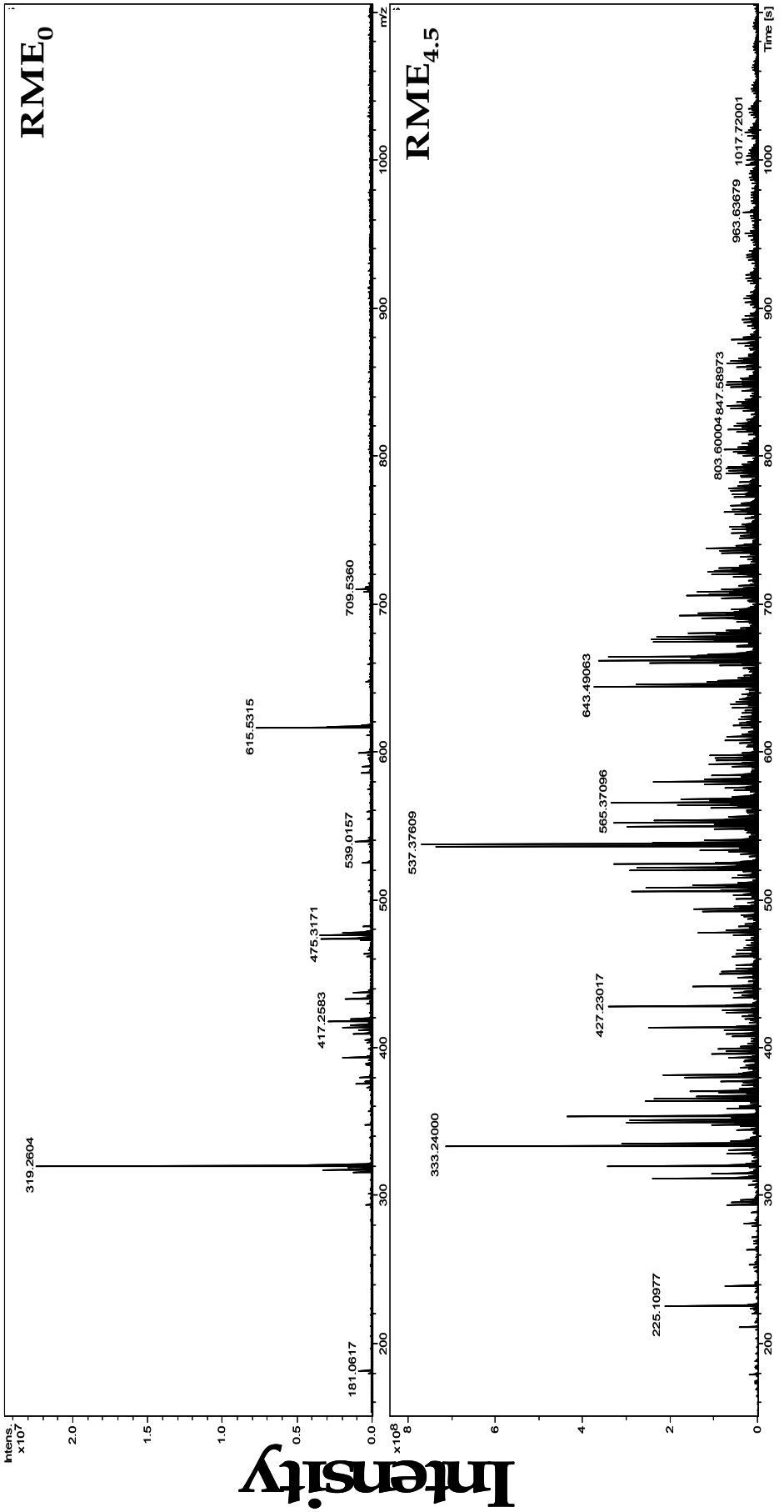


**Figure 3.14:** HR positive ion ESI-FT-ICR MS of $RME_0$ and $RME_{4.5}$

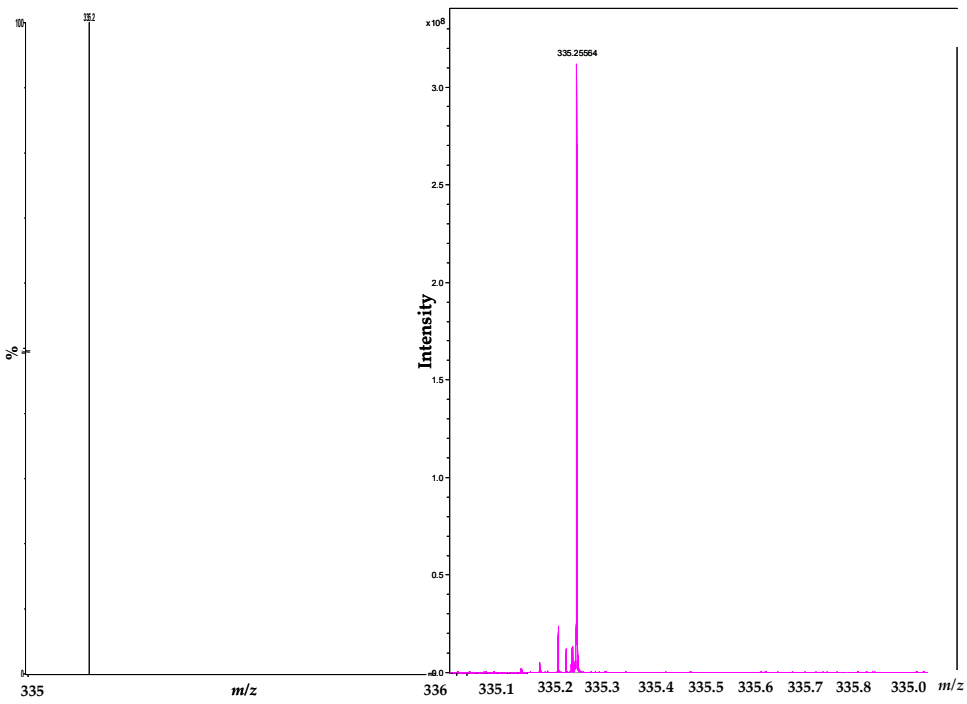


**Figure 3.15:** Expansion of a low resolution positive ion ESI-MS (left) and high resolution positive ion ESI-FT-ICR MS (right) over 1 *m*/*z* unit range of RME4.5.

ESI-MS is best suited for polar molecules, such as FAMEs. Non-polar compounds, such as petrodiesel or lubricant oil are not typically ionised *via* ESI-MS attributed to the absence of acidic/basic sites. This can be advantageous; samples which consist of RME, even as a minor component, can still be analysed. FAMEs can still be ionised, as can auto-oxidation products with the non-ionisable species being 'invisible' to the mass spectrometer (Figure 3.16). It should be noted that if analysing samples with large amounts of non-ionisable material the ion source will become contaminated quicker. If analysis of the matrices is also required this can be completed using other techniques, such as GC-MS.

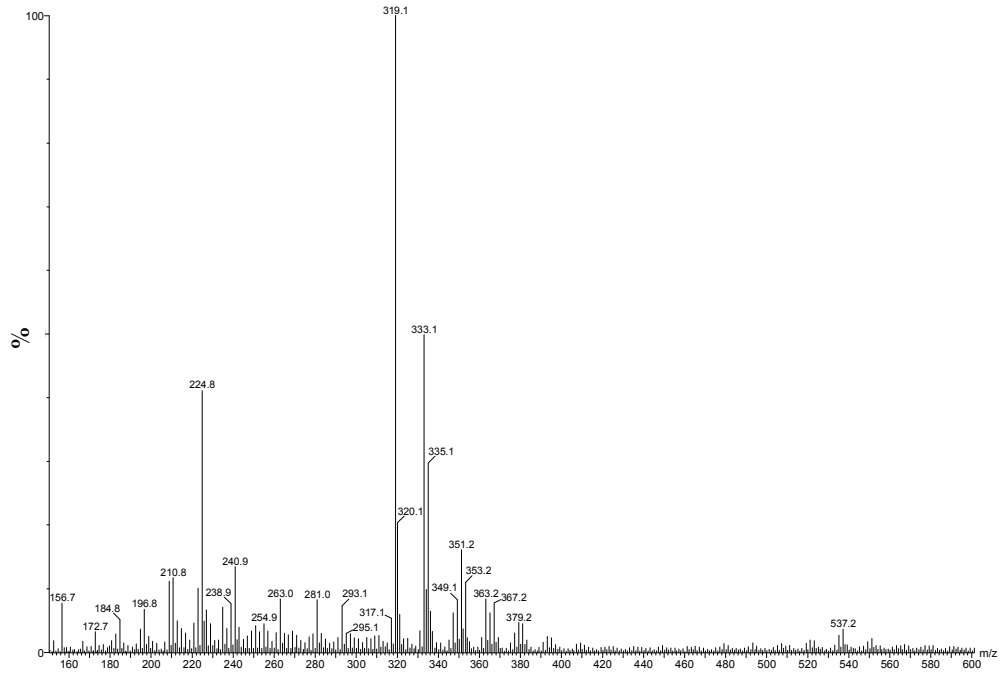


**Figure 3.16:** Low resolution positive ion-ESI-MS of B20.

Auto-oxidised RME has already been observed to be complex, and the presence of multiple species can affect ionisation. Ionisation efficiency of auto-oxidation products influence ionisation and this can cause ions with lower ionisation efficiencies to be suppressed. Chromatographic techniques compatible with ESI-MS were investigated to reduce ion suppression effects that occur with direct infusion ESI-MS. At a minimum, it was expected that components within RME and auto-oxidised RME would separate as groups. This was expected to be completed within a shorter time frame compared to GC-MS, with mass spectrometry used to separate and identify components in these group separations.

## 3.3. High Performance Liquid Chromatography-Mass Spectrometry

RP-HPLC-MS has been used in this research and has been coupled here to low resolution ESI-MS, the technique is limited by polarity of the sample, solubility of the sample in the mobile phase and ability of the compound to ionise, similar restrictions as with infusion ESI-MS. Whilst HPLC columns have a lower efficiency compared with GC-MS, run times can be or have been halved, a broader range of compounds can be analysed, with little restriction on molecular weight.

FAMEs were detected in their sodiated form as observed previously in direct infusion positive ion ESI-MS. However, unlike GC-MS, FAMEs were not baseline resolved under these conditions as detailed in Chapter 2.1. Distinct differences between RME and aged RME ($RME_4$) can be observed and identified through the use of HPLC positive ion ESI-MS (Figure 3.17).

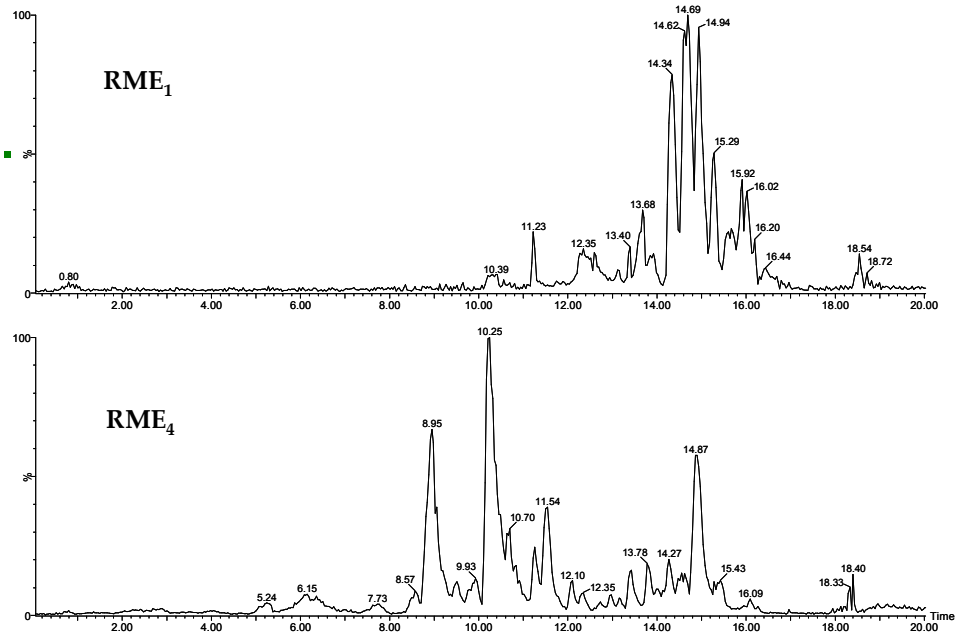


**Figure 3.17:** HPLC- positive ion ESI-MS BPICs of $RME_1$ and $RME_4$.

NP-HPLC-MS is less commonly used compared to RP-HPLC-MS.[132] The properties of NP-HPLC-MS, such as a non-polar mobile phase, are well placed to analyse and separate samples predominantly non-polar in nature. However, issues arise relating to the solubility of polar components, toxicity and low working limit exposure of some NP-HPLC mobile phase solvents and solvents are incompatible with the mass spectrometer. Additionally, as discussed previously, non-polar components typically do no ionise *via* ESI-MS (although this can be advantageous, *see* Figure 3.16).

An advantage of HPLC-MS analysis is the ease of addition of a UV detector. The UV detector is placed before the mass spectrometer and is a selective, non-destructive detector that can be used quantitatively (with certain requirements) and can give valuable information. Compounds that can be detected require a chromophore, typically found in conjugated $\pi$ systems. Much like ionisation, detection response is dependent on the extent of the conjugated $\pi$

system, with compounds which have an increased number of chromophores more intensely detected.

RP-HPLC ESI-MS and NP-HPLC ESI-MS are limited by sample polarity and sample solubility, and when applied to the analysis of a complex sample with varying components, such as biodiesel in petrodiesel have issues as discussed. SFC, a technique possessing beneficial properties from GC and HPLC techniques as previously discussed (Table 1.1) and coupled to ESI-MS and a UV detector possesses the ability to analyse FAMEs, auto-oxidation products and petrodiesel.

## 3.4. Supercritical Fluid Chromatography-Mass Spectrometry

SFC, a chromatography technique already discussed in Chapter 1, can be readily coupled to ESI-MS with little modification needed to the interface.

In this study a supercritical $CO_2$ mobile phase was used with varying amounts of methanol modifier, using unmodified silica for the stationary phase. Similar to HPLC-ESI-MS, ESI-SFC MS has a UV detector connected in series detecting compounds as they elute from the column. This instrument configuration has been used to aid identification of petrodiesel and FAMEs

Initially separation of individual C18 FAMEs was undertaken. By varying the amount of methanol modifier the polarity of the mobile phase can be altered drastically affecting the separation. Separation of C18 FAMEs was successfully completed using a low percentage of

methanol modifier. Optimal separation was obtained using 0.7% of methanol, see Figure 3.18.

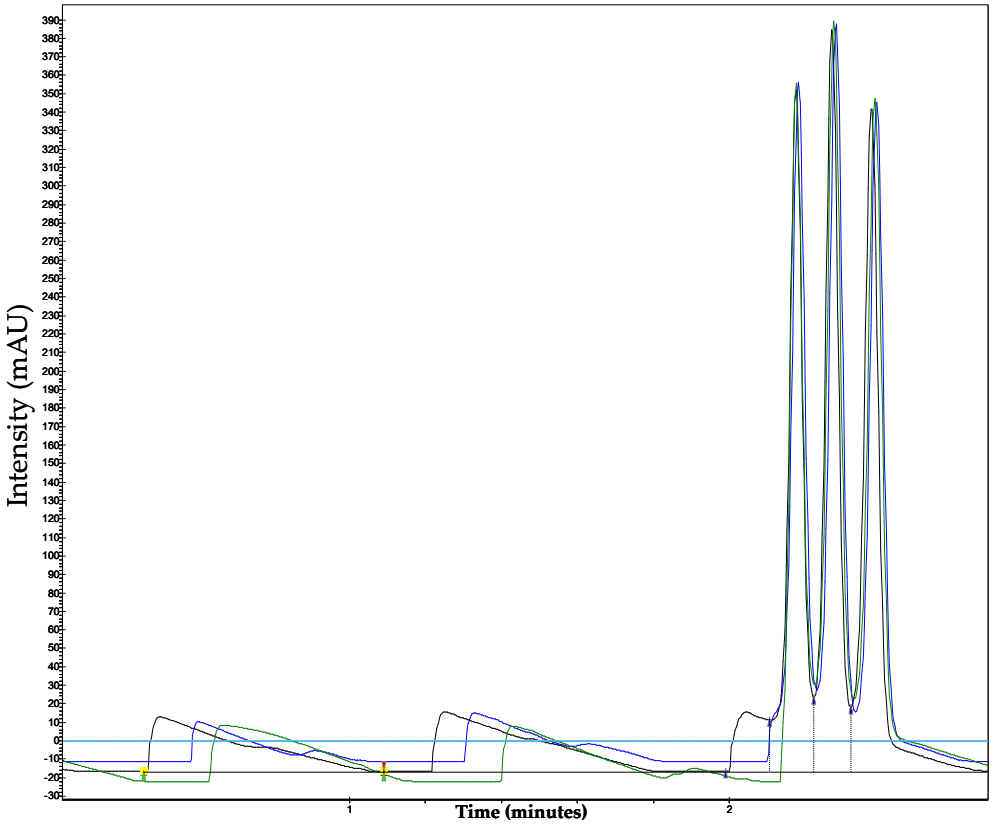


**Figure 3.18:** Overlay of 3 SFC-UV chromatograms at 210 nm of $RME_1$ analysis isocratic using $CO_2$ (0.7% methanol modifier).

However, problems arise with the instrumentation when using this low percentage of modifier. Whilst this technique displays good repeatability baseline stability is compromised and is unstable as displayed in Figure 3.18. The instrument struggles mechanically to deliver these low volumes of modifier in the $CO_2$ mobile phase. It was recommended that the instrument was operated using no less then 5% organic modifier, this being the minimum modifier percentage that can be used to produce a stable baseline.

The baseline resolution observed in Figure 3.18, is not achieved using 5% methanol modifier, C18:1, C18:2 and C18:3 co-elute (Figure 3.19). This is also true of auto-oxidation species observed in $RME_{4.8}$ although some group separation is achieved (Figure 3.20 and Figure 3.21).

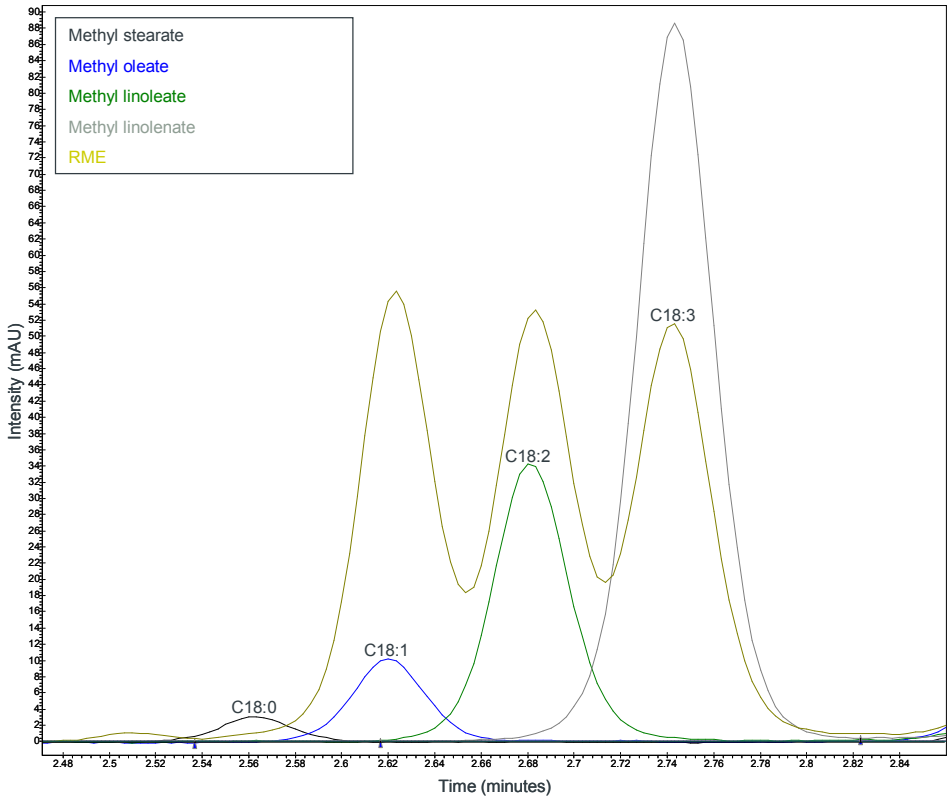


**Figure 3.19:** Overlay of SFC-UV chromatograms at 210 nm of C18:0, C18:1, C18:2, C18:3 and $RME_1$ analysis completed isocratically at 5% methanol modifier.

Auto-oxidation species have already proven to be analysed *via* positive ion ESI-MS (Figure 3.12, Figure 3.13 and Figure 3.14) and when compared to RP-HPLC-ESI-MS and GC-MS analysis times are significantly shorter, with a comparison of C18:3 retention times ~2 - 3.5 minutes (SFC MS), ~15 - 17 minutes (HPLC-MS) and 37.0 - 40.0 minutes (GC-MS).

RP/NP-HPLC-ESI-MS uses increased amounts of solvents compared to SFC, which are costly to purchase, dispose of and can be toxic and damaging to the environment. SFC poses a 'greener' technique using less solvent which is friendlier to the environment (when compared to RP/NP-HPLC-ESI-MS). Differences observed between RME samples of different ages are also detected using positive ion-ESI-SFC MS.

Use of isocratic (5% modifier) and a gradient programmed mobile phase was investigated (Figure 3.20 and Figure 3.21). As can be observed separation of individual FAMEs is not achieved, and low percentages of modifier cause instability in analysis. Therefore analysis was completed separating components into groups, as completed in RP-HPLC-ESI-MS. Analysis is rapid, with all peaks eluting in less than 8 minutes.

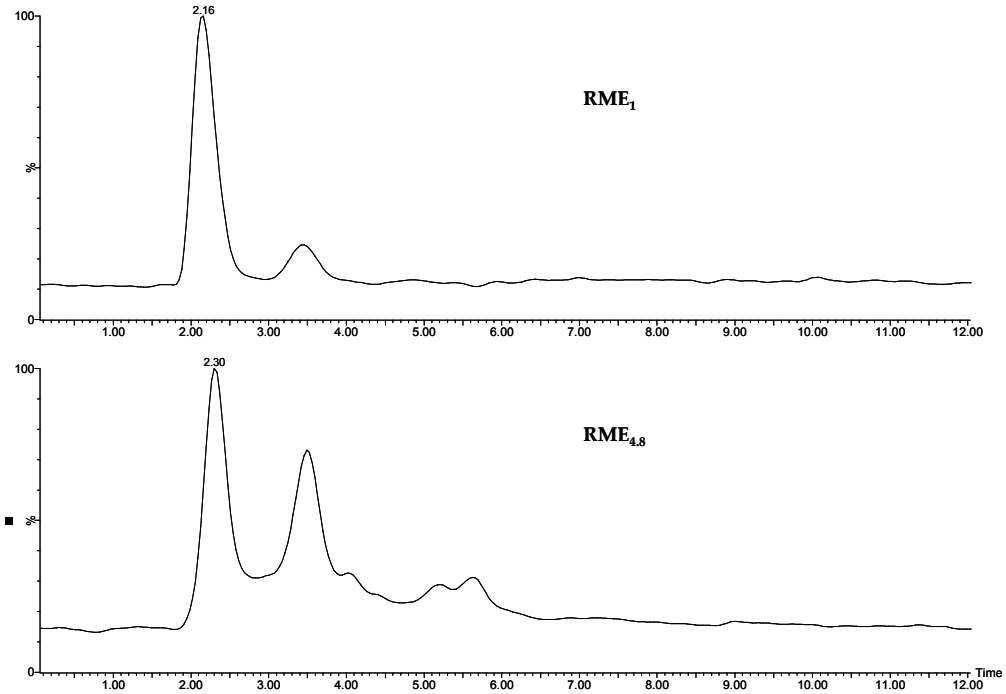


**Figure 3.20:** Positive ion ESI-SFC MS BPIC of $RME_1$ and $RME_{4.8}$ completed isocratically at 5% methanol modifier.

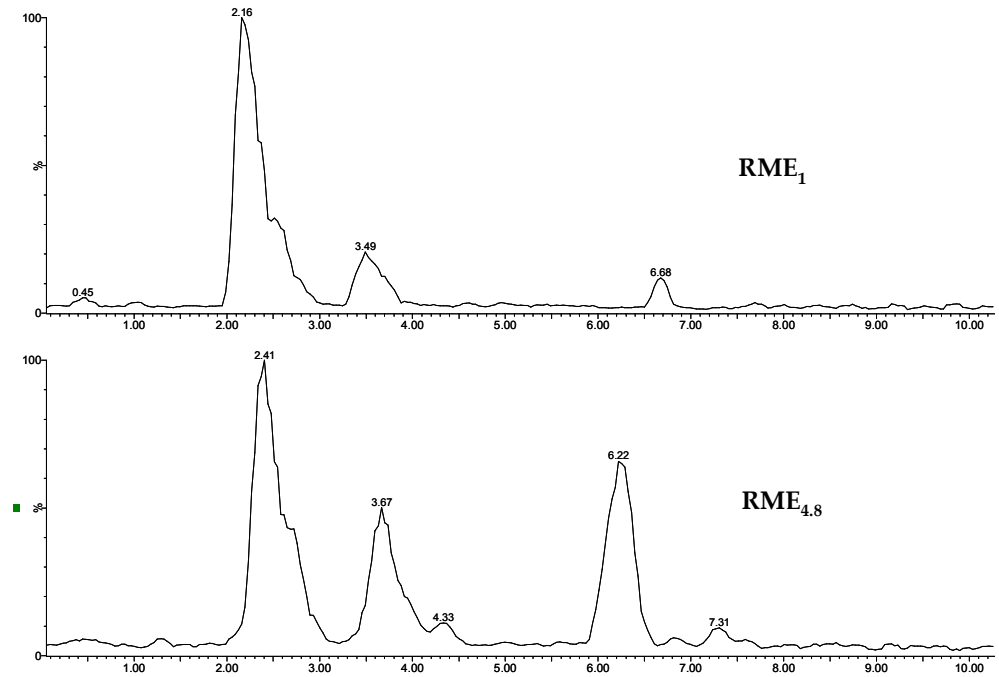


**Figure 3.21:** Positive ion ESI-SFC MS BPIC of $RME_1$ and $RME_{4.8}$ completed using a methanol modifier 5-50% gradient.

Another chromatography parameter that can be varied is the stationary phase. $C_{18}$ and silica stationary phases were investigated. FAME and auto-oxidation products in auto-oxidised RME eluted simultaneously when a $C_{18}$ stationary phase was used. Silica was established as the best stationary phase to separate FAMEs and auto-oxidation products observed in RME. Baseline separation was not observed, however ions separated into composite peaks. Two silica columns were used in series to analyse RME and auto-oxidised RME in isocratic conditions (5% modifier), as expected, the addition of another column increases retention time without significant increases in pressure. Addition of an extra silica column does not increase chromatographic resolution greatly compared with one silica column (Figure 3.22). Use of two silica columns better separates C18:1, C18:2 and C18:3 compared with one silica column, however baseline chromatographic resolution is still not achieved (Figure 3.22).

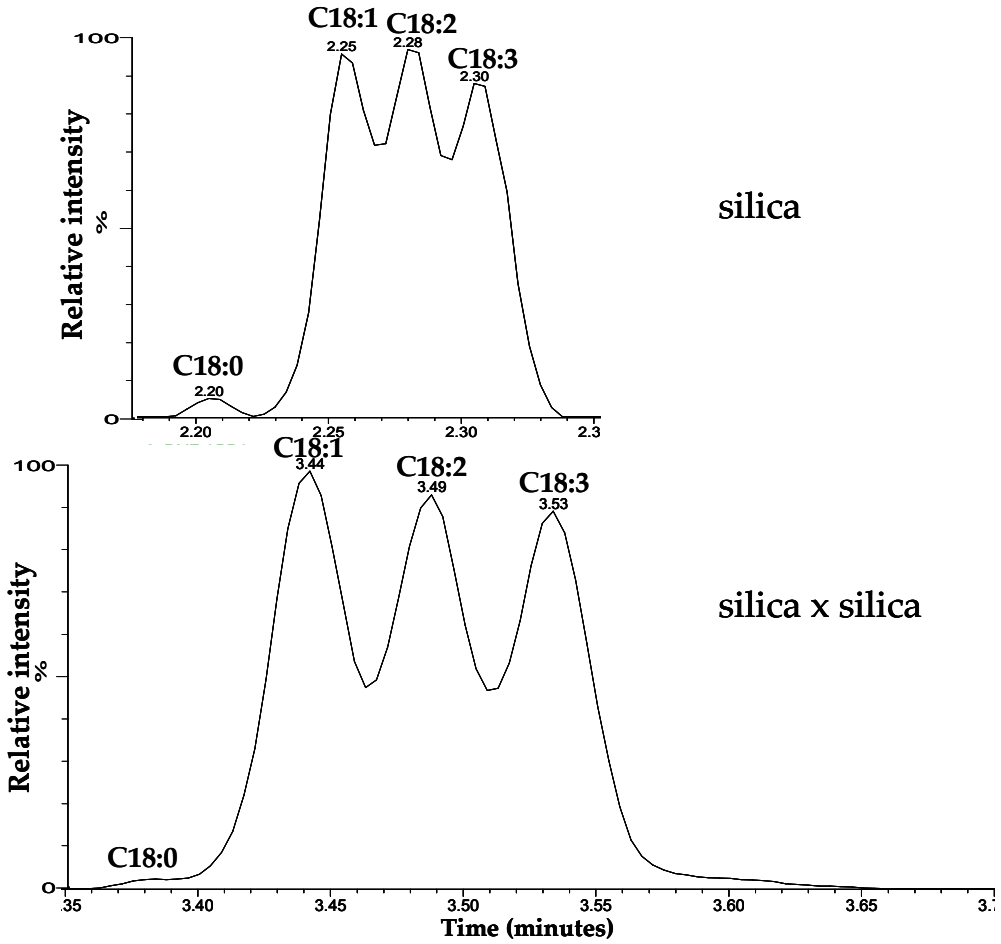


**Figure 3.22:** SFC-UV chromatograms at 210 nm of $RME_1$ displaying the difference in separation when an additional column is used completed isocratically at 5% methanol modifier.

As FAMEs auto-oxidise it is suggested that an oxygen atom is added to the starting FAMEs, this resulting in a series of compounds that are +16 Da apart. This series can be observed in the positive ion ESI-MS data (Figure 3.13 and Figure 3.14) and are also observed in the positive ion ESI-SFC MS data, *e.g.* for C18:2 species (317 *m*/*z*) relating to +16 Da (*m*/*z* 333, 349, 365, 381) can be extracted from the TICC (Figure 3.23). Polymerised auto-oxidation species are also observed, such as the ion *m*/*z* 537, which will be discussed in Chapter 4 - Detection of polymerised auto-oxidation products , and are successfully separated from the starting FAMEs and smaller auto-

oxidation species for example, those pre-described (+16 Da) (Figure 3.24). This will be discussed in more detail in Chapter 4.

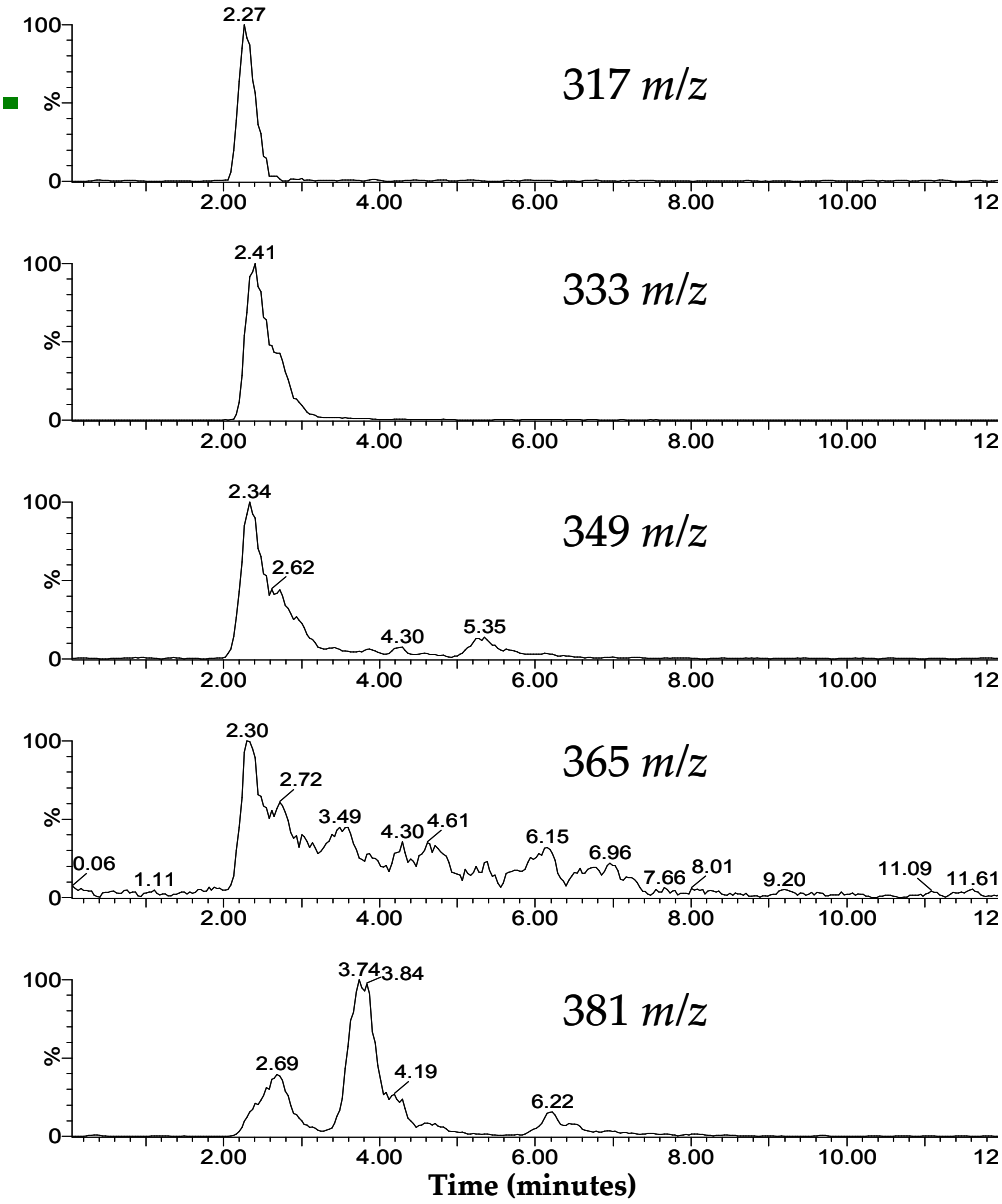


**Figure 3.23:** Positive ion-ESI-SFC MS EICC of $[C18:2 + Na + n16]^+$ series in Figure 3.20 $RME_{4.8}$.

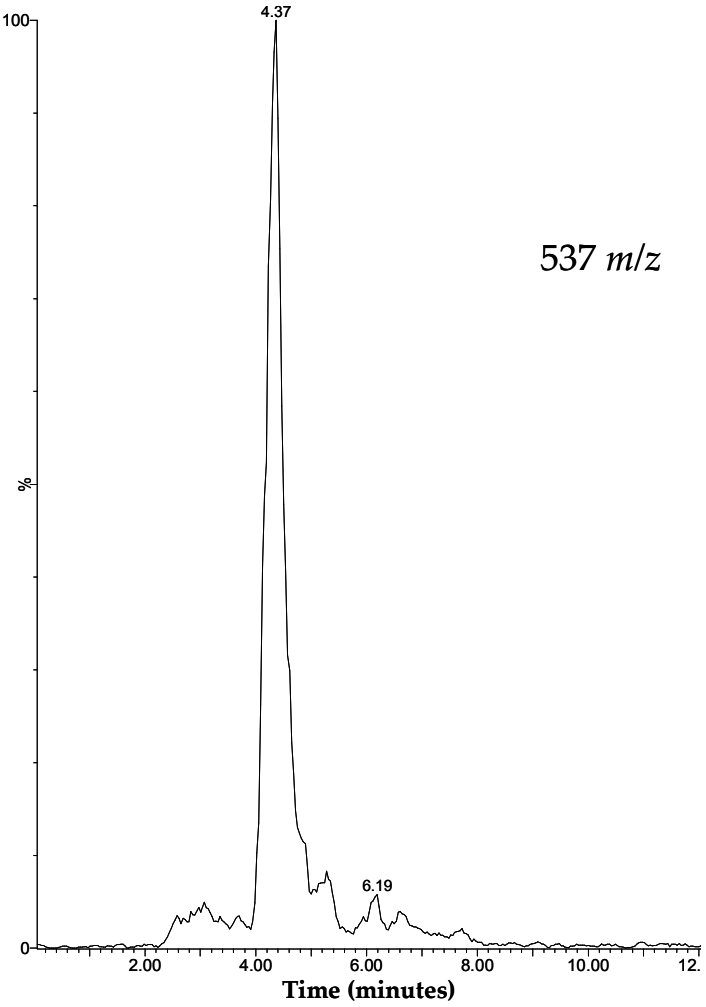


**Figure 3.24:** Positive ion-ESI-SFC MS EICC of *m/z* 537, gradient elution (methanol modifier 5% to 50%).

Through manipulation of the mobile phase, compounds of varying polarity can be separated, such as hydrocarbons and FAMEs. Initially investigated using 0.7% modifier, baseline separation of petrodiesel and RME in a B20 fuel mixture was obtained (Figure 3.25).

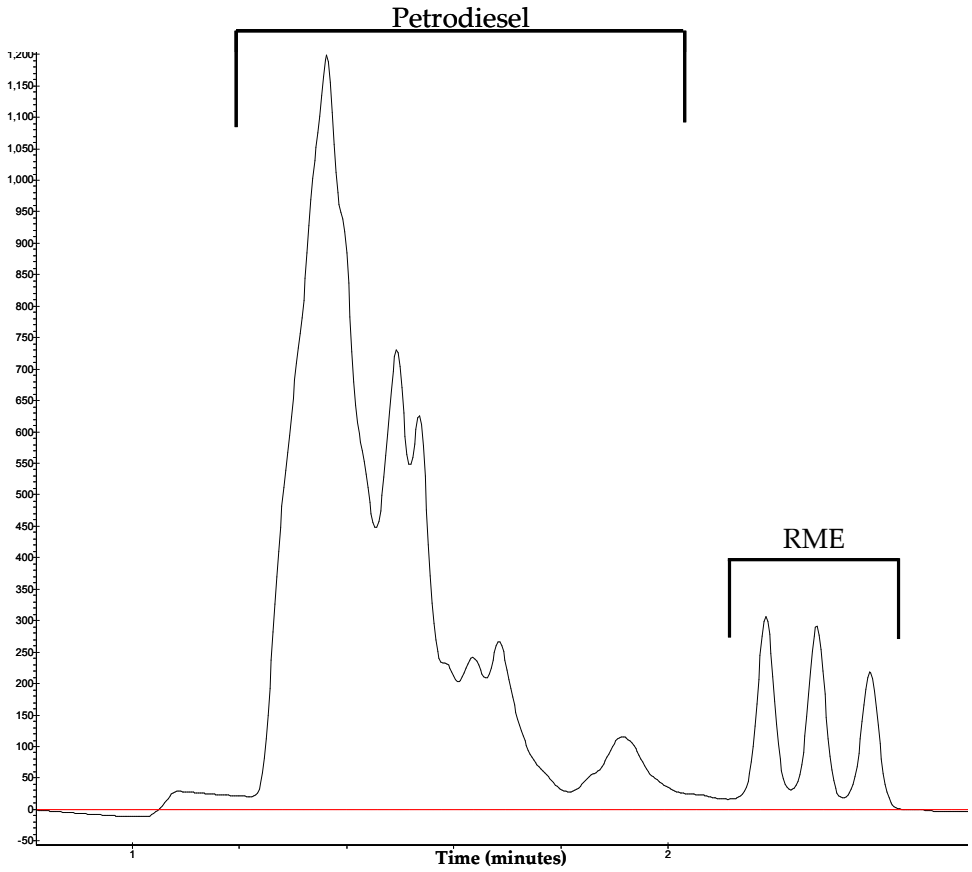


**Figure 3.25:** SFC-UV chromatogram of B20 (RME) at 210 nm completed at 0.7% methanol modifier using a silica column.

However, as discussed previously these conditions were not repeatable or sustainable with the instrumentation. B20 was then analysed using 5% modifier (Figure 3.26). A comparison of modifier percentages displays the better separation obtained using 0.7% modifier, with petrodiesel and biodiesel co-eluting when 5% modifier is used. However, with the addition of mass spectrometry FAMEs can still be identified and extracted (Figure 3.27 and Figure 3.28), this is attributed to the 'invisibility' of petrodiesel using positive ion ESI-MS.

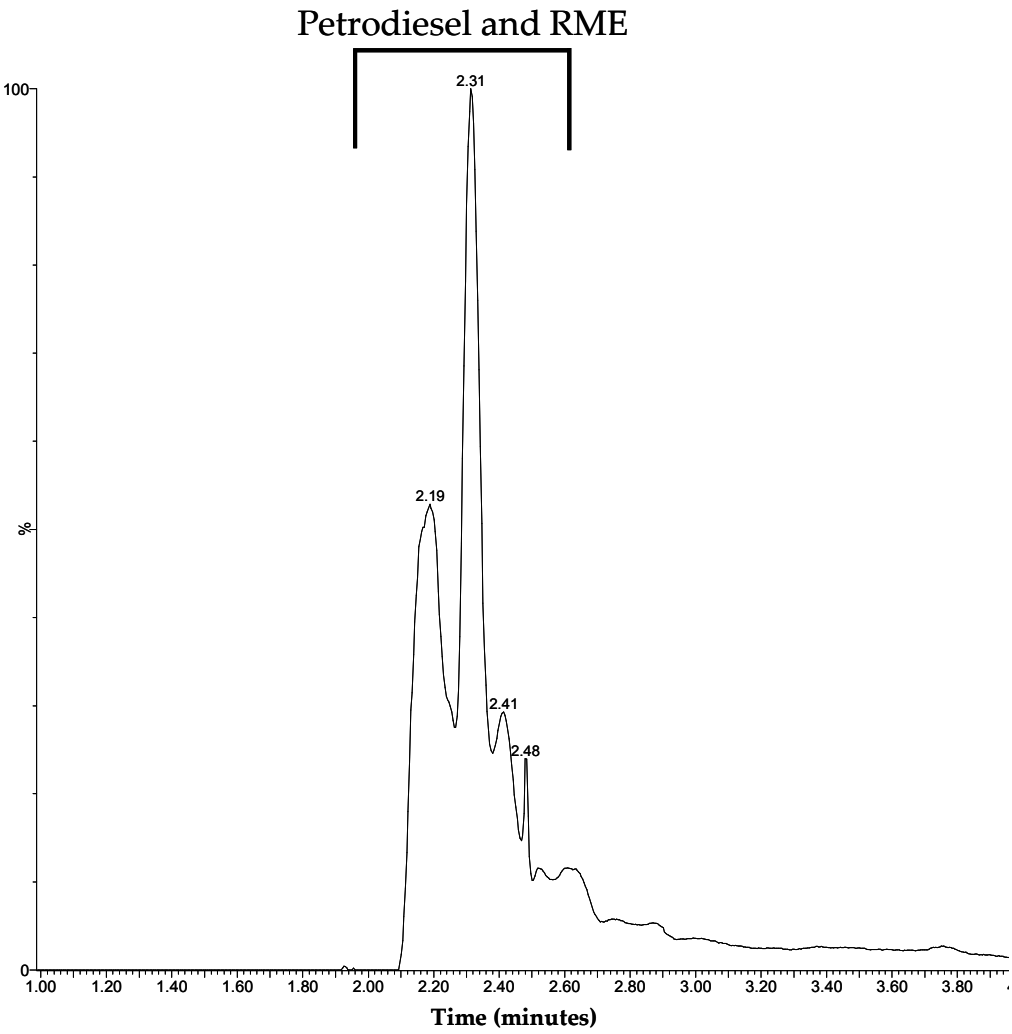


**Figure 3.26:** SFC-UV chromatogram of B20 (RME) at 210 nm completed at 5.0% methanol modifier using a silica column.

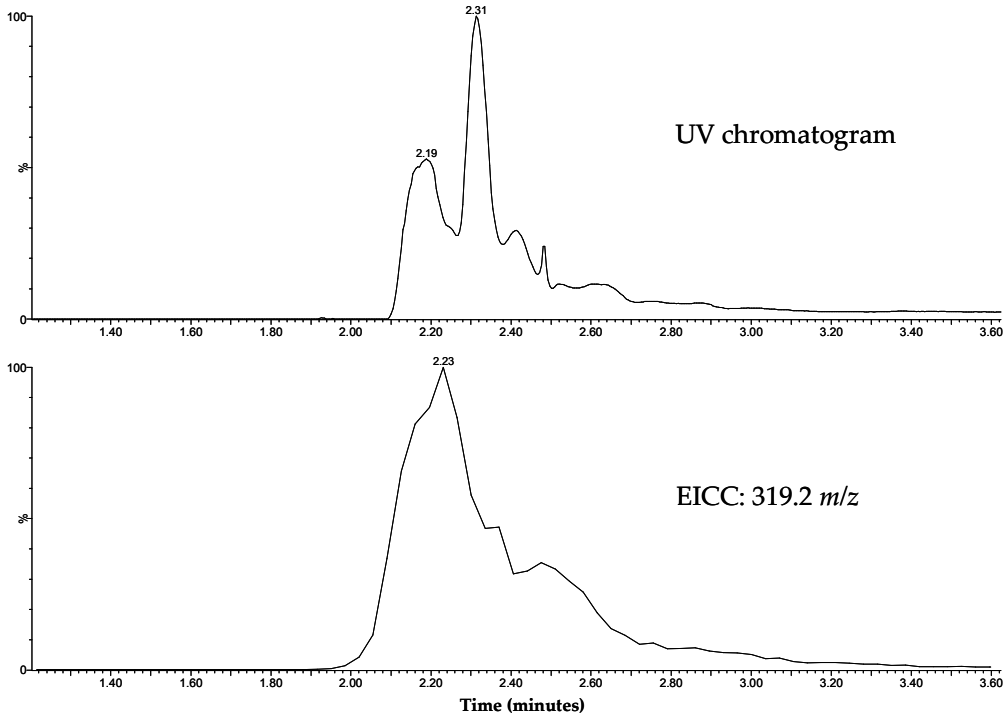


**Figure 3.27:** SFC-UV chromatogram at 210 nm of B20 (RME) (top) and B20 positive ion ESI-SFC MS EICC 319.2 *m/z*, completed at 5.0% methanol modifier using a silica column.

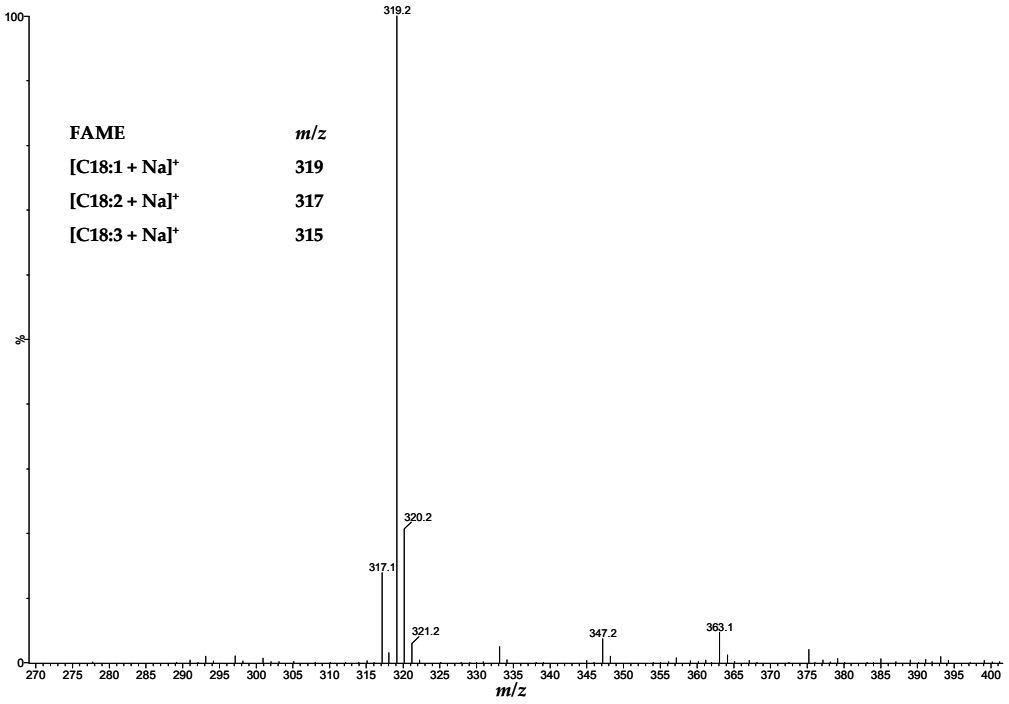


**Figure 3.28:** Positive ion ESI-MS of B20 displaying identification of FAMEs in a co-eluting petrodiesel/biodiesel mixture.

LODs obtained for positive ion-ESI-SFC MS are not as low as GC-MS, with methyl oleate (C18:1), methyl linoleate (C18:2) and methyl linolenate (C18:3) LODs 2.5, 5.0 and 7.5 ng on column respectively. This is not unexpected; firstly analysis was completed using RME (to represent a model RME fuel) in which methyl oleate is present at higher percentages (therefore lower LOD). Secondly FAMEs molecules have different ionisation efficiencies in positive ion-ESI-MS, therefore methyl linolenate is preferentially ionised over methyl oleate and methyl linoleate, and even if present at lower percentages would ionise preferentially.

## Summary

Detailed in this chapter is the use of several analytical techniques used to analyse auto-oxidised RME. GC-MS analyses volatile FAMEs and auto-oxidised products and detects differences between samples of RME auto-oxidised for different amounts of time. However, it is apparent when analysing auto-oxidised RME *via* infusion positive ion ESI-MS and positive ion ESI-FT-ICR MS that GC-MS is limited and does not describe the whole picture. GC-MS does not detect multiply oxygenated species of C18:2 and C18:3 FAMEs and detects C18:1 plus an additional oxygen atom, unlike API-MS techniques which identify a number of multiply oxygenated species for C18:1, C18:2 and C18:3. Detection of polymerised auto-oxidation products is also accomplished using API-MS techniques contrary to GC-MS where increasing volatility of auto-oxidation products limits analysis.

Analysis *via* positive ion ESI-FT-ICR MS exhibits in excess of 5000 ions in auto-oxidised $RME_{4.8}$, compared to GC-MS where ~30 species are observed and $RME_0$ where ~10 FAMEs are observed. The increased number of ions can lead to ion suppression and through the use of chromatography was reduced.

RP-HPLC and SFC were both coupled to MS. Through analysis using these techniques differences between RME and auto-oxidised RME have been identified. Whilst RP-HPLC positive ion ESI-MS separates some auto-oxidation products, RP-HPLC typically uses water and this is not suitable with petrodiesel or lubricant oil. NP-HPLC requires use of solvents that are incompatible with API-MS and was therefore deemed inappropriate for analysis of auto-oxidised RME.

Positive ion ESI-SFC-UV MS partially separates auto-oxidation species and this was completed in less than 10 minutes. SFC-UV MS possesses similar features of NP-HPLC-MS however is compatible with API techniques and does not use large amounts of hazardous solvents, perfectly placed for analysis of RME. The ability of SFC-UV MS to analyse RME and its mobile phase miscibility with petrodiesel and lubricant oil perfectly lend this technique for this analysis. SFC-UV MS is a complementary tool for fuel analysis alongside GC-MS, infusion ESI-MS (LR/FT-ICR) and HPLC-MS; RME and matrices can be detected *via* UV with petrodiesel and lubricant appearing invisible to the mass spectrometer.

# Chapter 4. Biodiesel Oxidation

FAMEs, the major components of biodiesel, are susceptible to auto-oxidation. Studies investigating auto-oxidation of methyl esters have been conducted by Holman and Elmer where it suggested that C18 FAEEs, the FAME counterparts the major components (>70%) of RME, auto-oxidise at a rate of 1:41:98 for C18 1:2:3 respectively.[23] This is not unexpected since FAMEs containing an increasing number of double bonds are likely to react faster due to the reactive nature of the pi bonds.

Biodiesel is composed of varying FAMEs and as previously discussed (Figure 1.3) different feedstock sources have different concentrations of $C_{14}$-$C_{24}$ FAMEs. The different FAMEs and percentage of FAME constituents influence the rate at which biodiesel produced from different feedstock sources degrade. For this study RME, the European standard biodiesel, and at times the pure constituents have been used.

Traditional hydrocarbon fuels can be stored for years before use with negligible if any degradation issues, however RME's susceptibility to auto-oxidation decreases its shelf life. As RME auto-oxidises increasing viscosity is observed, as auto-oxidation extends there is a presence of auto-oxidation products and this is not ideal. Auto-oxidation is also prevalent in engines, with increased temperature an ideal promoter of reactivity. Viscosity increase can be observed in auto-oxidised RME which can prevent proper workings of the engine and contribute to its damage alongside auto-oxidation products.[18, 133-135] For instance, when using high amounts of biodiesel *i.e.* B50/B100, Fontaras *et al.* described an increased wear of some parts

of the engine and postulated that this occurs because: biodiesel partially dissolves the lubricant, which increases friction of moving parts and through production of acidic species, which are formed during combustion (and auto-oxidation).[6, 136] Acidic species are dissolved into the lubricant and this can cause corrosion within the engine.[6, 136]

This chapter reports the investigation into RME at different auto-oxidation stages (ages) *via* a variety of analytical techniques, *i.e*. GC-MS, ESI MS, ESI-FT-ICR MS and SFC-UV MS, discussed in Chapter 3. In addition, this Chapter discusses the detection of auto-oxidation products and how these relate to suggested auto-oxidation pathways and expected products. Auto-oxidation is suggested to be completed *via* a radical pathway. Detection of radicals can be completed using analytical techniques such as electron paramagnetic resonance spectroscopy.[91, 137, 138] However, the purpose of this study is not to specifically investigate the production of radicals, it is to investigate production of auto-oxidation products *via* auto-oxidation of RME.

Ideally, compounds of RME auto-oxidation would be identified which could potentially be used as markers for RME auto-oxidation. These makers could then be used to identify the extent of auto-oxidation in RME and predict remaining shelf life. This project investigated and compared auto-oxidation of RME *via* three different approaches; natural auto-oxidation, forced oxidation mimicking simple RME auto-oxidation in an engine and electrochemical oxidation.

## 4.1. Investigating Natural Auto-oxidation of RME

Natural auto-oxidation occurs when a sample is stored in contact with air at ambient temperatures. To investigate natural auto-oxidation of RME, a sample was stored in contact with air at ambient temperature. As time progressed and the RME sample aged, small aliquots were taken and subsequent auto-oxidation was monitored using the analytical techniques discussed in Chapter 3. For RME and auto-oxidised RME samples a naming system is in place: $RME_x$ where x represents the length of time, in years, that the RME has been oxidised, where 0 denotes fresh RME.

### Depletion of Starting FAMEs

RME is predominantly composed of C18:X FAMEs (Figure 1.3) with other FAMEs present in minor percentages. Investigation using GC-MS shows a decrease in the abundance of C18:1, C18:2 and C18:3 over time, with C18:2 and C18:3 fully depleted (Figure 4.1).

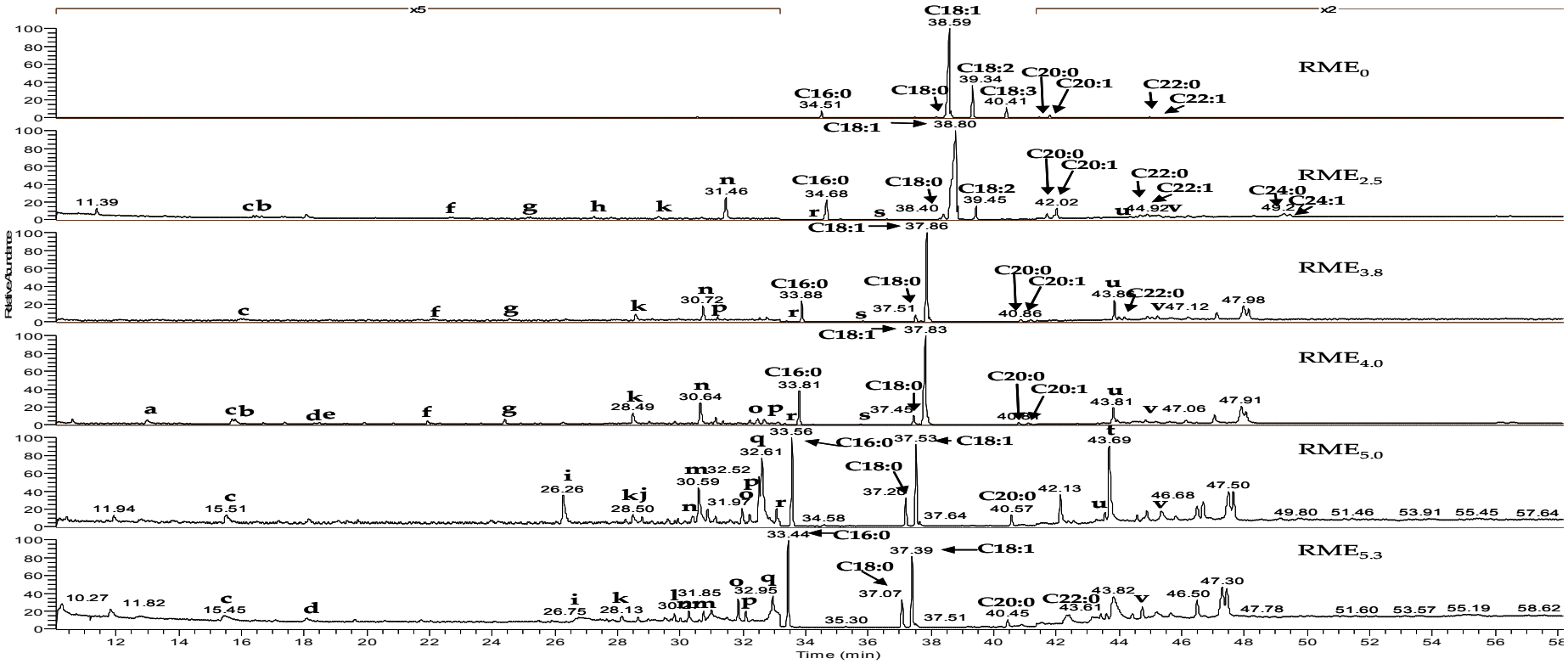


**Figure 4.1:** GC-MS TICCs of $RME_0$, $RME_{2.5}$, $RME_{3.8}$, $RME_{4.0}$, $RME_{5.0}$ and $RME_{5.3}$; $t_R$ 10-33.4 min. expanded x5 and $t_R$ 40.5-60 min. x2.

Where a) octanal, b) nonanal, c) methyl octanoate, d) methyl nonanoate, e) decanal, f) 2-decenal, g) 2-undecenal, h) 2,4-decadienal, i) hexanoic acid, j) heptanoic acid, k) methyl 8-oxooctanoate, l) octanedioic acid dimethyl ester, m) octanoic acid, n) methyl 9-oxononanoate, o) nonanedioic acid dimethyl ester, p) methyl 9-oxodecanoate, q) nonanoic acid, r) methyl 8-hydroxyoctanoate, s) methyl 10-oxo-8-decanoate, t)nonanedioic acid monomethyl ester, u) methyl *cis*-9, 10-epoxystearate, v) methyl 9-oxostearate.

These depletions were also observed using positive ion ESI-MS (Figure 4.2) where ions relating to C18:2 or C18:3 became absent over time. This was especially observed at extended time; as $[C18:1 + Na]^+$ (319 *m*/*z*), $[C18:2 + Na]^+$ (317 *m*/*z*) and $[C18:3 + Na]^+$ (315 *m*/*z*) become extinct, other ions dominate the spectrum (Figure 4.2).

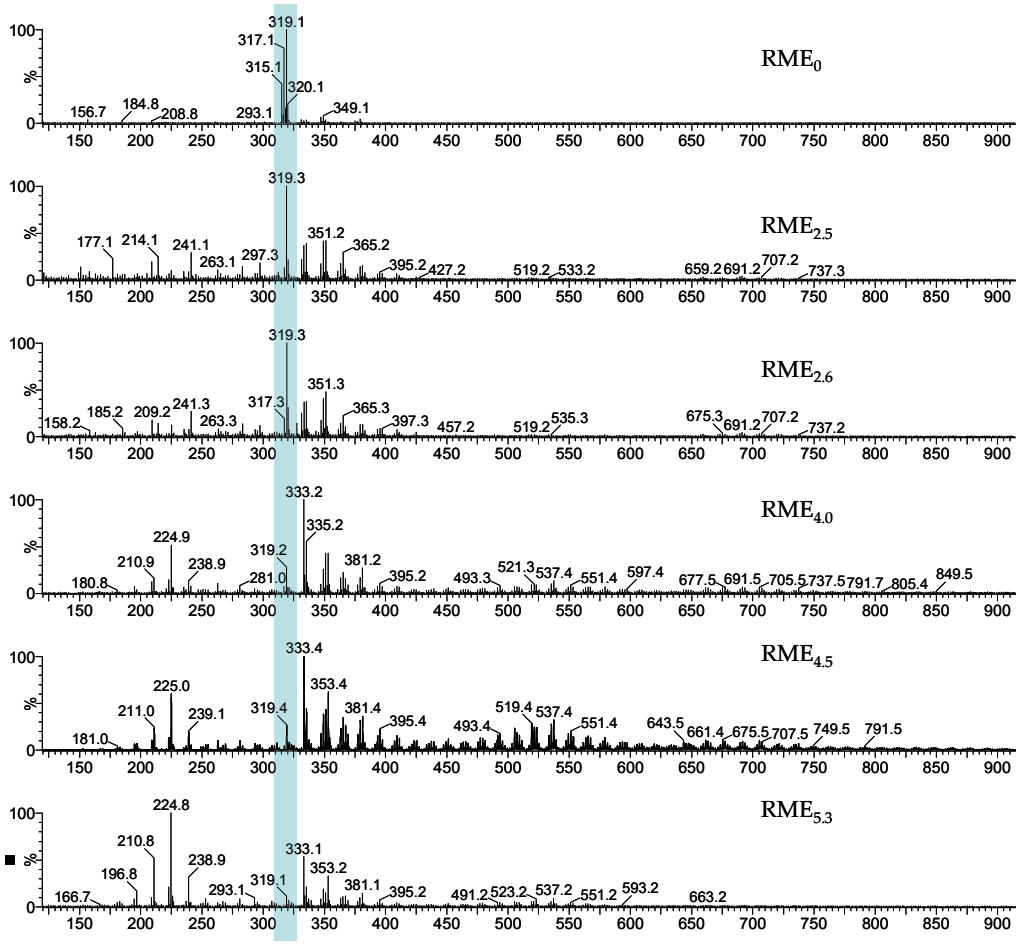


**Figure 4.2:** Positive ion ESI-MS of $RME_0$, $RME_{2.5}$, $RME_{2.6}$, $RME_{4.0}$, $RME_{4.5}$ and $RME_{5.3}$, blue shaded region represents $[M + Na]^+$ of C18:1, C18:2 and C18:3.

Auto-oxidation of saturated FAMEs appears to be a slow process with little percentage change detected for C16:0 and C18:0 (Figure 4.1). Whilst the relative intensity of C16:0 and C18:0 appears to have increased this is a relative issue. The unsaturated FAMEs have

depleted giving this impression whereas C16:0 and C18:0 remain relatively constant throughout (Figure 4.1). This decrease in abundance of the unsaturated FAMEs can be observed in the SFC-MS data, see Figure 4.3. SFC-UV chromatograms of $RME_{1.2}$ and $RME_{4.8}$ when overlaid demonstrate the decrease of C18:1, C18:2 and C18:3 and the constant presence of C18:0 (Figure 4.3).

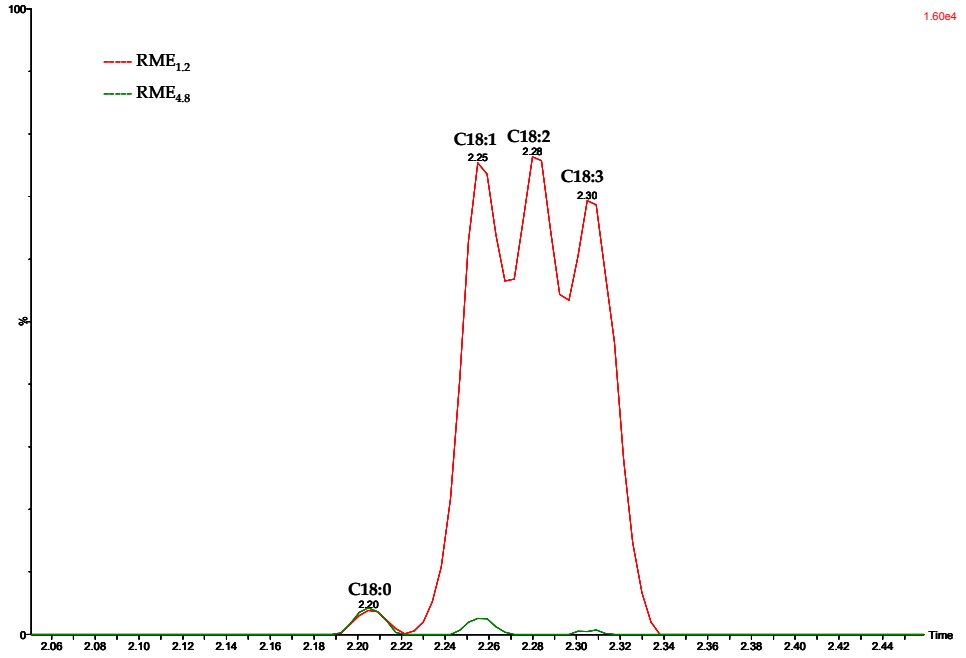


**Figure 4.3:** SFC-UV chromatograms of auto-oxidised $RME_{1.2}$ (red) and $RME_{4.8}$ (green**).**

From the GC-MS data (Figure 4.1) many auto-oxidation products, such as methyl 9-oxononanoate (n) become more pronounced as auto-oxidation progresses. Similarly, ions produced *via* auto-oxidation dominate positive ion ESI-MS spectra obtained using low resolution (Figure 4.2) and high resolution (Figure 4.4) instruments. Ions attributed to auto-oxidation products dominate positive ion ESI-MS spectra because of their increased oxygen content,

which reduces the ionisation potential of these species and are thus preferentially ionised.

Auto-oxidation products initially formed from FAMEs are suggested to be; FAMEs with addition of (multiple) oxygen atoms; smaller chain degradation products; and polymerisation products. Typically, addition of an oxygen atom occurs at a methylene group located next to a double bond. If a FAME contains multiple double bonds it will react faster and potentially many times, this can produce auto-oxidation species that contain multiple oxygens and/or addition of other auto-oxidation products.[22, 23, 139, 140]

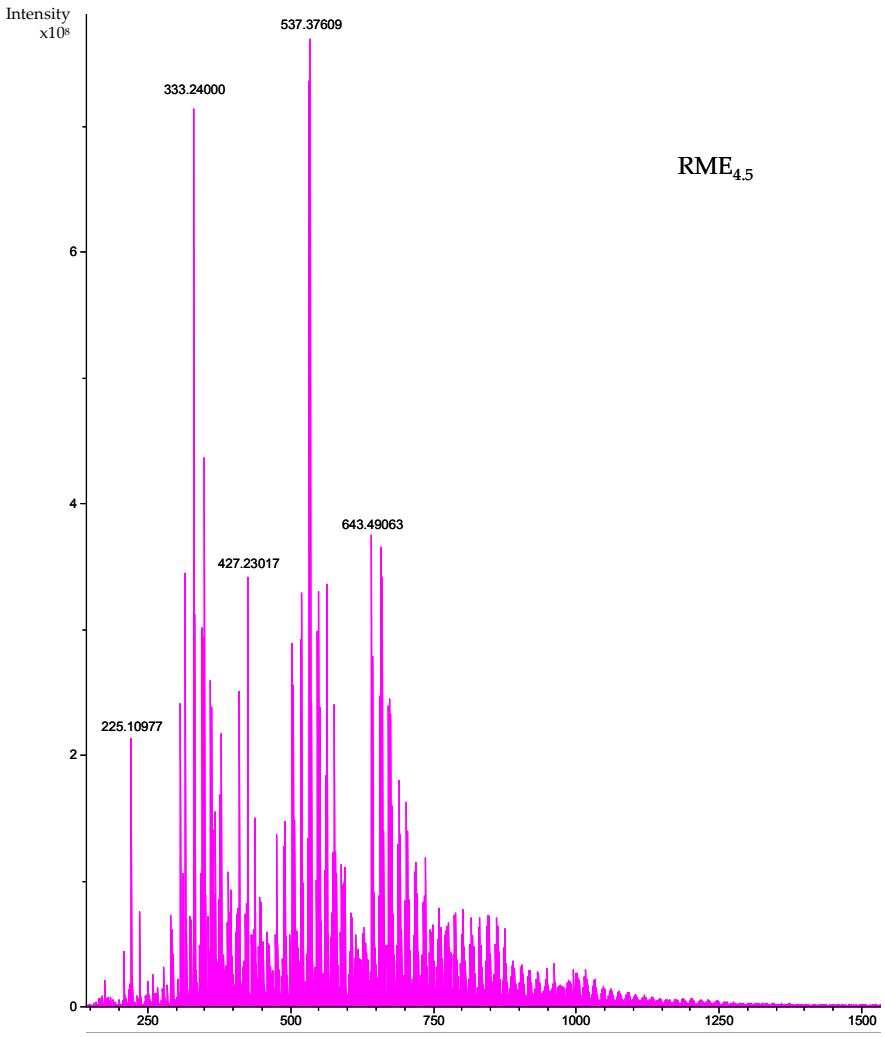


**Figure 4.4:** Positive ion ESI-FT-ICR MS of $RME_{4.5}$.

## Auto-oxidation Pathways

There are three steps to auto-oxidation: initiation, propagation and termination (Equations 4.1-4.5).[22, 139-143] Auto-oxidation of FAMEs is well documented and proceeds *via* a radical pathway producing hydroperoxide (OOH) FAMEs.[22, 139, 140] Through hydroperoxide decomposition many auto-oxidation products are formed including propagating species which continue to react until a stable terminal auto-oxidation product is formed.

*Initiation*

$$RH \xrightarrow{-H^{\cdot}} R^{\cdot} \qquad \text{Equation 4.1}$$

*Propagation*

$$R^{\cdot} + O_2 \longrightarrow ROO^{\cdot} \qquad \text{Equation 4.2}$$

$$ROO^{\cdot} + RH \longrightarrow ROOH + R^{\cdot} \qquad \text{Equation 4.3}$$

$$ROOH \xrightarrow{-OH^{\cdot}} RO^{\cdot} \qquad \text{Equation 4.4}$$

*Termination*

$$RX^{\cdot} + RX^{\cdot} \longrightarrow \text{non-radical species} \qquad \text{Equation 4.5}$$

X= $R'OO^{\cdot}$ or $R'O^{\cdot}$

Production of OOH FAMEs is achieved *via* multiple steps[22, 139, 142] First, hydrogen is abstracted producing a FAME radical and through double bond migration several FAME radical forms are possible (Equation 4.1).[22, 139-141] Through addition of $O_2$ and hydrogen abstraction (Equation 4.2 and 4.3), OOH FAME radicals of each FAME isomer are produced.[22, 139-141] This has been modelled using C18:1 (Figure 4.5) whereby 8-OOH, 9-OOH, 10-OOH and 11-OOH FAME are

produced[22, 139-141] C18:2 and C18:3 produce a number of OOH FAMEs attributed to the number and placement of double bonds within each molecule (Table 4.1).[22, 139, 140] The large number of hydroperoxides which can be formed from three methyl esters alone further complicates an already complex sample.

**Table 4.1:** Auto-oxidation products potentially produced *via* homolytic β-scission of C18:1/C18:2/C18:3 RO·.[22, 140, 144]

| FAME | x-OOH x = FAME position | Potential auto-oxidation products |
|---|---|---|
| C18:1 | 8 | 2-undecenal, C7:0, decanal, methyl 8-oxooctanoate |
| C18:1 | 9 | 2-decenal, C8:0 , methyl 9-oxononanoate, nonanal |
| C18:1 | 10 | methyl 9-oxononanoate, methyl 10-oxo-8 decenoate, nonanal, octane |
| C18:1 | 11 | heptane, methyl 10-oxodecanoate, methyl 11-oxo-9-undecenoate, octanal |
| C18:2 | 9 | 2,4 decadienal, 3-nonenal, C8:0, methyl 9-oxononanoate |
| C18:2 | 10 | 2-octene, 2-octen-1-ol, 3-nonenal, methyl 9-oxononanoate, methyl 10-oxo-8-decenoate |
| C18:2 | 12 | 2-heptenal, hexanal, methyl 9-undecenoate, methyl 12-oxo-9-dodecenoate |
| C18:2 | 13 | 1-pentanol, hexanal, methyl 12-oxo-9-dodecanoate, methyl 13-oxo-9,11, tridecadienoate, pentane, pentanal |
| C18:3 | 9 | 2,4,7-decatrienal, 3,6-nonadienal, C9:0, methyl 9-oxononanoate |
| C18:3 | 10 | 2,5-octadiene, 2,5-octadien-1-ol, 3,6-nonadienal, methyl 9-oxononanoate, methyl 10-oxo-8-decenoate |
| C18:3 | 12 | 2,4-heptadienal, 3-hexenal, methyl 9-undecenoate, methyl 12-oxo-9-dodecenoate |
| C18:3 | 13 | 2-pentenal, 2-penten-1-ol, 2-pentene, 3-hexenal, methyl 12-oxo-9-dodecenoate, methyl 13-oxo-9,11-tridecadienoate |
| C18:3 | 15 | 2-butenal, methyl 9,12-butadecadienoate, methyl 15-oxo-9,12-pentadecadienoate, propanal |
| C18:3 | 16 | ethane, propanal, methyl 15-oxo-9,12-pentadecadienoate, methyl 16-oxo-9,12,14-hexadecatrienoate |

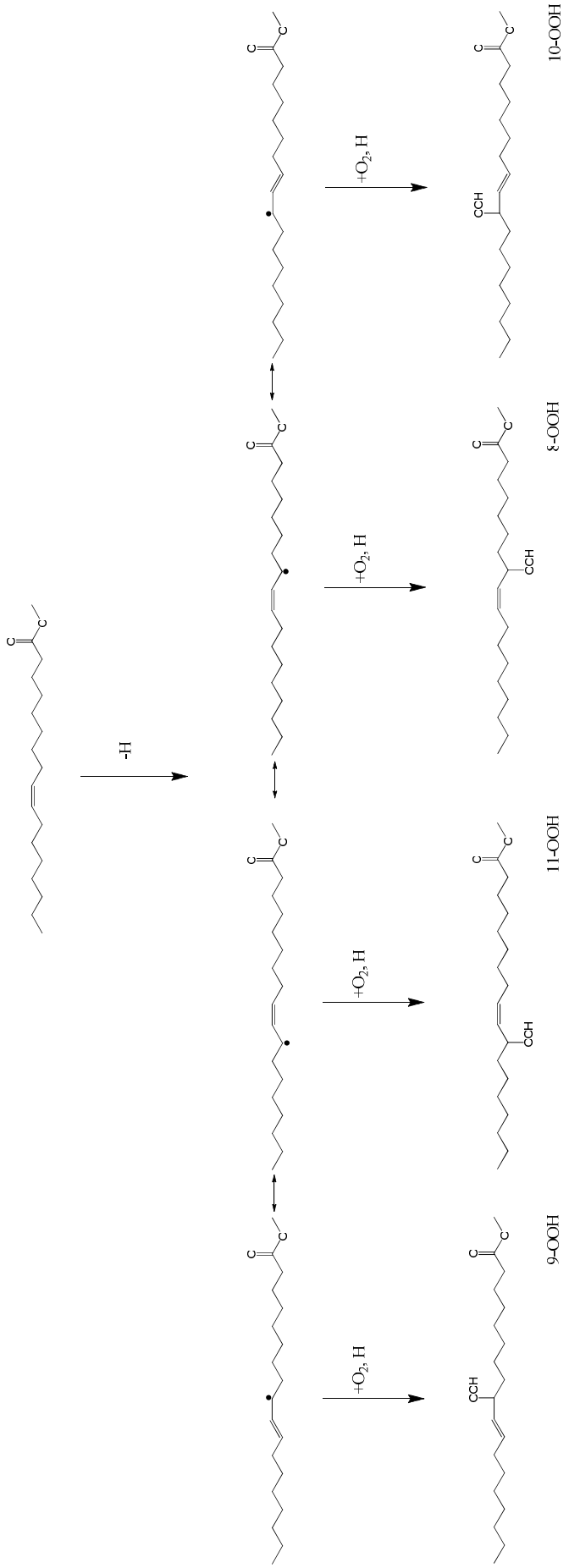


**Figure 4.5:** Auto-oxidation pathway of C18:1 depicting production of 8-OOH, 9-OOH, 10-OOH and 11-OOH FAMEs.[22, 140, 141, 144]

After production of OOH-FAMEs (Figure 4.5) several auto-oxidation routes are suggested to occur. The first auto-oxidation route that will be discussed is an auto-oxidation pathway that produces an epoxide intermediate followed by smaller chain degradation products.[22, 133, 139, 140, 144, 145] Using GC-MS methyl *cis*-9, 10-epoxystearate ($C_{19}H_{36}O_3$, 'u' Figure 4.1) has been detected in all auto-oxidised RME samples except $RME_0$, an example EI mass spectrum and library spectrum are shown in comparison in Figure 4.6.

## Auto-oxidation Pathway *via* an Epoxide Intermediate

Lipid oxidation is an area of interest that has and continues to be researched. Epoxides are produced through lipid oxidation and are found in the human body. Production of epoxides in lipid oxidation are heavily studied, with studies suggesting epoxides play a role in the production of cancerous cells.[146-148] Discussed herein is the identification of an epoxide produced through the auto-oxidation of FAME present in RME.

Initially, as C18:1, C18:2 and C18:3 deplete, methyl *cis*-9, 10-epoxystearate is detected in the GC-MS TICC of samples $RME_{3.8}$ and $RME_{4.0}$ (Figure 4.1). However as time extended the epoxide was observed to be consumed and was depleted in the $RME_{5.3}$. Through the use of positive ion ESI-MS (Figure 4.2) an ion at *m*/*z* 335.2 was observed for the $RME_{5.3}$ sample. Whilst it is suggested that this is methyl *cis*-9, 10-epoxystearate, the structural composition is unknown and therefore this species could additionally be an auto-oxidation compound of the same nominal mass.

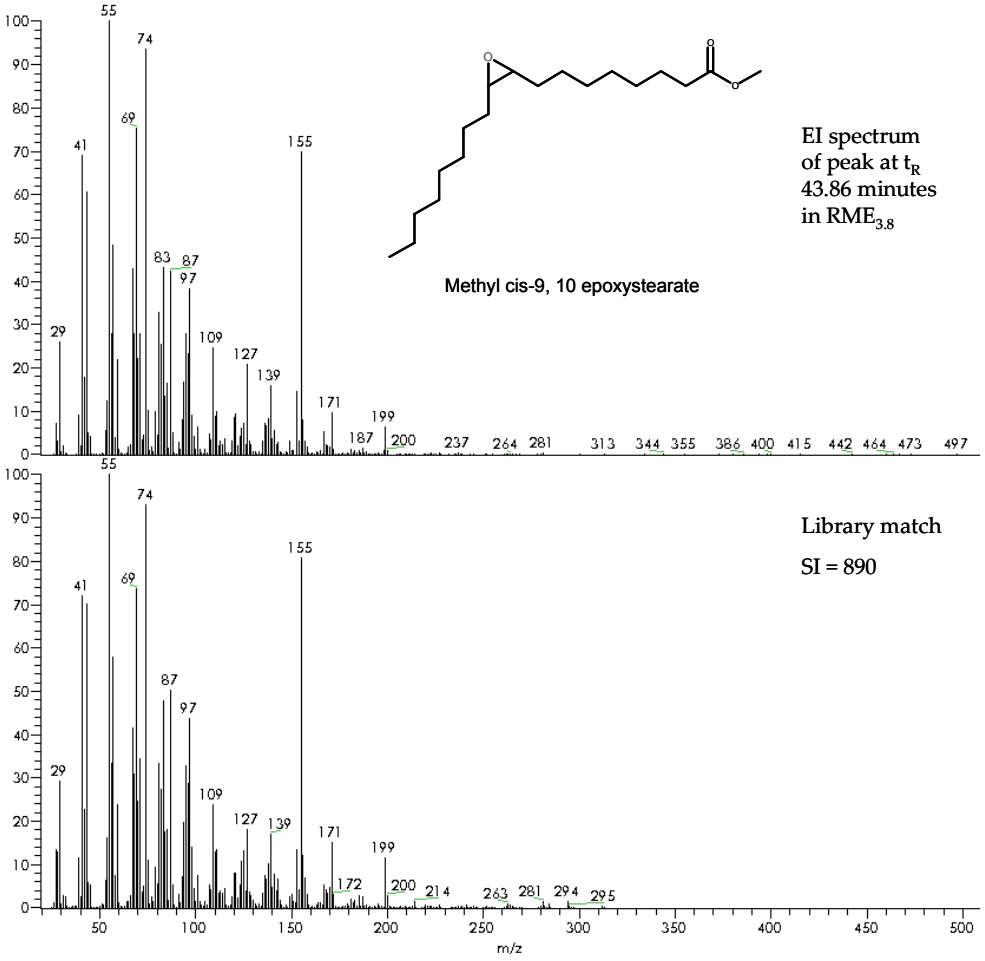


**Figure 4.6:** EI mass spectrum obtained using GC-MS of peak at $t_R$ 43.86 minutes in $RME_{3.8}$ and the resulting library match from the NIST database, consistent with methyl *cis*-9,10-epoxystearate (SI = 890).

Epoxides are formed with loss of $OH^{\cdot}$ and a double bond from OOH FAMEs.[22, 140, 142, 149, 150] Through this route methyl *cis*-9, 10-epoxystearate is observed and is suggested to be produced from C18:1. Potentially, more than one epoxide is produced from auto-oxidation of RME (Figure 4.7). However only methyl *cis*-9, 10-epoxystearate was detected which suggests either other epoxides are not present or are not detected as they are below the LOD. Methyl *cis*-9, 10-epoxystearate can be produced from two different OOH FAME: 9-OOH and 10-OOH (Figure 4.7.)[22, 140, 151]

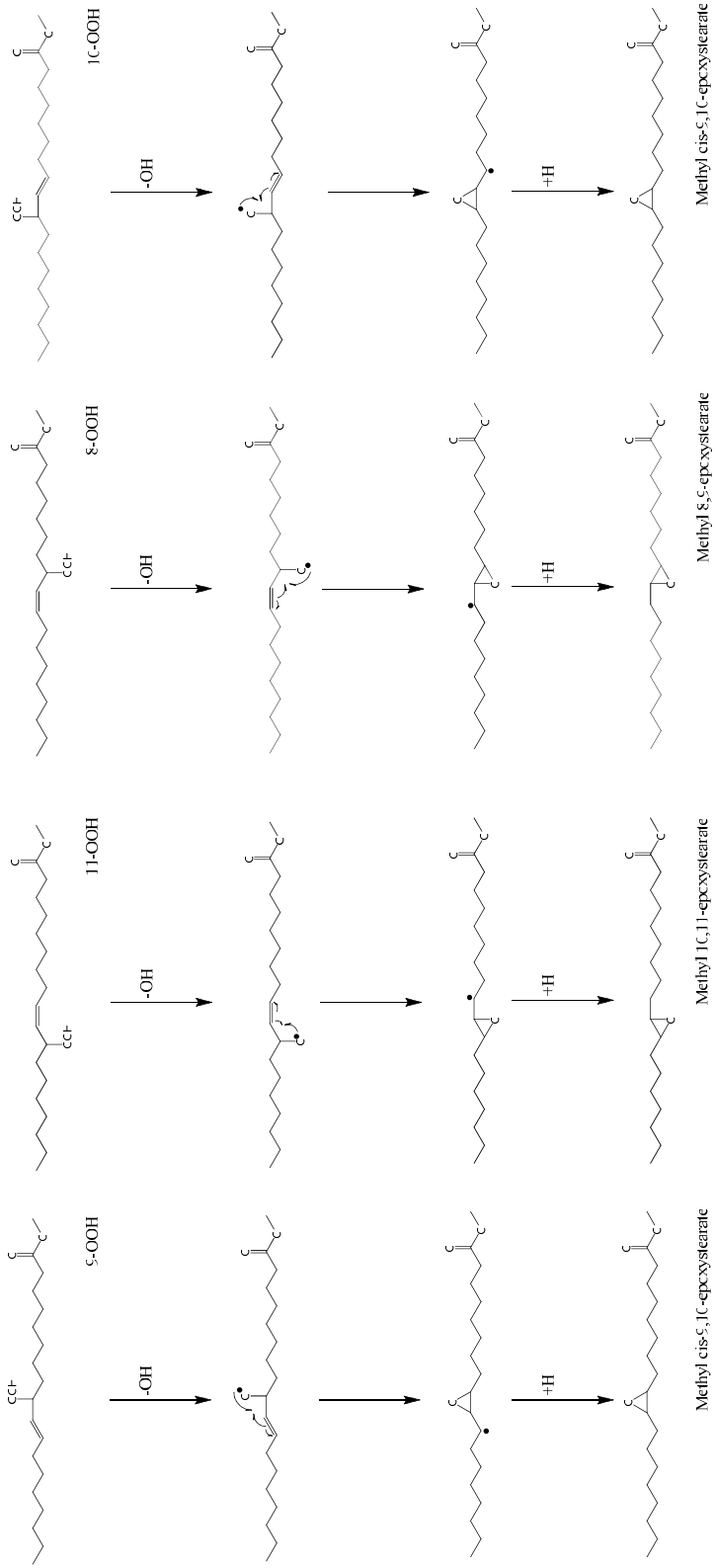


**Figure 4.7:** Auto-oxidation pathway of C18:1 depicting production of epoxides produced from 8-OOH, 9-OOH, 10-OOH and 11-OOH FAMEs.[22, 140, 142, 150, 152]

Positive ion ESI-FT-ICR MS of $RME_{4.5}$ suggested the presence of C18:X FAMEs each with an additional oxygen atom. The following species were observed; $[C18:1 + O + Na]^+$ 335.2556 *m/z* (0.08 ppm error), $[C18:2 + O + Na]^+$ 333.2400 *m/z* (0.06 ppm error) and $[C18:3 + O + Na]^+$ 331.2243 *m/z* (0.10 ppm error) (Figure 4.4). HDX experiments using LR positive ion ESI-MS have allowed the structure of $[C18:X + nO + Na]^+$ to be probed. These experiments have shown that there are species present in auto-oxidised RME, specifically $[C18:X + nO + Na]^+$ species that contain exchangeable *e.g.* OH and non-exchangeable species *e.g.* epoxides and carbonyls.[153] Ions observed at +16 Da from the starting C18:X FAME show little change when diluted in deuterated methanol, this suggest these species to be fixed and are suggested to be epoxides or carbonyl species, this is supported by species observed in GC-MS (Figure 4.1 and Figure 4.6).[153] Ions at +32Da from the starting C18:X FAME show some changes when diluted into methanol and deuterated methanol.[153] Ions present in the spectrum of RME diluted into methanol are still present when RME is diluted into deuterated methanol, however additional ions can be observed in this region, this suggests that these species contain a hydroxyl functional group.[153]

## Detection of Smaller Chain Degradation Products

Epoxides are notoriously unstable and reactive. Epoxide instability leads to production of other auto-oxidation products, including smaller chain degradation products.[22, 140, 142, 150] Some of the smaller chain degradation products were detected using GC-MS and positive ion ESI-MS. Through decomposition of methyl *cis*-9, 10 epoxystearate, the products nonanal ($C_9H_{18}O$) and methyl 9-oxononanoate ($C_{10}H_{18}O_3$) are expected (Figure 4.7) and were detected

using GC-MS (Figure 4.1 'b' and 'n', respectively).[22, 140, 142] These species were successfully matched to EI-MS library entries (Figure 4.8 and Figure 4.9). Methyl 9-oxononanoate was also suggested to be observed using positive ion ESI-FT-ICR MS ($[C_{10}H_{18}O_3 + Na]^+$ 209.1149 *m/z* (0.21 ppm error) Figure 4.4). Additionally, nonanedioic acid monomethyl ester was detected ('t', Figure 4.1; $[C_{10}H_{18}O_4 + Na]^+$ 225.1098 *m/z* (0.18 ppm) error Figure 4.4) which possesses a methyl ester and a carboxylic acid functionality produced *via* 9-OOH and 10-OOH epoxide decomposition pathway (Figure 4.10).[22, 140, 142]

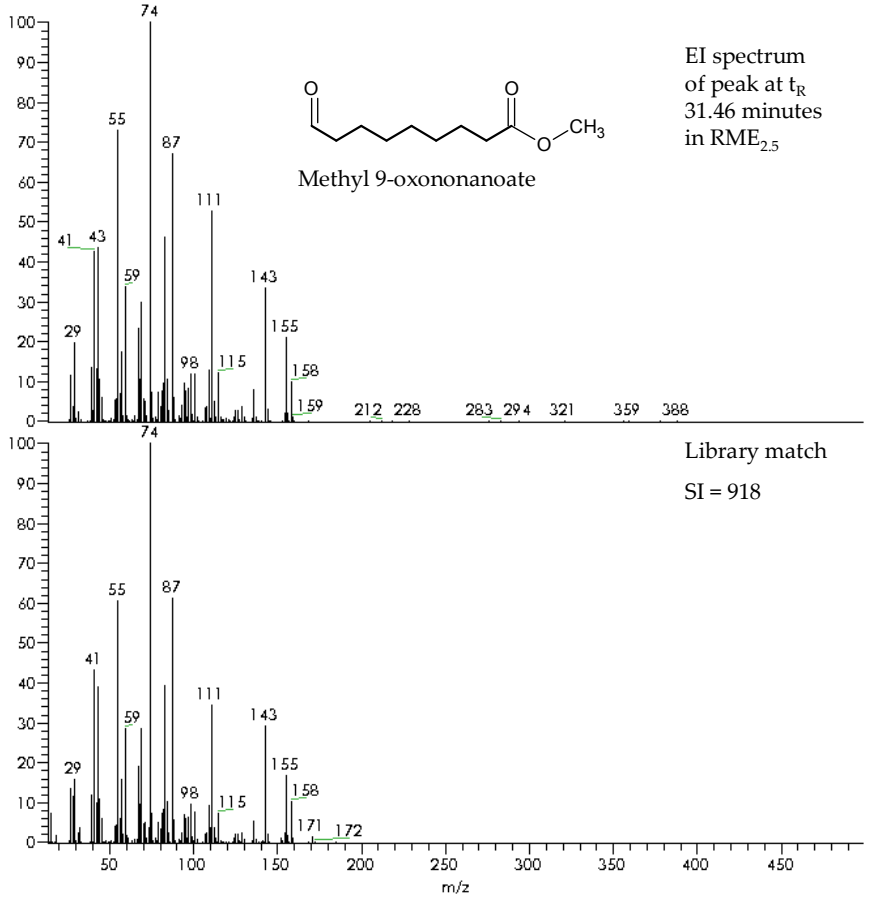


**Figure 4.8:** EI mass spectrum of methyl 9-oxononanoate ('n' in Figure 4.1), obtained using GC-MS of the peak at $t_R$ 31.46 minutes in $RME_{2.5}$ compared to the NIST spectral database spectrum of methyl 9-oxononanoate (SI = 918).

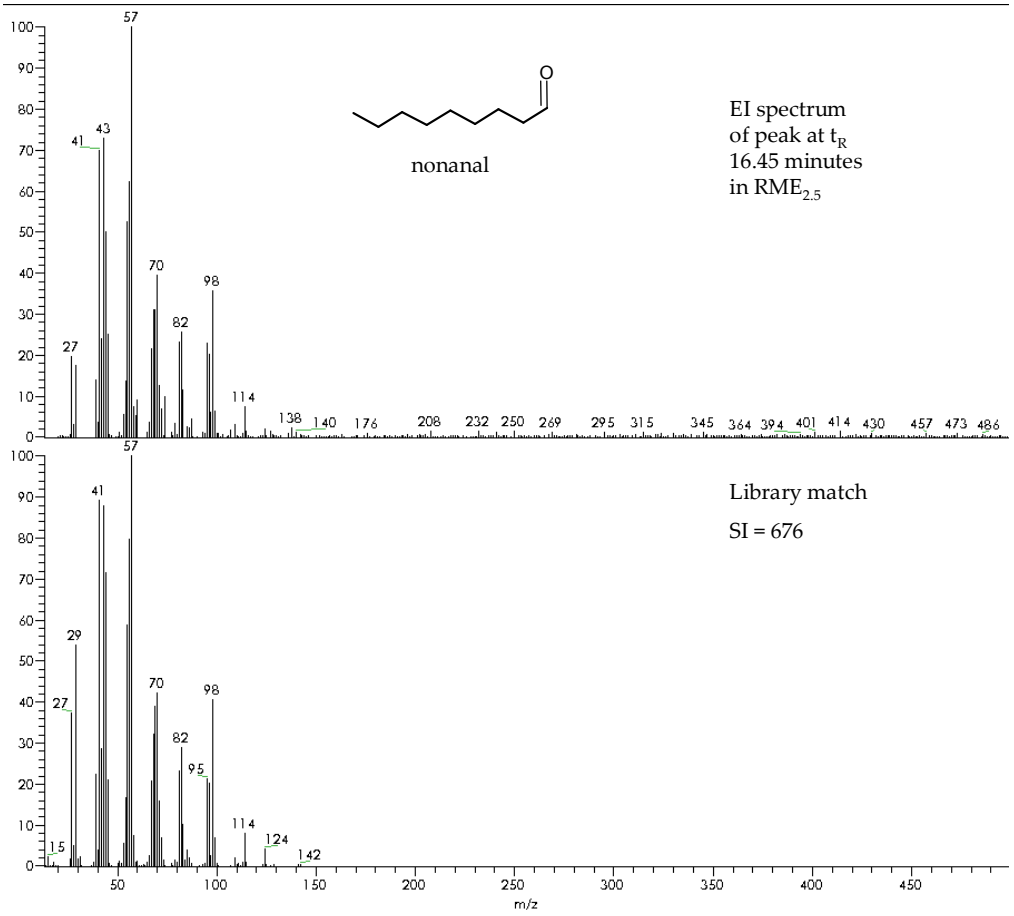


**Figure 4.9:** EI mass spectrum obtained using GC-MS of the peak at $t_R$ 16.45 minutes in $RME_{2.5}$ and the resulting library match from the NIST database suggested to be nonanal 'b' (SI = 676).

Epoxides produced from 8-OOH and 10-OOH C18:1 were not detected, however breakdown products suggested to be produced *via* an epoxide pathway (Figure 4.10) were detected (octanal 'a' Figure 4.1 and methyl 8-oxooctanoate 'k' Figure 4.1; $[C_9H_{16}O_3 + Na]^+$ 195.0993 *m/z* (0.45 ppm error) Figure 4.4). Ions with corresponding molecular formulae of counterpart auto-oxidation species produced *via* 8-OOH C18:1 and 10-OOH C18:1 ($[C_{11}H_{20}O_3 + Na]^+$ 223.1305 *m/z* 0.17 ppm error; $[C_{11}H_{20}O_4 + Na]^+$ 239.1254 *m/z* 0.12 ppm error; $[C_9H_{16}O_3 + Na]^+$ 195.0992 *m/z* 0.45 ppm error; $[C_9H_{16}O_4 + Na]^+$ 211.0941 *m/z* 0.22 ppm

error) were detected using positive ion ESI-FT-ICR MS (Figure 4.4), however they are in small abundance. This suggests either the auto-oxidation route (8-OOH and 11-OOH) is not favoured and therefore counterparts are below the LOD, counterpart auto-oxidation products are involved in extended auto-oxidation or these species are produced *via* an alternate auto-oxidation radical pathway.

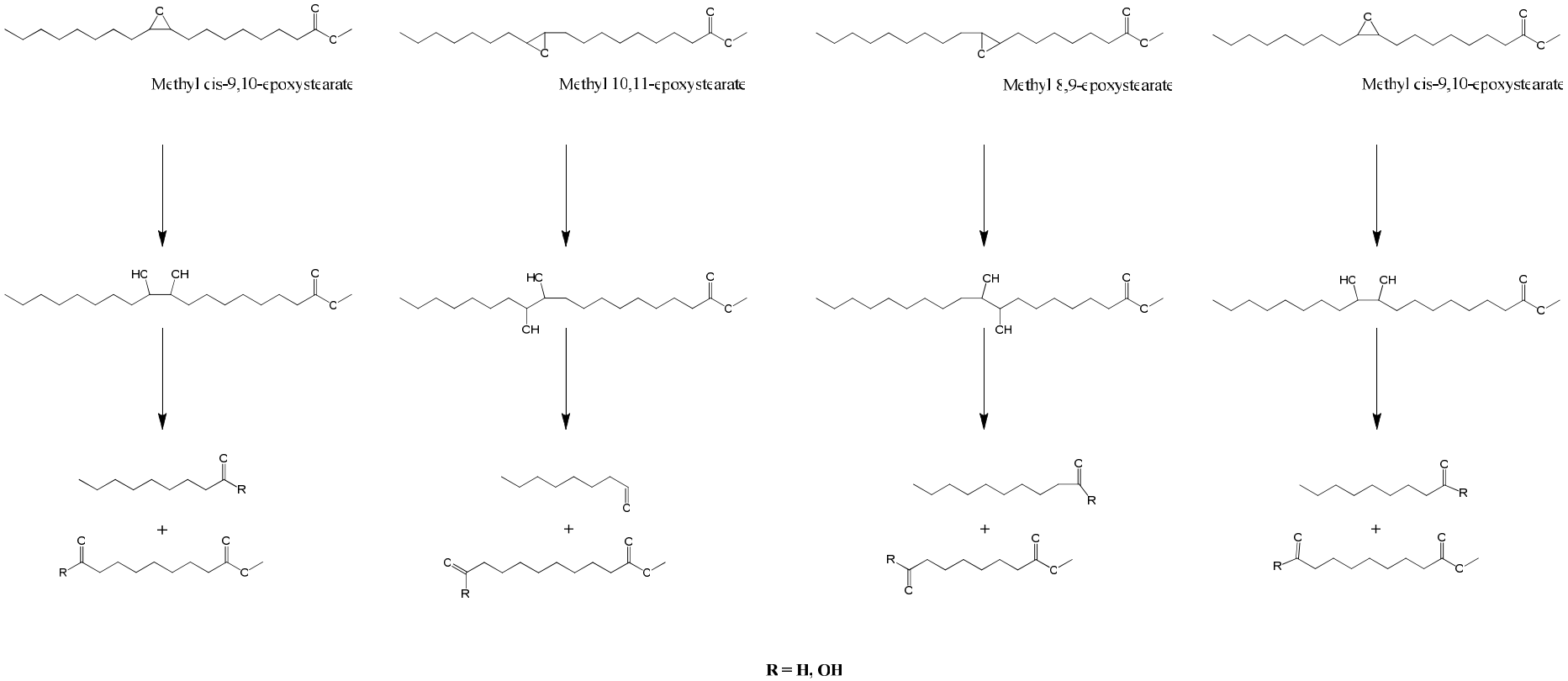


**Figure 4.10:** Auto-oxidation pathways of C18:1 depicting production of small chain degradation products produced from epoxides observed in Figure 4.7.[22, 140, 142, 144, 152, 154]





119

Alongside nonanal, octanal, methyl 8-oxooctanoate and methyl 9-oxononanoate, other smaller chain degradation products were observed that cannot be explained by the C18:1 epoxide pathway route. These products are classified into the following functional groups: shorter FAMEs (<C14), aldehydes, ketones and smaller dual functionality compounds. From the identified auto-oxidation products it is anticipated auto-oxidation markers can be identified that can be used in conjunction with methyl *cis*-9, 10 epoxystearate to indicate extent of auto-oxidation.

FAME <C14:0 are not naturally present in RME (Figure 1.3). Methyl octanoate (C8:0) ('c', Figure 4.1) and methyl nonanoate (C9:0) ('d', Figure 4.1) were detected in auto-oxidised RME using GC-MS. C8:0 was detected throughout, with C9:0 detected in later samples. It is suggested that FAMEs species are produced from an alternate radical pathway (Figure 4.11) compared to the epoxide route (Figure 4.7).[22, 139, 140, 150, 155]

Through homolytic β- scission a variety of auto-oxidation products can be formed, such as smaller chain methyl esters, described here for 9-OOH C18:1 FAME.[22, 139, 140] Auto-oxidation products produced *via* this pathway can further react, propagating the auto-oxidation process.

**Figure 4.11:** Homolytic β-scission of FAME monohydroperoxides produced from auto-oxidation of C18:1 as displayed in Figure 4.7.[22, 140, 144]

Along with smaller chain methyl esters, hexanoic acid ('i' Figure 4.1), heptanoic acid ('j' Figure 4.1 ), octanoic acid ('m' Figure 4.1) and nonanoic acid ('q' Figure 4.1 ) were also detected. These acids are present at later stages of auto-oxidation and their presence can promote auto-oxidation and other reactions through acidic conditions. Additionally acids can cause corrosion of a cars engine and reduce the lifetime of lubricant oil, rubber seals and the engine. By their very nature acids are corrosive and the presence of acids can have damaging consequences if allowed to build up. In an engine lubricant is used that contains various additives to combat acids and other auto-oxidation products. These additives are used to minimise the harmful effects caused by auto-oxidation products. Additives will be discussed further in Chapter 5.

Similar to nonanal other smaller chain aldehydes were detected by GC-MS which are produced through auto-oxidation of RME. Aldehydes detected include: 2-decenal ('f', Figure 4.1), 2-undecenal ('g', Figure 4.1), 2,4-decadienal ('h', Figure 4.1) and decanal ('e', Figure 4.1). These aldehydes were not detected in auto-oxidised RME after 4 years, it is believed these species undergo further auto-oxidation due to the presence of double bonds which still remain in the molecule. It is postulated they undergo addition of oxygen atoms and contribute to the production of polymerised auto-oxidation species, discussed later.

## Dual-functionality Auto-oxidation Products

In addition to mono-functional auto-oxidation products, production of species retaining the methyl ester functionality and gaining an additional functionality, *e.g.* a methyl ester/ketone type

compound, have been detected. These include methyl 8-hydroxyoctanoate ('r', Figure 4.1; $[C_9H_{18}O_3 + Na]^+$ 197.149 *m/z* (0.36 ppm error) Figure 4.4), methyl 10-oxo-8-decanoate ('s', Figure 4.1; $[C_{11}H_{18}O_3 + Na]^+$ 221.1148 *m/z* (0.28 ppm error) Figure 4.4), methyl 9-oxodecanoate ('p', Figure 4.1; $[C_{11}H_{20}O_3 + Na]^+$ 223.1305 *m/z* (0.17 ppm error) Figure 4.4) methyl 9-oxostearate ('v', Figure 4.1; $[C_{19}H_{36}O_3 + Na]^+$ 335.2556*m/z* 0.08 ppm error Figure 4.4), nonanedioic acid dimethyl ester ('o', Figure 4.1; $[C_{11}H_{20}O_4 + Na]^+$ 239.1254 *m/z* (0.12 ppm error) Figure 4.4), and octanedioic acid dimethyl ester ('l', Figure 4.1; $[C_{10}H_{18}O_4 + Na]^+$ 225.1098 *m/z* (0.18 ppm error) Figure 4.4). These additional functionalities ensure these species are beacons of auto-oxidation when analysed using positive ion ESI-MS techniques. Presence of additional functionalities facilitates rapid detection of auto-oxidation products *via* positive ion ESI-MS techniques.

It is postulated that these auto-oxidation species discussed above were produced *via* the epoxide mechanism (Figure 4.10) or by degradation of C18:1, C18:2 and C18:3 species *via* homolytic β-scission (Figure 4.11).[22]

Additionally, primary and secondary peroxyls are suggested to terminate *via* the Russell mechanism. This mechanism has been suggested to operate *via* a transition state produced from two primary or secondary peroxyl radicals, producing a ketone, alcohol and oxygen. [22, 139, 155-157] It is suggested the Russell mechanism could be an alternate pathway for the production of methyl 9-oxostearate ('v', Figure 4.1).This again demonstrates the variety of pathways that FAMEs undergo when auto-oxidising and the resulting complex data (Figure 4.4).

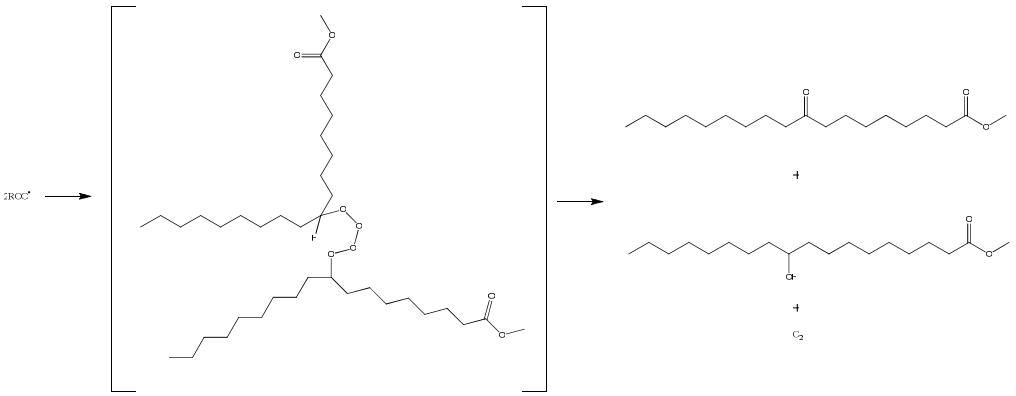

**Figure 4.12:** Russell mechanism observed in auto-oxidation, demonstrated here for 2 9-OO· FAME.[22, 155-157]

Figure 4.4 clearly shows many ions present that cannot be attributed to the auto-oxidation products described above. These ions can be identified and molecular formulae suggested when analysed using positive ion ESI-FT-ICR MS and are undetected using GC-MS.

Small degradation products detected have been compared to auto-oxidation products that could be produced by homolytic β-scission of C18:1, C18:2 and C18:3 (Table 4.2).[22, 140] The majority of degradation products observed using GC-MS relate to decomposition of C18:1. C18:1 is present at 51.0-71.0% (Figure 1.3) in RME and when auto-oxidised produces some of the expected auto-oxidation products. It is suggested that auto-oxidation products that are expected but not detected are below the LOD. Similarly, C18:2 and C18:3 which are present in smaller percentages (15.0-30.0 and 5.0-14.0%, Figure 1.3), expected auto-oxidation products may be below the LOD and not be detected. This is further fuelled by the present of multiple double bonds, which result in more auto-oxidation products, subsequently forming many species of low abundance therefore possibly below the LOD. Positive ion ESI-FT-ICR MS did not detect many smaller degradation products, some of these species were not detected because

the lower mass range was not measured, whilst others are either volatile, below the LOD or not compatible with electrospray ionisation (Table 4.2). However, the data obtained from analysis of auto-oxidised $RME_{4.5}$ contains over 5000 ions (when discounting the $^{13}C$ isotope) (Figure 4.4). These ions are auto-oxidation products of RME and are observed at masses in excess of the starting FAMEs. Auto-oxidation producing methyl *cis*-9, 10 epoxystearate has been previously reported, however auto-oxidation producing FAMEs containing multiple oxygen atoms is evident (Figure 4.2 and Figure 4.4). Epoxides relating to C18:2 and C18:3 FAMEs were not detected using GC-MS, this is possibly linked to the age of samples analysed or to volatility issues.

**Table 4.2:** Comparison of auto-oxidation products expected from homolytic β-scission and those detected *via* GC-MS (Figure 4.1) and positive ion ESI-FT-ICR MS (Figure 4.4).[22, 140]

| **Auto-oxidation product** | **Molecular formula** | **FAME produced from:** | **Detected using GC-MS?** | **Formula detected using positive ion ESI-FT-ICR MS?** |
|---|---|---|---|---|
| 2-undecenal | $C_{11}H_{20}O$ | C18:1 | Y | N |
| C7:0 | $C_8H_{16}O_2$ | C18:1 | N | N |
| Decanal | $C_{10}H_{20}O$ | C18:1 | Y | N |
| methyl 8-oxooctanoate | $C_9H_{16}O_3$ | C18:1 | Y | Y |
| 2-decenal | $C_{10}H_{18}O$ | C18:1 | Y | N |
| C8:0 | $C_9H_{18}O_2$ | C18:1/C18:2 | Y | N |
| methyl 9-oxononanoate | $C_{10}H_{18}O_3$ | C18:1/C18:2/C18:3 | Y | Y |
| Nonanal | $C_9H_{18}O$ | C18:1 | Y | N |
| methyl 10-oxo-8 decenoate | $C_{11}H_{18}O_3$ | C18:1/C18:2/C18:3 | Y | Y |
| Octane | $C_8H_{18}$ | C18:1 | N | N |
| Heptane | $C_7H_{16}$ | C18:1 | N | N |
| methyl 10-oxodecanoate | $C_{11}H_{20}O_3$ | C18:1 | N | Y |
| methyl 11-oxo-9-undecenoate | $C_{12}H_{20}O_3$ | C18:1 | N | N |
| Octanal | $C_8H_{16}O$ | C18:1 | Y | N |
| 2,4 decadienal | $C_{10}H_{16}O$ | C18:2 | Y | N |
| 3-nonenal | $C_9H_{16}O$ | C18:2 | N | N |
| 2-octene | $C_8H_{16}$ | C18:2 | N | N |
| 2-octen-1-ol | $C_8H_{16}O$ | C18:2 | N | N |
| 3-nonenal | $C_9H_{18}$ | C18:2 | N | N |
| 2-heptenal | $C_7H_{12}O$ | C18:2 | N | N |
| Hexanal | $C_6H_{12}O$ | C18:2 | N | N |
| C11:1 | $C_{12}H_{22}O_2$ | C18:2/C18:3 | N | N |
| methyl 12-oxo-9-dodecenoate | $C_{13}H_{22}O_3$ | C18:2/C18:3 | N | Y |
| 1-pentanol | $C_5H_{12}O$ | C18:2 | N | N |
| methyl 13-oxo-9,11, tridecadienoate | $C_{14}H_{22}O_3$ | C18:2 | N | N |
| Pentane | $C_5H_{12}$ | C18:2 | N | N |
| Pentanal | $C_5H_{10}O$ | C18:2 | N | N |

| **Auto-oxidation product** | **Molecular formula** | **FAME produced from:** | **Detected using GC-MS?** | **Formula detected using positive ion ESI-FT-ICR MS?** |
|---|---|---|---|---|
| 2,4,7-decatrienal | $C_{10}H_{14}O$ | C18:3 | N | N |
| 3,6-nonadienal | $C_9H_{14}O$ | C18:3 | N | N |
| C9:0 | $C_{10}H_{20}O_2$ | C18:3 | Y | N |
| 2,5-octadiene | $C_8H_{14}$ | C18:3 | N | N |
| 2,5-octadien-1-ol | $C_8H_{14}O$ | C18:3 | N | N |
| 2,4-heptadienal | $C_7H_{10}O$ | C18:3 | N | N |
| 3-hexenal | $C_6H_{10}O$ | C18:3 | N | N |
| 2-pentenal | $C_5H_8O$ | C18:3 | N | N |
| 2-penten-1-ol | $C_5H_{10}O$ | C18:3 | N | N |
| 2-pentene | $C_5H_{10}$ | C18:3 | N | N |
| 2-butenal | C4H6O | C18:3 | N | N |
| methyl 9,12-butadecadienoate | $C_{15}H_{26}O_2$ | C18:3 | N | N |
| methyl 15-oxo-9,12-pentadecadienoate | $C_{16}H_{26}O_3$ | C18:3 | N | N |
| propanal | $C_3H_6O$ | C18:3 | N | N |
| ethane | $C_2H_6$ | C18:3 | N | N |
| methyl 16-oxo-9,12,14-hexadecatrienoate | C $_{17}H_{26}O_3$ | C18:3 | N | N |

## Detection of Multiply Oxygenated Auto-oxidation Products

Auto-oxidation of FAMEs has been most prevalent in C18:3, with products containing up to 8 additional oxygen atoms detected ($[C18:3 + nO + Na]^+, n \leq 8$) (Table 4.3). C18:3 possess 3 double bonds which are all able to react facilitating increased auto-oxidation and presence of highly oxygenated species, such as $[C18:3 + 8O + Na]^+$. Auto-oxidation products of C18:1 and C18:2 have been identified which contain up to the same amount of additional oxygen atoms

(n≤6) (Table 4.3). A limitation of addition of oxygen atoms is suggested to be steric hindrance. C18:2 possess 2 double bonds and if oxygen atoms added across both double bonds, steric hindrance could limit the size of this group and thus further reactivity. C18:1 possesses only one double bond and therefore the only limiting space factor is the rest of the FAME molecule.

Positive ion ESI-FT-ICR MS data (Figure 4.4) provides no structural information for detected ions, therefore all structures relating to these ions are postulations. It is postulated that auto-oxidation products with multiple oxygen atoms are formed *via* the auto-oxidation routes described, however instead of degradation, these species can form multiply oxygenated auto-oxidation products (Figure 4.13), which can subsequently degrade.[22, 140]

**Table 4.3:** Addition of oxygen atoms auto-oxidation series observed in positive ion ESI-FT-ICR MS (Figure 4.4) for C18:1, C18:2 and C18:3.

| C18:1 | C18:2 | C18:3 |
|---|---|---|
| $C_{19}H_{36}O_2$ | $C_{19}H_{34}O_2$ | $C_{19}H_{32}O_2$ |
| $C_{19}H_{36}O_3$ | $C_{19}H_{34}O_3$ | $C_{19}H_{32}O_3$ |
| $C_{19}H_{36}O_4$ | $C_{19}H_{34}O_4$ | $C_{19}H_{32}O_4$ |
| $C_{19}H_{36}O_5$ | $C_{19}H_{34}O_5$ | $C_{19}H_{32}O_5$ |
| $C_{19}H_{36}O_6$ | $C_{19}H_{34}O_6$ | $C_{19}H_{32}O_6$ |
| $C_{19}H_{36}O_7$ | $C_{19}H_{34}O_7$ | $C_{19}H_{32}O_7$ |
| $C_{19}H_{36}O_8$ | $C_{19}H_{34}O_8$ | $C_{19}H_{32}O_8$ |
| | | $C_{19}H_{32}O_9$ |
| | | $C_{19}H_{32}O_{10}$ |

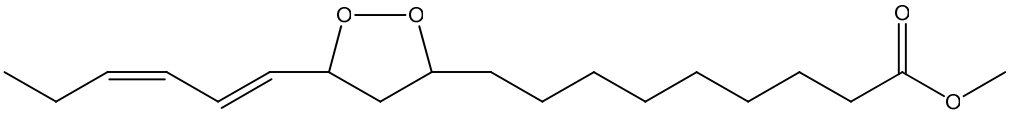

**Figure 4.13:** Suggested multi-oxygen containing species produced from C18:3.[22, 145, 158]

## Detection of Polymerised Auto-oxidation Products

Supplementary to this series was the presence of ions at higher mass range (>400 Da). These higher mass ions are suggested to be polymerised auto-oxidised products. These products were detected using positive ion ESI-MS and positive ion ESI-FT-ICR MS in extended auto-oxidised RME (*e.g.* Figure 4.2 and Figure 4.4). Polymerised auto-oxidised products contain multiple oxygen atoms and, unlike the pre-described series, also contain increased numbers of carbon and hydrogen atoms compared to the starting FAMEs (Figure 1.3). Polymerised auto-oxidised species present were not only detected using positive ion ESI-FT-ICR MS, but were also investigated using APCI-MS. The latter technique detected these ions (Figure 4.14) and confirmed these species to be covalently bonded species present in auto-oxidised RME4.3. This suggests that polymerised auto-oxidation species detected are not a result of the electrospray desolvation/ionisation process.

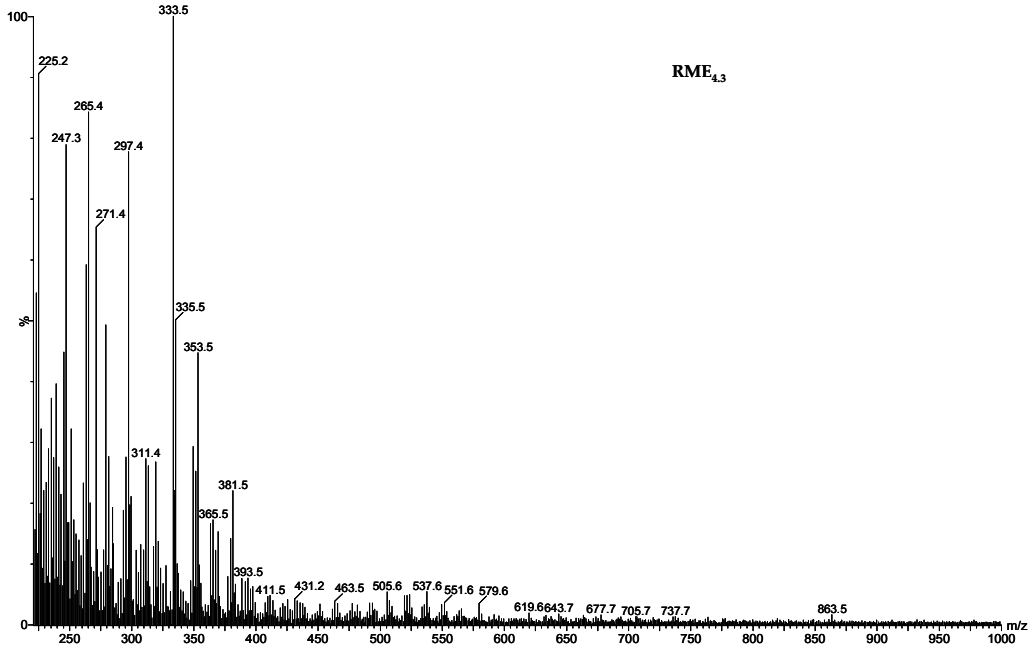


**Figure 4.14:** Positive ion APCI-MS spectrum of $RME_{4.3}$.

Many polymerised auto-oxidation ions were present and will not be discussed here, however a common ion observed throughout MS data of auto-oxidised RME was an ion at 537.4 *m*/*z*. This ion is the base peak in Figure 4.4 and can be more accurately referred to as 537.3761 *m*/*z*. The molecular formulae suggested for this compound is $[C_{29}H_{54}O_7 + Na]^+$, displaying increased C, H and O compared to the starting FAME, as pre-mentioned. Auto-oxidised polymer species have also been detected by Miyashita *et al.*[159, 160], Neff *et al.*[161], Dunn[134] and Khoury *et al.*.[133, 134]

To understand this species better it is necessary to know its structure. Whilst positive ion ESI-FT-ICR MS alone does not provide structural data, the use of tandem mass spectrometry, namely positive ion ESI-FT-ICR MS/MS, can aid elucidation. This technique was applied to analysis of the ion $[C_{29}H_{54}O_7 + Na]^+$ (Figure 4.15).

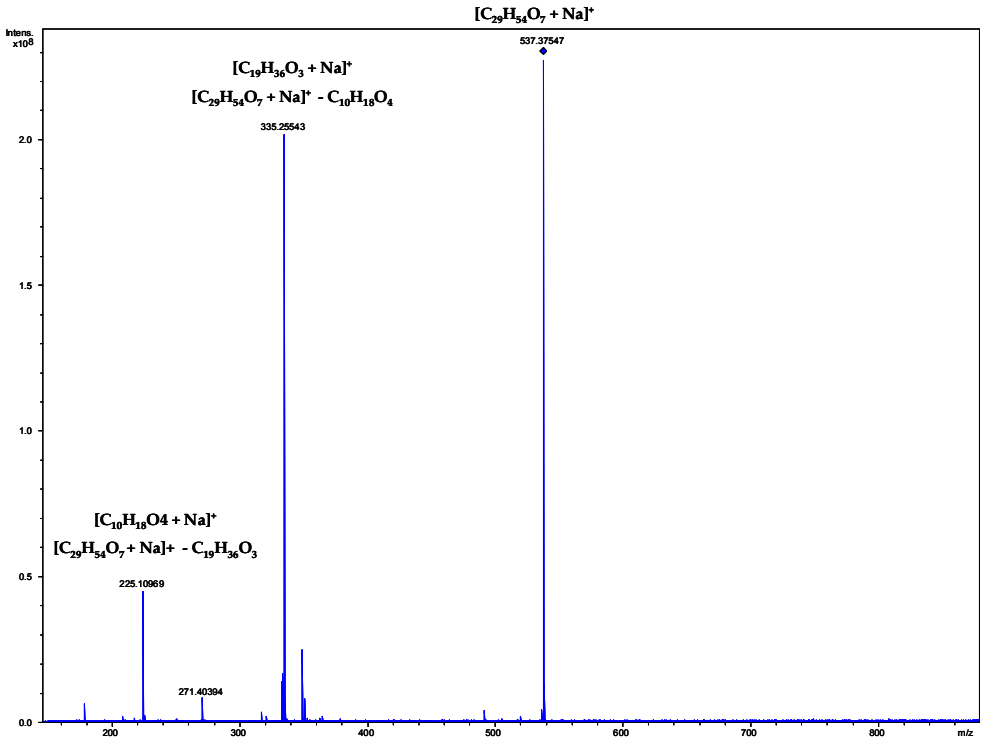


**Figure 4.15:** Positive ion ESI-FT-ICR MS/MS of pre-cursor ion 537.3755 *m/z* $RME_{4.5}$.

Through the use of MS/MS the pre-cursor ion 537.3755 *m/z* was fragmented and information about its structure obtained. Figure 4.15 displays the positive ion ESI-FT-ICR MS/MS spectrum of 537.3755 *m/z* and two distinct product ions were observed: 335.2554 *m/z* and 225.1097 *m/z*. These ions correspond to loss of $C_{10}H_{18}O_4$ and $C_{19}H_{36}O_3$ respectively, which compose the pre-cursor ion. Compounds with these molecular formulae were detected previously: $C_{10}H_{18}O_4$ - nonanedioic acid methyl ester ('t', Figure 4.1; $[C_{10}H_{18}O_4 + Na]^+$ 225.1098 *m/z* 0.18 ppm error Figure 4.4) or octanedioic acid dimethyl ester ('l', Figure 4.1; $[C_{10}H_{18}O_4 + Na]^+$ 225.1098 *m/z* 0.18 ppm error Figure 4.4) and methyl *cis*-9,10-epoxystearate ($C_{19}H_{36}O_3$, 'u' Figure 4.1; [C18:1 + O +Na]$^+$ 335.2556 *m/z* (0.08 ppm error Figure 4.4) or methyl 9-oxostearate. However, no structural data is available for the product

ions and therefore they could be the suggested species or an isomer of these species.

Auto-oxidised polymerisation products only appear limited by steric hindrance, with a molecule with multiple double bonds potentially able to propagate the polymerisation process producing high molecular weight species, *e.g.* Figure 4.16. Species identified in auto-oxidised RME using positive ion ESI-FT-ICR MS (Figure 4.4) contain over $C_{60}$ and $O_{20}$.

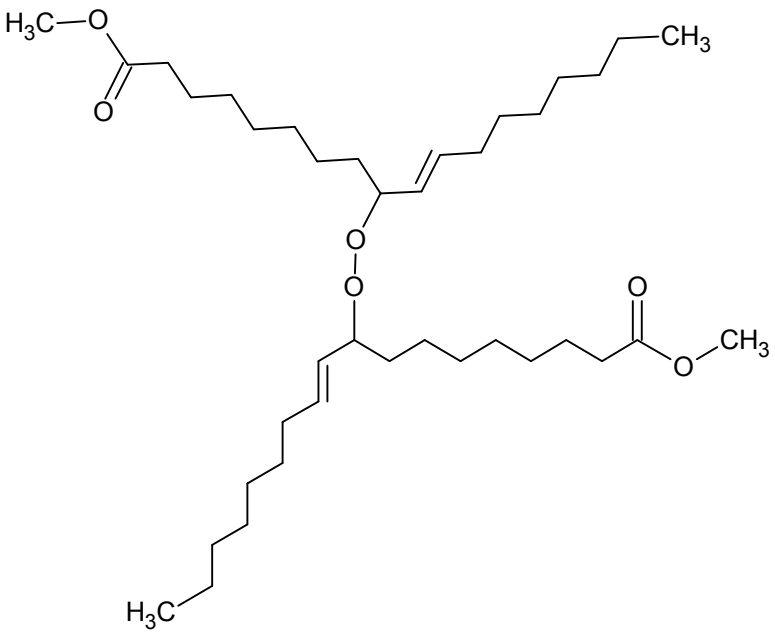


**Figure 4.16:** Suggested auto-oxidation polymer product: $C_{38}H_{35}O_6$, 587.2434 *m/z*.

Polymerised auto-oxidation products are also susceptible to decomposition forming smaller degradation products, such as methyl 9-oxononanoate, which has been a key breakdown product observed throughout analysis. It is believed that polymerised auto-oxidised products, along with the other auto-oxidation products, contribute to the increase in viscosity of aged FAMEs.

Polymerisation auto-oxidation products are suggested to be formed from auto-oxidation radicals. This pathway which occurs at extended auto-oxidation adds to the complexity of analysis, this characteristic of auto-oxidised RME requires instrumentation that can aid analysis of complex data sets. Positive ion ESI-FT-ICR MS is one such instrument, with resolution able to identify several peaks across 1 *m*/*z* unit mass range. An alternate analysis method is the use of chromatography, this not only reduces ion suppression effects but can separate nominally isobaric ions and simplify the mass spectra.

## Investigation of Auto-oxidation of RME Using Positive Ion ESI-SFC-UV MS

Positive ion ESI-SFC-UV MS was used to investigate auto-oxidation of RME. Unlike positive ion ESI-FT-ICR MS this technique utilises a low resolution mass spectrometer which is unable to separate nominal mass isobars. The addition of chromatography will allow compounds that are different species or structural isomers to be separated, as was observed using GC-MS (methyl *cis*-9,10-epoxystearate and methyl 9-oxostearate Figure 4.1).

Positive ion ESI-SFC-UV MS discussed herein was completed using a silica column (250 x 4.6 mm, 5 μm 60 Å). Baseline separation of FAMEs was not required for analysis using this approach. Whilst SFC does not separate the FAMEs, mass spectrometry analysis allows the individual FAMEs to be separated by *m*/*z* values. Instead, the aim of analysis was to separate FAMEs and auto-oxidation products into small groups of ions dependent on the molecules interaction with the column. Separation of auto-oxidation products and FAMEs into small

groups will help reduce ion suppression and enable easier analysis, again with mass spectrometry aiding separation of ions *via* auto-oxidation species and FAMEs ions *m*/*z*. GC-MS is sufficient to identify smaller degradation products as described earlier these products are of low molecular weight (<300 Da) and are readily volatile. However larger auto-oxidation products are not amenable for analysis by GC-MS due to increased molecular weight (>350 Da) and involatile nature, in comparison with smaller degradation products and therefore positive ion ESI-SFC-UV MS was explored as an option for the analysis of these species. Positive ion ESI-SFC-UV MS was preferentially chosen over RP/NP-HPLC-MS. HPLC-MS suffers from some issues when analysing biodiesel, such as, longer retention times, issues of compatibility of mobile phases (RP-HPLC-MS water) with petrochemical matrices and issues of compatibility with API techniques (NP-HPLC-MS). Already discussed is the presence of highly oxygenated species: addition of oxygen atoms to C18:1, C18:2 and C18:3 FAMEs ($[C18:1 + nO + Na]^+$, $[C18:2 + nO + Na]^+$, $[C18:3 + nO + Na]^+$ Table 4.3) and polymerised auto-oxidation products, these were explored using positive ion ESI-SFC-UV MS.

The use of this technique successfully separated RME FAMEs and its auto-oxidation products into small groups of ions (Figure 4.17). Figure 4.17 shows the presence of two composite peaks for $RME_1$ and three composite peaks in $RME_{4.8}$, indicative of more advanced auto-oxidation in $RME_{4.8}$.

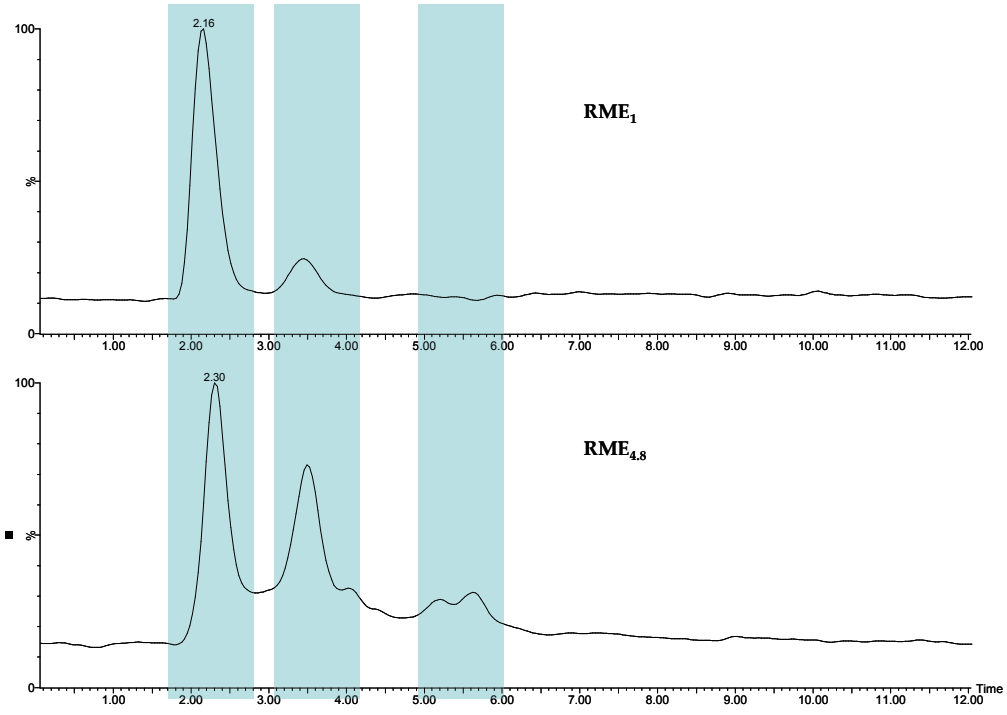


**Figure 4.17:** Positive ion ESI-SFC MS BPIC of $RME_1$ and $RME_{4.8}$.

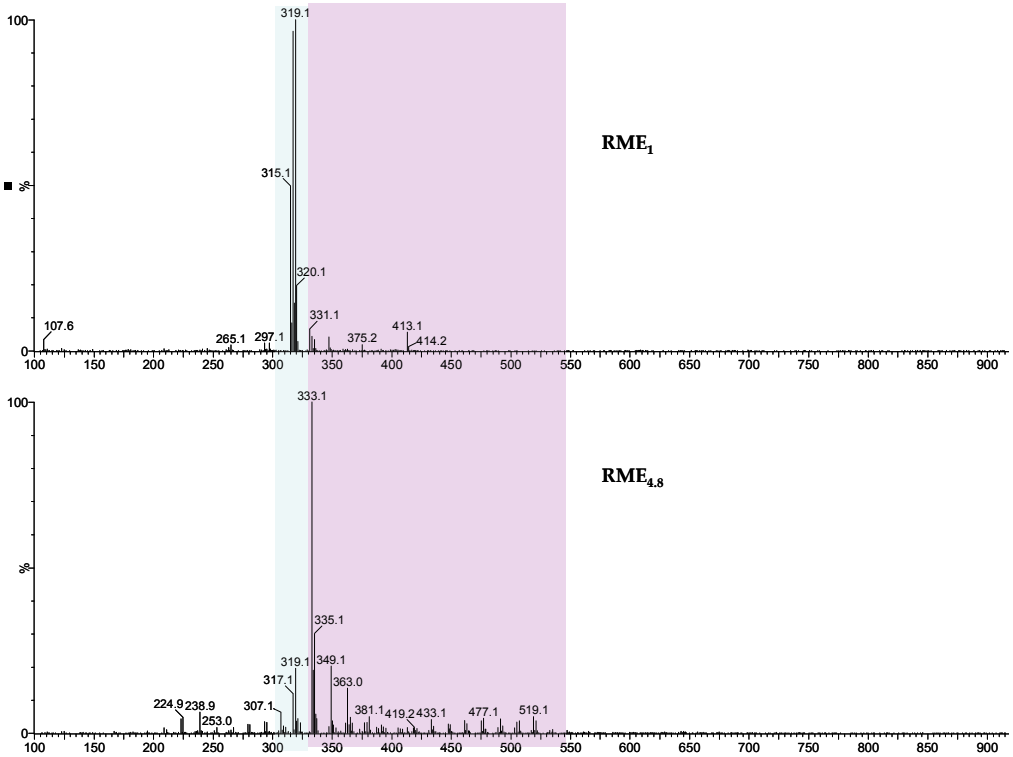


**Figure 4.18:** Positive ion ESI-MS of $RME_1$ and $RME_{4.8}$ first composite peak in Figure 4.17 at $t_R$ 1.8-2.5 minutes, blue highlights $[C18:1 + Na]^+$, $[C18:2 + Na]^+$, $[C18:3 + Na]^+$, purple highlights auto-oxidation products observed.

As can be observed in Figure 4.18, different profiles are obtained from the first composite peak ($t_R$ 2.00-2.75 minutes). Highlighted in blue is the presence of FAMEs C18:1 and C18:2. C18:3 was not detected and this supports data observed throughout and the propensity of C18:3 to auto-oxidise. C18:2 was detected in auto-oxidised $RME_{4.8}$, which is contrary to other MS techniques, with GC-MS (Figure 4.1), positive ion ESI-FT-ICR MS (Figure 4.4) and positive ion ESI-MS (Figure 4.2) not detecting C18:2; this could be attributed to the use of chromatography for reducing ion suppression associated with the electrospray ionisation process.

The purple region highlighted in Figure 4.18, shows the range where auto-oxidation products were expected to be observed. The

mass spectrum of $RME_{4.8}$ shows many products are present in comparison with $RME_1$ (Figure 4.8). Auto-oxidation is in its initial stages in $RME_1$, with only a few ions related to the additional oxygen series observed. Further analysis of this sample suggests it is undergoing auto-oxidation by not only the presence of these ions but also a second composite peak in the positive ion ESI- SFC-UV MS (Figure 4.17). Positive ion ESI-MS (Figure 4.19) suggest the presence of other auto-oxidation products in $RME_1$ and $RME_{4.8}$, with emphasis on smaller degradation products expected again displaying different profiles with ions observed *via* positive ion ESI-FT-ICR MS (Figure 4.1).

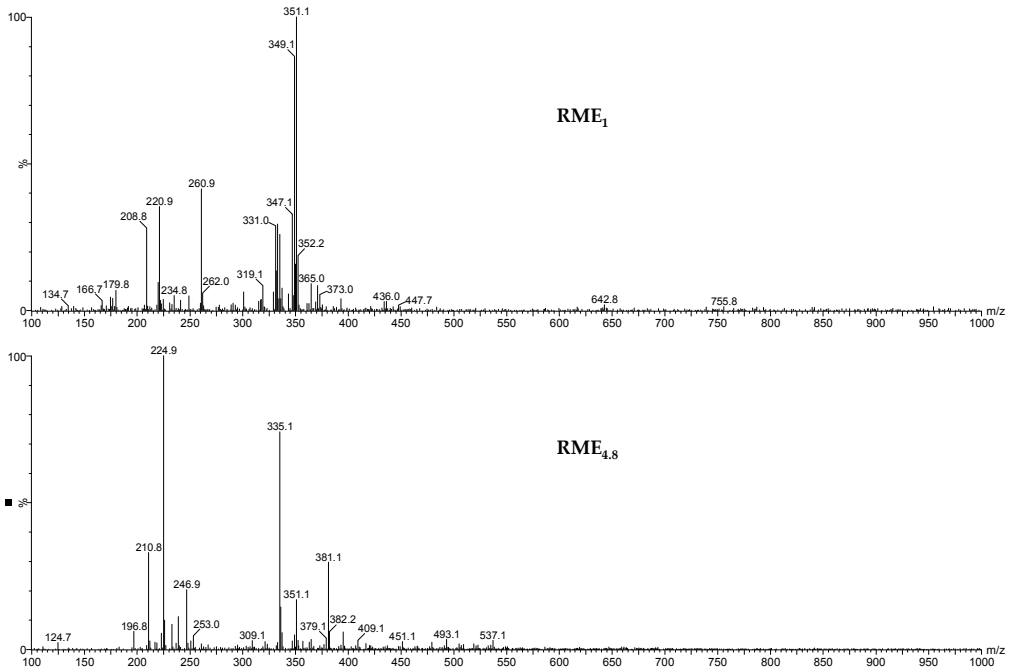


**Figure 4.19:** Positive ion ESI-MS of $RME_1$ and $RME_{4.8}$ second composite peak in Figure 4.17 at $t_R$ 3.2-4.0 minutes of positive ion ESI-SFC MS (Figure 4.17).

$RME_{4.8}$ is auto-oxidised to a further extent than $RME_1$ and it would be expected that more products are present, this was observed

by evidence of a third and fourth composite peak in Figure 4.17 at $t_R$ 5.0-6.0 minutes (Figure 4.20).

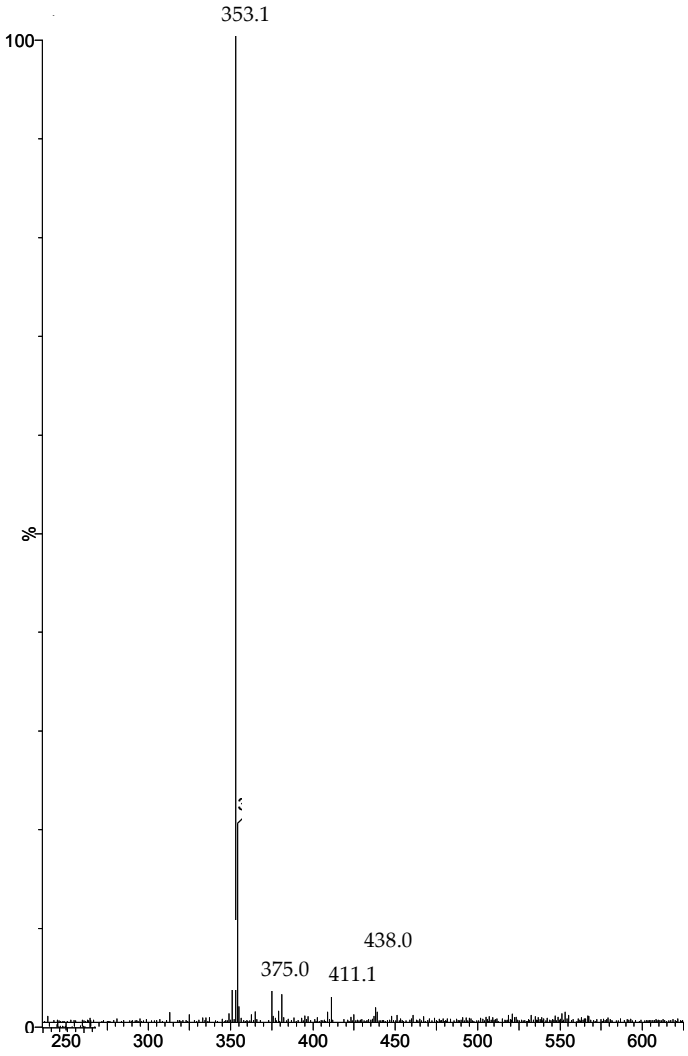


**Figure 4.20:** Positive ion ESI-MS of $RME_{4.8}$ third/fourth composite peak in Figure 4.17 at $t_R$ 5.0-6.0 minutes positive ion ESI-SFC MS (Figure 4.17).

Whilst positive ion ESI-SFC-UV MS was utilised and observed to separate ions into small groups it was also able to aid separation of structural isomers.

The addition of oxygen atoms to C18:1, C18:2 and C18:3 has been discussed and this will be further explored. The masses of

compounds listed in Table 4.3 were extracted from positive ion ESI-SFC-UV MS BPIC as $[M + Na]^+$ species. The resulting EICCs (Figure 4.21, Figure 4.22, Figure 4.23, Figure 4.24, Figure 4.25, Figure 4.26, Figure 4.27, Figure 4.28, Figure 4.29 and Figure 4.30) display the selectivity offered by positive ion ESI-SFC-MS. Individual *m*/*z* values of interest can be extracted from the BPIC and examples of this are displayed below. The mass spectra of positive ion ESI-SFC EICC form part of the aforementioned composite peaks and will not be included (Figure 4.18, Figure 4.19 and Figure 4.20).

In $RME_1$, ions suggested to be $[C18:1 + 3O + Na]^+$ were observed (Figure 4.21). In $RME_{4.8}$, C18:1 with 7 additional oxygen atoms was detected (Figure 4.22). However, using positive ion ESI-FT-ICR MS (Table 4.3) compounds containing 8 oxygen atoms were detected in $RME_{4.5}$. Detection of a lesser number of additional oxygens could be related to reduced sensitivity of positive ion ESI-SFC-UV MS used here, solubility of these species in the mobile phase used ($CO_2$ with 5% methanol modifier), or possible increased polarity of these species. There was also little suggestion that $[C18:1 + 5O + Na]^+$ and $[C18:1 + 6O + Na]^+$ were detected using positive ion ESI-SFC-UV MS, possibly due to the decreased sensitivity of SFC positive ion instrumentation compared with positive ion ESI-FT-ICR MS.

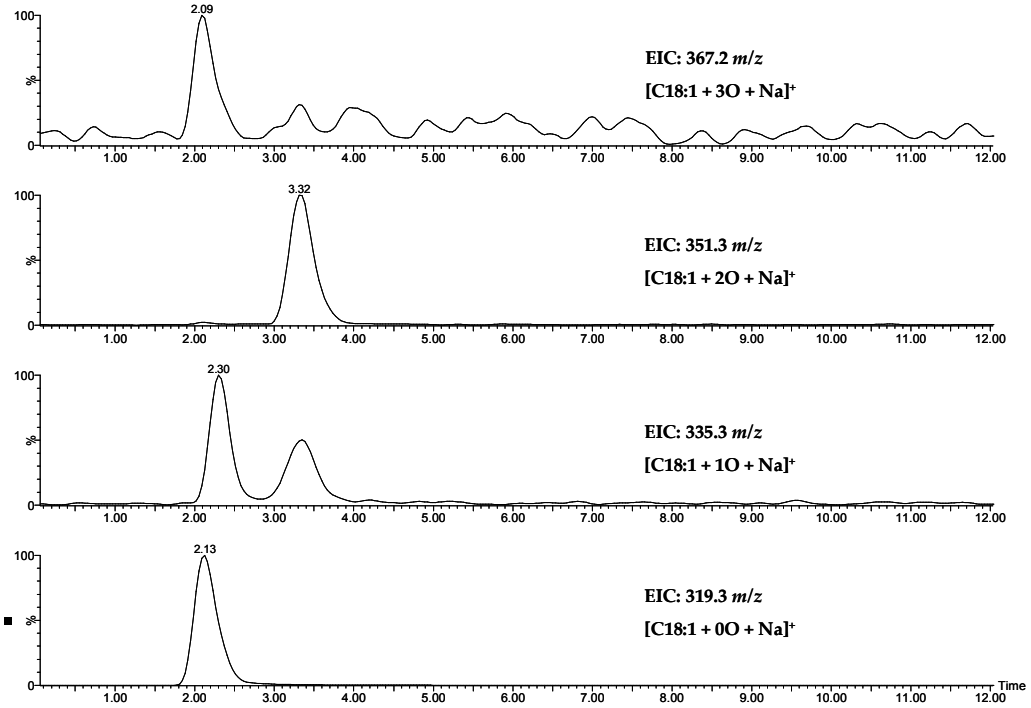


**Figure 4.21:** Positive ion ESI-SFC MS EICC of 319.3, 335.3, 351.3 and 367.2 *m*/*z* postulated to be $[C18:1 + nO + Na]^+$ in $RME_1$ where n = 0-3.

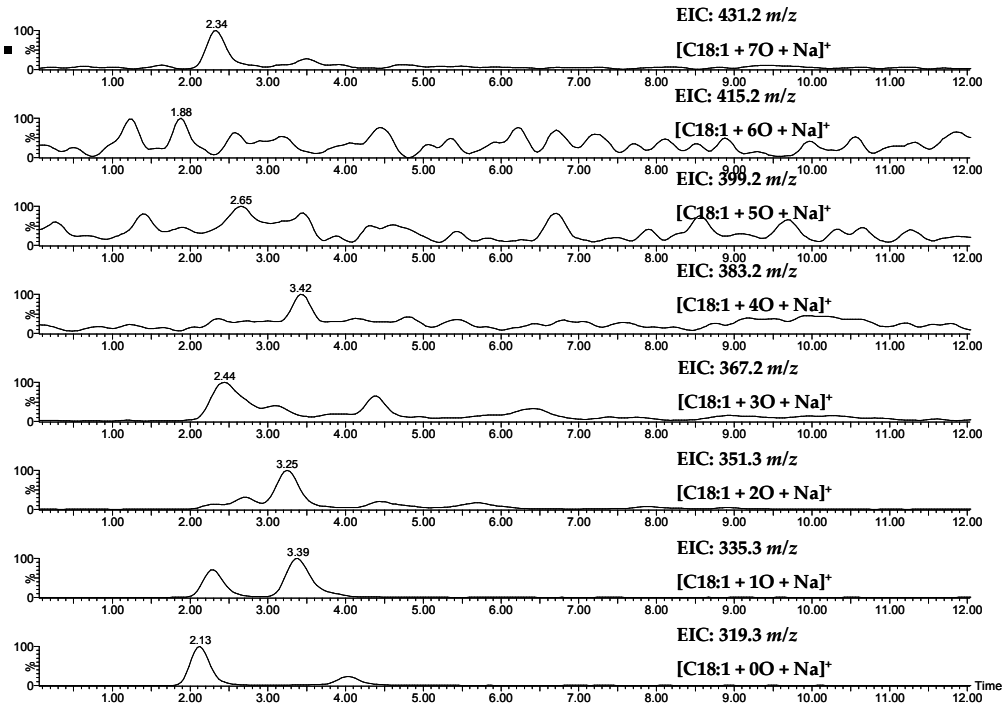


**Figure 4.22:** Positive ion ESI-SFC MS EICC of 319.3, 335.3, 351.3, 367.2, 383.2, 399.2, 415.2 and 431.2 *m*/*z* postulated to be $[C18:1 + nO + Na]^+$ in $RME_{4.8}$ where n = 0-7.

Multiple peaks were observed in some EICCs *i.e. m/z* 319.3, 335.3, 351.3 and 367.2, with the EICC of *m/z* 335.3 showing most clearly two distinct peaks ($t_R$ 2.30 min. and $t_R$ 3.39 min.), stressing the necessity of chromatography for analysis of auto-oxidation of RME. Comparison of EICC of this ion in $RME_1$ and $RME_{4.8}$ (Figure 4.23) displays different abundances of each peak at the different stages of auto-oxidation. Positive ion ESI-SFC-UV MS EICC suggests the presence of two isomers in auto-oxidised RME and further suggests that over time a different mechanism exists in which the production of one of these species is favoured or alternatively is consumed by further auto-oxidation pathways.

GC-MS analysis of auto-oxidised RME (Figure 4.1) identified two structural isomers; methyl *cis*-9,10-epoxystearate and methyl 9-oxostearate, which are C18:1 with an additional oxygen atom. These compounds contain different functional groups and it is expected they will behave differently when interacting with the silica stationary phase. Epoxidation of FAMEs is suggested to occur initially, followed by degradation and addition of multiple oxygens through auto-oxidation. Therefore it is suggested methyl *cis*-9,10-epoxystearate elutes first ($t_R$ 2.30 min.) and methyl 9-oxostearate second ($t_R$ 3.39 min.).

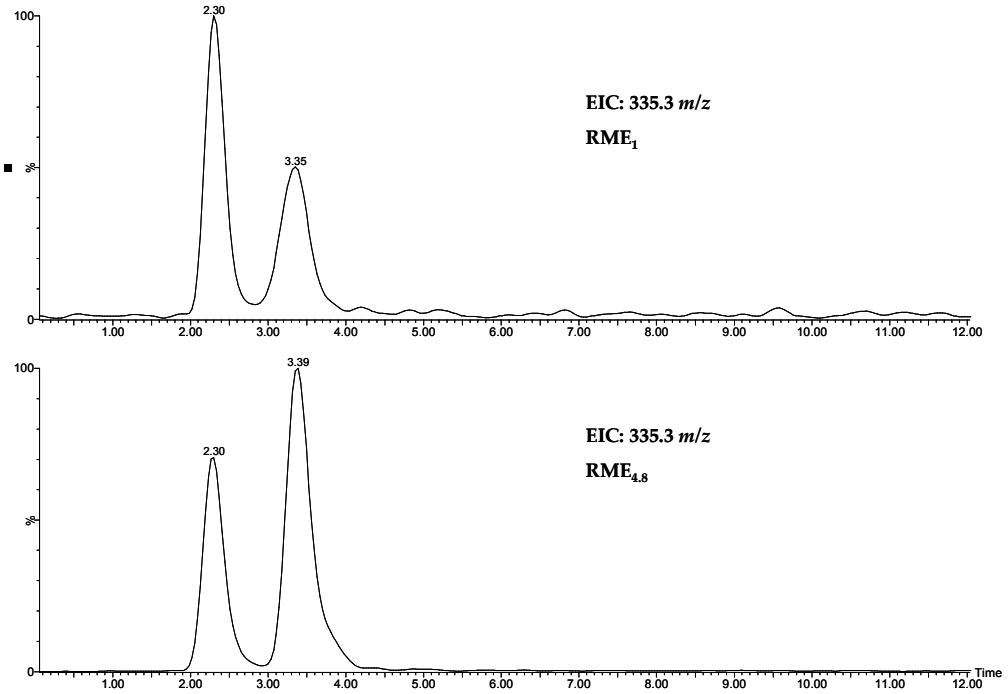


**Figure 4.23:** Positive ion ESI-SFC MS EICC of 335.3 *m/z* postulated to be $[C18:1 + 1O + Na]^+$ in $RME_1$ and $RME_{4.8}$.

EICCs for auto-oxidation compounds identified which are suggested to be formed from C18:2 (Figure 4.24 and Figure 4.25) and C18:3 (Figure 4.27 and Figure 4.28) display similar characteristics.

An increased number of C18:2 auto-oxidation products were detected in $RME_1$ (Figure 4.24) compared with C18:1 (Figure 4.21). However, this is still limited in comparison with multiple oxygenated species detected *via* positive ion ESI-FT-ICR MS ; $[C18:2 + 6O + Na]^+$ is detected in $RME_{4.8}$ using positive ion ESI-SFC-UV MS compared with compounds containing an additional 8 oxygen atoms (Table 4.3) detected in $RME_{4.5}$ using positive ion ESI-FT-ICR MS. As observed in C18:1 (Figure 4.23) two auto-oxidation products suggested to be $[C18:2 + 1O + Na]^+$ were detected ($t_R$ 2.34 and 3.40 minutes) (Figure 4.24 and Figure 4.25), with the latter not detected in 4.8 years, this is different compared to $[C18:1 + 1O + Na]^+$. No structural data is available for auto-oxidation species relating to C18:2 and C18:3. C18:2 possess two

double bonds which increases the potential number of auto-oxidation products which could be formed. This is highlighted in Figure 4.26 whereby 3 species of the same nominal mass (349.2 *m*/*z*) were observed, with depletion of two of these species observed over time.

Alternatively these species could be produced from addition of water across a double bond achieved through the presence of lone pairs on the water molecule. The addition of water across a double bond produces a FAME with an alcohol functionality and an ion +18Da would be observed. The alcohol functionality (R-OH) is considered exchangeable and can be identified through HDX experiments *via* the increase in *m*/*z* of H exchanged for D on alcohol (exchangeable) functionality. Whilst ions in this region are observed, HDX experiments demonstrate that ions identified at 331-337 *m*/*z* are composed of an oxygen atom functionality that is non-exchangeable.[153] Therefore it is postulated that these species are primarily epoxides and/or carbonyl functionality FAMEs not produced from water addition across the double bond.

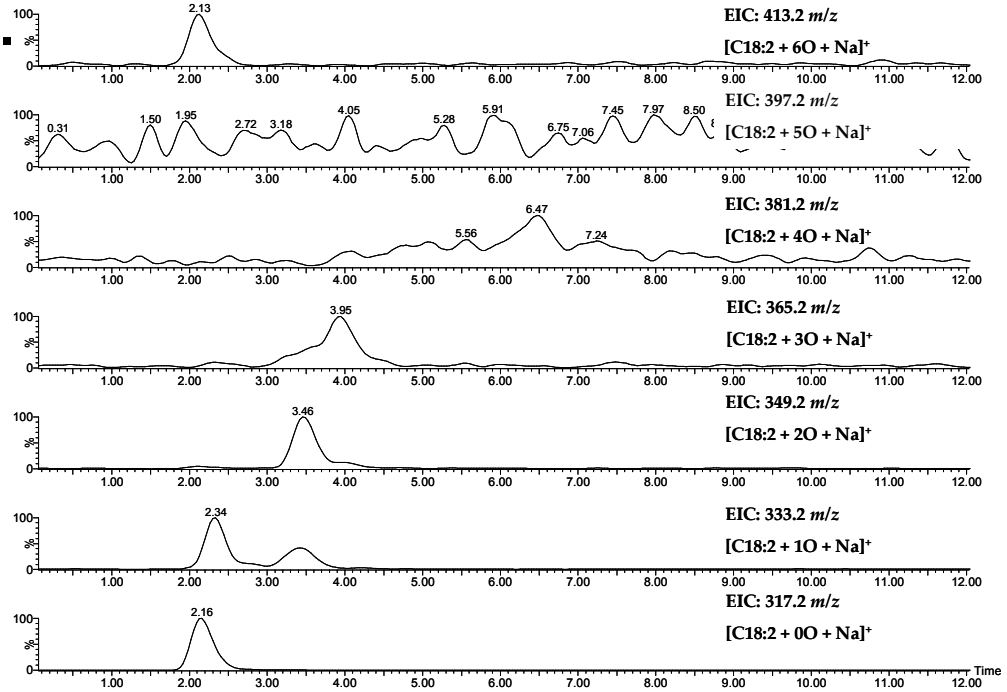


**Figure 4.24:** Positive ion ESI-SFC MS EICC of 317.2, 333.2, 349.2, 365.2, 381.2, 397.2 and 413.2 *m*/*z* postulated to be $[C18:2 + nO + Na]^+$ in $RME_1$ where n = 0-6.

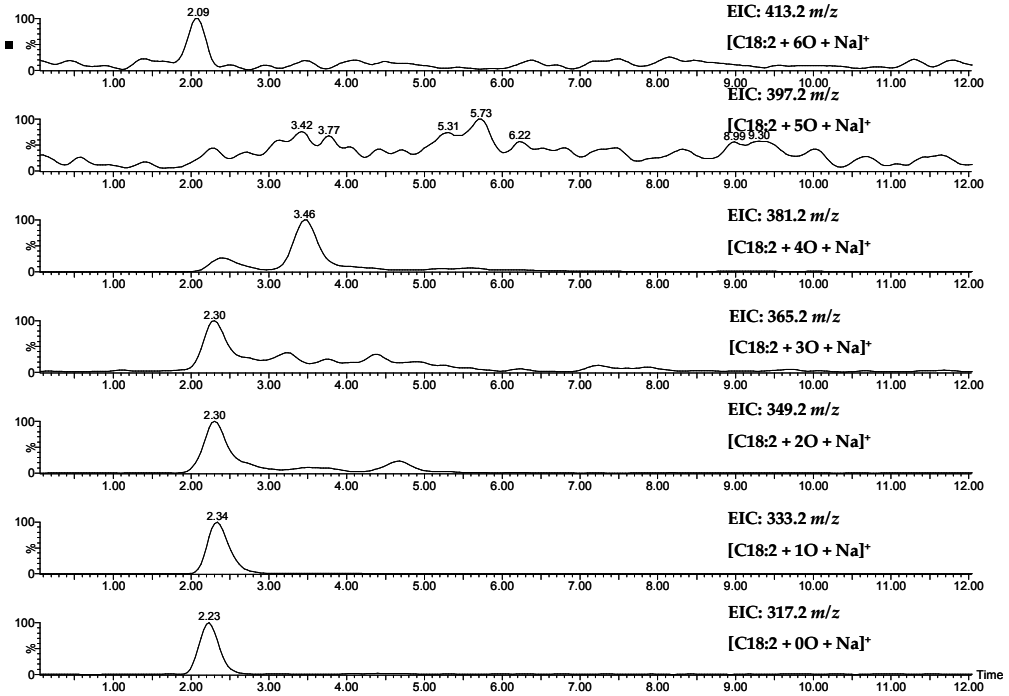


**Figure 4.25:** Positive ion ESI-SFC MS EICC of 317.2, 333.2, 349.2, 365.2, 381.2, 397.2 and 413.2 *m/z* postulated to be $[C18:2 + nO + Na]^+$ in $RME_{4.8}$ where n = 0-6.

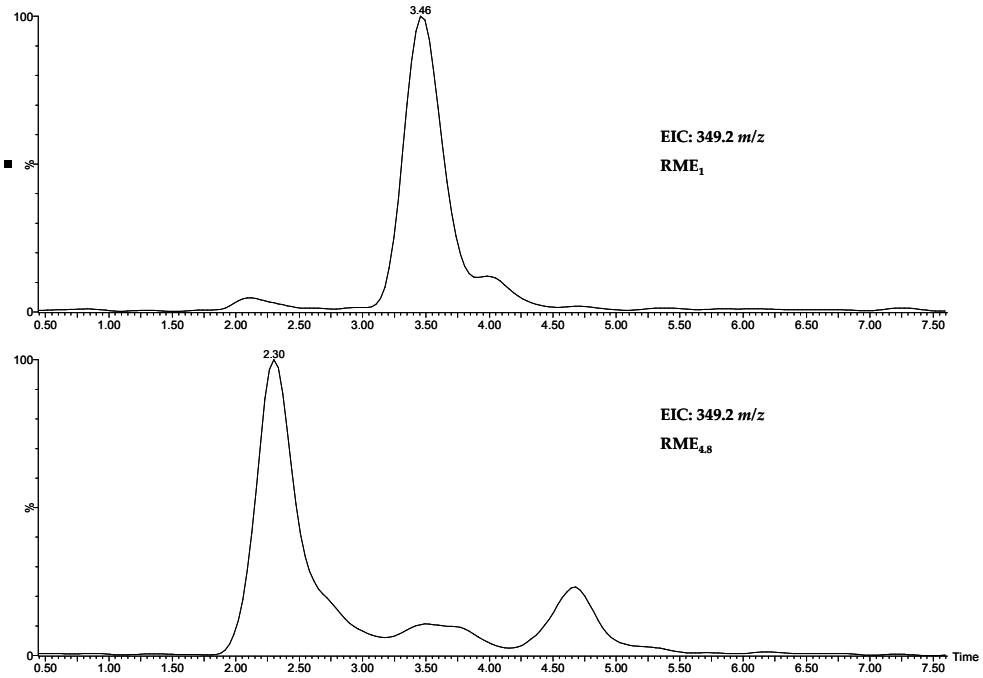


**Figure 4.26:** Positive ion ESI-SFC MS EICCs of 349.2 *m/z* postulated to be $[C18:2 + 2O + Na]^+$ in $RME_1$ and $RME_{4.8}$.

As observed for C18:1 auto-oxidation species, auto-oxidation products detected for C18:3 $RME_1$ (Figure 4.27) were reduced compared to $RME_{4.8}$. Similarly to C18:2, auto-oxidation products identified in $RME_{4.8}$ (Figure 4.28) using positive ion ESI-SFC MS were not identified to the same extent as in positive ion ESI-FT-ICR MS (Figure 4.4). It is postulated that detection of C18:3 auto-oxidation products is affected by the low percentage of C18:3 present in RME (5.0-14.0%, Figure 1.3). C18:3 reacts the fastest when compared with C18:1 and C18:2 and auto-oxidation products produced can continue to react. This coupled with the number of double bonds and thus number of potential auto-oxidation products limits the concentration of auto-oxidation products present in auto-oxidised RME. As auto-oxidation extends and products are used in further auto-oxidation reactions, such as production of polymerised auto-oxidation species,

the sensitivity of this instrument becomes a limiting factor to detect auto-oxidised compounds of C18:3 and C18:3 itself. Detection of these species is important to understand the effect auto-oxidation species will have on the other components of RME. Whilst this low percentage of C18:3 increases the stability of RME, a technique that can identify lower percentages of C18:3 and the resulting auto-oxidation products is beneficial.

As expected, multiple peaks with the same nominal mass were detected with an example given in Figure 4.29, which is synonymous (by auto-oxidation type) with C18:2 species. Again, three peaks are present in the EICCs of $[C18:3 + 2O + Na]^+$ species (349 *m*/*z*) from $RME_1$ and $RME_{4.8}$ A shift in ionisation abundance of these peaks can be observed in samples $RME_1$ and $RME_{4.8}$ with only one peak remaining, suggesting that these auto-oxidation products (suggested to be $[C18:2 + 2O + Na]^+$ and $[C18:3 + 2O + Na]^+$) are linked and follow similar degradation profiles.

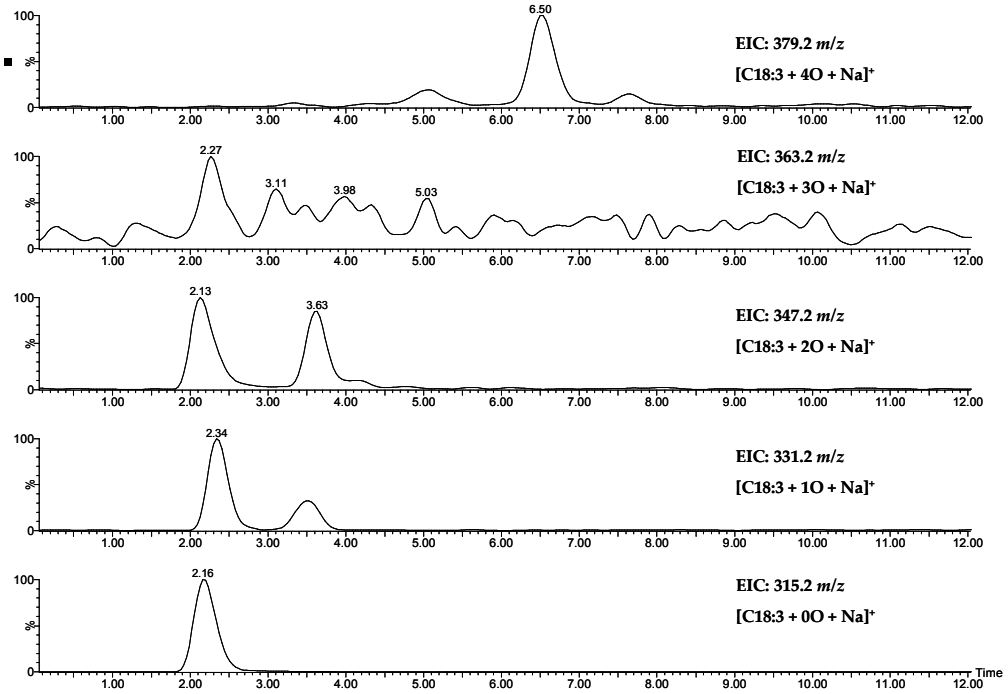


**Figure 4.27:** Positive ion ESI-SFC MS EICC of 315.2, 331.2, 347.2, 363.2 and 379.2 *m/z* postulated to be $[C18:3 + nO + Na]^+$ in $RME_1$ where n = 0-4.

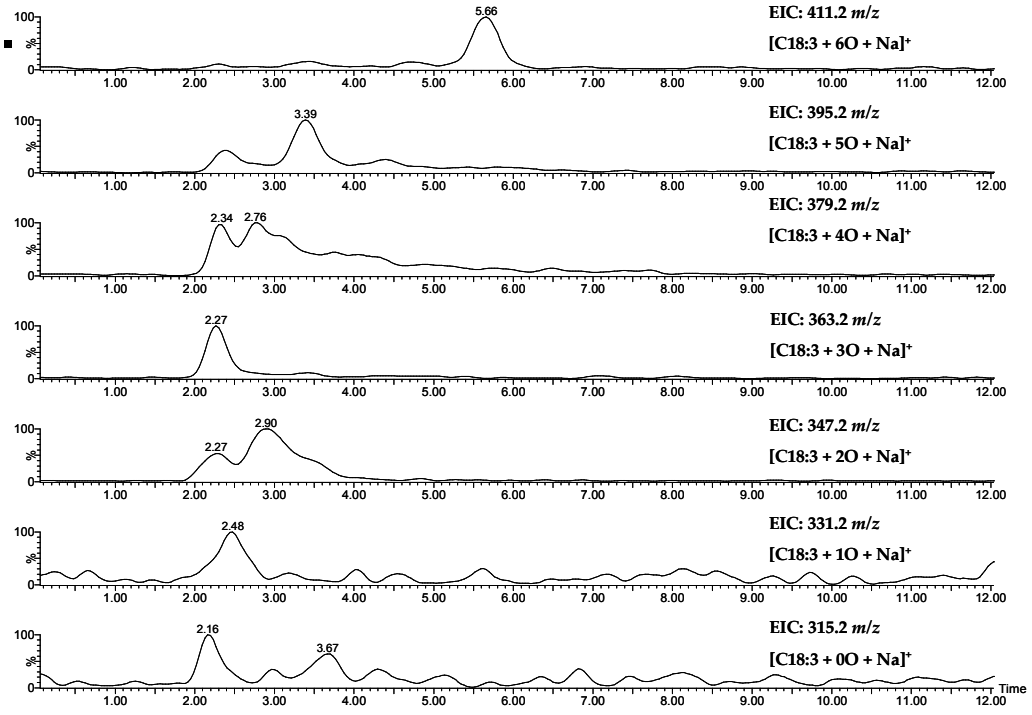


**Figure 4.28:** Positive ion ESI-SFC MS EICC of 315.2, 331.2, 347.2, 363.2, 379.2, 395.2 and 411.2 *m/z* postulated to be $[C18:3 + nO + Na]^+$ in $RME_{4.8}$ where n = 0-6.

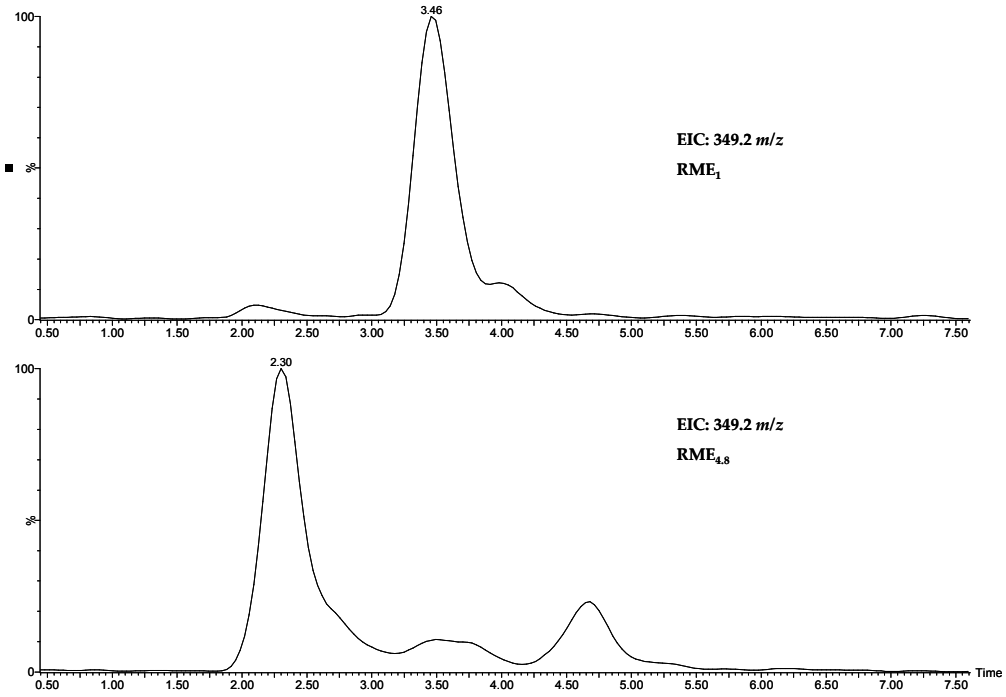


**Figure 4.29:** Positive ion ESI-SFC MS EICC of 349.2 *m/z* postulated to be $[C18:3 + 2O + Na]^+$ species from $RME_1$ and $RME_{4.8}$.

Positive ion ESI-SFC-UV MS also aids some separation (from FAMEs and other smaller degradation products) and detection of polymeric species as displayed in Figure 4.31, and the focus here is on the previously discussed ion at *m/z* 537.2. This was detected in short analysis times (<5 minutes) and is indicative of extended auto-oxidation (Figure 4.30 and Figure 4.31). The detection of all of these species suggests this technique could be utilised to measure the extent of auto-oxidation *via* the use of similar species as auto-oxidation markers. Not only can FAMEs be detected, but it has been demonstrated that multiply oxygenated auto-oxidised species can be detected and structural isomers easily separated.

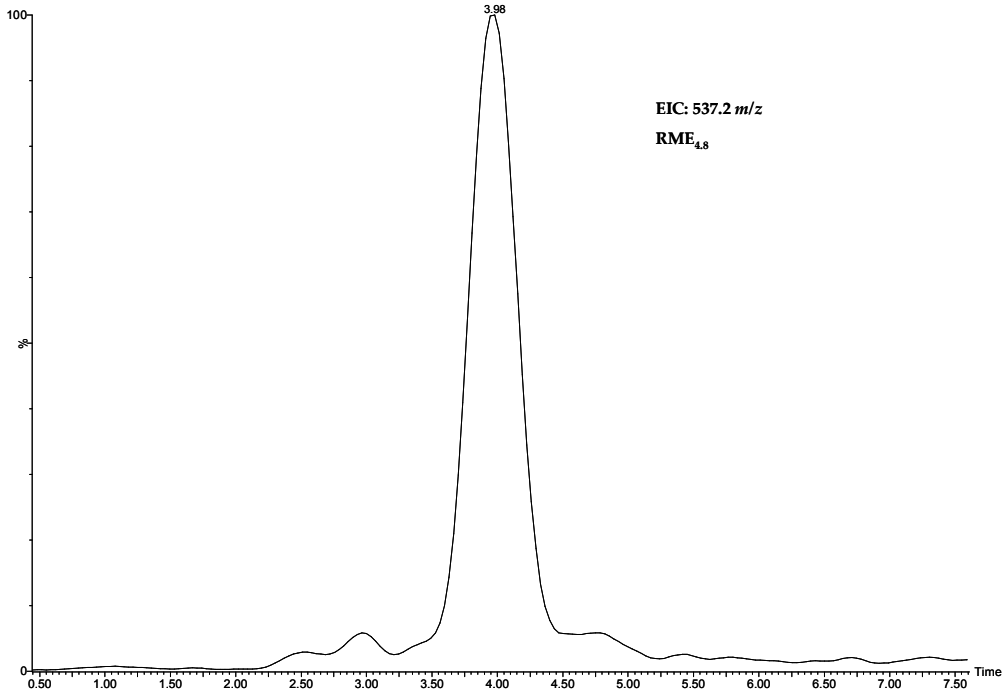


**Figure 4.30:** Positive ion ESI-SFC MS EICC of 537.2 *m/z* postulated to be a polymeric auto-oxidation species in $RME_{4.8}$.

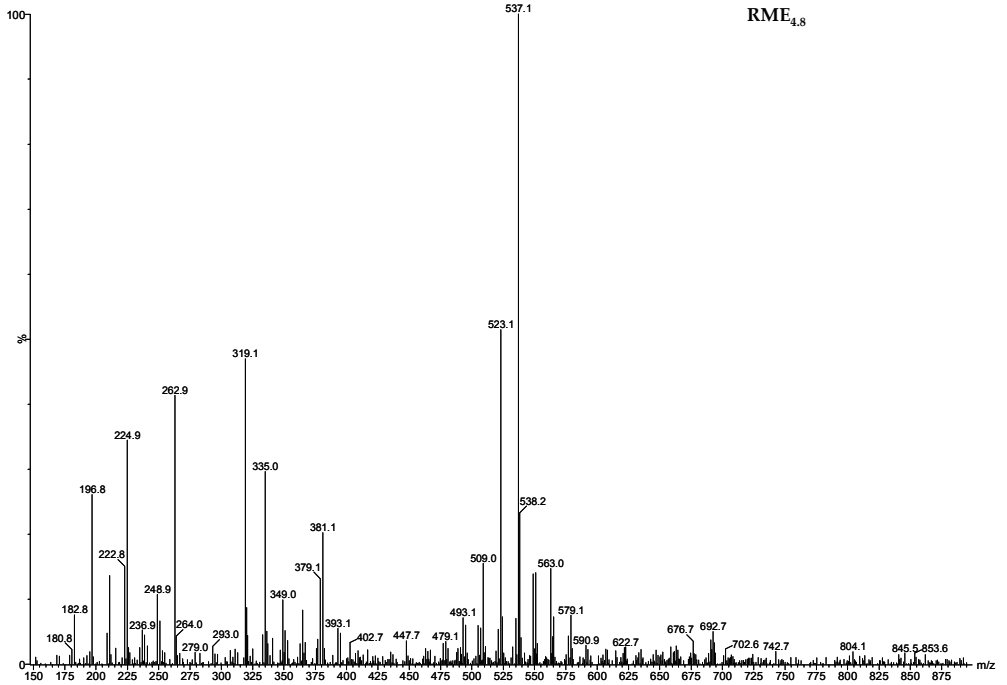


**Figure 4.31:** Positive ion ESI-SFC-MS from $t_R$3.6-4.4 min. of positive ion ESI-SFC MS EICC of 537.2 *m/z* in $RME_{4.8}$ as observed in Figure 4.30.

## Summary

Natural auto-oxidation observed here mimics auto-oxidation observed during storage of RME. Auto-oxidation of RME was monitored over a long time period and analysed using several techniques. This analysis has shown the complexity of auto-oxidised RME and the challenges needed to be overcome to analyse it.

GC-MS, positive ion ESI-FT-ICR MS, positive ion ESI-MS and positive ion ESI-SFC-UV MS have proved to be invaluable. GC-MS allowed C18:1, C18:2 and C18:3 depletion to be observed, together with production of small chain degradation products. Whereas, positive ion ESI-MS techniques have capitalised on the ionisation affinity of auto-oxidation species which is attributed to the increased number of oxygen atoms present in auto-oxidation products. The resolution of positive ion ESI-FT-ICR MS afforded nominal ions to be separated, exposing the transformation of RME from 10 starting components to an auto-oxidised sample containing over 5,000 new species after 4.5 years. Positive ion ESI-SFC-UV MS has demonstrated the necessity of chromatography techniques, reducing ion suppression effects and separating nominally isobaric ions.

Through the use of these analytical techniques, auto-oxidation products identified were compared with other studies and auto-oxidation pathways have been suggested.[22, 140] It is also suggested that auto-oxidation occurs through all the pathways as discussed, however, for initial auto-oxidation the epoxide route is likely favoured.

Auto-oxidation of RME is complex and is readily promoted and propagated by species generated by the auto-oxidation process. To better understand RME auto-oxidation a simplified model would be

required, such as investigating the forced oxidation of FAMEs, in a controlled environment. This model could aid the identification of markers to be used to measure extent of auto-oxidation and be used diagnostically to test other RME sources for auto-oxidation. Ultimately complementary techniques (GC-MS, ESI-MS (LR/HR), APCI-MS and SFC-MS) are required to aid understanding of auto-oxidation.

## 4.2. Forced Oxidation of RME: Engine Simulation Studies

Forced oxidation tests were conducted on RME by BP; a sample of RME was heated at 165 °C and stirred to allow air to be mixed into the sample. This was completed to simulate auto-oxidation of RME and it was anticipated that the raised temperature would increase auto-oxidation. This investigation was undertaken using RME with no matrices, primarily to reduce matrices effects, *e.g.* lubricant contains anti-oxidants which could prevent some stages of auto-oxidation, but also to not add to the already observed complexity of the samples. An issue related to auto-oxidation of RME is the increase in viscosity observed as time extends. During the forced oxidation engine simulation study samples were also taken at different time points and their viscosities were measured using the KV40 standard test (completed by BP).[133] The KV40 standard test is a test which measures the viscosity of the sample at 40 °C. [133] These samples were then investigated using GC-MS and positive ion ESI-FT-ICR MS. Results were compared as time extended to investigate degradation of C18:X FAMEs and auto-oxidation together with the viscosity measurements. From analysis of GC-MS and positive ion ESI FT-ICR MS data obtained from these tests, auto-oxidation markers will be suggested and discussed.

This test was run until the KV40 of RME had doubled, with samples taken periodically (0, 10, 17, 18, 19, 21, 23, 24, 25, 26, 42, 43, 44, 45, 46, 47, 50, 51, 52, 66, 67, 70 hours). Initially GC-MS was used to quantify FAMEs present in the samples and other auto-oxidation products that arose as the test continued. Methyl octadecanoate-d35 (Figure 3.8) was used as the internal standard.

All major FAMEs (C16:0, C18:0, C18:1, C18:2 and C18:3) were observed to decrease compared to the starting percentage (Figure 1.3, Figure 4.32). Overall C18:1, C18:2 and C18:3 deplete at a faster rate, observed by the steep gradient, compared to C16:0 and C18:0 which deplete very slowly represented by a shallower gradient (Figure 4.32). At the end of this forced oxidation test, C18:1, C18:2 and C18:3 were observed to still be present, suggesting that viscosity increases occur within initial auto-oxidation. Throughout the RME forced oxidation studies small spikes can be observed when monitoring depletion of FAMEs (Figure 4.32, Figure 4.33, Figure 4.34, Figure 4.37, Figure 4.38 and Figure 4.39) and detection of auto-oxidation products, these are attributed to sampling errors. Depletion of FAMEs and production of auto-oxidation species can still be monitored, with the overall trend of FAME depletion and production of auto-oxidation species of most importance.

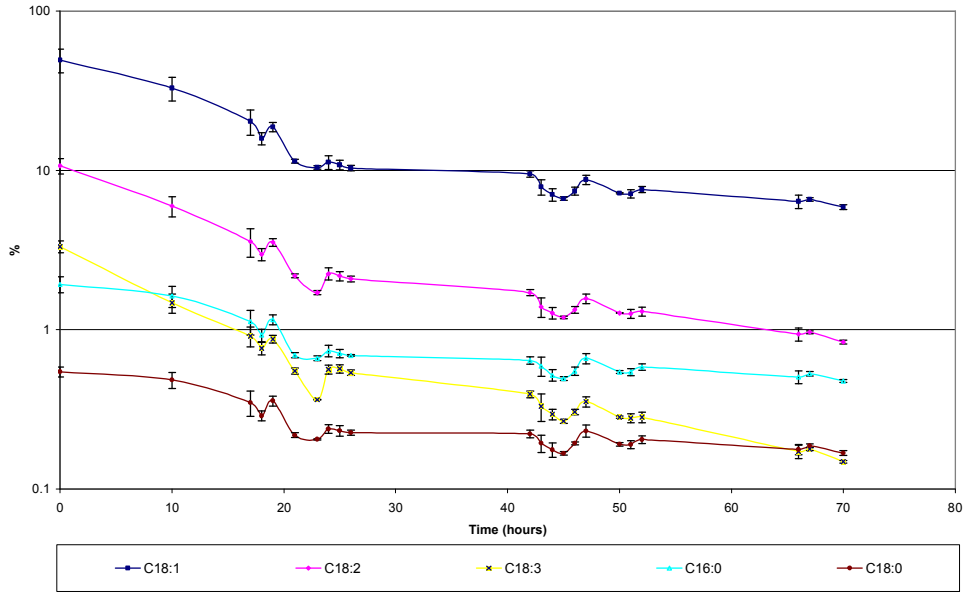


**Figure 4.32:** C16:0, C18:0, C18:1, C18:2 and C18:3 percentages in RME auto-oxidised samples.

C16:0, C18:0, C18:1, C18:2 and C18:3 FAMEs are present at different percentages in RME and whilst Figure 4.32 describes the loss of C16:0, C18:0, C18:1, C18:2 and C18:3 as a percentage in RME, it does not illustrate the loss of each individual FAME. Overall depletion is best described as a percentage of the starting FAME (Figure 4.33). C18:3 displays the biggest percentage loss (96%), followed by C18:2 (92%), C18:1 (88%), C18:0 (69%) and C16:0 (75%). This supports previous data with C18:3 auto-oxidising fastest, closely followed by C18:2 and C18:1.

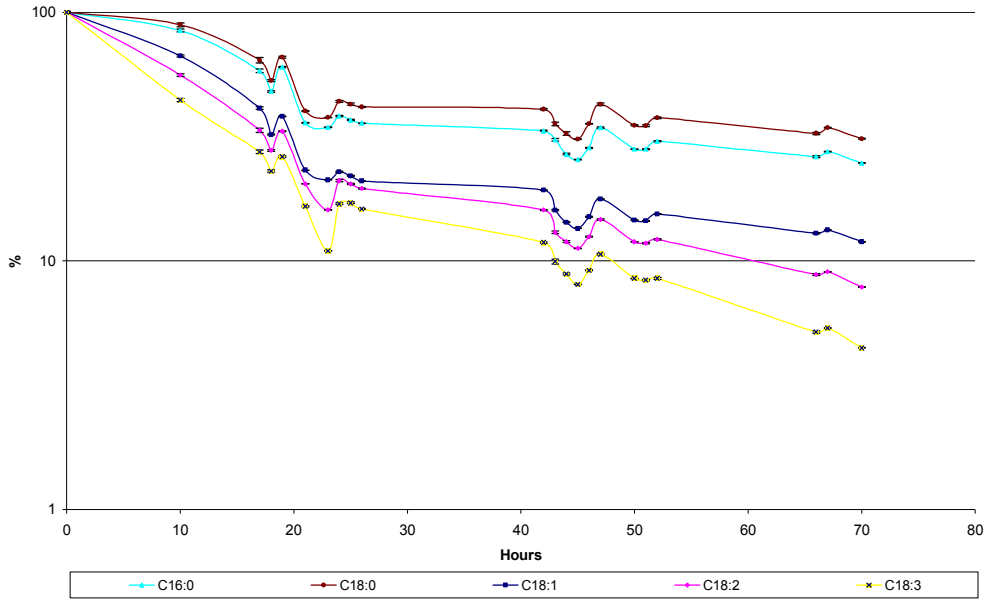


**Figure 4.33:** C16:0, C18:0, C18:1, C18:2 and C18:3 percentages in RME auto-oxidised samples, where at t = 0 FAME content of each individual FAME is 100% of that FAME.

An inverse relationship is observed where; as the concentrations of the starting FAMEs are depleted, viscosity increases (Figure 4.34).

Initially, degradation of FAMEs appears rapid, there is an excess of FAMEs and auto-oxidation appears to be rapid with the

biggest loss observed within the first 24 hours. Within this time period C18:1 is depleted by 77% of its initial percentage in RME, similar trends are observed for C16:0 (62%), C18:0 (56%), C18:2 (79%) and C18:3 (83%) (Figure 4.34). Again, this demonstrates the increased reactivity of species with more double bonds (C18:3>C18:2.C18:1>C18:0 depletion in the first 24 hours) (Figure 4.34). A similar trend is observed with viscosity whereby a steeper gradient of increasing viscosity was observed for the first 24 hours compared with the rest of the study, although viscosity increases as FAMEs % depletes (Figure 4.34). These viscosity increases are attributed to the depletion of FAMEs and production of auto-oxidation species, with FAMEs possessing an increased number of double bonds (C18:3) contributing to a larger degree (C18:3>C18:2>C18:1>C18:0) (Figure 4.34).

After this time period (24-70 hours (end)) a smaller decrease in percentages was observed: C16:0 (13%), C18:0 (13%), C18:1 (11%), C18:2 (13%), C18:3 (13%) with all FAMEs auto-oxidising at a similar rate. This suggests that auto-oxidation occurs at the fastest rate within the first 24 hours. After this time period auto-oxidation seemingly slows, with other auto-oxidation (propagation reactions) suggested to be more favourable, see Figure 4.11. The induction period is suggested to be below 10 hours, however without data for auto-oxidised RME sampled before this point no conclusions as to the exact time point can be drawn. Viscosity measurements also display a similar gradient profile comparable with depletion of FAMEs, (although an inverse relationship is present, this suggesting increased viscosity is a result of the production of auto-oxidation species and depletion of FAMEs.

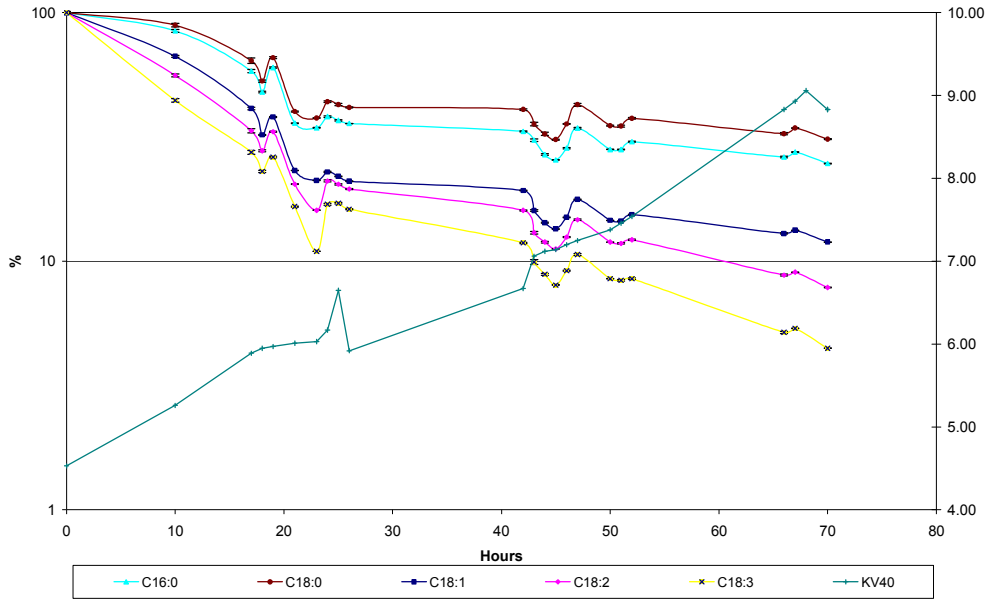


**Figure 4.34:** C16:0, C18:0, C18:1, C18:2 and C18:3 percentages in RME auto-oxidised samples as a percentage of the amount present at t = 0 hours and KV40 values (cSt) at each time point.

The occurrence of auto-oxidation is evident from the depletion of FAMEs and the presence of auto-oxidation products (Figure 4.35 and Figure 4.36). Auto-oxidation is apparent in sample t = 0, where it has begun to auto-oxidise during storage, further supporting this technique to be used as a screening method to detect auto-oxidation rapidly due to 'beacon' multiple oxygenated auto-oxidation products. Simply measuring the depletion of FAMEs is not indicative of auto-oxidation; different RME (and biodiesel sources) possess different percentages of FAMEs (Figure 1.3). Throughout auto-oxidation, the concentration of C16:0, C18:0, C18:1, C18:2 and C18:3 FAMEs can be observed to deplete. Depletion of C16:0, C18:0, C18:1, C18:2 and C18:3 alter the percentage of FAMEs in the sample and thus when analysed, this sample could potentially contain ratios of FAMEs that mimic a different feedstock source. If an unknown sample of unknown auto-oxidation time was analysed in this way, it could be wrongly

characterised, this could lead to complications, such as, it could be used in place of the correct fuel. Additionally, if the comparator t = 0 sample is not available comparisons cannot be made as the original percentage composition is not known, again the extent of auto-oxidation is not known or even feedstock source. This could cause issues when assessing whether a fuel has been adulterated. To identify extent of auto-oxidation it is proposed that auto-oxidation products can be used, termed as auto-oxidation markers. Forced oxidation samples will be analysed and auto-oxidation products that could be used as markers of auto-oxidation will be selected. The selected auto-oxidation markers concentration will then be compared to the extent of auto-oxidation and viscosity.

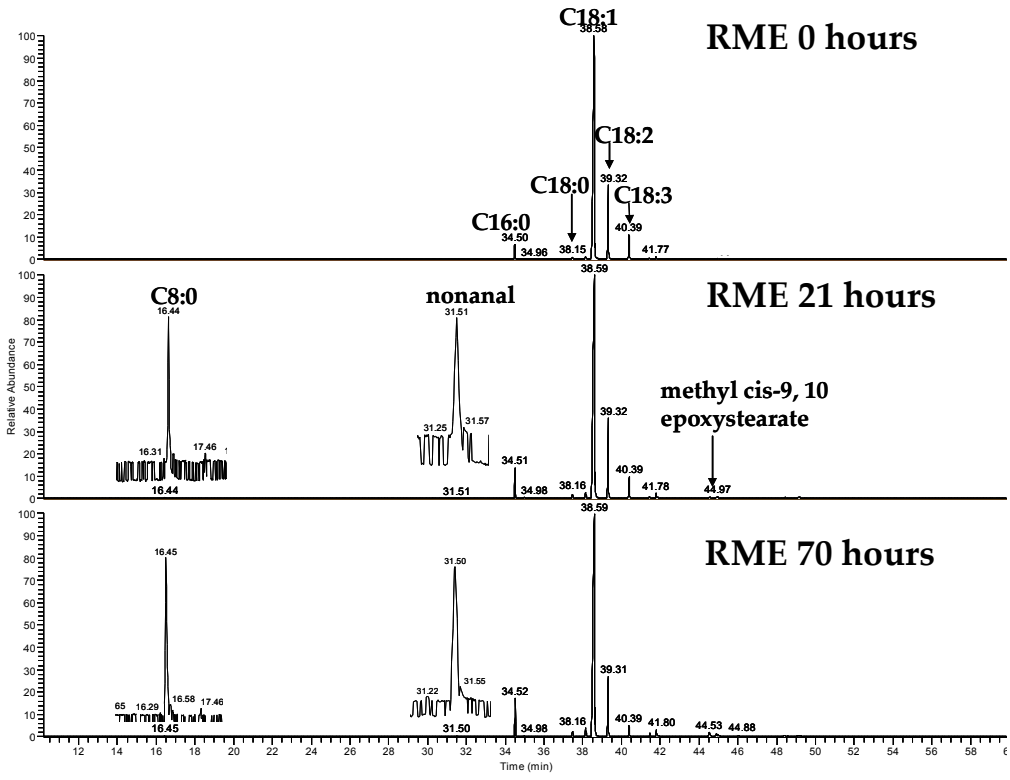


**Figure 4.35:** GC-MS TICCs of RME 0 hours, 24 hours and 70 hours from forced oxidation studies highlighting C8:0 (inserted), nonanal

(inserted) and methyl *cis*-9, 10-epoxystearate suggested auto-oxidation markers.

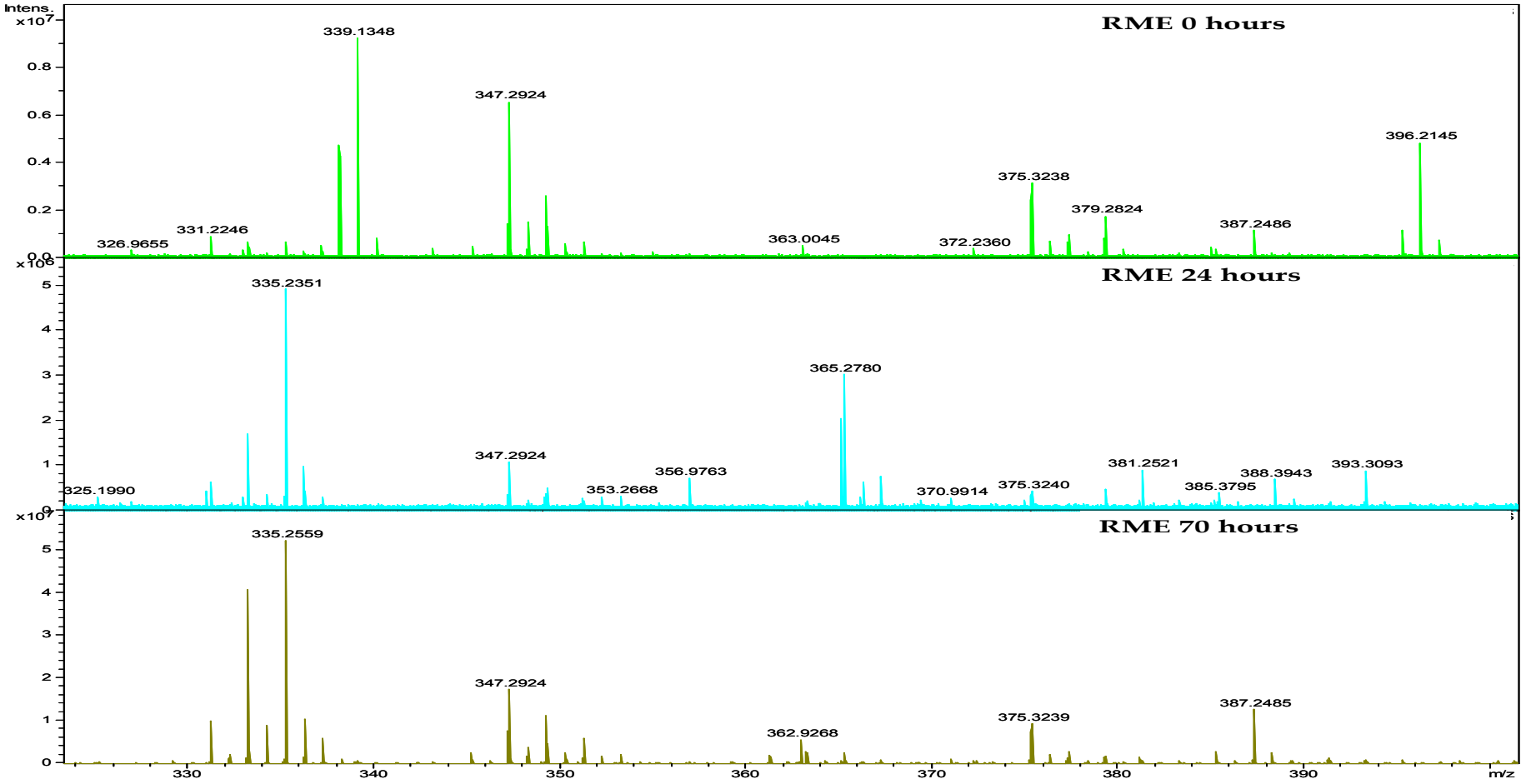


**Figure 4.36:** Positive ion ESI-FT-ICR MS of RME 0 hours, 24 hours and 70 hours from forced oxidation studies.

GC-MS data of natural auto-oxidation (Figure 4.1) contains many species that cannot be attributed to FAMEs, this is not true for forced oxidation, where only 9 new species were detected (Figure 4.35, Table 4.4). Positive ion ESI-FT-ICR MS spectra (Figure 4.36) shows auto-oxidation has progressed with many auto-oxidation products present that have not been detected using GC-MS possibly due to their involatility.

Auto-oxidation species identified in the GC-MS of auto-oxidised samples include: C7:0, C8:0, C15:0, 2-decenal, 2-undecenal, methyl 8-oxooctanoate, nonanal, methyl *cis*-9,10-epoxystearate and methyl 10-oxohexadecanoate (Table 4.4). Many of these species were also detected in natural auto-oxidation, with the only exceptions C7:0, C15:0 and methyl 10-oxohexadecanoate. The presence of these species supports the hypothesis of multiple pathways that RME can undergo to auto-oxidise (Figure 4.5, Figure 4.7, Figure 4.10-Figure 4.12). It was observed that different auto-oxidation products were detected in RME auto-oxidised to different extents (years) (Table 4.1). There are only three auto-oxidation products detected that are detected throughout this study in all auto-oxidised samples supplied (except t = 0): C8:0, nonanal and methyl *cis*-9,10-epoxystearate and it is suggested these could be used as auto-oxidation markers in conjunction with GC-MS analysis.

**Table 4.4:** Auto-oxidation products identified using GC-MS in forced oxidised RME samples, where Y = detected, N = not detected.

| | Auto-oxidation products | | | | | | | | |
|---|---|---|---|---|---|---|---|---|---|
| Auto-oxidised RME sample (hours) | C7:0 | C8:0 | 2-decenal | 2-undecenal | methyl 8-oxooctanoate | nonanal | C15:0 | methyl *cis*-9,10-epoxysterate | methyl 10-oxohexadecanoate |
| 0 | N | N | N | N | N | N | N | N | N |
| 10 | N | Y | N | N | N | Y | N | Y | N |
| 17 | N | Y | N | N | N | Y | N | Y | N |
| 18 | N | Y | N | N | N | Y | N | Y | N |
| 19 | N | Y | N | N | N | Y | N | Y | N |
| 21 | N | Y | N | N | N | Y | N | Y | N |
| 23 | N | Y | N | N | N | Y | N | Y | N |
| 24 | N | Y | N | N | N | Y | N | Y | N |
| 25 | N | Y | N | N | N | Y | N | Y | N |
| 26 | N | Y | N | N | N | Y | N | Y | N |
| 42 | N | Y | N | N | N | Y | N | Y | N |
| 43 | N | Y | N | N | N | Y | N | Y | N |
| 44 | N | Y | N | N | N | Y | N | Y | N |
| 45 | N | Y | N | Y | N | Y | N | Y | N |
| 46 | N | Y | Y | Y | N | Y | N | Y | N |
| 47 | N | Y | Y | Y | N | Y | N | Y | N |
| 50 | Y | Y | Y | Y | N | Y | N | Y | Y |
| 51 | Y | Y | Y | Y | N | Y | N | Y | Y |
| 52 | Y | Y | Y | Y | N | Y | N | Y | Y |
| 66 | Y | Y | Y | Y | Y | Y | N | Y | Y |
| 67 | Y | Y | Y | Y | Y | Y | N | Y | Y |
| 70 | Y | Y | Y | Y | Y | Y | Y | Y | Y |
| Natural auto-oxidation (letter in Figure 4.1) | N | Y (c) | Y (f) | Y (g) | Y (k) | Y (b) | N | Y (u) | N |

In the first RME auto-oxidised sample (10 hours), C8:0, nonanal and methyl *cis*-9,10-epoxystearate were observed (Figure 4.37) and were repeatedly observed (in varying concentrations, Figure 4.37) as time extended. The profile of these auto-oxidation species is similar

and the percentage of these auto-oxidation species as detected by GC-MS is low.

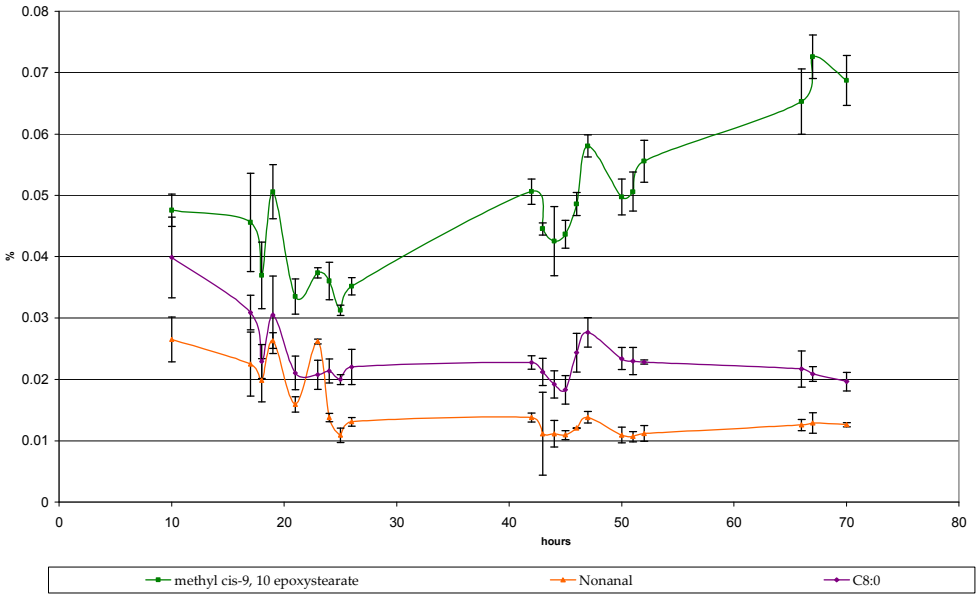


**Figure 4.37:** Percentages of C8:0, nonanal and methyl *cis*-9,10-epoxysterate in forced oxidised RME samples.

Initially C8:0, nonanal and methyl *cis*-9,10-epoxysterate were observed to overall deplete (10 hours – 25 hours) (Figure 4.37). It was observed (Figure 4.34) that during forced oxidation tests auto-oxidation was at its quickest in the first 24 hours. As FAMEs deplete, auto-oxidation products are formed and it is suggested C8:0, nonanal and methyl *cis*-9,10-epoxysterate are involved in further auto-oxidation reactions. After 24 hours the rate of depletion of FAMEs slowed and C8:0 and nonanal concentration was observed to overall plateau, with methyl *cis*-9,10 epoxystearate seemingly increased (Figure 4.37). It is suggested in this time period C8:0 and nonanal abundance in auto-oxidised RME remains constant, with other auto-oxidation products favoured for further auto-oxidation reactions. Evidence of other auto-oxidation products is present from forced

oxidised RME sample 45 hours, where C7:0, 2-decenal, 2-undecenal, methyl 8-oxooctanoate, C15:0, methyl 10-oxohexadecanoate are additionally detected (Table 4.4). However, with added sensitivity (positive ion ESI-FT-ICR MS), auto-oxidation species are prevalent in earlier samples (Figure 4.36). Auto-oxidation species detected using positive ion ESI-FT-ICR MS have not been structurally identified and without additionally information auto-oxidation markers cannot be suggested.

The presence of auto-oxidation products is suggested to cause the increase in viscosity. Auto-oxidation products C8:0 (0.80 g/mL) and nonanal (0.83 g/mL) have viscosities similar to RME (0.88 g/mL).[18] Whereas, methyl *cis*-9,10-epoxystearate has an increased viscosity (0.93 g/mL) and this contributes to the viscosity increase observed. It is not suggested that this species alone increases the viscosity; other auto-oxidation products, as discussed in Section 4.1, are all believed to contribute. It is also suggested that non-covalent interactions, such as, hydrogen bonds, of auto-oxidation products with RME could play a role and aid thickening.

C8:0, nonanal and methyl *cis*-9,10-epoxystearate, suggested auto-oxidation markers could be used to identify auto-oxidation, however to measure extent simply measuring the abundance is not effective. The profile of the biodiesel is ever-changing and presence of C8:0, nonanal and methyl *cis*-9,10-epoxystearate is not diagnostic to identify degree of auto-oxidation. It is suggested instead to compare auto-oxidation product abundance to C18:0 abundance (Figure 4.38).[133] C18:0 is present in a small percentage range in RME (Figure 1.3), it also possesses the smallest depletion overall (69%, Figure 4.34). Auto-oxidation products present are dependent on the starting FAMEs and comparison to these would be beneficial. Comparison of auto-

oxidation products abundance to the abundance of a component in RME would allow a ratio to be obtained that could be used diagnostically to identify extent of auto-oxidation.

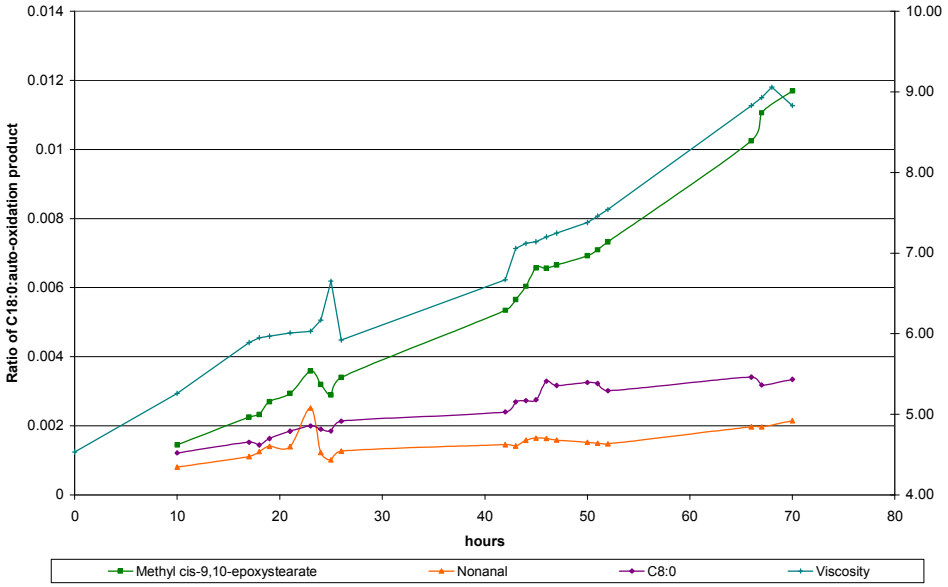


**Figure 4.38:** C18:0:auto-oxidation product ratios and viscosity of forced oxidised RME samples.

From Figure 4.38 it can be seen that similar trends are observed for C18:0:auto-oxidation product (C8:0, nonanal and methyl *cis*-9,10-epoxysterate) and follow a similar trend observed in viscosity (Figure 4.37). Ratios increase as time extends and this is attributed to the depletion of C18:0 and increase in auto-oxidation products. Comparisons between viscosity and ratios of C18:0:auto-oxidation products display a similar correlation and Figure 4.38 suggests that the ratio of % of C18:0 to methyl *cis*-9,10 epoxystearate in the RME sample could be used diagnostically to identify the extent of auto-oxidation. For example, in the forced oxidised RME 10 hour sample a small ratio of C18:0 to methyl *cis*-9,10 epoxystearate (0.002) is observed when auto-oxidation is not as prevalent and viscosity is close to the starting values. However as time extends (RME forced oxidised for 70 hours)

the C18:0 to methyl *cis*-9,10 epoxystearate ratio is in excess of 0.012 and viscosity has doubled. Analysis of RME samples of unknown auto-oxidation time could potentially be completed using this ratio technique, with extended auto-oxidation identified and a rough estimate, in terms of starting viscosity, could be suggested.

Whilst C18:0:methyl *cis*-9,10-epoxystearate ratio could be utilised to identify extent of auto-oxidation in RME, other feedstock sources have different percentages of FAMEs. Comparisons of C18:0 to other FAME abundance is suggested to overcome the different percentages of FAMEs as used by Khoury *et al*.[133], as observed in Figure 4.39. Correlations were observed using comparisons of C18:0 to other FAME abundance and similar trends with viscosity can be observed. C18:0:FAME abundance could be useful to identify the extent of auto-oxidation in RME. Further investigation is needed to investigate ratios of FAMEs in other biodiesel.

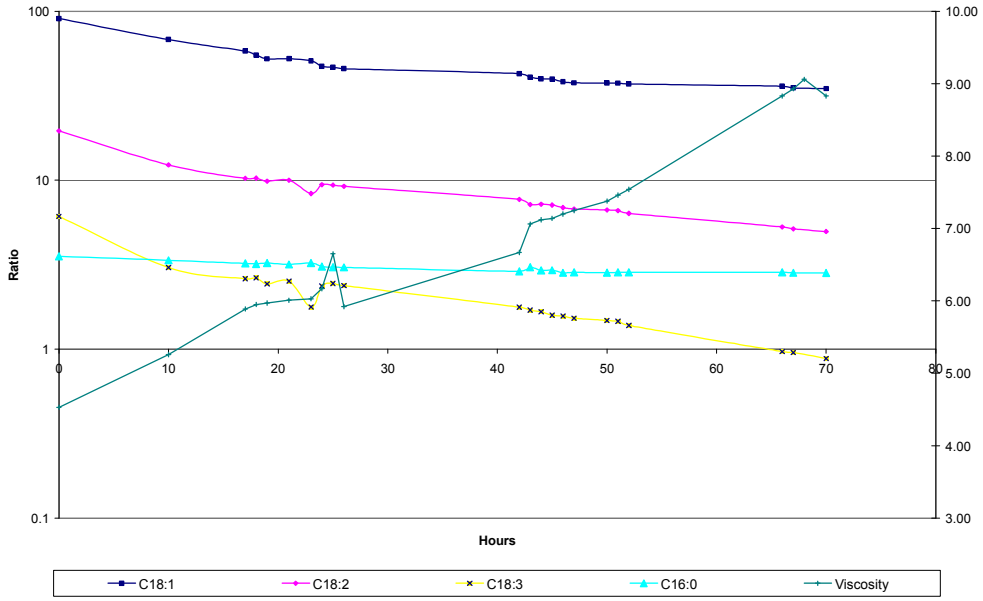


**Figure 4.39:** C18:0:C18:1/C18:2/C18:3/C16:0 ratios and viscosity of forced oxidised RME samples.

Using GC-MS the number of auto-oxidation products detected in RME forced oxidised sample was few. Through the use of positive ion ESI-FT-ICR MS auto-oxidation products were detected (Figure 4.36), with multiple oxygens typically improving ionisation. C18:1, C18:2 and C18:3 were detected using ESI-MS; $[C18:1 + Na]^+$ 319.2607, *m/z* (0.3 ppm error); $[C18:2 + Na]^+$, 317.2451 *m/z* (0.0 ppm error) and $[C18:3 + Na]^+$, 315.2296 *m/z* (0.5 ppm error) (Figure 4.40) and contrary to GC-MS were observed in every sample. Molecular formula $[C_{19}H_{34}O_3 + Na]^+$ consistent with methyl *cis*-9,10-epoxystearate was also suggested using positive ion ESI-FT-ICR MS (Figure 4.40).

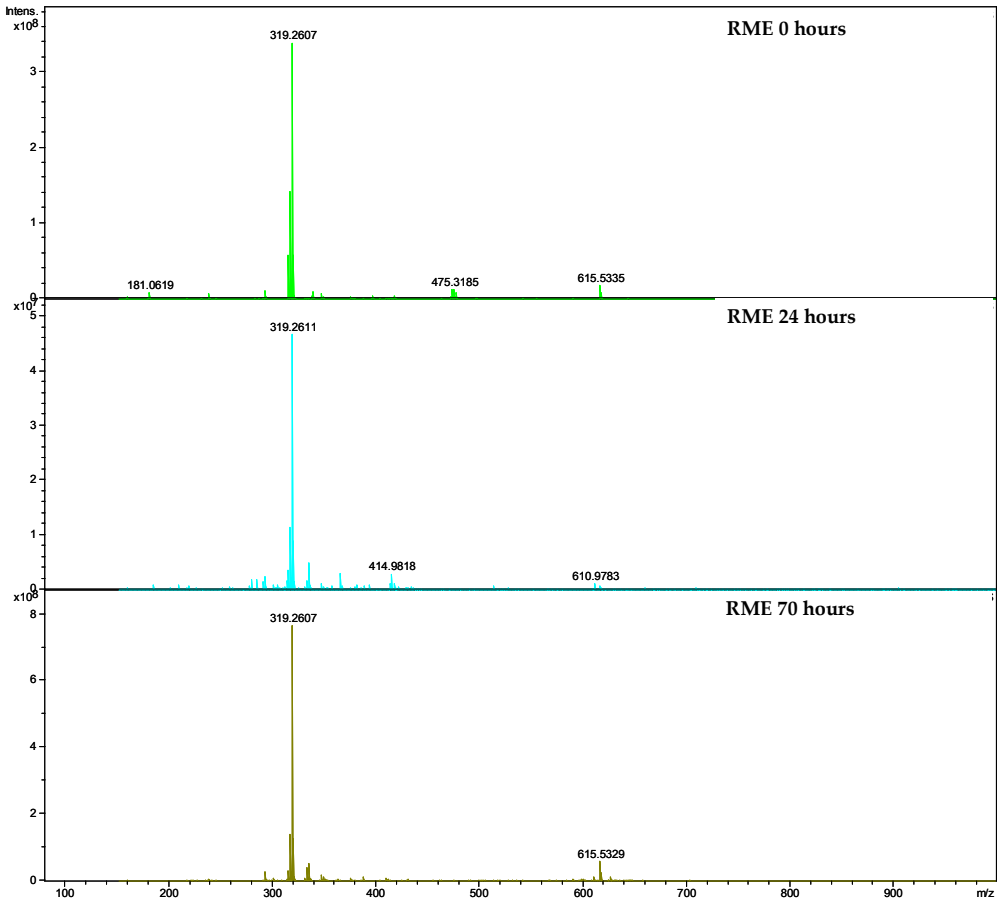


**Figure 4.40:** Positive ion ESI-FT-ICR MS of auto-oxidised RME 0, 24 and 70 hours.

As discussed for natural auto-oxidation (Table 4.3), a series relating to the addition of oxygen atoms to FAMEs was detected. This series was observed in auto-oxidised RME samples. Over the course of this study, species postulated to be C18:1, C18:2 and C18:3 with additional oxygen atoms can be observed (Table 4.5). As already discussed C18:3 auto-oxidises to a larger extent and this was evident when forced oxidised samples were analysed using positive ion ESI-FT-ICR MS (Table 4.5). Addition of oxygen atoms was not as extensive as observed in natural auto-oxidation (Table 4.3), however this is not surprising as this test was conducted over 70 hours, with natural auto-oxidation samples in excess of 5 years.

**Table 4.5:** Values for maximum n for auto-oxidation products of the series $[C18:X + nO + Na]^+$ observed in forced oxidised RME samples, where X = 1-3. All auto-oxidation products identified less than 2 ppm error.

| | FAME | | |
|---|---|---|---|
| Auto-oxidised RME sample (hours) | C18:1 (n) | C18:2 (n) | C18:3 (n) |
| 0 | 2 | 2 | 4 |
| 10 | 2 | 4 | 4 |
| 17 | 2 | 4 | 4 |
| 18 | 2 | 4 | 4 |
| 19 | 2 | 4 | 4 |
| 21 | 2 | 3 | 4 |
| 23 | 2 | 4 | 6 |
| 24 | 2 | 2 | 2 |
| 25 | 3 | 4 | 4 |
| 26 | 3 | 4 | 3 |
| 42 | 3 | 3 | 4 |
| 43 | 3 | 6 | 4 |
| 44 | 3 | 4 | 3 |
| 45 | 3 | 4 | 5 |
| 46 | 3 | 4 | 4 |
| 47 | 2 | 3 | 4 |
| 50 | 3 | 3 | 4 |
| 51 | 2 | 2 | 3 |
| 52 | 2 | 3 | 3 |
| 66 | 3 | 3 | 3 |
| 67 | 2 | 3 | 3 |
| 70 | 4 | 4 | 5 |

Polymerised auto-oxidation products were detected at extended time (Figure 4.41). These species contribute to the viscosity increases, with $[C_{29}H_{54}O_7 + Na]^+$, 537.37646 *m/z* (0.54 ppm error) also detected.

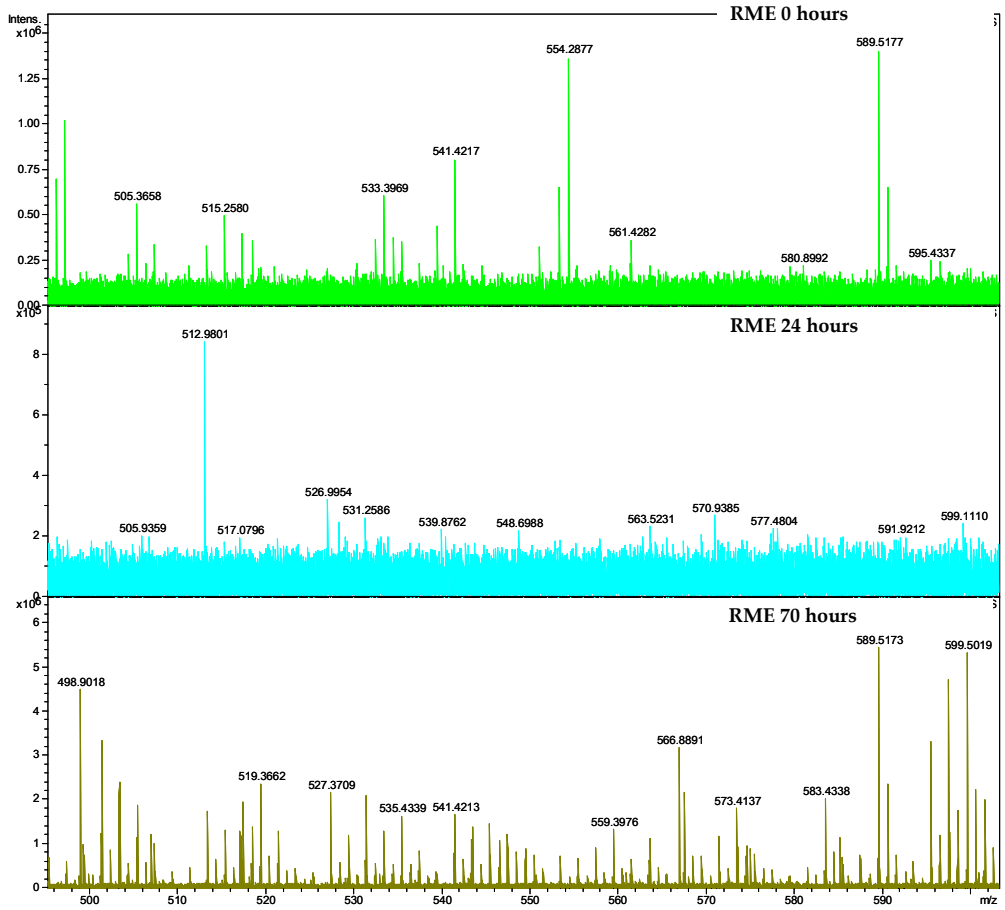


**Figure 4.41:** Positive ion ESI-FT-ICR MS of RME 0 hours, 24 hours and 70 hours from forced oxidation studies displaying polymerised auto-oxidation species.

Data obtained using positive ion ESI-FT-ICR MS is not quantitative and therefore conclusions about amounts of auto-oxidation products in each sample cannot be easily determined. However, the presence of auto-oxidation products can be utilised lending this technique to be used as a quick screening method, with samples possessing certain characteristics, such as auto-oxidation markers (C8:0, nonanal and methyl *cis*-9,10-epoxystearate), to be further analysed.

## Summary

Forced oxidation tests simulate RME auto-oxidation in an engine environment. RME was used without matrices to investigate a simplified model of auto-oxidation. Through this study data has shown that FAMEs deplete at different rates with C18:3>C18:2>C18:1>C18:0. A collection of auto-oxidation species were detected using GC-MS (Table 4.4) with three auto-oxidation products suggested to be used as auto-oxidation markers; C8:0, nonanal and methyl *cis*-9,10-epoxystearate. Viscosity measurements taken confirm that viscosity increases are related to the depletion of FAMEs and thus the presence of auto-oxidation products.

Markers identified in GC-MS can be used in conjunction with C18:0 and ratios of C18:0:auto-oxidation markers were shown to follow similar trends to viscosity in forced oxidised RME samples (Figure 4.38). Other species, such as $[C_{29}H_{54}O_7 + Na]^+$, 537.37646 *m*/*z* (0.54 ppm error) can be used diagnostically to identify extended auto-oxidation. Exploitation of the positive ion ESI-MS ionisation process, which preferentially ionises multiply oxygenated species, could lend this technique to be used as a quick screening method with analysis completed in minutes compared to *ca* 1 hour for GC-MS.

## 4.3. Electrochemical Oxidation of C18:1, C18:2, C18:3 and RME

Natural auto-oxidation was monitored over a number of years and forced oxidation was monitored over hours, however these time scales are still quite long. Another way to monitor oxidation is through the use of an electro-chemical cell and this can be completed on the minutes time scale.

The ROXY potentiostat is an instrument that is used to control redox reactions[162-164] It can be coupled to a mass spectrometer to monitor oxidation (Figure 4.42). The system is composed of a syringe driver which is loaded with the sample to be oxidised. This is connected to a cell where the sample flows over an electrode and continuous oxidation occurs. The oxidised sample then flows to be collected or flows into the mass spectrometer (Figure 4.42). The ability to collect the oxidised solution allows samples to be analysed off-line *via* other techniques, such as HPLC-MS, furthermore, the oxidised solution can be further oxidised, mimicking an extended oxidation process. Alternatively, a mass spectrometer can be used to detect species produced.

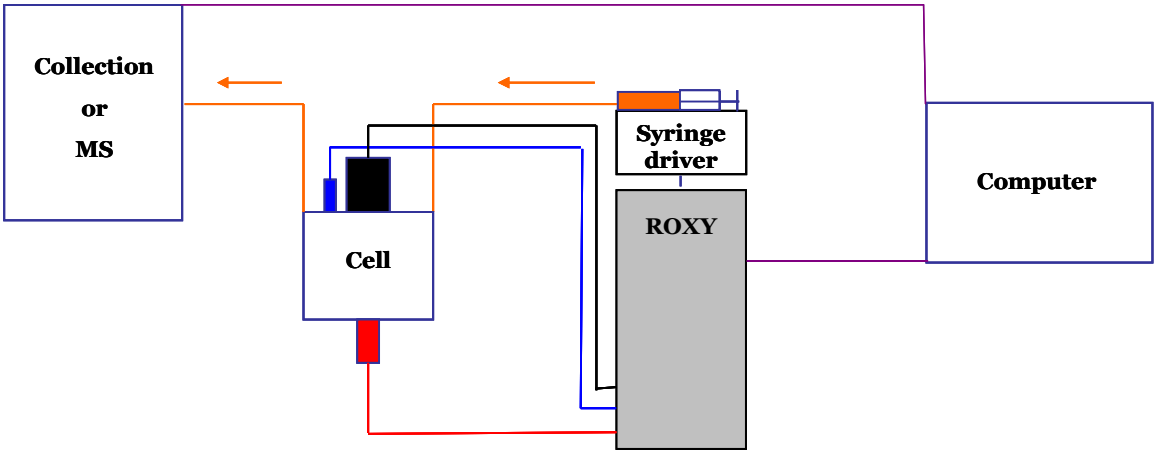


**Figure 4.42:** Schematic of the ROXY potentiostat coupled to a mass spectrometer.

There are two different cells that can be used on this system: ReactorCell or μ-PrepCell. The ReactorCell has a maximum capacity of 70 nL and has four different types of electrodes: glassy carbon, magic diamond, platinum and gold. The μ-PrepCell has a larger capacity of 12 μL and can be used with two different types of electrode: glassy carbon and magic diamond.

In this study C18:1, C18:2, C18:3 and RME were forced oxidised using the ROXY potentiostat using the μ-PrepCell and glassy carbon electrode (Figure 4.43). The cell was chosen for the larger sample volume, therefore the sample spends longer in the cell and is oxidised for an extended period of time. The glassy carbon electrode used due to its higher maximum voltage (1.8 V). This was coupled to a mass spectrometer and monitored using positive ion ESI-MS.

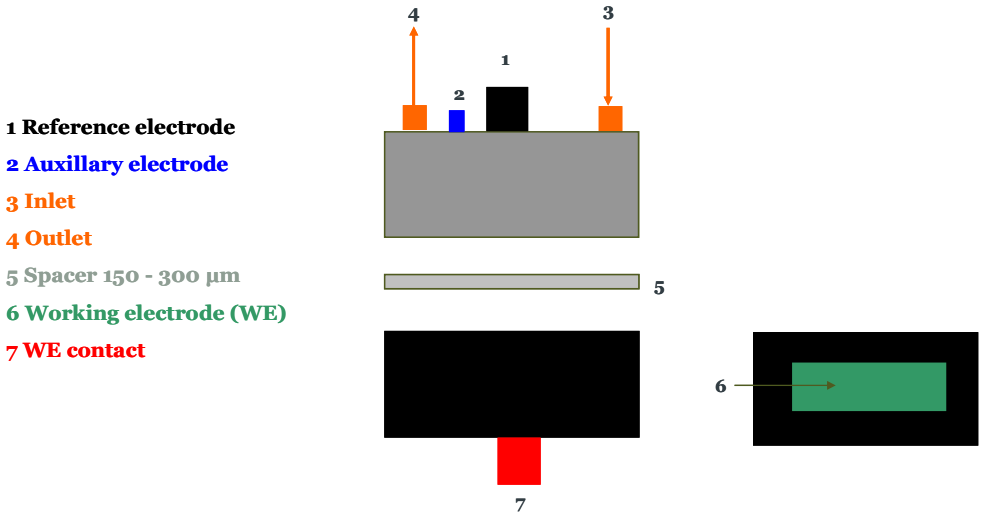


**Figure 4.43:** Schematic of the µ-PrepCell.

C18:1, C18:2 and C18:3 were initially electrochemically oxidised to monitor individual FAME oxidation which will aid understanding of the RME oxidation process. RME was then electrochemically oxidised and analysed *via* mass spectrometry, with comparisons drawn between C18:1, C18:2 and C18:3 FAMEs. Firstly, all samples were analysed with the electrochemical cell at 0 V, mimicking FAME in its least oxidised state, *i.e.* no oxidation, completed to replicate t = 0. These samples were then electrochemically oxidised at 1.8 V, the maximum voltage possible for the glassy carbon electrode. As the sample exited the EC cell it was monitored *via* positive ion ESI-MS. It was postulated that electrochemical oxidation would closely mimic auto-oxidation in FAMEs so that it can be used as a tool to investigate auto-oxidation of FAMEs.

## C18:1

Initially the electrochemical oxidation of C18:1 was investigated with analysis completed at a cell potential of 0 V and 1.8 V. Once the cell was turned on obvious differences in the TICC were observed (Figure 4.44). As C18:1 is oxidised an increase in the intensity of the TICC is observed (Figure 4.44). As electrochemical oxidation proceeded, oxidation products were formed containing increased multiple oxygenated species which are more amenable to ionise *via* positive ion ESI-MS (Figure 4.45). As can be observed (Figure 4.45) the C18:1 sample under investigation has already undergone some auto-oxidation, with ions present at *m/z* 335.2.

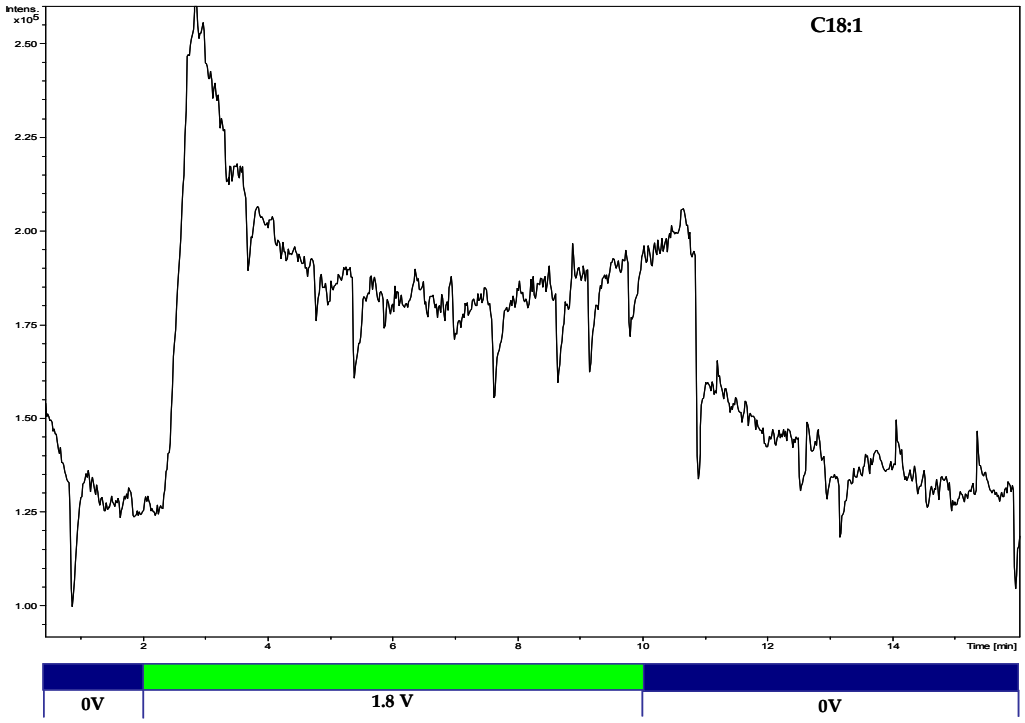


**Figure 4.44:** Positive ion ESI-MS TICC of C18:1 with the μ-PrepCell at 0 V and 1.8 V, where blue indicates the EC cell is at 0 V and green indicates where the EC cell is at 1.8 V.

Comparisons of positive ion ESI-MS spectra of electrochemically oxidised C18:1 at 0 and 1.8 V (Figure 4.45) confirm the effectiveness of using electrochemical oxidation to force oxidise by the presence of additional ions when a higher voltage is applied. The base peak of each spectrum is $[C18:1 + Na]^+$, 319.2609 (at 0 V, 0.5 ppm error), 319.2607 *m/z* (at 1.8 V, 0.0 ppm error) caused by the constant supply of C18:1 to the electrochemical cell. The intensity of this ion decreased as new species were formed and was observed to deplete as oxidation species of C18:1 occurred (Figure 4.46). This is comparable with C18:1 depletion observed in natural auto-oxidation (Figure 4.1) and forced oxidation (Figure 4.34).

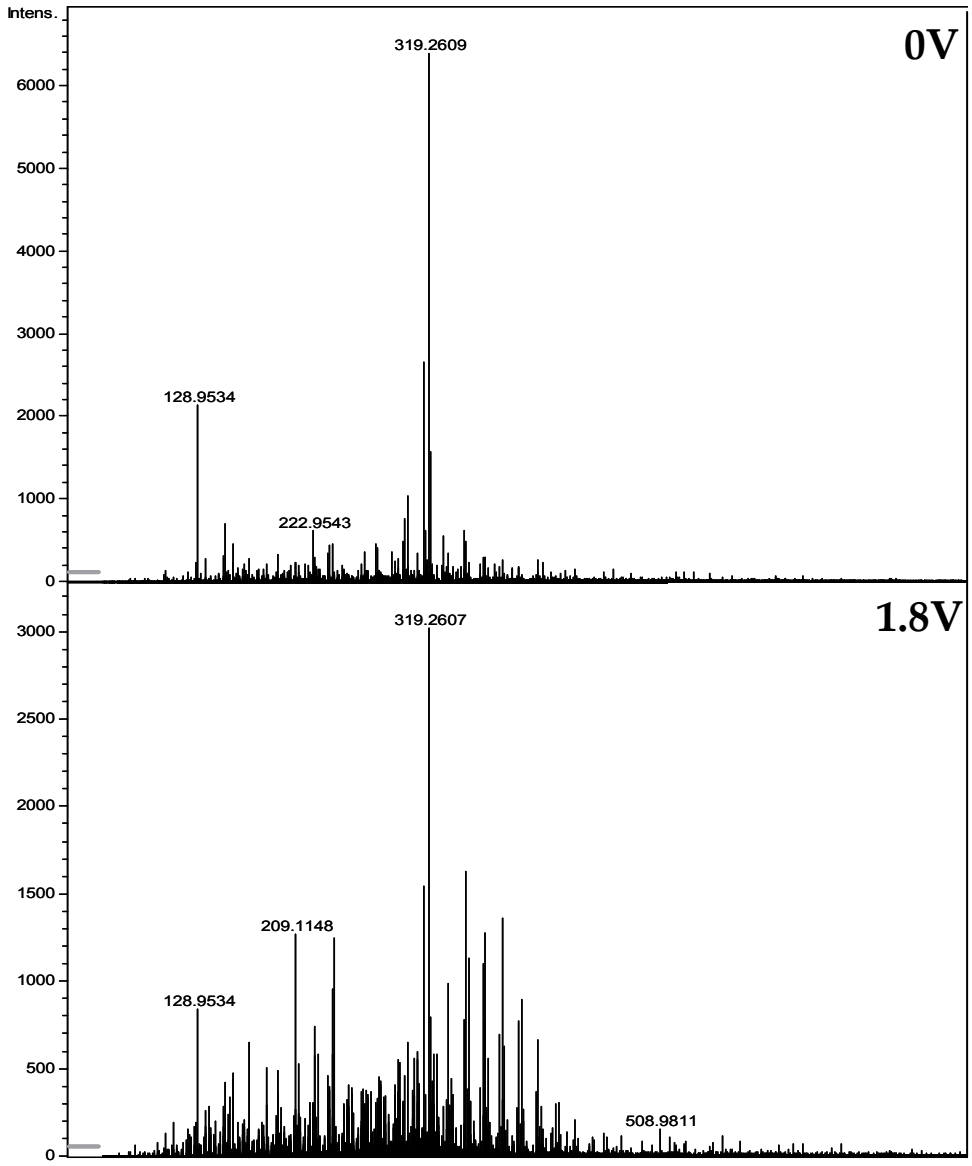


**Figure 4.45:** Positive ion ESI-MS of C18:1 at 0 V (top) and 1.8 V (bottom).

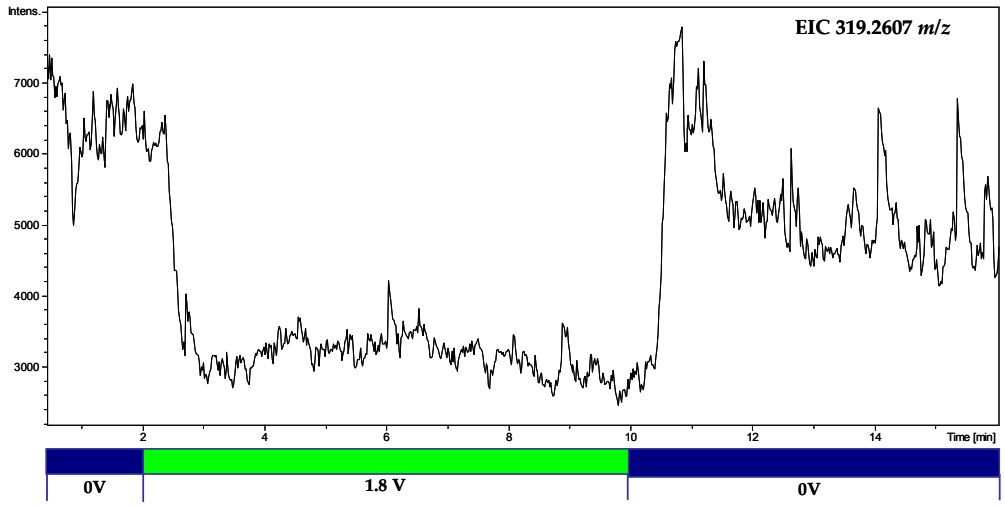


**Figure 4.46:** Positive ion ESI-MS EICC of 319.2609 *m/z*, $[C18:1 + Na]^+$, where blue indicates the EC cell is at 0 V and green indicates where the EC cell is at 1.8 V.

Auto-oxidation products discussed in natural and forced oxidation have included small chain degradation products, multiple oxygen atom containing FAMEs and polymerised auto-oxidation products. Through the use of electrochemical oxidation auto-oxidation products discussed in natural and forced oxidation can be further investigated. Investigation of auto-oxidation products will allow comparisons to be drawn between the suitability of this technique to investigate the oxidation process of RME. In addition, auto-oxidation markers suggested can be explored and correlated with auto-oxidised RME. This will describe detection of suggested auto-oxidation markers which will be used to demonstrate the effectiveness of EC oxidation.

Small chain degradation products identified using GC-MS and suggested to be detected by positive ion ESI-FT-ICR MS produced by auto-oxidation of C18:1 (Table 4.4) were investigated (methyl 8-oxooctanoate, methyl 9-oxooctanoate, methyl 10-oxo-8decenoate and

methyl 10-oxodecanoate). It can be observed from EICCs of these species (Figure 4.47) that when the cell was turned on the extracted ions concentration (which have the same *m/z* as the sodiated ion of: methyl 8-oxooctanoate, methyl 9-oxooctanoate, methyl 10-oxo-8decenoate and methyl 10-oxodecanoate) appear to have reached a maximum and then plateau. It is suggested methyl 8-oxooctanoate, methyl 9-oxooctanoate, methyl 10-oxo-8decenoate and methyl 10-oxodecanoate are produced as the C18:1 is oxidised and continue to be further oxidised as the sample travels across the cell.

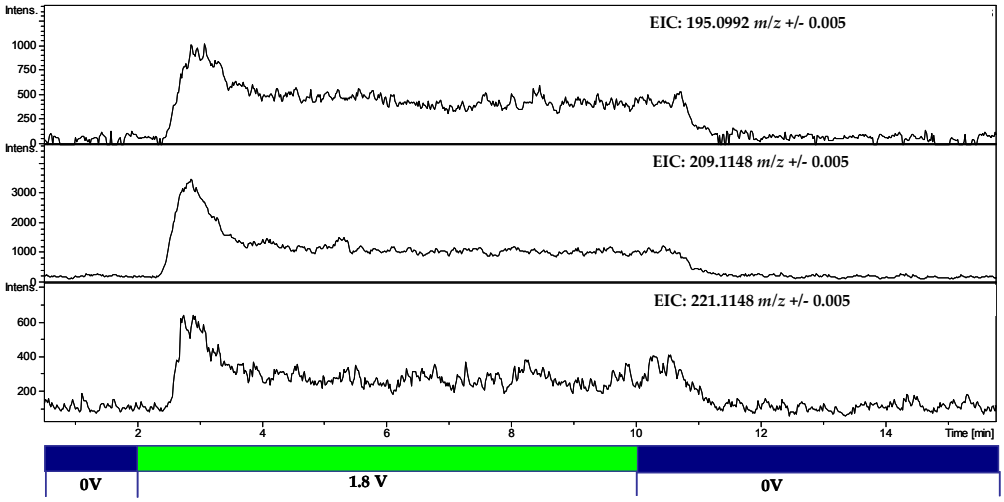


**Figure 4.47:** Positive ion ESI-MS EICCs of auto-oxidation species detected in natural auto-oxidation, $[C_9H_{16}O_3 + Na]^+$ (195.0992 *m/z*), $[C_{10}H_{18}O_3 + Na]^+$ (209.1148 *m/z*), $[C_{11}H_{18}O_3 + Na]^+$ (221.1148 *m/z*), where blue indicates the EC cell is at 0 V and green indicates where the EC cell is at 1.8 V.

A key series identified using positive ion ESI-FT-ICR MS is the addition of oxygen atoms to the starting FAME. In natural auto-oxidation, species related to C18:1 plus multiple oxygens were detected containing up to 8 oxygens (Table 4.3) and in forced oxidation up to 4 oxygen atoms (Table 4.5). In electrochemical oxidation of

C18:1 compounds with up to an additional 4 oxygens were observed (Figure 4.48), with a possible 5 additional oxygens observed. Most evident from addition of oxygen atoms to C18:1 EICCs is the lack of change observed in 335.2557 *m/z* EICC. As previously discussed it is suggested that an auto-oxidation pathway of FAMEs produces the parent molecule +16 Da, suggested to be an epoxide (*via* GC-MS) and $[C18:1 + O + Na]^+$ (*via* positive ion ESI-FT-ICR MS) and was detected in natural and forced oxidation (Figure 4.1, Figure 4.4, Figure 4.35, Figure 4.36 and Figure 4.37). Studies by Lohmann *et al.* have demonstrated that oxidation *via* the ROXY potentiostat does not produce epoxides.[162] This further supports the presence of the epoxide auto-oxidation route of FAME by the absence and lack of change in the 335.2557 *m/z* EICC (Figure 4.48). The presence of other auto-oxidation species in the absence of this epoxide also highlights the multiple routes FAMEs use to auto-oxidise (Figure 4.5, Figure 4.7, Figure 4.11 and Figure 4.12).

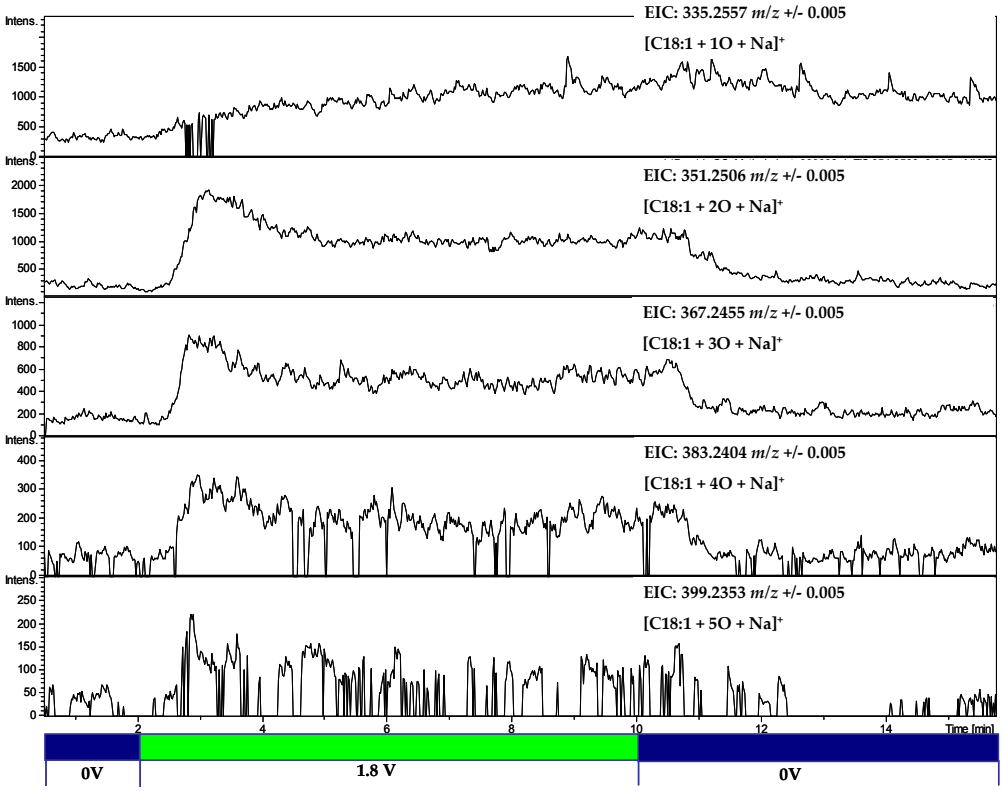


**Figure 4.48:** Positive ion ESI-MS EICC of multiple oxygen atom auto-oxidation products produced from C18:1: $[C18:1 + 1O + Na]^+$, $[C18:1 + 2O + Na]^+$, $[C18:1 + 3O + Na]^+$, $[C18:1 + 4O + Na]^+$ and $[C18:1 + 5O + Na]^+$, where blue indicates the EC cell is at 0 V and green indicates where the EC cell is at 1.8 V.

Polymerised auto-oxidation products were identified in natural auto-oxidation (Figure 4.4) and forced oxidation (Figure 4.36) at extended times with $[C_{29}H_{54}O_7 + Na]^+$ 537.3762 *m/z* investigated. As can be observed from Figure 4.49 $[C_{29}H_{54}O_7 + Na]^+$ and $[C_{19}H_{36}O_3 + Na]^+$ ion abundance did not change throughout oxidation and were not detected. The small chain degradation product $[C_{10}H_{18}O_4 + Na]^+$ was detected (225.1097 *m/z*) 0.0 ppm error. It is suggested, as demonstrated in Figure 4.15 that 537 *m/z* ($[C_{29}H_{54}O_7 + Na]^+$ as identified using positive ion ESI-FT-ICR MS) is the sodiated species produced from $C_{19}H_{36}O_3$ and $C_{10}H_{18}O_4$.

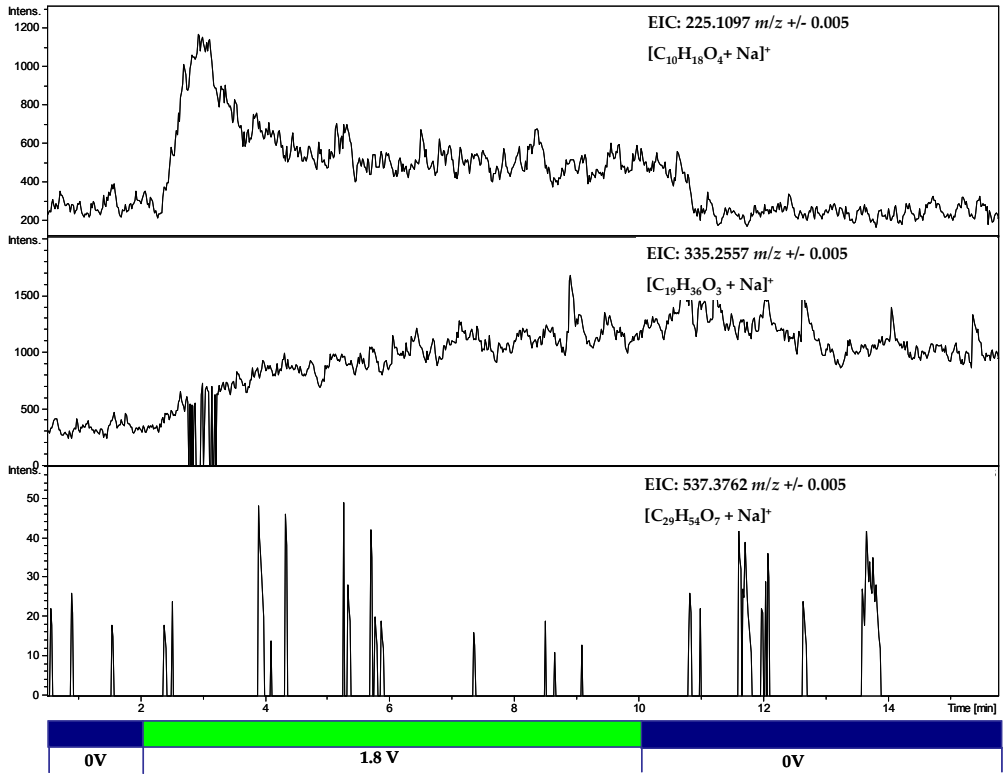


**Figure 4.49:** Positive ion ESI-MS EICC of polymerised auto-oxidation species $[C_{29}H_{54}O_7 + Na]^+$ and ions detected by MS/MS (Figure 4.15), where blue indicates the EC cell is at 0 V and green indicates where the EC cell is at 1.8 V.

Lastly, auto-oxidation markers suggested from forced oxidation studies, C8:0 and nonanal, were investigated, together with methyl *cis*-9,10-epoxystearate already discussed. Ions suggested to be $[C8:0/nonanal + Na]^+$ can be observed in Figure 4.50, with changes in profile are observed as the cell potential is increased from 0 V to1.8 V. Identification of these species suggests that these markers are comparable across different RME oxidation platforms. Intensity of the ions suggested to be C8:0 and nonanal are low, this is attributed to the presence of other oxidation compounds which ionise preferentially and/or the cell voltage. Investigation of other voltages was not completed therefore it is unknown whether ions suggested to be $[C8:0/nonanal + Na]^+$ are present in high abundance at lower voltages.

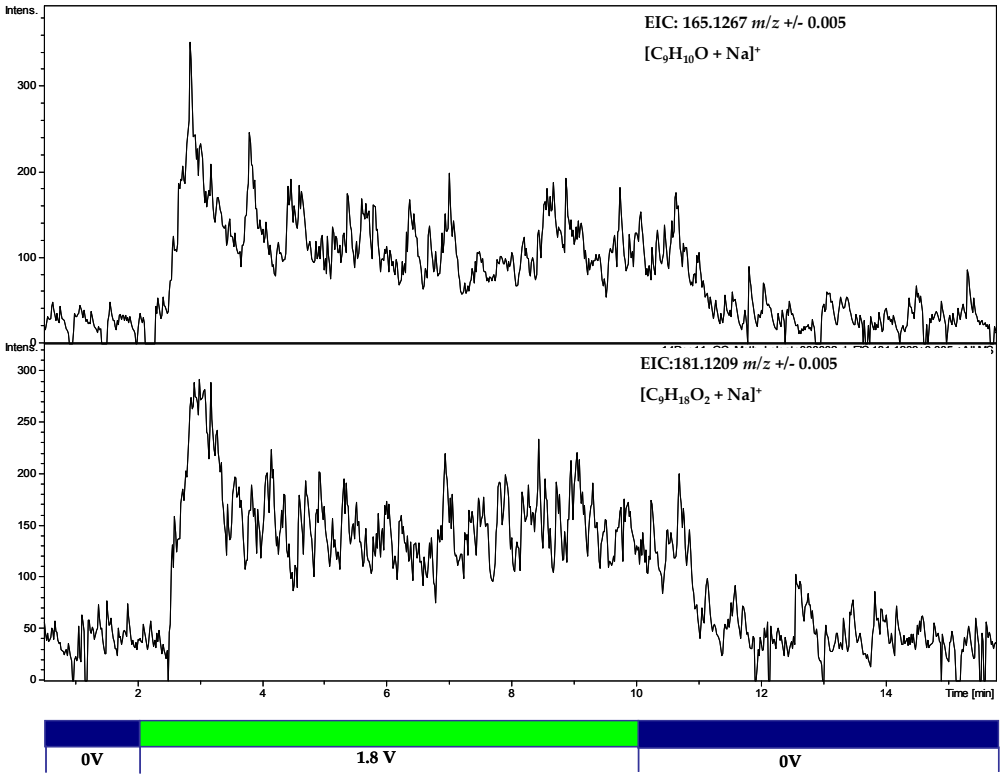


**Figure 4.50:** Positive ion ESI-MS EICCs of suggested auto-oxidation markers from forced oxidation engine tests: $[C_9H_{10}O + Na]^+$ and $[C_9H_{18}O_2 + Na]^+$, where blue indicates the EC cell is at 0 V and green indicates where the EC cell is at 1.8 V.

## C18:2

Electrochemical oxidation was completed for C18:2 as per C18:1. TICCs display similar patterns, with an overall increase in intensity and depletion of C18:2 observed as the cell was switched to 1.8 V when oxidation occurs (Figure 4.51).

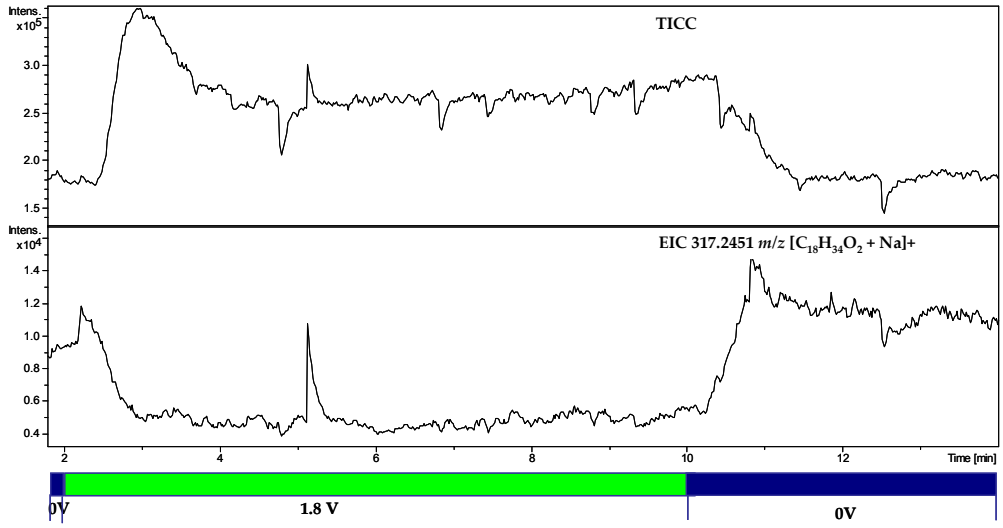


**Figure 4.51:** Positive ion ESI-MS TICC of electrochemical oxidation of C18:2 and EICC of *m/z* 317.2451, where blue indicates the EC cell is at 0 V and green indicates where the EC cell is at 1.8 V.

Unlike C18:1, C18:2 does not remain the base peak once oxidation occurs and this is related to its propensity to auto-oxidise, producing more oxidation species compared to C18:1 (Figure 4.52). Oxidation of C18:2 produced many oxidation products, with C18:2 observed to have auto-oxidised before the cell has been switched on. This is suggested to have occurred off-line, during storage of the FAME and not through investigation using EC. Mass spectral data obtained are complex (Figure 4.52), and oxidation was completed on C18:2 alone.

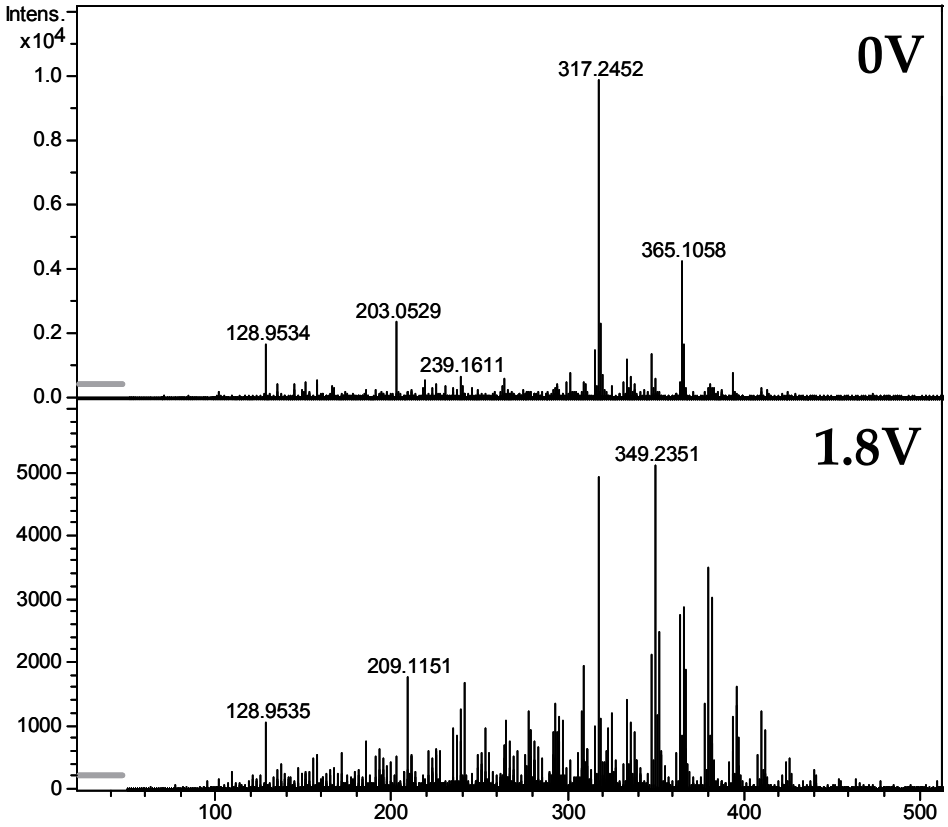


**Figure 4.52:** Positive ion ESI-MS electrochemical oxidation of C18:2 at 0 V and 1.8 V, where blue indicates the EC cell is at 0V and green indicates where the EC cell is at 1.8 V.

Auto-oxidation products identified in natural auto-oxidation positive ion ESI-FT-ICR MS (Table 4.2) which are attributed to C18:2 are methyl 9-oxononanoate, methyl 10-oxo-8 decenoate and methyl 12-oxo-9-dodecenoate. Profiles of electrochemical oxidation of these species from C18:2 were monitored and identified to be oxidation species from C18:2 (Figure 4.53).

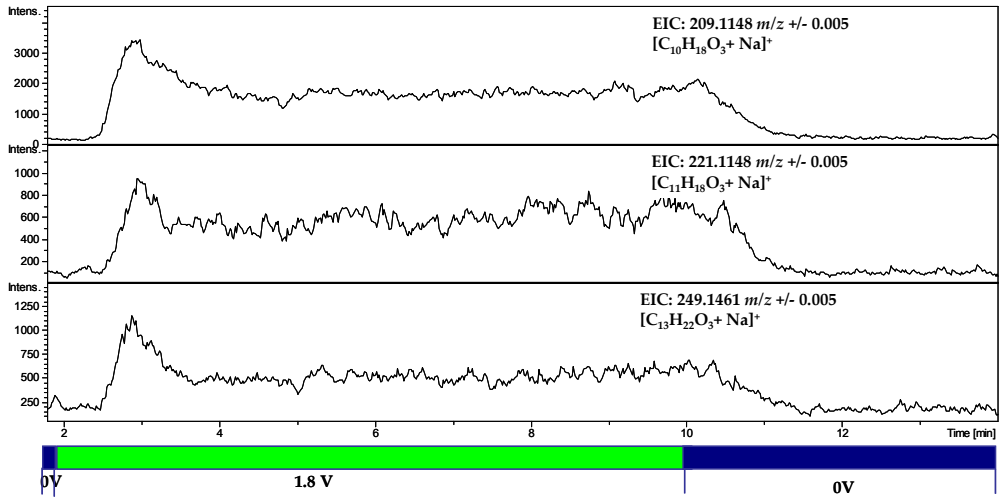


**Figure 4.53:** Positive ion ESI-MS EICC of auto-oxidation products identified in natural auto-oxidised RME (Table 4.2) samples attributed to C18:2: $[C_{10}H_{18}O_3 + Na]^+$, $[C_{11}H_{18}O_3 + Na]^+$ and $[C_{13}H_{22}O_3 + Na]^+$, where blue indicates the EC cell is at 0 V and green indicates where the EC cell is at 1.8 V.

Once the cell was turned on and C18:2 oxidised, 349.2351 *m/z* ($[C_{19}H_{34}O_4 + Na]^+$ 0.6 ppm error) was observed to be the base peak (Figure 4.52). 349.2351 *m/z* ($[C_{19}H_{34}O_4 + Na]^+$) is suggested to be part of the multiple oxygen atom containing FAME series as observed in natural and forced oxidation (Table 4.3 and Table 4.5) and the equivalent series observed in electrochemical oxidation of C18:1 (Figure 4.48). Unlike natural and forced oxidation (8O and 4O respectively) and C18:1 electrochemical oxidation only species containing up to 3 additional oxygens are detected for oxidation of C18:2 in EC conditions (Figure 4.54). Again, species suggested to be an epoxide $[C_{19}H_{34}O_3 + Na]^+$ 333.2400 *m/z* 0.6 ppm error were not detected, supporting production of auto-oxidation products in RME *via* many routes. An ion (181.199 *m/z*) which is suggested to be C8:0, a suggested auto-oxidation marker, can be observed at low intensities in

the electrochemical oxidation of C18:2 (Figure 4.55). Further research is required to investigate auto-oxidation markers in electrochemical oxidation, with more understanding of the mechanisms needed.

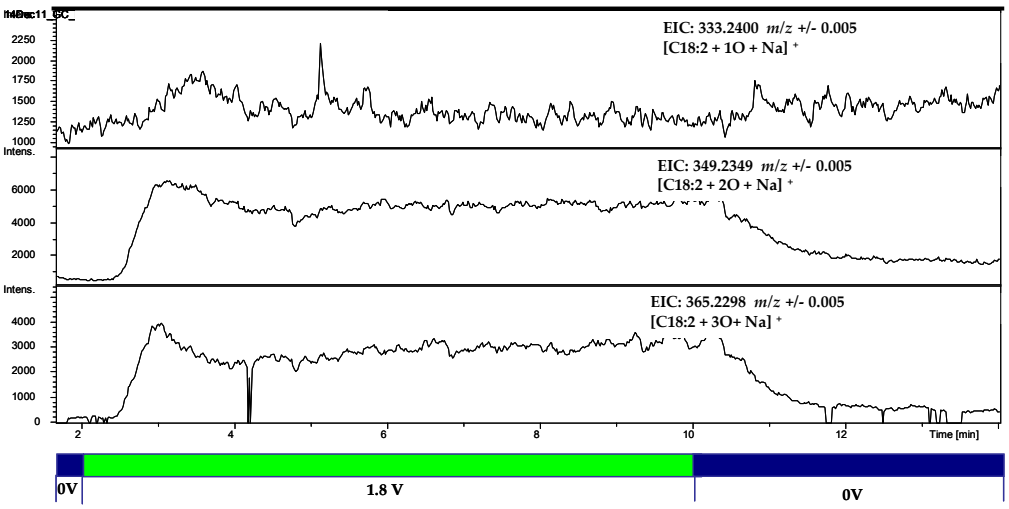


**Figure 4.54:** Positive ion ESI-MS EICCs of $[C18:2 + 1O + Na]^+$, $[C18:2 + 2O + Na]^+$ and $[C18:2 + 3O + Na]^+$ in electrochemically oxidised C18:2, where blue indicates the EC cell is at 0 V and green indicates where the EC cell is at 1.8 V.

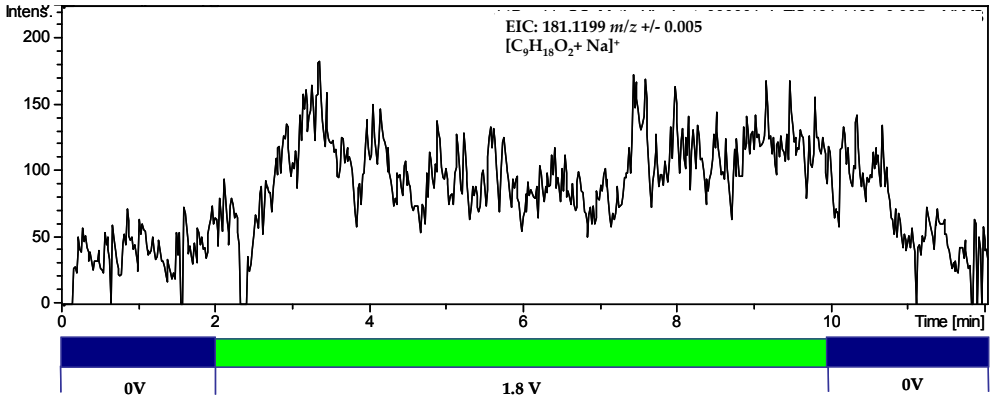


**Figure 4.55:** Positive ion ESI-MS EICC of auto-oxidation marker C8:0 ($[C_9H_{18}O_2 + Na]^+$) as described in forced oxidation of RME, where blue indicates the EC cell is at 0 V and green indicates where the EC cell is at 1.8 V.

## C18:3

C18:3 had undergone auto-oxidation whilst being stored before commencing the electrochemical oxidation process (Figure 4.56). However, after electrochemical oxidation the complexity of oxidised C18:3 increases, following a similar trend to C18:2, with C18:3 ($[C_{19}H_{32}O_2 + Na]^+$ 315.2291 *m*/*z*) no longer the base peak of the positive ion ESI-MS (Figure 4.56). This is attributed to the number of carbon-carbon double bonds on the fatty acid chain in this molecule (3) and therefore its increased reactivity.

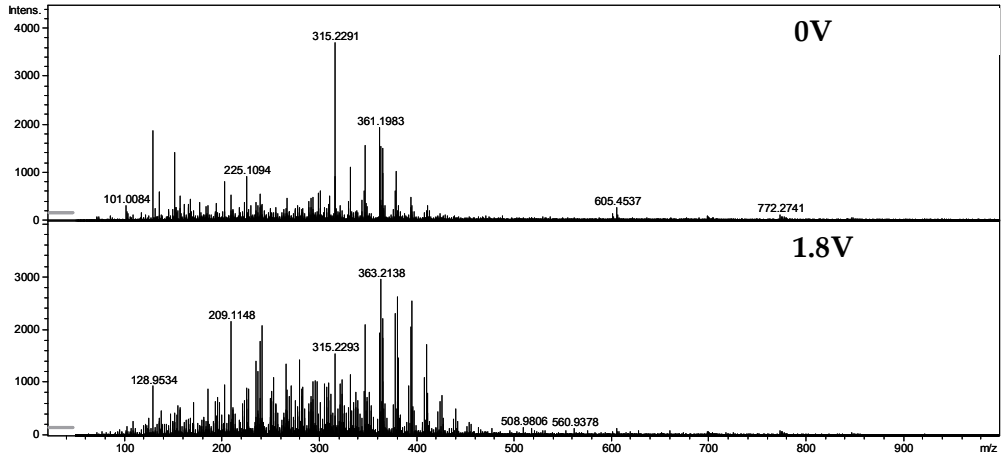


**Figure 4.56:** Positive ion ESI-MS of electrochemically oxidised C18:3 at 0 V and 1.8 V.

The TICC was observed to increase as oxidation products were produced, with C18:3 observing an opposite trend as the C18:3 concentration depletes (Figure 4.57). Oxidation products containing multiple oxygen atoms have been detected with a maximum addition of 3 oxygen atoms observed (Figure 4.57). Similarly to C18:1 and C18:2, C18:3 exhibits oxidation products not produced *via* an epoxide

route, with no ions relating to $[C18:3 + 1O + Na]^+$, suggested to be an epoxide detected (Figure 4.57).

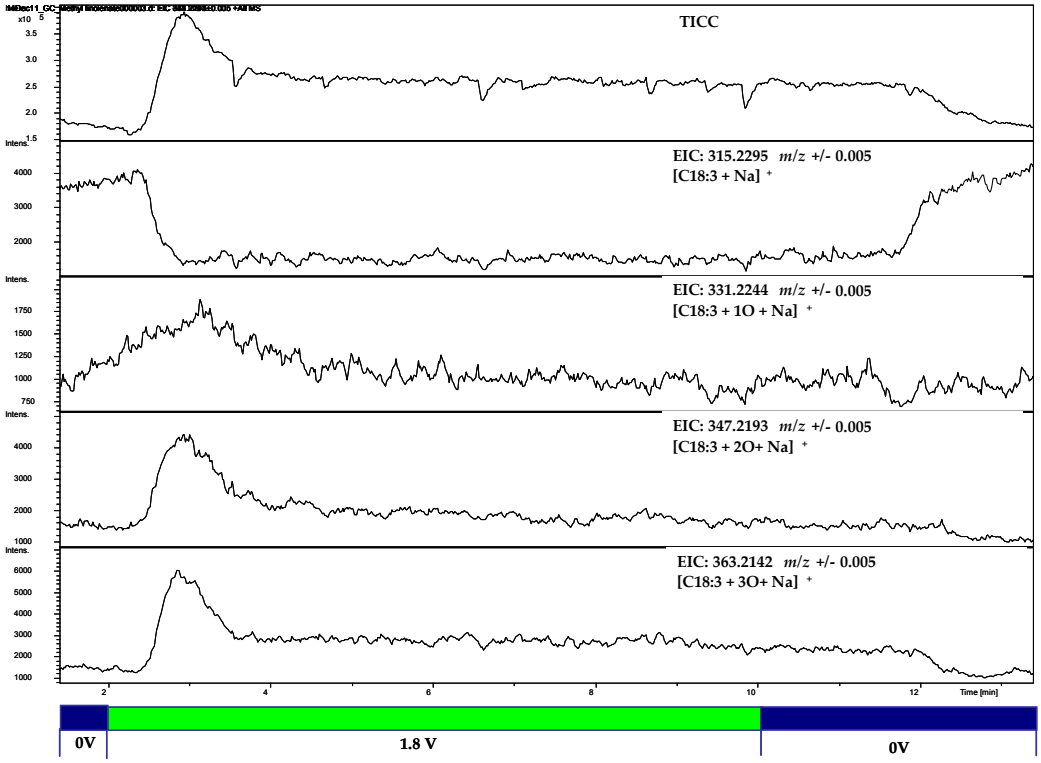


**Figure 4.57:** Positive ion ESI-MS TICC of electrochemically oxidised C18:3 and EICC of $[C18:3 + Na]^+$, $[C18:3 + 1O + Na]^+$, $[C18:3 + 2O + Na]^+$ and $[C18:3 + 3O + Na]^+$, where blue indicates the EC cell is at 0 V and green indicates where the EC cell is at 1.8 V.

Auto-oxidation products identified *via* positive ion ESI-FT-ICR MS (Table 4.2) (methyl 9-oxononanoate, methyl 10-oxo-8 decenoate and methyl 12-oxo-9-dodecenoate) were detected
Figure 4.58) in oxidised C18:3 as expected. This demonstrates the application of this technique to investigate oxidation of FAMEs.

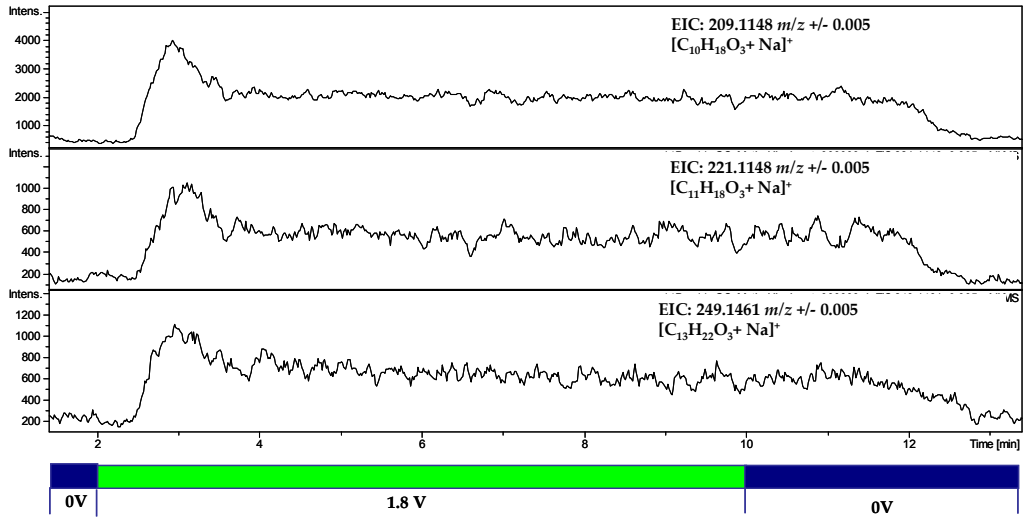


**Figure 4.58:** Positive ion ESI-MS EICC of auto-oxidation products identified in natural auto-oxidation (Table 4.2): $[C_{10}H_{18}O_3 + Na]^+$, $[C_{11}H_{18}O_3 + Na]^+$ and $[C_{13}H_{22}O_3 + Na]^+$, where blue indicates the EC cell is at 0 V and green indicates where the EC cell is at 1.8 V.

Through a forced oxidation study three markers have been identified that could be used to identify extent of auto-oxidation of RME: C8:0, nonanal and methyl *cis*-9,10-epoxystearate. Ions which correspond to C8:0 and nonanal have been successfully identified in C18:1 and C8:0 has been suggested to be identified in C18:2 and C18:3 (Figure 4.59). Whilst not used quantitatively, presence of C8:0 and nonanal suggests that oxidation *via* electrochemical cell does mimic some auto-oxidation of FAMEs. However, methyl *cis*-9,10-epoxystearate was not identified and was observed to visibly decrease when present in the starting sample (Figure 4.57). Electrochemical oxidation is a useful tool to further understand the oxidation processes of FAMEs.

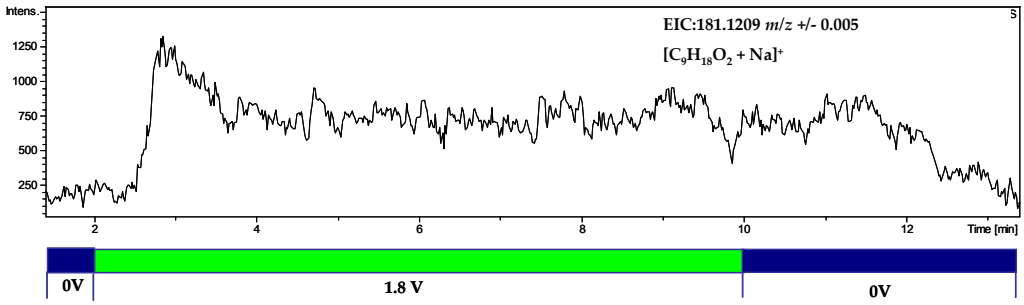


**Figure 4.59:** Positive ion ESI-MS EICC of auto-oxidation marker C8:0 ($[C_9H_{18}O_2 + Na]^+$) as suggested in forced oxidation studies, where blue indicates the EC cell is at 0 V and green indicates where the EC cell is at 1.8 V.

## RME

RME was electrochemically oxidised as per the individual FAMEs. This was completed to identify whether RME oxidised electrochemically mimics RME that has undergone auto-oxidation. C18:1, C18:2 and C18:3 oxidation products identified by oxidation of C18:1, C18:2 and C18:3 *via* the ROXY potentiostat closely mimicked auto-oxidation products observed in natural/forced auto-oxidation conditions.

Unfortunately, auto-oxidation of RME had already begun with 331.2240 *m/z* $[C_{19}H_{32}O_3 + Na]^+$ 1.1 ppm error observed as the base peak of positive ion ESI-MS of RME when the cell is at 0 V. However, through electrochemical oxidation is not produced, again suggesting this species is an epoxide.[162] Absence of ions suggested to be epoxides ($[C18:1/2/3 + O + Na]^+$) is evident in oxidised RME (Figure 4.60) whereby *m/z* 349.2349 $[C_{19}H_{34}O_4 + Na]^+$ 0.2 ppm error was the base peak. This suggests preference for C18:2 oxidation (compared with

C18:1 and C18:3), suggested to be attributed to the auto-oxidation process which has already begun.

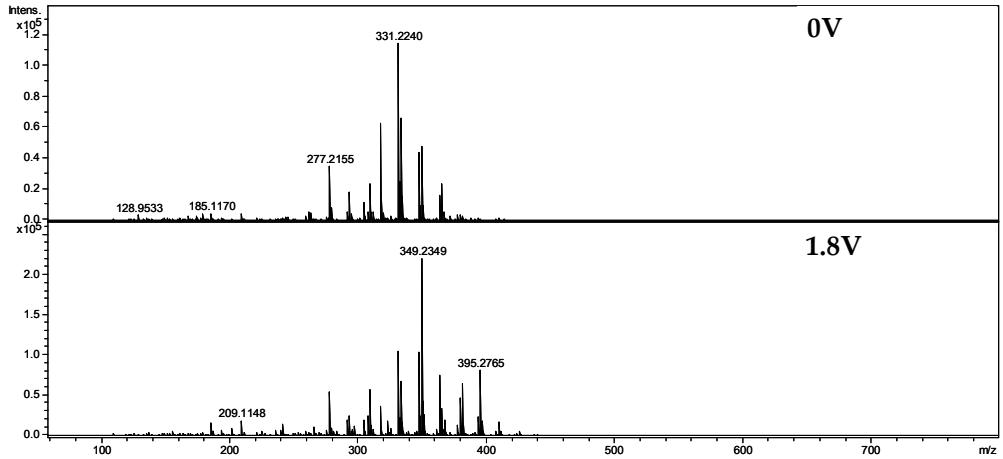


**Figure 4.60:** Positive ion ESI-MS of electrochemically oxidised RME at 0 V and 1.8 V.

Another feature that is noticeably absent from electrochemical oxidation was the presence of polymerised species (Figure 4.61). Currently it is unknown why polymerised species are not present however it is proposed that RME would require more extensive oxidation using this technique, by re-oxidising RME and analysing it offline.

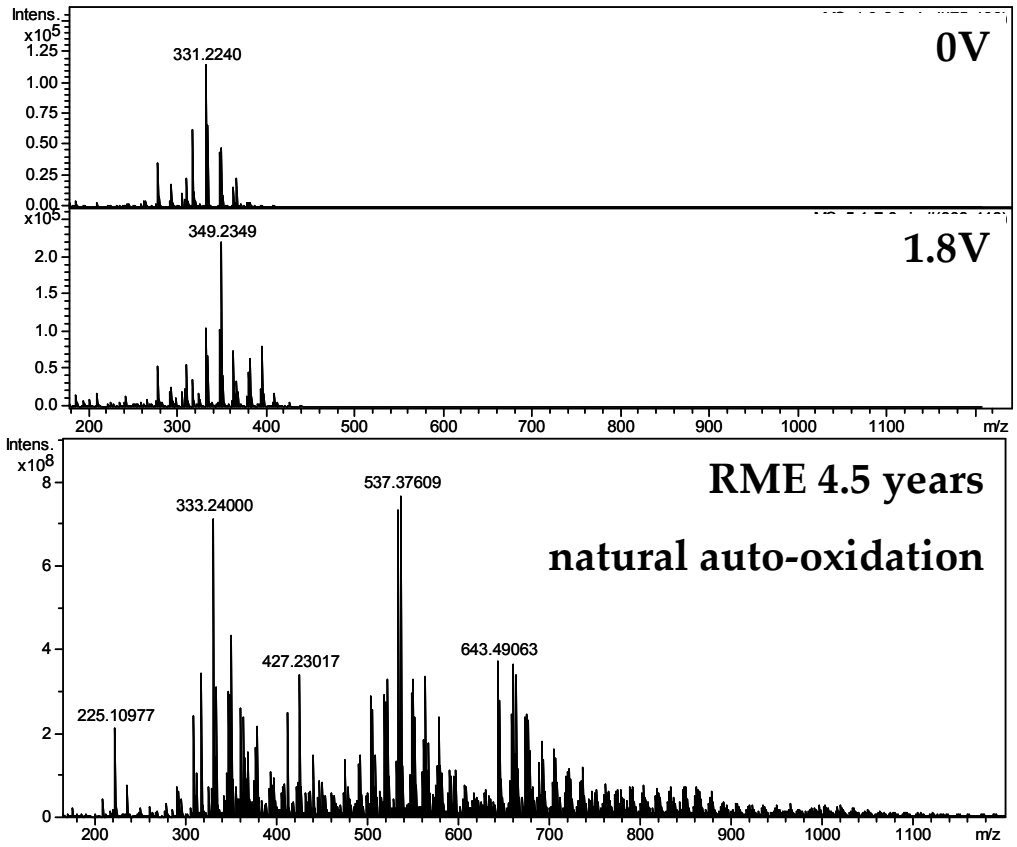


**Figure 4.61:** Comparison of positive ion ESI-MS RME electrochemically oxidised at 0 V and 1.8 V and auto-oxidised $RME_{4.5}$.

Depletion of C18:1 and C18:2 *via* oxidation in RME is evident (Figure 4.62), however there is little evidence of C18:3 depletion. The RME sample that was oxidised had already undergone some auto-oxidation and it is postulated that C18:3 had already depleted below the LOD.

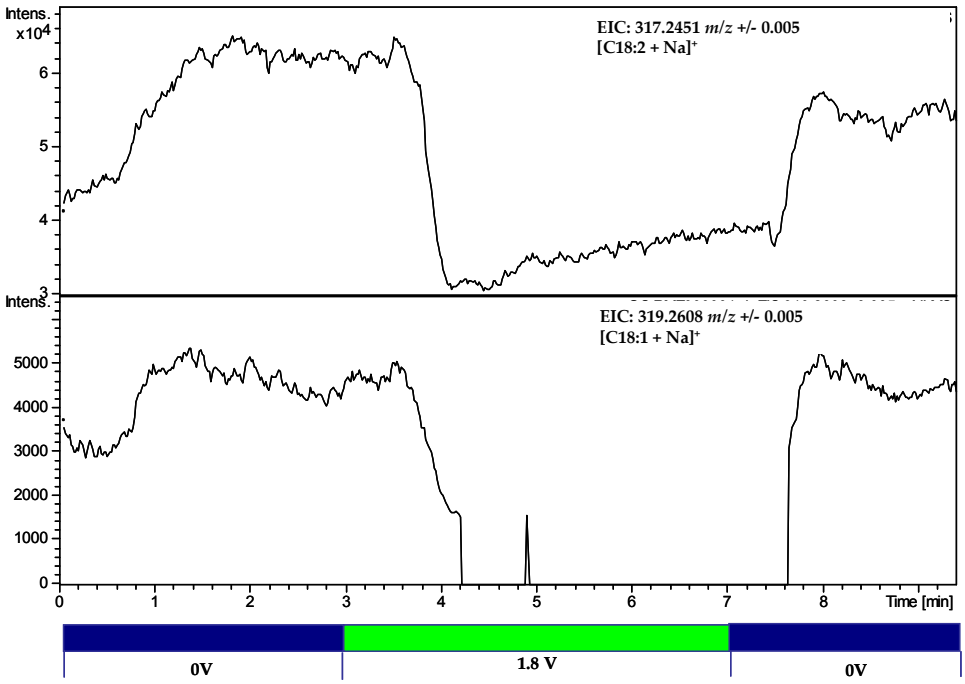


**Figure 4.62:** Positive ion ESI-MS EICC of $[C18:1 + Na]^+$ and $[C18:2 + Na]^+$ in electrochemically oxidised RME, where blue indicates the EC cell is at 0 V and green indicates where the EC cell is at 1.8 V.

Discussed throughout this section is the inability of electrochemical auto-oxidation to produce epoxides. Species present in auto-oxidised RME that are FAMEs +16 Da have been identified, however were not detected in electrochemical oxidation studies. Auto-oxidation of RME had already begun before this sample was oxidised using the ROXY potentiostat, and when FAMEs +16 Da were monitored a depletion was observed (Figure 4.63). It is suggested that the +16 Da species is an epoxide, evidenced by the absence of a +16 Da series. Additionally epoxide products present in auto-oxidised RME undergo further oxidation. The unstable nature of the epoxide ring ensures that when oxidised electrochemically they are converted to other oxidation products, such as, C18:3 + 2O.

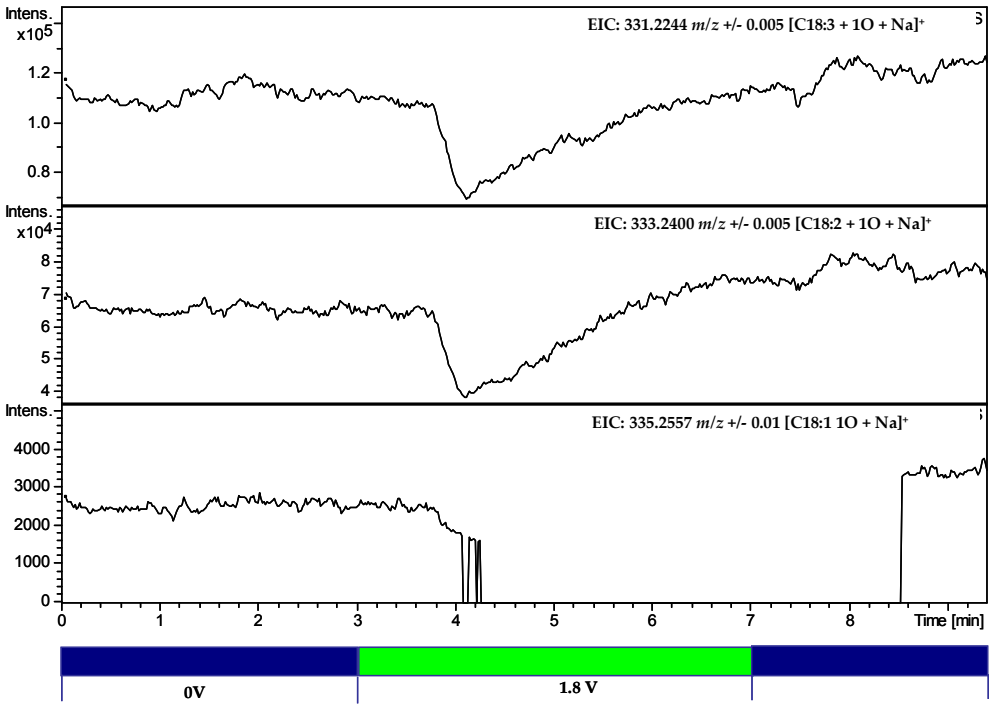


**Figure 4.63:** Positive ion ESI-MS EICC of $[C18:3 + 1O + Na]^+$, $[C18:2 + 1O + Na]^+$ and $[C18:3 + 1O + Na]^+$ in electrochemically oxidised RME, where blue indicates the EC cell is at 0 V and green indicates where the EC cell is at 1.8 V.

Detected in C18:1, C18:2 and C18:3, the auto-oxidation markers nonanal and C8:0 were also observed upon electrochemical oxidation of RME (Figure 4.64). This verifies the importance and validity of these compounds to be used as auto-oxidation markers, with further research into the electrochemical oxidation pathway required.

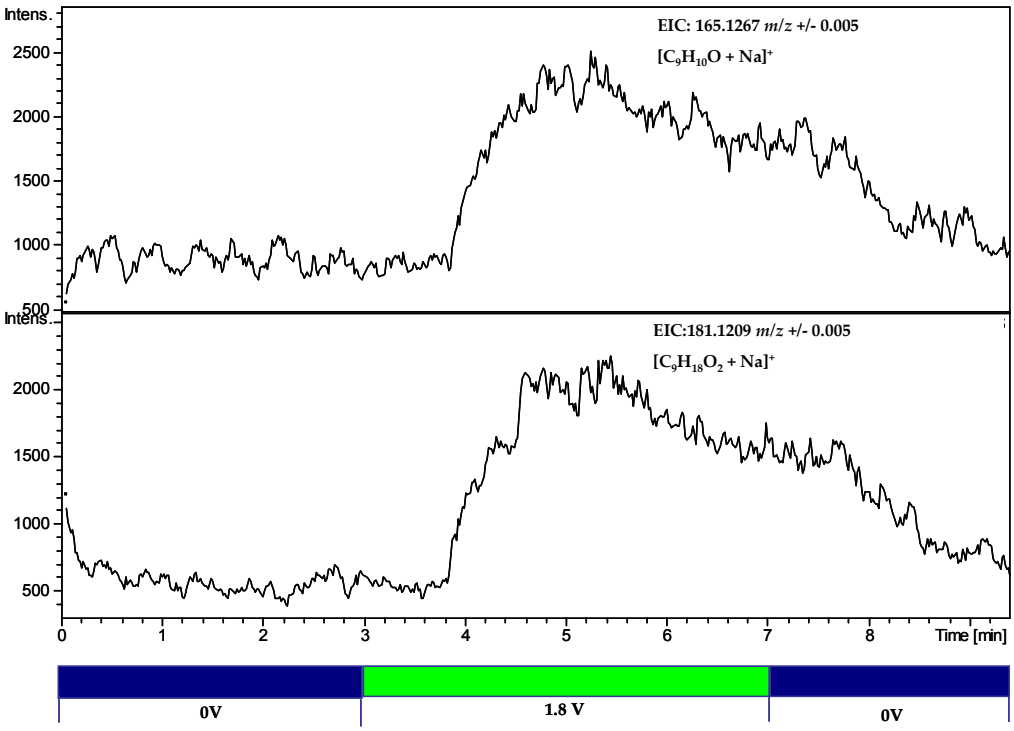


**Figure 4.64:** Positive ion ESI-MS EICCs of auto-oxidation markers as suggested in forced oxidised auto-oxidation studies: $[C_9H_{18}O + Na]^+$ and $[C_9H_{18}O_2 + Na]^+$, where blue indicates the EC cell is at 0 V and green indicates where the EC cell is at 1.8 V.

## Summary

It has been demonstrated that oxidation completed electrochemically mimics parts of the auto-oxidation process of RME. Through this electrochemical oxidation, the origin of products formed can be linked to C18:1, C18:2 and C18:3 with more certainty and support data observed throughout all oxidation experiments (natural and forced oxidation). Through electrochemical oxidation epoxides are not produced, through the use of this technique it has been proved that RME undergoes auto-oxidation *via* more than one route. This is increasingly evident in electrochemical oxidation of RME which has

already undergone auto-oxidation where species believed to be epoxides are depleted (Figure 4.63).

Oxidation of C18:1, C18:2, C18:3 and RME does not appear as extended as in natural auto-oxidation (Figure 4.61), however through collection and re-oxidation of the sample it is expected this could be mimicked. In addition, slowing the transit time of the sample in the cell could increase oxidation and thus produce higher oxygenated species. Collection of electrochemically oxidised RME can also be completed and analysed off-line and this could be used in conjunction with force oxidising FAMEs several times to investigate extended electrochemical oxidation.

Throughout this study, the presence of auto-oxidation markers identified in forced oxidation tests has been prevalent. This demonstrates the presence of these auto-oxidation markers in oxidised C18:1, C18:2, C18:3 and RME and the application of using these markers to detect auto-oxidation in conjunction with other techniques, such as GC-MS as described previously.

It is also suggested that this technique could be utilised to investigate compounds which can prevent/slow oxidation. Completed in minutes, compounds which could be used as antioxidants could be injected alongside the FAME and oxidation products monitored *via* mass spectrometry. This would also afford a catalogue of compounds to be analysed, with promising compounds taken further for more comprehensive testing, saving time, testing a wider variety of compounds and reducing costs. This approach could also be used to investigate these antioxidant compounds with individual FAMEs, potentially tailoring anti-oxidants to a higher degree.

# Chapter 5. Lubricant Oil Additives

Lubricant oils are designed to reduce friction, address problems that arise due to engine working conditions and maintain a healthy working engine environment whilst meeting strict legislation requirements.[165-167] Lubricant is composed of base oil and a lubricant additive package that varies dependent on use *e.g.* the country where it is being used.[166-168]

An engine is an environment which constantly changes; temperatures fluctuate, fuel decomposition products are generated, oxidation of fuel and base oil occurs producing various residues and deposits including sludge.[167] Therefore, an additive package is required in lubricant oil that can adapt to these conditions whilst still maintaining an appropriate working environment.[166] The additive package consists of varying percentages of compounds which are described as: detergents, dispersants, viscosity improvers, oxidation/corrosion inhibitors, anti-wear agents, anti-oxidants and pour point depressants.[165-167, 169] These additives are designed to enhance the properties of the base oil and are used to prolong the life of the lubricant oil by tackling contamination products and oxidation, which allows the lubricant oil to minimise wear and damage to the engine by reducing friction.[165-167]

Lubricant oil formulation is often not disclosed. As legislation becomes increasingly stricter, the more traditional approach of 'bucket science' to produce a working formulation is being discouraged with more understanding required about the roles of the additives and the individual/cumulative effects of these.

Traditionally, each lubricant additive has one specific role within the engine, however they can work synergistically enhancing/aiding the properties of other additives. This is often at a cost, *e.g.* reducing the benefit of its primary function. This can lead to over-loading of the base oil with lubricant additives in an attempt to achieve an appropriate balance. As legislation grows increasingly tighter, a reduction in the amount of lubricant additives used will be required, affecting the dynamic of the lubricant additives.

Whilst specific lubrication packages are a closely guarded secret, the fundamental composition of the lubricant additives is well known.[166, 167] The focus of this work is on dispersant additives. Dispersants are composed of a hydrocarbon tail (typically polyisobutylene (PiB)), a hook (typically maleic anhydride) and a polar head (typically an amine or alcohol) (Figure 5.1).[166, 167, 170] Their primary function is to aid the stabilisation of unwanted products generated from the fuel process during an engine's operation.[165-167]

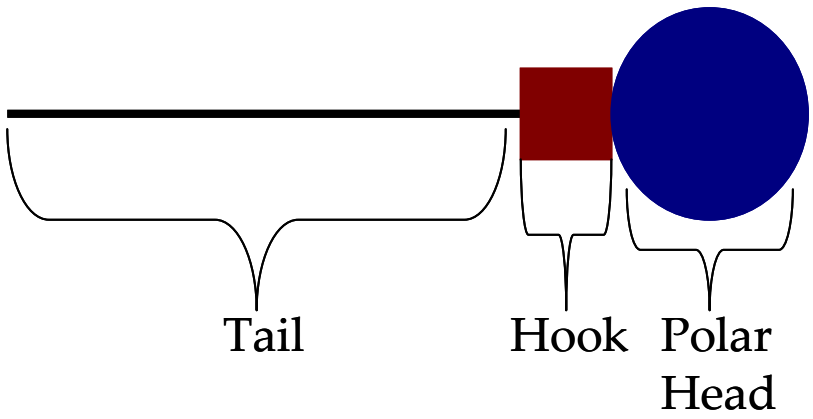


**Figure 5.1:** Fundamental dispersant structure.

Initially, a PiB succinic anhydride (PiBSA) polymer is produced *via* reaction of PiB (hydrocarbon tail) and maleic anhydride (the hook).

This is completed *via* one of two processes, either $AlCl_3$ or $BF_3$ routes, producing differing PiBSA polymers (Figure 5.2).[165-167]

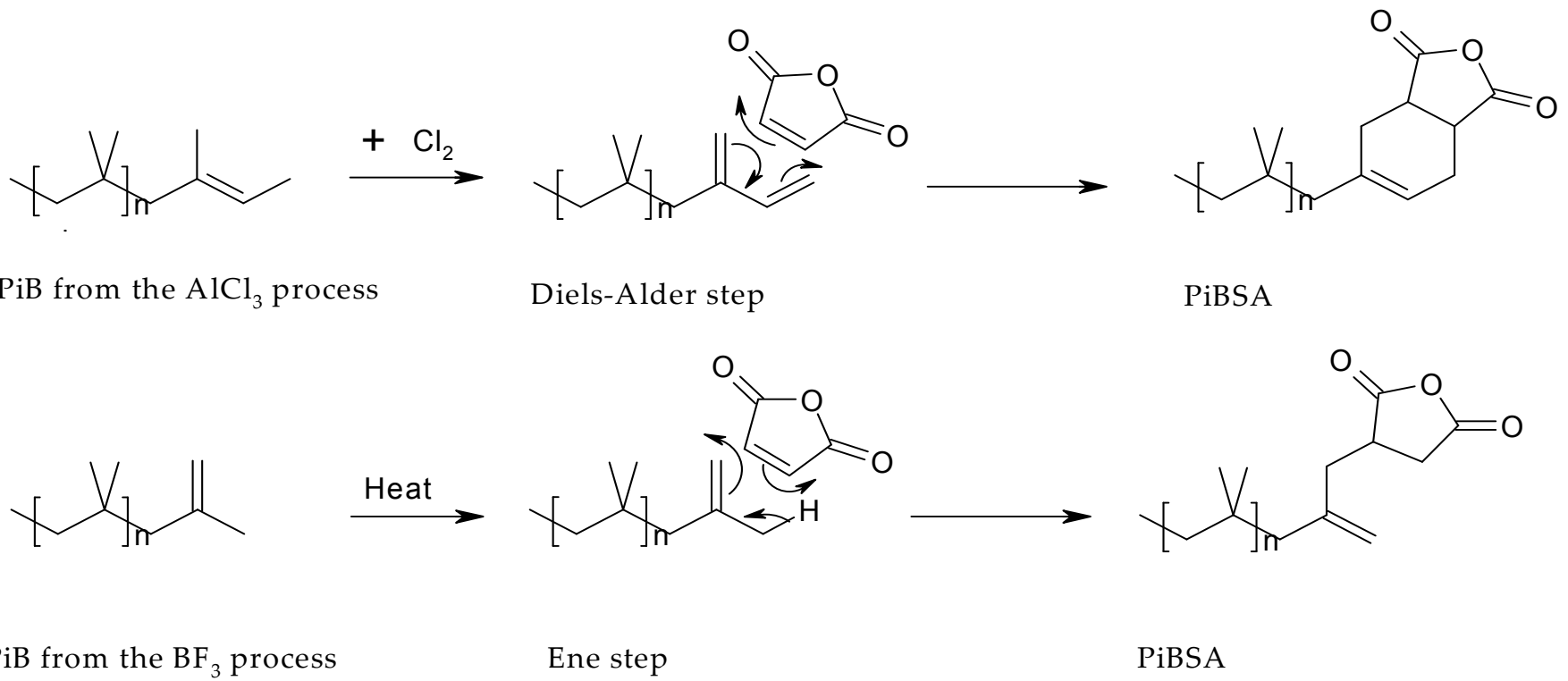


**Figure 5.2:** Production of PiBSA polymers from $AlCl_3$ and $BF_3$ processes.

To produce the final dispersant the PiBSA polymer is reacted with either an alcohol to produce a succinic ester or with an amine to produce a PiB succinimide polymer (Figure 5.3).[167, 170] The latter being the most common dispersant used in lubricant packages.[167]

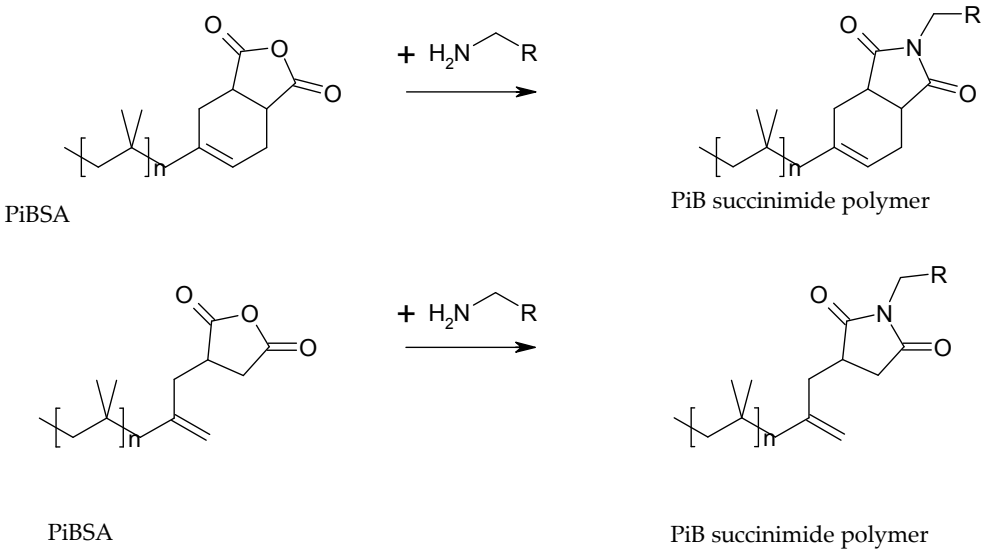


**Figure 5.3:** Reaction schemes describing the production of a PiB succinimide polymer from a PiBSA polymer produced *via* an $AlCl_3$ (top) and $BF_3$ (bottom) pathway.

Production of a multi-functional lubricant oil additive that can target multiple issues is advantageous. With emphasis on greener fuel technology a multi-functional additive which reduces the amount of additives in lubricant oil would be welcomed. A multi-functional additive could potentially reduce production costs and time, meet stringent legislation whilst maintaining a lubricant oil package that continues to work effectively in an engine.[167-170]

## 5.1. PiBSA Polymers and Dispersant Type Molecule Analysis

This work focuses on the analysis of a dual-functionality novel dispersant additive that has been synthesised at BP.

Synthesis of a PiB succinimide polymer dispersant was completed at BP in two steps. Initially, PiBSA polymer **(**Figure 5.2**)** and N-vinylimidazole (VIMA) (Figure 5.4) were reacted with the aim of grafting multiple VIMA groups to the hydrocarbon tail of the PiB repeat unit (Figure 5.4). This sample (VIMA intermediate) was then reacted with N-phenyl-p-phenylenediamine (polar head group) to produce a dispersant (Figure 5.3), preferably with multiple VIMA grafts (final dispersant).

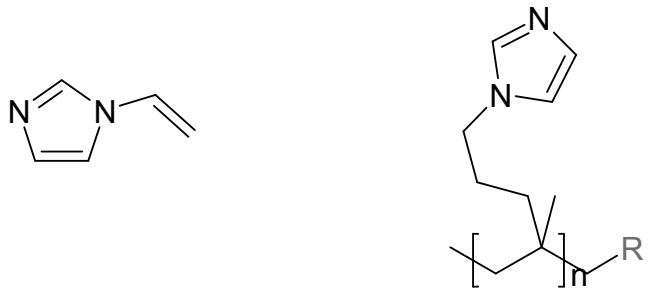


**Figure 5.4:** N-vinylimidazole (VIMA) (left) and the postulated structure of the desired VIMA grafted a) PiBSA polymer, where R = hook (maleic anhydride), b) PiB succinimide dispersant, where R = hook and polar head group (maleic anhydride and N-phenyl-p-phenylenediamine) (right).

Analysis was completed on four samples: PiBSA, VIMA, VIMA intermediate and final dispersant. This was undertaken to establish the components in each sample including identification of: PiBSA polymer type, success of VIMA graft and final succinimide dispersant.

Polymer analysis can be a difficult task, polydispersity ensures that higher concentrations of sample are required for analysis, with wider dispersed polymers harder to analyse. Additionally, polymers are hard to ionise *via* gas phase ionisation techniques, with softer ionisation techniques usually required *e.g.* MALDI. As the reaction proceeds, different products (desired and unwanted) can be generated. Polymeric products contain a repeat unit and if this is present in a mixture with other polymer series, such as starting polymer material (PiBSA polymer) or side reaction polymers, the sample will contain a complex mixture of compounds. Compounds found in the different samples (PiBSA, VIMA, VIMA intermediate and final dispersant) possess varying functionality which complicate analysis. For analysis of these samples a technique was required that was able to analyse a variety of different chemistries. To reduce the complexity of analysis a chromatography technique is required, coupled to a suitable detector; in this case a UV detector and mass spectrometer were used.

Samples from this reaction scheme were not soluble in typical ESI-MS solvents (MeOH, MeCN and $H_2O$), however were found to be soluble in hexane. The insoluble nature of the samples in MeOH, MeCN and $H_2O$ ruled out the use of reversed phase HPLC-MS. Normal phase HPLC-MS was considered, however it is not readily compatible with API techniques, additionally the use of large volumes of hazardous solvents deemed this technique unsuitable. The samples of interest were not sufficiently volatile for GC-MS. It was expected this sample would be complex as it was analysis of a polymer and the different reaction steps further complicated this, therefore a chromatography technique was required to try and simplify this. SFC-UV MS was determined to be the most suitable chromatographic

technique, with $CO_2$ providing density and diffusion of a liquid and viscosity of a gas.

Analysis is of a two step reaction, whilst PiBSA polymer is a starting reagent, other compounds, such as VIMA grafted PiBSA polymer and a VIMA grafted PiB succinimide polymer are likely to be present. These compounds contain (potentially) many nitrogen atoms, therefore +ve ESI-MS was deemed most appropriate for analysis of these compounds.

Previous studies into PiBSA polymers have focussed on the use of –ve ion ESI-MS however the nature of the expected intermediates and dispersant meant that positive ion ESI-MS was more appropriate. [165, 166]

### 5.1.1. PiBSA

The first sample analysed was PiBSA. Analysis suggests that the PiBSA polymer supplied was produced using a $BF_3$ process (Figure 5.2). PiBSA polymers eluted across a 3.2-6.6 minute retention time range (Figure 5.5) and were observed as the sodiated species. The repeat unit of PiBSA ($C_4H_8$, 56 *m*/*z*) was observed throughout the +ve ion ESI-MS across the elution range 3.2-6.6 minutes (Figure 5.6). Different repeat units of n = 3-20 were detected above the LOD for these PiBSA polymers. Whilst baseline separation was not achieved, small differences in separations are observed (Figure 5.5).

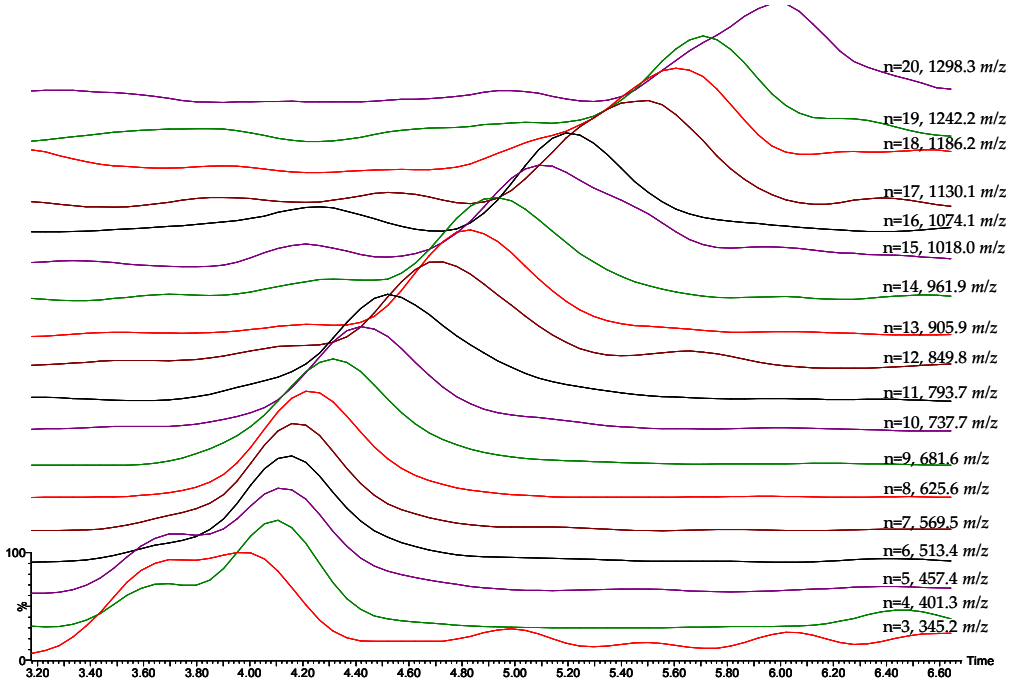


**Figure 5.5:** EICCs of [PiBSA + Na]$^+$ polymer series in the PiBSA sample, detected at repeat units of n = 3-20.

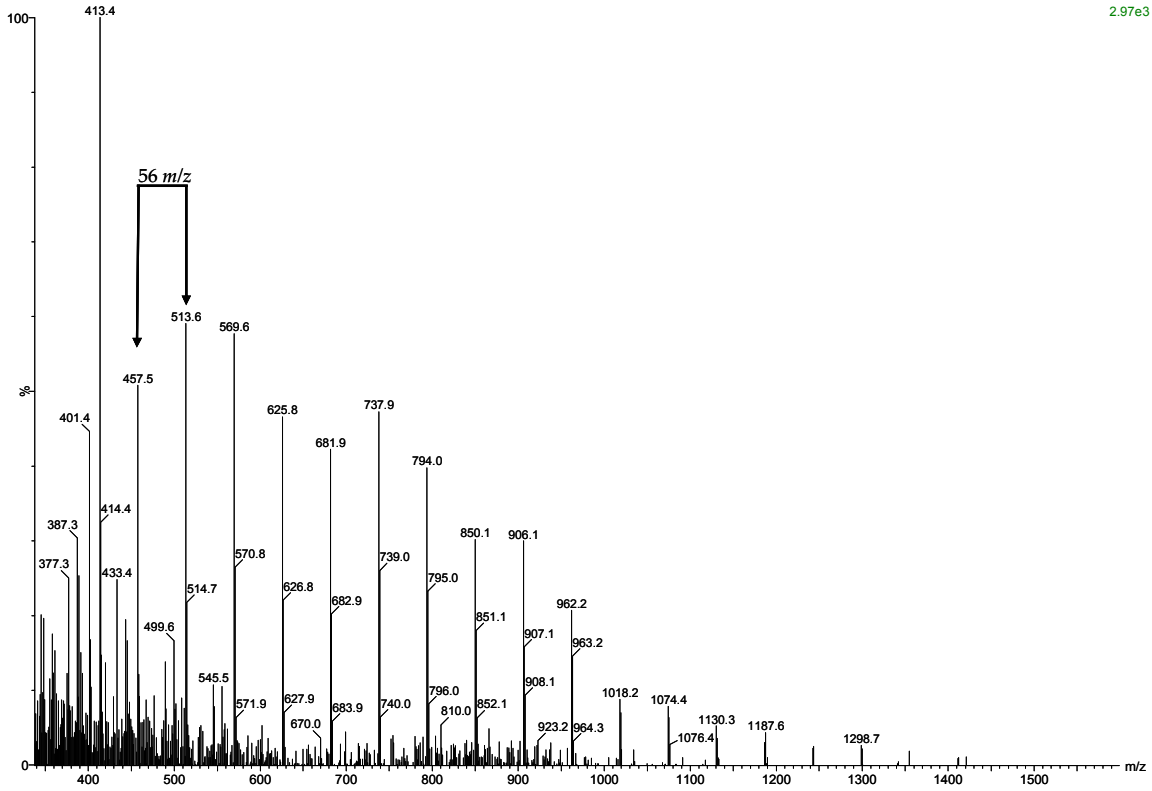


**Figure 5.6:** Positive ion ESI-MS from the PiBSA sample across a 3.2-6.6 minute retention time range highlighting the repeat unit of 56 *m/z* units and the $[PiBSA + Na]^+$ polymer series.

Alongside the PiBSA polymer series another polymer series was detected. PiBSA polymers undergo reactions with water *via* hydrolysis producing a PiB dicarboxylic acid polymer (Figure 5.7).[165, 166] Analysis of the PiBSA sample suggests this species is present and is detected in its sodiated form, however this polymer contains two interchangeable protons. The interchangeable nature of these hydrogens can complicate analysis, whereby the $[PiB\ dicarboxylic\ acid + Na]^+$ polymer series is isobaric with the [PiB monosodium carboxylate monocarboxylic acid + $H]^+$ (Figure 5.7) polymer series and is not distinguishable by mass spectrometry. +ve ion ESI-MS data suggests the presence of a PiB monosodium carboxylate monocarboxylic acid polymer series with one H

interchanged for sodium, which is detected as the +H and +Na adducts; [PiB dicarboxylic acid + Na]$^+$ polymer series and [PiB disodium carboxylate + H]$^+$ polymer series (Figure 5.7). These species elute at an increased retention time (13.9-22.0 minutes, Figure 5.8) compared to the PiBSA polymer series (3.2-6.6 minutes) (Figure 5.5), as would be expected, and this is attributed to the strong interactions with the silica stationary phase.

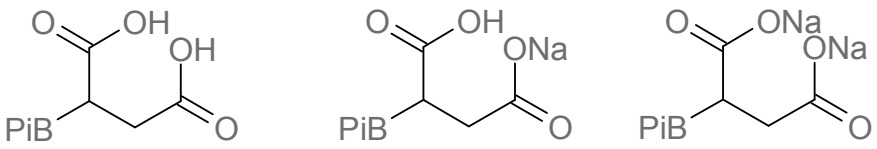


**Figure 5.7:** PiB dicarboxylic acid polymer, PiB monosodium carboxylate monocarboxylic acid and PiB disodium carboxylate.

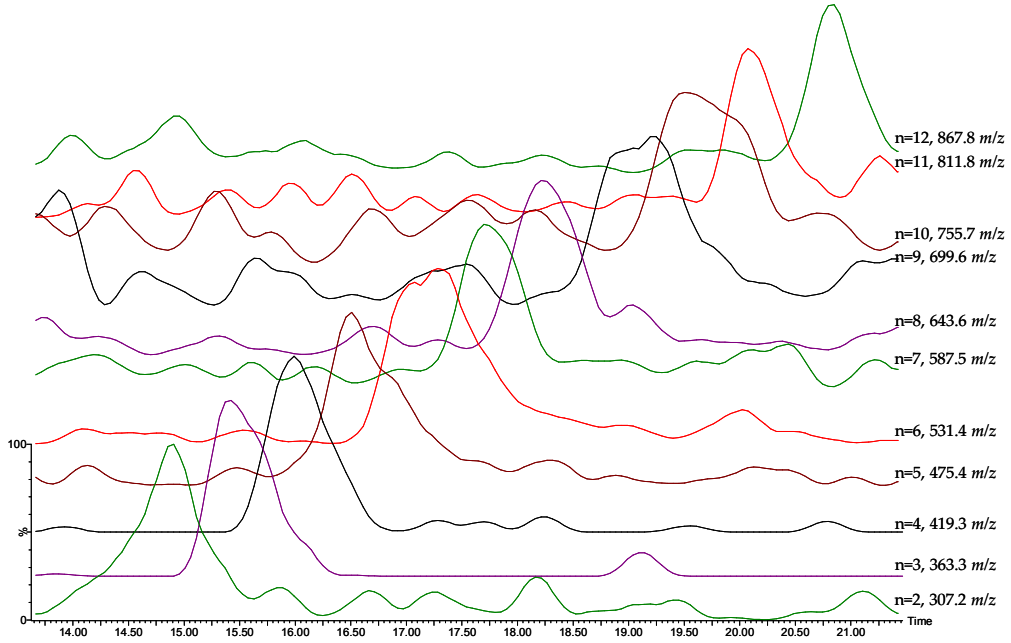


**Figure 5.8:** EICCs of [PiB dicarboxylic acid - H + Na + H]$^+$ / [PiB dicarboxylic acid + Na]$^+$ polymer series detected in the PiBSA sample at repeat units of n = 2-12.

## 5.1.2. VIMA grafted PiBSA

The next stage of the synthetic route was to react the PiBSA sample with VIMA with the aim of producing a multi-grafted PiBSA. Analysed independently, VIMA was observed to elute at a longer retention time (~19 minutes) in comparison to the PiBSA polymer (3.2-6.6 minutes) (Figure 5.9). These conditions were not optimised for analysis of VIMA and this can be observed by the poor peak shape obtained (Figure 5.9).

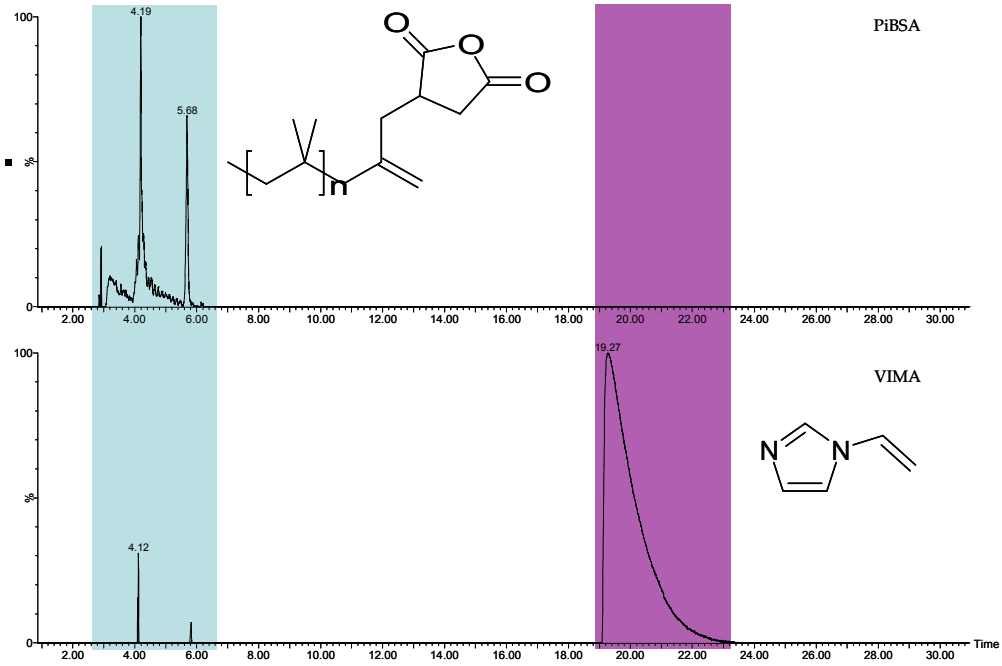


**Figure 5.9:** UV chromatogram comparison of PiBSA and VIMA samples. Shaded blue region represents PiBSA polymer elution range, shaded purple region represents VIMA elution range.

The VIMA intermediate sample was physically different, with the sample appearing green/grey compared to the paler gold colour of the PiBSA polymer and of increased viscosity. Comparison of PiBSA, VIMA intermediate and VIMA UV chromatograms exhibit similar features in VIMA intermediate suggested to be residual reagent (Figure 5.10).

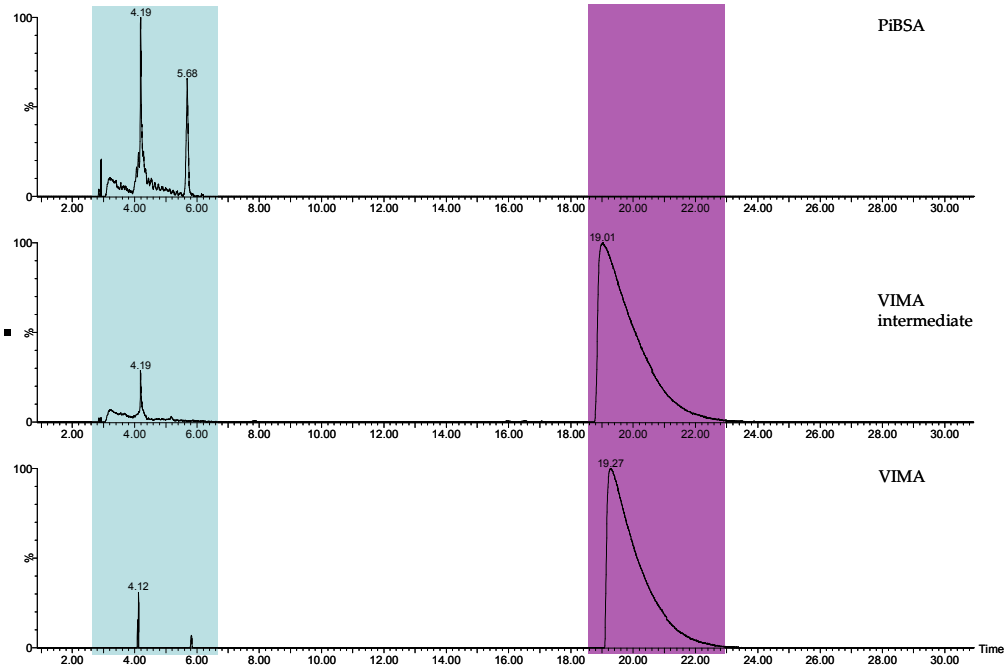


**Figure 5.10:** UV chromatogram comparison of PiBSA, VIMA intermediate and VIMA samples. Shaded blue region represents PiBSA polymer elution range, shaded purple region represents VIMA elution range.

The PiBSA polymer, eluting at 3.2-6.6 minutes, was observed in the VIMA intermediate sample using UV (Figure 5.10) and mass spectrometry detection. This suggests that not all the PiBSA polymer underwent a reaction with VIMA. As expected, no PiBSA polymer was detected in the VIMA sample. VIMA was observed in the VIMA sample and residual unreacted VIMA was observed in the VIMA intermediate sample (~19 minutes) (Figure 5.10).

Alongside VIMA and the PiBSA polymer series, a polymer series was observed to elute at 5.2-8.0 minutes with the same 56 *m*/*z* repeat unit as the PiBSA polymer series (Figure 5.11). This polymer series is suggested to be a VIMA grafted PiBSA polymer. However, contrary to expectation (Figure 5.4), +ve ion ESI-MS data were consistent with the presence of only one VIMA graft per PiBSA

polymer and was detected with repeat unit n = 2-11 (Figure 5.11), a much shorter range than its PiBSA polymer counterpart (n = 3-20) (Figure 5.5). VIMA is suggested to be attached *via* the double bond or on the ring of the hook group (Figure 5.12). The data suggest that a double bond in the VIMA grafted PiBSA polymer (Figure 5.12) is broken during grafting of the VIMA, with a polymer series observed at +2 *m/z* compared to addition of a single VIMA to PiBSA with the double bond still intact. This is further supported by species observed in the final dispersant sample. It is suggested that this double bond has been lost from the hydrocarbon backbone (Figure 5.12).

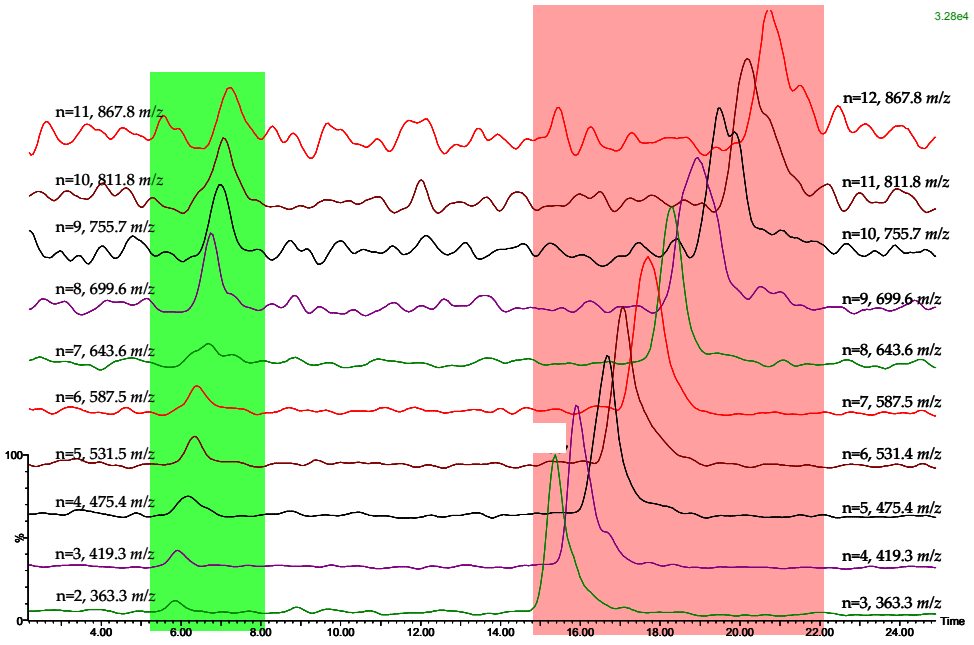


**Figure 5.11:** EICCs of [PiB dicarboxylic acid - H + Na + H]$^+$ / [PiB dicarboxylic acid + Na]$^+$ polymer series (shaded pink) detected at repeat units of n = 2-12 which is isobaric with [PiBSA with VIMA graft and LDB + H]$^+$ polymer series (shaded green) detected in the VIMA intermediate sample at repeat units of n = 2-11, where LDB = loss of double bond.

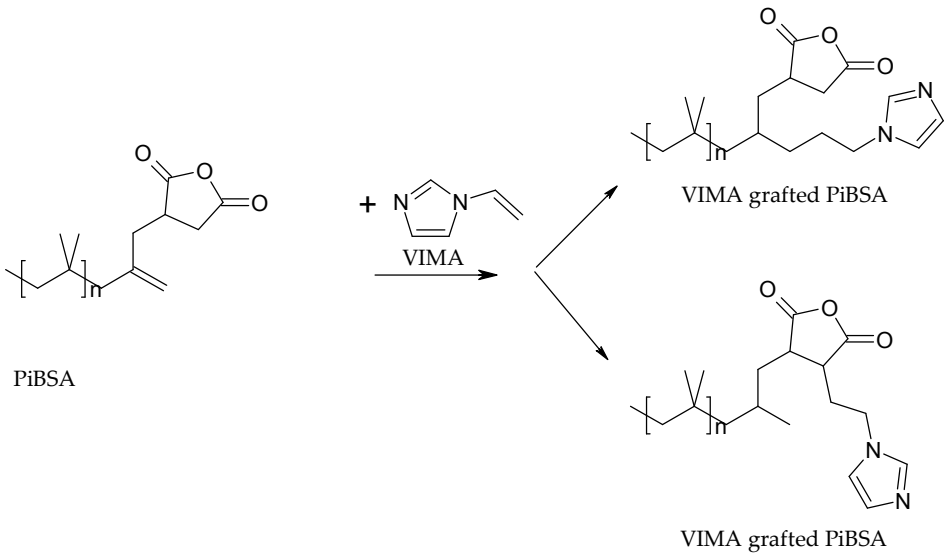


**Figure 5.12:** Proposed structures for PiBSA with a single VIMA graft and LDB polymer as detected using +ve ion ESI-MS adding across the double bond (top) and onto the ring of the hook group (bottom).

Similarly to species observed in PiBSA, this species (PiBSA + VIMA graft and loss of a double bond polymer series) is isobaric with the previously discussed PiB dicarboxylic acid 1H/Na exchange polymer. The SFC data suggests that both postulated species are present (Figure 5.11). EICCs of this *m*/*z* polymer series show two sets of peaks observed at 5.2-8.0 and 13.9-22.0 minutes, with the former present only in the VIMA intermediate sample (Figure 5.1, Figure 5.11). The polymer series eluting at 5.2-8.0 minutes is suggested to be a singly grafted PiBSA with VIMA and loss of a double bond polymer (Figure 5.12). The polymer series present at 13.9-22.0 minutes is suggested to be (as previously observed in the PiBSA sample (Figure 5.5)) the PiB dicarboxylic acid with 1 H/Na exchange. The retention times also suggest very different chemistry between these eluted analytes, further supporting this assignment.

### 5.1.3. VIMA Grafted Dispersant

The final sample was the product of the VIMA intermediate sample reacted with n-phenyl-p-phenylenediamine to produce a VIMA grafted PiB succinimide polymer. Comparisons of PiBSA, VIMA, VIMA intermediate and the final dispersant sample UV chromatograms display obvious differences (Figure 5.13). Unreacted VIMA was still present in the final sample, alongside small amounts of PiBSA polymer, with little evidence to suggest the presence of the PiB dicarboxylic acid or its exchangeable species. +ve ion ESI-MS analysis across 11.5-14.5 minutes of the final sample (Figure 5.15) suggests the presence of a grafted VIMA PiB succinimide polymer. Similar to species observed in the VIMA intermediate sample, +ve ion ESI-MS analysis suggests a PiB succinimide polymer with a single VIMA graft (Figure 5.14 and Figure 5.15), contrary the expectation of a dispersant with multiple grafts *e.g.* Figure 5.4. This species (Figure 5.14) is also consistent with loss of a double bond within the molecule, suggested to occur in the previous step (Figure 5.12).

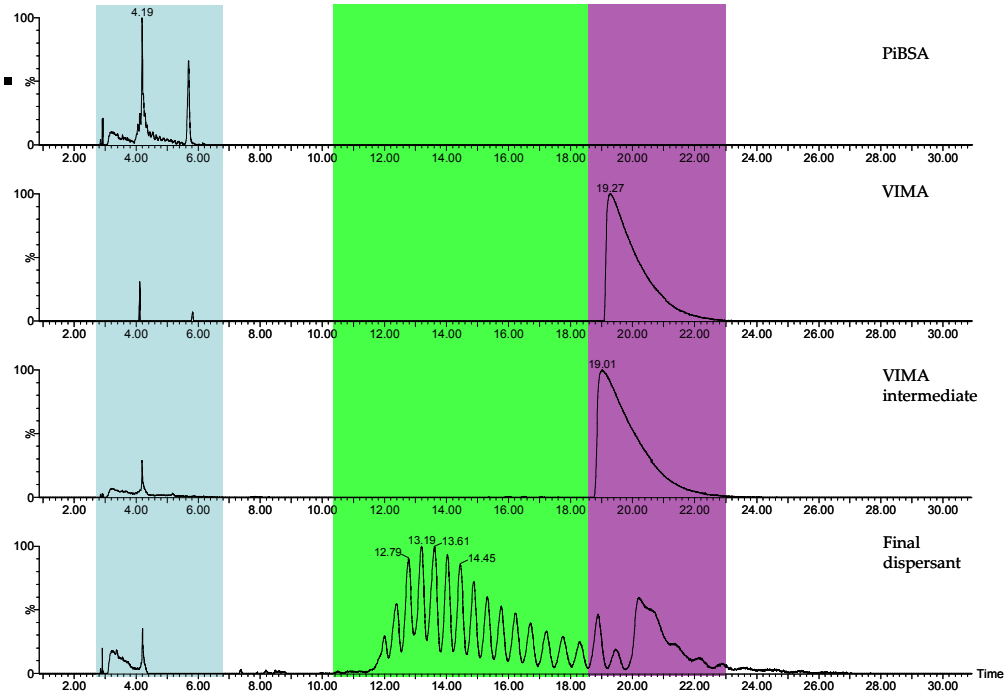


**Figure 5.13:** SFC-UV chromatogram comparison of PiBSA, VIMA intermediate, final dispersant and VIMA samples. Shaded blue region represents PiBSA polymer elution range, shaded purple region represents VIMA elution range, shaded green region represents final dispersant polymer elution range.

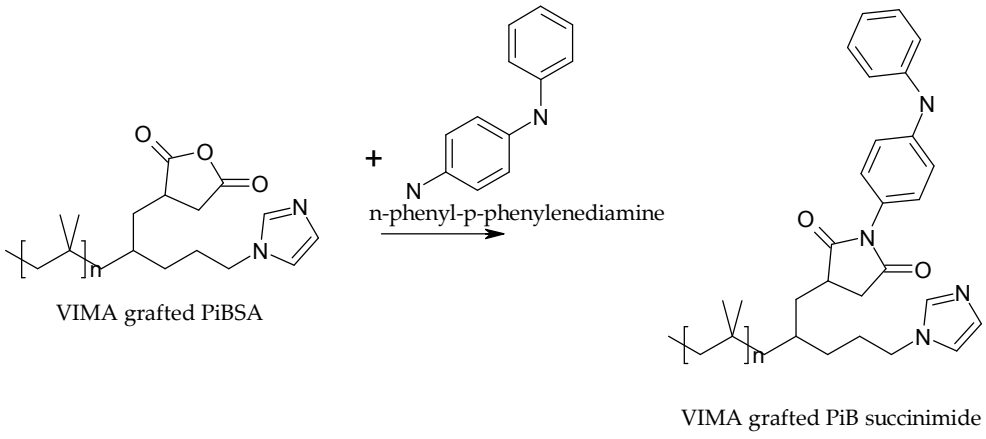


**Figure 5.14**: Proposed structure for the VIMA grafted PiB succinimide.

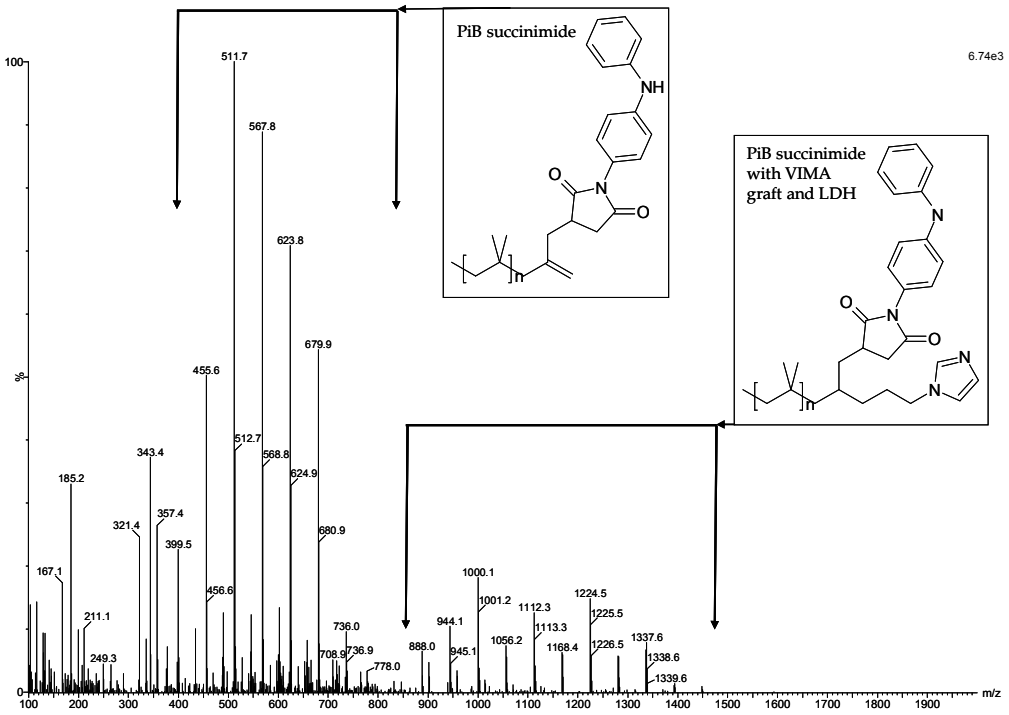


**Figure 5.15:** Positive ion ESI-MS spectrum across an 11.5-14.5 minute retention time highlighting the presence of [PiB succinimide + Na]$^+$ polymer series and [PiB succinimide with VIMA graft with LDB + Na]$^+$ polymer series as detected in the final dispersant sample.

Baseline separation of the different repeat unit VIMA grafted PiB succinimide polymers with loss of double bond is not observed, although separation is equivalent to other polymers identified (Figure 5.16). This polymer series is successfully separated from PiBSA and PiBSA grafted with VIMA with loss of the double bond polymer series (Figure 5.5 and Figure 5.11). Although co-elution with unreacted VIMA occurs this does not present a problem.

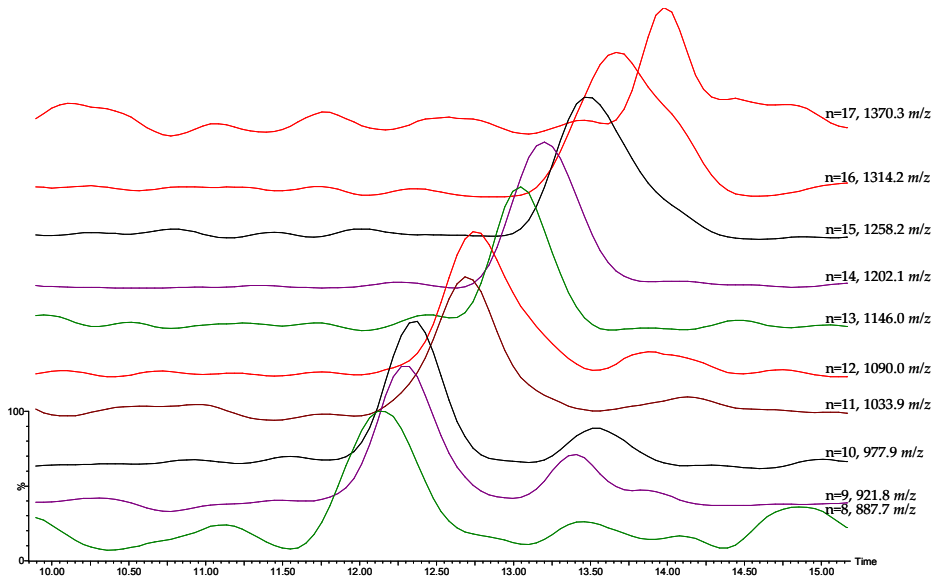


**Figure 5.16:** EICCs of [PiB succinimide with VIMA graft and LDB + Na]$^+$ polymer series detected at repeat units of n = 8-17 in the final dispersant sample .

Observation of reduced PiBSA polymer in the final sample is suggested to be linked to production of an un-grafted dispersant polymer (Figure 5.16). Both PiBSA polymer and VIMA grafted PiBSA polymer undergo the same reaction with N-phenyl-p-phenylenediamine. This produces a more traditional type dispersant; a PiB succinimide polymer with observed repeat units of n = 2-13 (Figure 5.17). Again, some co-elution between polymer series is observed, however with the aid of chromatography the complexity of analysis is reduced (Figure 5.18).

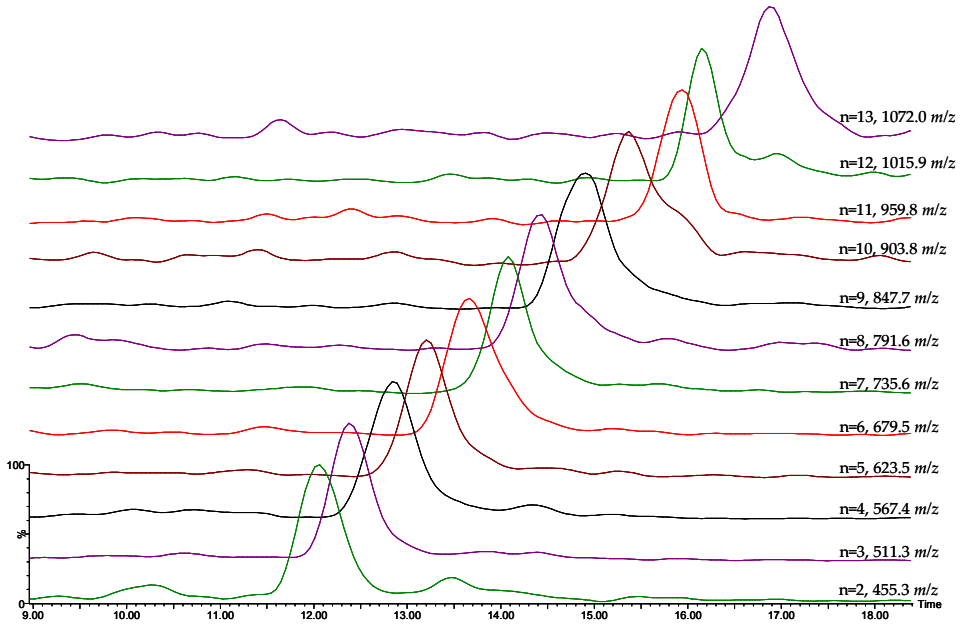


**Figure 5.17:** EICCs of [PiB succinimide + Na]$^+$ polymer series detected at repeat units of n = 2-13 in the final dispersant sample.

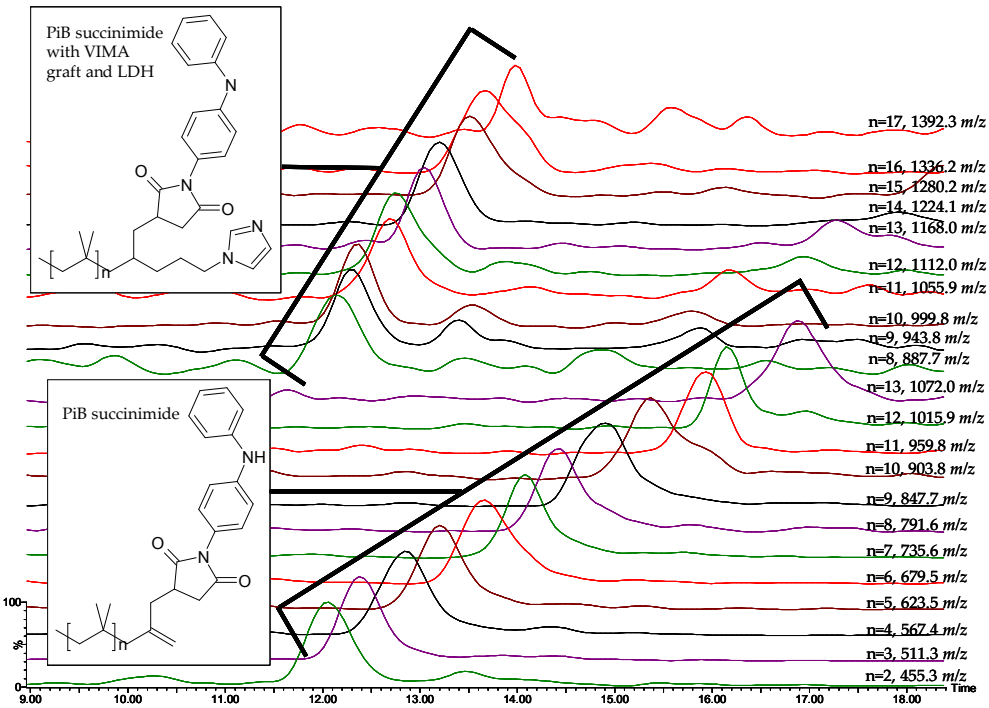


**Figure 5.18:** EICCs of polymer series detected in the final dispersant sample: [PiB succinimide with VIMA graft and LDB + Na]$^+$ and [PiB succinimide + Na]$^+$.

In comparison, the PiB succinimide polymer is detected with the double bond intact contrary to observations of the VIMA grafted PiB succinimide polymer. Therefore it is postulated loss of the double bond is directly related to addition of the VIMA. It is further speculated that VIMA adds across the double bond as depicted in Figure 5.12 (top) and throughout from this point onwards.

## 5.2. Conclusion

Several compounds with varying chemistries within the reaction mixtures were identified and this was only possible with SFC-UV MS. Analysis *via* infusion and RP-HPLC-MS was unsuitable due to the insoluble nature of these samples in MeOH, MeCN and DCM.

Products identified included PiBSA polymer, PiB dicarboxylic acid polymer, VIMA grafted PiBSA polymer, VIMA grafted PiB succinimide polymer and PiB succinimide polymer. Chromatography simplified analysis with PiBSA, VIMA grafted PiBSA and VIMA grafted PiB succinimide successfully separated from one another. Separation of individual repeat units within each series proved harder, with baseline resolution not observed for any polymer series here. However, analysis was required to identify whether the graft had been successful and therefore baseline separation was not required. Some separation of repeat units in polymer series is observed and with the aid of the mass spectrometer co-elution does not present a problem for analysis.

The use of SFC-UV MS is also advantageous for analysis of individual lubricant additives and *in situ* lubricant additives; Base oil and petrodiesel are predominantly non-polar contrary to additives

which are typically polar. These compounds are compatible and are able to be analysed with this technique: petrodiesel and base oil can be detected by the UV detector and appear invisible in ESI-MS, whilst lubricant additives, as shown here, can be detected *via* both techniques.

# Chapter 6. Final Conclusions

This research has demonstrated the complexity of auto-oxidised RME and the necessity of the appropriate techniques for analysis with GC-MS, infusion positive ion ESI-FT-ICR MS, positive ion EC-ESI-TOF-MS, HPLC-positive ion ESI-MS and positive ion ESI-SFC-UV MS have all been used to investigate auto-oxidised RME and RME in petrodiesel. It has highlighted for these techniques to be used in tandem and the need to understand the chemistry to allow successful application of analytical technique. GC-MS and positive ion ESI-MS have been used extensively and have proven to be key techniques; used alongside positive ion ESI-SFC-UV-MS the information obtained has given insight into the auto-oxidation of RME.

Through this study the auto-oxidation of FAMEs in RME has been observed to be related to the number of double bonds in the fatty acid chain, supporting previous work. It has been established that the auto-oxidation rate of the major FAMEs in RME is decreased as the number of double bonds decrease, *i.e.* C18:3>C18:2>C18:1>C18:0.

Through the use of the aforementioned techniques, it has been observed that as the FAMEs deplete there is a number of new ions detected (in all ionisation techniques) that were not present in previous (less auto-oxidised) samples. It is proposed that these auto-oxidation products are produced from auto-oxidation of FAMEs. As auto-oxidation extends, viscosity of the aged RME increases and it is suggested that this is due to the presence of auto-oxidation products.

It has been observed in positive ion ESI-FT-ICR-MS alone that over 5000 ions are present in aged RME all suggested to be auto-

oxidation species, and this does not account for isobaric ions. Within this study a number of auto-oxidation products were the main focus, small chain degradation products (compared to the starting FAMEs), multiple oxygenated addition to the starting FAME and polymeric oxygenated auto-oxidation products. Through identification of auto-oxidation compounds in auto-oxidised RME, auto-oxidation pathways were suggested and comparisons were drawn between the detected auto-oxidation species in aged RME and expected compounds as reported in the literature.

GC-MS is a good technique to analyse small chain auto-oxidation products, the volatility and typical fragmentation pathways allow ease of analysis and successful identification. Species detected using this technique are in agreement with expected auto-oxidation species observed in other studies. However, whilst applicable to small chain auto-oxidation products, it is not a viable technique for larger auto-oxidation species. Using GC-MS a number of ions are present which are not FAMEs, however these are less than 50.

When analysing the same sample by positive ion ESI-MS techniques, there are many more ions present, in excess of 100, with positive ion ESI-FT-ICR MS displaying over 5000 new ions. This demonstrates how highly suited positive ion ESI-MS is to analyse auto-oxidation species, this is in large part to the presence of multiple oxygens within auto-oxidised FAMEs. With molecules containing increased oxygen preferentially ionised.

Using positive ion ESI-MS a series of ions +16 Da repeat series from the starting FAMEs were detected. This series is suggested to be FAMEs with addition oxygens, *I.e.* $[C18:1/2/3 + nO + Na]^+$. Through the use of positive ion ESI-SFC-UV-MS these species in the series can be observed to be related. It is suggested that compounds undergo auto-

oxidation through production of a peroxide which then reacts by: forming an epoxide, which can react further to initially produce multiply oxygenated compounds, *via* homolytic β-scission producing smaller chain auto-oxidation products or terminating propagation *via* the Russell mechanism. These auto-oxidation pathways are suggested as evidenced by the presence of *cis*-9, 10-methyl epoxystearate (epoxide), the presence of smaller chain auto-oxidation species (homolytic β-scission) and methyl 9-oxostearate (Russell mechanism).

Additionally, polymeric species were identified using positive ion ESI-MS, with species containing $C_{60}$ and $O_{20}$ detected. MS/MS was used to investigate one polymeric species ($C_{29}H_{54}O_7$), with product ions detected with molecular formula $C_{19}H_{36}O_3$ and $C_{10}H_{18}O_4$, suggesting that polymeric species are composed of other auto-oxidation species. It is postulated that these species are present at later stages of auto-oxidation and this is evidenced through the absence of these ions in less aged RME.

This research has also identified, through the use of different oxidation models, the need for auto-oxidation markers to aid identification of auto-oxidation and extent of auto-oxidation.

Alongside natural auto-oxidation, forced oxidation (engine test and electrochemical) techniques were used to investigate auto-oxidation of RME, in more appropriate time frames (hours and minutes, respectively). Through analysis of auto-oxidised RME using these techniques it was postulated that auto-oxidation pathways could be probed, auto-oxidation markers established and the relationship between FAMEs depletion, auto-oxidation species produced and viscosity proven.

From forced oxidation engine tests potential auto-oxidation markers were identified (C8:0, nonanal and methyl *cis*-9, 10-

epoxystearate) and were observed to be present in natural auto-oxidation. The relationship between the suggested auto-oxidation markers and the major FAMEs in RME were probed and related to viscosity, with strong correlations detected. It was suggested that a ratio of C18:0 compared to the percentage of auto-oxidation product most closely mimicked viscosity increases observed in auto-oxidised RME samples, with methyl *cis*-9, 10-epoxystearate the most close-fitting.

Electrochemical oxidation allowed RME oxidation or be probed on a very small time frame, minutes, compared to the natural auto-oxidation time frame of years. Overall, electrochemistry oxidation produced many oxidation products identified in natural auto-oxidised RME. However, as previous work has shown, this technique does oxidise compounds *via* epoxide routes. This was observed clearly in the oxidation of individual FAMEs were ions suggested to be $[C18:1/2/3 + O + Na]^+$ were not produced. This technique offers valuable insight into the oxidation behaviour of RME, and supports the multiple auto-oxidation pathways described in natural auto-oxidation. It is suggested that electrochemistry could be used to rapidly screen possible oxidation inhibitors before taken on to lengthy tests or to screen the oxidation capacity of biodiesel fuel stocks.

This work has further demonstrated the application of positive ion ESI-SFC-UV-MS to analyse other fuel related compounds, namely dispersant compounds. This technique was utilised to analyse different stages of a PiB succinimide dispersant synthesis. The complexity of polymer analysis and requirement of a separation technique to reduce complexity was apparent through analysis of the samples.

Positive ion ESI-SFC-UV-MS proved useful to analyse PiB succinimide dispersant samples which would not dissolve in typical positive ion ESI-SFC-MS solvents (MeOH, MeCN and $H_2O$). Initially, PiBSA and VIMA were reacted to produce a grafted PiBSA, which was then reacted to produce a PiB succinimide, with the end product being a multi-functional dispersant containing a VIMA graft. However, through the use of positive ion ESI-SFC-UV-MS when PiBSA and VIMA were reacted, analysis suggested that only VIMA had grafted onto the molecule. This was further supported in the end sample, where only ions correlating to a PiB succinimide series with only one VIMA was identified, with ions correlating to the multiply grafted VIMA dispersant absent. In addition, this technique proved useful in detecting residual reagents, such as PiBSA and VIMA and more traditional dispersant molecules, with ions suggested to be a PiB succinimide dispersant also detected.

# Further Work

This study has focussed on the development and application of chromatography and mass spectrometry techniques to investigate the auto-oxidation of RME. From this study areas of further work have been identified and will be discussed herein, these include: continued monitoring of RME auto-oxidation, monitoring of individual FAME and biodiesel produced from other feedstock sources auto-oxidation, further investigation of auto-oxidation markers, the use of EC-MS to investigate forced oxidation and prevention/decreased oxidation and investigation of multiply oxygenated species using MS/MS.

It is suggested that RME is continued to be monitored as it auto-oxidises. This will help gain a better comprehension of auto-oxidation at extended times and allow for the continued mapping of auto-oxidation species. Additionally, this will further aid the understanding of auto-oxidation processes in RME, with the focus of investigation polymerised auto-oxidation products.

Alongside continued monitoring of RME, it would be a benefit to monitor: auto-oxidation of biodiesel produced from other feedstock sources and the major FAME components of biodiesel commonly in use. Monitoring biodiesel other than RME and individual FAMEs using the techniques described within this research, using natural and forced oxidation processes, will aid identification of auto-oxidation products.

Further work is suggested to investigate the use of auto-oxidation markers. Proposed in this study is the use of C8:0, nonanal and methyl *cis*-9, 10-epoxystearate as auto-oxidation markers in RME

that can be used comparatively with C18:0 to identify extent of viscosity. It is suggested that this method should be applied to samples of RME of known auto-oxidation time to assess the validity and robustness of this technique across different RME sources. Additionally, biodiesel of different feedstock sources should be investigated to identify whether this application can be directly translated to other biodiesel feedstock sources.

EC-MS was used to investigate the oxidation of C18:1, C18:2, C18:3 and RME. This work was completed to compare this technique as an application to monitor FAME/RME oxidation on a quick time scale. However, during this application polymerised species observed in natural auto-oxidation were not detected. It is suggested that this is one area of focus for further work using EC-MS, with recirculation of already EC auto-oxidised FAME/RME, offline analysis of the EC-oxidised sample and using a longer electrode key areas of interest. Another focus of further work of EC-MS, is the use of this technique to investigate oxidation inhibitors. It is suggested that this technique could be used to investigate anti-oxidants, with the technique potentially used as a screening method for potential anti-oxidant compounds.

MS/MS was used in this study to investigate a polymerised auto-oxidation product, however it is evident from positive ion ESI-MS spectra that there are multiple polymerised auto-oxidation species. Further work is suggested to investigate polymerised auto-oxidation species and the $[C18:x + nO + Na]^+$ series *via* MS/MS, $MS^3$ and $MS^4$,to gain a better understanding of the auto-oxidation mechanism and how these species contribute to the increased viscosity of auto-oxidised biodiesel.

# References


[1] A. Demirbas, *Energy Convers. Manage.*, **2008**, *49*, 2106.

[2] Department for Transport, *Consultation On The Draft Renewable Transport Fuel Obligations Order*, **2007**.

[3] S. Şensöz, D. Angin, S. Yorgun, *Biomass Bioenergy*, **2000**, *19*, 271.

[4] A. Demirbas, *Energy Convers. Manage.*, **2009**, *50*, 14.

[5] N. M. Ribeiro, A. C. Pinto, C. M. Quintella, G. O. da Rocha, L. S. G. Teixeira, L. L. N. Guarieiro, M. D. Rangel, M. C. C. Veloso, M. J. C. Rezende, R. S. da Cruz, A. M. de Oliveira, E. A. Torres, J. B. de Andrade, *Energ. Fuel*, **2007**, *21*, 2433.

[6] G. Knothe, J. Van Gerpen, J. Krahl, *The Biodiesel Handbook*, AOCS Press, Urbana, **2005**.

[7] R. M. Mortier, M. Fox, F., S. T. Orszulik, *The Chemistry and Technology of Lubricants*, Springer, **2010**.

[8] Renewable Fuels Agency, *Year Two of the RTFO: Renewable Fuels Agency report on the Renewable Transport Fuel Obligation 2009/2010*, **2011**, 16

[9] A. C. Pinto, L. L. N. Guarieiro, M. J. C. Rezende, N. M. Ribeiro, E. A. Torres, W. A. Lopes, P. A. D. Pereira, J. B. de Andrade, *J. Braz. Chem. Soc.*, **2005**, *16*, 1313.

[10] J. Van Gerpen, *Fuel Process. Technol.*, **2005**, *86*, 1097.

[11] E. H. Pryde, *J. Am. Oil Chem. Soc.*, **1983**, *60*, 1557.

[12] H. L. Wang, H. Y. Tang, S. Salley, K. Y. S. Ng, *J. Am. Oil Chem. Soc.*, **2010**, *87*, 215.

[13] H. Y. Tang, R. De Guzman, S. Salley, K. Y. S. Ng, *J. Am. Oil Chem. Soc.*, **2010**, *87*, 337.

[14] R. A. Moreau, K. M. Scott, M. J. Haas, *J. Am. Oil Chem. Soc.*, **2008**, *85*, 761.

[15] E. Goering, W. Schwab, J. Daugherty, H. Pryde, J. Heakin, *T ASAE*, **1979**, *25*, 1472.

[16] R. W. Pryor, M. A. Hanna, J. L. Schinstock, L. L. Bashford, *T ASAE*, **1982**, *26*, 333.

[17] CODEX, *Standard for named vegetable oils*, **2003**,

[18] T. Hoshino, Y. Iwata, H. Koseki, *Therm. Sci.*, **2007**, *11*, 87.

[19] D. Y. C. Leung, B. C. P. Koo, Y. Guo, *Bioresour. Technol.*, **2006**, *97*, 250.

[20] G. Knothe, K. R. Steidley, *Fuel*, **2005**, *84*, 1059.

[21] C. Ragonese, P. Q. Tranchida, D. Sciarrone, L. Mondello, *J. Chromatogr. A*, **2009**, *1216*, 8992.

[22] E. N. Frankel, *Lipid Oxidation*, 2 ed., The Oily press, Bridgwater, **2005**.
[23] R. T. Holman, O. C. Elmer, *J. Am. Oil Chem. Soc.*, **1947**, *22*, 127.
[24] M. Canakci, A. Monyem, J. Van Gerpen, *T ASAE*, **1999**, *42*, 1565.
[25] H. Prankl, H. Schindlbauer, *Biomass for Energy and Industry*, **1998**, 594.
[26] European Commitee for Standardization, in *EN14112*, **2003**.
[27] C. D. Gamlin, N. K. Dutta, N. Roy Choudhury, D. Kehoe, J. Matisons, *Thermochim. Acta*, **2002**, *392-393*, 357.
[28] M. Tswett, *Berichte der Deutschen botanischen Gesellschaft*, **1906**, *24*, 316.
[29] M. Tswett, *Berichte der Deutschen botanischen Gesellschaft*, **1906**, *24*, 384.
[30] H. H. Strain, J. Sherma, *J. Chem. Educ.*, **1967**, *44*, 235.
[31] L. S. Ettre, *Pure Appl. Chem.*, **1993**, *65*, 819.
[32] A. T. James, J. P. Martin, *Biochem. J*, **1952**, *50*, 679.
[33] H. M. McNair, J. M. Miller, *Basic gas chromatography*, 2 ed., John Wiley & Sons, Inc., Hoboken, **2009**.
[34] D. R. Gere, *Science*, **1983**, *222*, 253.
[35] K. Yaku, F. Morishita, *J. Biochem. Bioph. Methods*, **2000**, *43*, 59.
[36] E. Klesper, A. H. Corwin, D. A. Turner, *J. Org. Chem.*, **1962**, *27*, 700.
[37] T. A. Berger, J. F. Deye, *J. Chromatogr. A*, **1991**, *547*, 377.
[38] A. Cazenave-Gassiot, R. Boughtflower, J. Caldwell, L. Hitzel, C. Holyoak, S. Lane, P. Oakley, F. Pullen, S. Richardson, G. J. Langley, *J. Chromatogr. A*, **2009**, *1216*, 6441.
[39] J. D. Pinkston, *Eur. J. Mass Spectrom.*, **2005**, *11*, 189.
[40] C. J. Welch, W. R. Leonard, J. O. DaSilva, M. Biba, J. Albaneze-Walker, D. W. Henderson, B. Laing, D. J. Mathre, *LC GC Europe*, **2005**, *18*, 264.
[41] T. R. Covey, B. A. Thomson, B. B. Schneider, *Mass Spectrom. Rev.*, **2009**, *28*, 870.
[42] M. Yamashita, J. B. Fenn, *J. Phys. Chem.*, **1984**, *88*, 4451.
[43] J. B. Fenn, M. Mann, C. K. Meng, S. F. Wong, C. M. Whitehouse, *Science*, **1989**, *246*, 64.
[44] M. Dole, L. L. Mack, R. L. Hines, R. C. Mobley, L. D. Ferguson, M. B. Alice, *J. Chem. Phys.*, **1968**, *49*, 2240.
[45] S. F. Wong, C. K. Meng, J. B. Fenn, *J. Phys. Chem.*, **1988**, *92*, 546.
[46] M. Yamashita, J. B. Fenn, *J. Phys. Chem.*, **1984**, *88*, 4671.
[47] W. M. A. Niessen, *J. Chromatogr. A*, **1999**, *856*, 179.
[48] G. Taylor, *Proceedings of the Royal Society A*, **1964**, *280*, 383.
[49] B. A. Thomson, J. V. Iribarne, *J. Chem. Phys.*, **1979**, *71*, 4451.
[50] P. Kebarle, U. H. Verkerk, *Mass Spectrom. Rev.*, **2009**, *28*, 898.

[51] J. V. Iribarne, B. A. Thomson, *J. Chem. Phys.*, **1976**, *64*, 2287.
[52] L. L. Mack, P. Kralik, A. Rheude, M. Dole, *J. Chem. Phys.*, **1970**, *52*, 4977.
[53] R. B. Cole, *J. Mass Spectrom.*, **2000**, *35*, 763.
[54] J. B. Fenn, *J. Am. Soc. Mass. Spectrom.*, **1993**, *4*, 524.
[55] J. Fernández de la Mora, *Anal. Chim. Acta,* **2000**, *406*, 93.
[56] P. Kebarle, M. Peschke, *Anal. Chim. Acta,* **2000**, *406*, 11.
[57] G. Wang, R. B. Cole, *Anal. Chim. Acta,* **2000**, *406*, 53.
[58] M. Gamero-Castaño, J. Fernández de la Mora, *Anal. Chim. Acta,* **2000**, *406*, 67.
[59] G. Wang, R. B. Cole, *Anal. Chem.*, **1998**, *70*, 873.
[60] E. de Hoffman, V. Stroobant, *Mass Spectrometry: Principles and Applications*, 3 ed., John Wiley & Sons Ltd, Chichester, **2007**.
[61] IUPAC, *Compendium of Chemical Terminology*, 2 ed., Blackwell Scientific Publications, Oxford, **1997**.
[62] W. Paul, H. Steinwedel, *Naturforsch,* **1953**, 448.
[63] D. J. Douglas, *Mass Spectrom. Rev.,* **2009**, *28*, 937.
[64] P. H. Dawson, *Mass Spectrom. Rev.,* **1986**, *5*, 1.
[65] S. D. Tanner, V. I. Baranov, *J. Am. Soc. Mass. Spectrom.*, **1999**, *10*, 1083.
[66] W. E. Stephens, *Bull. Am. Phys. Soc.*, **1946**, *21*, 22.
[67] W. C. Wiley, I. H. McLaren, *Rev. Sci. Instrum.*, **1955**, *26*, 1150.
[68] M. Guilhaus, *J. Mass Spectrom.*, **1995**, *30*, 1519.
[69] M. L. Vestal, P. Juhasz, S. A. Martin, *Rapid Commun. Mass Spectrom.*, **1995**, *9*, 1044.
[70] R. S. Brown, J. J. Lennon, *Anal. Chem.*, **1995**, *67*, 1998.
[71] J. H. Watson, D. O. Sparkman, *Introduction to Mass Spectrometry*, 4th ed., John Wiley and Sons Ltd, Chichester, **2007**.
[72] A. Staub, J. Schappler, S. Rudaz, J.-L. Veuthey, *Electrophoresis,* **2009**, *30*, 1610.
[73] A. G. Marshall, C. L. Hendrickson, G. S. Jackson, *Mass Spectrom. Rev.*, **1998**, *17*, 1.
[74] K. D. Henry, E. R. Williams, B. H. Wang, F. W. McLafferty, J. Shabanowitz, D. F. Hunt, *Proc. Natl. Acad. Sci. USA,* **1989**, *86*, 9075.
[75] I. J. Amster, *J. Mass Spectrom.*, **1996**, *31*, 1325.
[76] M. B. Comisarow, A. G. Marshall, *Chem. Phys. Lett.*, **1974**, *25*, 282.
[77] ISO Standard 3104, **1994**.
[78] British Standards*, Vol. BS EN14214*, **2008**.
[79] R. P. Rodgers, A. M. McKenna, *Anal. Chem.*, **2011**, *83*, 4665.
[80] British Standards*, Vol. BS EN 14103*, **2011**.

[81] F. Ulberth, R. G. Gabernig, F. Schrammel, *J. Am. Oil Chem. Soc.*, **1999**, *76*, 263.
[82] F.-F. Hsu, J. Turk, *J. Am. Soc. Mass. Spectrom.*, **2008**, *19*, 1673.
[83] J. A. Zirrolli, R. C. Murphy, *J. Am. Soc. Mass. Spectrom.*, **1993**, *4*, 223.
[84] H. L. Fang, T. L. Alleman, R. L. McCormick, *SAE International,* **2006**, *01*.
[85] British Standards, *Vol. BS EN 14078*, **2009**.
[86] G. Knothe, *Eur. J. Lipid Sci. Technol.*, **2006**, *108*, 493.
[87] J. Samuelsson, M. Johansson, *J. Am. Oil Chem. Soc.*, **2001**, *78*, 1191.
[88] P. H. Cui, R. K. Duke, B. N. Tattam, C. C. Duke, *Chem. Phys. Lipids,* **2008**, *152*, 65.
[89] G. Knothe, J. A. Kenar, *Eur. J. Lipid Sci. Technol.*, **2004**, *106*, 88.
[90] V. M. Mello, F. C. C. Oliveira, W. G. Fraga, C. J. do Nascimento, P. A. Z. Suarez, *Magn. Reson. Chem.*, **2008**, *46*, 1051.
[91] A. Szterk, I. Stefaniuk, B. Waszkiewicz-Robak, M. Roszko, *J. Am. Oil Chem. Soc.*, **2011**, *88*, 611.
[92] J. S. Buyer, *J. Microbiol. Methods,* **2003**, *54*, 117.
[93] A. L. Michaud, M. P. Yurawecz, P. Delmonte, B. A. Corl, D. E. Bauman, J. T. Brenna, *Anal. Chem.*, **2003**, *75*, 4925.
[94] C. Y. Peng, C. H. Lan, Y. T. Dai, *Chemosphere,* **2006**, *65*, 2054.
[95] V. Vrkoslav, K. Urbanova, J. Cvacka, *J. Chromatogr. A,* **2010**, *1217*, 4184.
[96] S. Hauff, W. Vetter, *Anal. Bioanal. Chem.*, **2010**, *396*.
[97] J. R. Pedersen, A. Ingemarsson, J. O. Olsson, *Chemosphere,* **1999**, *38*, 2467.
[98] L. Hejazi, D. Ebrahimi, M. Guilhaus, D. B. Hibbert, *Anal. Chem.*, **2009**, *81*, 1450.
[99] W. Tsuzuki, K. Ushida, *Lipids,* **2009**, *44*, 373.
[100] H. Devle, E. O. Rukke, C. F. Naess-Andresen, D. Ekeberg, *J. Sep. Sci.*, **2009**, *32*, 3738.
[101] K. Eder, *J. Chromatogr. B-Bio. Med. Appl.*, **1995**, *671*, 113.
[102] British Standards, *Vol. BS EN14331*, **2004**.
[103] S. Schober, I. Seidl, M. Mittelbach, *Eur. J. Lipid Sci. Technol.*, **2006**, *108*, 309.
[104] F. Adam, F. Bertoncini, V. Coupard, N. Charon, D. Thiebaut, D. Espinat, M. C. Hennion, *J. Chromatogr. A,* **2008**, *1186*, 236.
[105] W. Tiyapongpattana, P. Wilairat, P. J. Marriott, *J. Sep. Sci.*, **2008**, *31*, 2640.
[106] C. Villegas, Y. Zhao, J. M. Curtis, *J. Chromatogr. A,* **2010**, *1217*, 775.

[107] M. Kaminski, E. Gilgenast, A. Przyjazny, G. Romanik, *J. Chromatogr. A,* **2006**, *1122*, 153.
[108] J. Huang, R. Chen, D. Cavagnin, E. Long, *App. Note 389: A Robust Method for the Analysis if Biodiesel Using a Self-cleaning API source*, **2007**.
[109] T. Madl, M. Mittelbach, *Analyst,* **2005**, *130*, 565.
[110] G. Di Nicola, M. Pacetti, F. Polonara, G. Santori, R. Stryjek, *J. Chromatogr. A,* **2008**, *1190*, 120.
[111] C. Orellana-Coca, D. Adlercreutz, M. M. Andersson, B. Mattiasson, R. Hatti-Kaul, *Chem. Phys. Lipids,* **2005**, *135*, 189.
[112] T. A. Foglia, K. C. Jones, J. G. Phillips, *Chromatographia,* **2005**, *62*, 115.
[113] R. H. Smith, M. Hyytiainen, A. V. Felipe, P. M. Morris, *J. Sep. Sci.,* **2001**, *24*, 208.
[114] R. M. Smith, S. Cocks, *Anal. Proc.,* **1991**, *28*, 11.
[115] A. Nomura, J. Yamada, K. Tsunoda, K. Sakaki, T. Yokochi, *Anal. Chem.,* **1989**, *61*, 2076.
[116] J. Cole, J. Lefler, R. Chen, *LC GC North America,* **2008**, 40.
[117] J. W. Diehl, F. P. DiSanzo, *J. Chromatogr. Sci.,* **2007**, *45*, 690.
[118] R. M. Smith, S. Cocks, *Analyst,* **1994**, *119*, 921.
[119] R. M. Smith, M. Hyytiäinen, A. V. Felipe, P. M. Morris, *J. Sep. Sci.,* **2001**, *24*, 208.
[120] I. Eide, K. Zahlsen, *Energ. Fuel,* **2007**, *21*, 3702.
[121] R. R. Catharino, H. M. S. Milagre, S. A. Saraiva, C. M. Garcia, U. Schuchardt, M. N. Eberlin, R. Augusti, R. C. L. Pereira, M. J. R. GuimarÃes, G. F. de SÃ¡, J. M. R. Caixeiro, V. de Souza, *Energ. Fuel,* **2007**, *21*, 3698.
[122] L. S. Eberlin, P. V. Abdelnur, A. Passero, G. F. de Sa, R. J. Daroda, V. de Souza, M. N. Eberlin, *Analyst,* **2009**, *134*, 1652.
[123] P. V. Abdelnur, L. S. Eberlin, G. F. de Sa, V. de Souza, M. N. Eberlin, *Anal. Chem.,* **2008**, *80*, 7882.
[124] S. Cai, J. A. Syage, *Anal. Chem.,* **2006**, *78*, 1191.
[125] I. Eide, G. Neverdal, F. Westad, *Energ. Fuel,* **2010**, *24*, 3661.
[126] R. G. D. Prates, R. Augusti, I. C. P. Fortes, *Energ. Fuel,* **2010**, *24*, 3183.
[127] British Standards, *Vol. BS EN14112*, **2004**.
[128] British Standards, *Vol. BS EN 15751*, **2009**.
[129] British Standards, *Vol. BS EN 16091*, **2011**.
[130] F. W. McLafferty, F. Turecek, *Interpretation of Mass Spectra*, Fourth Edition ed., University Science Books, Sausalito, **1993**.
[131] British Standards, *Vol. BS EN 14103*, **2003**.
[132] R. E. Majors, *LC GC North America,* **1997**, *15*, 1009.

[133] R. R. Khoury, D. Ebrahimi, L. Hejazi, M. P. Bucknall, R. Pickford, D. B. Hibbert, *Fuel,* **2011**, *90*, 2677.
[134] R. O. Dunn, *Biofuels, Bioprod. Biorefin.,* **2008**, *2*, 304.
[135] R. O. Dunn, *Fuel Process. Technol.,* **2005**, *86*, 1071.
[136] G. Fontaras, G. Karavalakis, M. Kousoulidou, T. Tzamkiozis, L. Ntziachristos, E. Bakeas, S. Stournas, Z. Samaras, *Fuel,* **2009**, *88*, 1608.
[137] S. Y. Qian, H. P. Wang, F. Q. Schafer, G. R. Buettner, *Free Radical Biol. Med.,* **2000**, *29*, 568.
[138] S. Venkataraman, F. Q. Schafer, G. R. Buettner, *Antioxid. Redox Signal.,* **2004**, *6*, 631.
[139] M. J. Perkins, *Radical Chemistry: The Fundamentals*, Oxford University Press, New York, **2000**.
[140] E. N. Frankel, *Prog. Lipid Res.,* **1980**, *19*, 1.
[141] M. Lucarini, G. F. Pedulli, *Chem. Soc. Rev.,* **2010**, *39*, 2106.
[142] A. Köckritz, A. Martin, *Eur. J. Lipid Sci. Technol.,* **2008**, *110*, 812.
[143] J. L. Bolland, G. Gee, *Trans. Faraday Soc.,* **1946**, *42*, 244.
[144] L. Niczke, F. Czechowski, I. Gawel, *Prog. Org. Coat.,* **2007**, *59*, 304.
[145] W. E. Neff, E. N. Frankel, D. Weisleder, *Lipids,* **1981**, *16*, 439.
[146] C. Morisseau, *Biochimie,* **2008**, *95*, 91.
[147] M. Poirot, S. Silvente-Poirot, *Biochimie,* **2013**, *95*, 622.
[148] J. Jin, Y. X. Zheng, W. E. Boeglin, A. R. Brash, *J. Lipid Res.,* **2013**, *54*, 754.
[149] L. Attanatho, P. Thepkhun, A. Suemanotham, K. Petchtabtim, Y. Thanmongkhon, P. Jenvanitpanjakull, Y. Yoshimura, in *3rd Biomass-Asia Workshop*, **2006**.
[150] N. A. Porter, K. A. Mills, R. L. Carter, *J. Am. Chem. Soc.,* **1994**, *116*, 6690.
[151] G. Lercker, M. T. Rodriguez-Estrada, M. Bonoli, *J. Chromatogr. A,* **2003**, *985*, 333.
[152] E. N. Frankel, W. E. Neff, W. K. Rohwedder, B. P. S. Khambay, R. F. Garwood, B. C. L. Weedon, *Lipids,* **1977**, *12*, 901.
[153] G. J. Langley, J. M. Herniman, M. Gower, S. Lamond, P. McMahon, T. Lynch, H. Preston, in *56th ASMS Conference on Mass Spectrometry and Allied Topics* Denver, USA, **2008**.
[154] D. A. Lillard, E. A. Day, *J. Amer. Oil Chem. Soc.,* **1964**, *41*, 549.
[155] J. A. Howard, K. U. Ingold, *J. Am. Chem. Soc.,* **1968**, *90*, 1056.
[156] G. A. Russell, *J. Am. Chem. Soc.,* **1957**, *79*, 3871.
[157] S. Miyamoto, G. R. Martinez, M. H. G. Medeiros, P. Di Mascio, *J. Am. Chem. Soc.,* **2003**, *125*, 6172.
[158] N. A. Porter, *Acc. Chem. Res.,* **1986**, *19*, 262.

[159] K. Miyashita, K. Fujimoto, T. Kaneda, *Agric. Biol. Chem.,* **1984**, *48*, 2511.
[160] K. Miyashita, N. Hara, K. Fujimoto, T. Kaneda, *Lipids,* **1985**, *20,* 578.
[161] W. E. Neff, E. N. Frankel, K. Fujimoto, *J. Am. Oil Chem. Soc.,* **1988**, *65*, 616.
[162] W. Lohmann, A. Baumann, U. Karst, *Lc Gc North America,* **2010**, *28*, 470.
[163] A. Baumann, W. Lohmann, B. Schubert, H. Oberacher, U. Karst, *J. Chromatogr. A,* **2009**, *1216*, 3192.
[164] F. Pitterl, J. P. Chervet, H. Oberacher, *Anal. Bioanal. Chem.,* **2010**, *397*, 1203.
[165] E. Rivera-Tirado, D. J. Aaserud, C. Wesdemiotis, *J. Appl. Polym. Sci.,* **2011**, *124*, 2682.
[166] T. V. Liston, *Lubr. Eng.,* **1992**, *48*, 389.
[167] R. M. Mortier, M. F. Fox, S. T. Orszulik, *Chemistry and Technology of Lubricants*, Springer, London, **2010**.
[168] M. A. Mekewi, *Mater. Res. Innovations,* **2002**, *6*, 214.
[169] N. S. Ahmed, A. M. Nassar, A. A. Abdel-Azim, *Int. J. Polymer. Mater.,* **2008**, *57*, 114.
[170] J. Hancsók, M. Bubálik, Á. Beck, J. Baladincz, *Chem. Eng. Res. Des.,* **2008**, *86*, 793.